

**ASSESSMENT OF PHARMACOKINETIC INTERACTION
OF
L-DOPA AND BENSERAZIDE**

ANIMAL MODEL, MECHANISTIC MATHEMATICAL MODELS, AND ALLOMETRIC
SCALING ACROSS SPECIES

Inauguraldissertation

zur

Erlangung der Würde eines Doktors der Philosophie

vorgelegt der

Philosophisch-Naturwissenschaftlichen Fakultät

der Universität Basel

von

Susanna Sarah Grange

aus Fribourg (FR)

Basel, 2004

Genehmigt von der Philosophisch-Naturwissenschaftlichen Fakultät auf Antrag der Herren

Professor Dr. T.W. Guentert

Professor Dr. N.H.G. Holford

Professor Dr. U.A. Meyer

Basel, den 8. Juni 2004

Professor Dr. M. Tanner

Dekan

To see a world in a grain of sand
And a heaven in a wild flower
Hold infinity in the palm of your hand
And eternity in an hour
Auguries of innocence, William Blake

to my parents

ACKNOWLEDGEMENTS

The present thesis was supported by F. Hoffmann-La Roche Ltd, Pharma Division, Non-Clinical Drug Safety, 4070 Basel, Switzerland.

I wish to thank:

Theodor W. Guentert for acting as my supervisor and academic referee, for his mentorship in clinical pharmacology, for giving me the opportunity to do a thesis under his guidance, and for the broad scientific training I received.

Urs A. Meyer for acting as my academic co-referee.

Nicholas H.G. Holford for acting as my scientific adviser, for his coaching, and for teaching me the know-how in modeling and simulation.

Jean-Louis Steimer for his scientific input, for the helpful discussions on modeling, and for the kindness to let me use the software ACSL in his department during summer 1998.

Ronald Gieschke for his scientific input and for all the fruitful discussions about mathematical and modeling issues.

Bärbel Fotteler for her input on programming issues in SAS and NONMEM, for her scientific advice, and for the much appreciated friendship.

Klaas Zuideveld, Florence Hourcade-Potelleret, and the modeling & simulation group for the scientific discussions, for the NONMEM support, and for their encouragement.

Bruno Reigner for his helpful scientific discussions, for his mentorship in clinical pharmacology, and for his encouragement.

Guy Fischer for teaching me the techniques to determine L-dopa, 3-OMD, benserazide, and Ro 04-5127 in plasma and for supporting my efforts in the world of analytics.

Karin Tosch, Guy Fischer, and Thierry Delemonte for accepting my presence in their lab.

Herbert Birnböck for his helpful discussions on analytical issues.

Mirjana Lazendic for her technical assistance during the animal experiment.

Jo Meyer for his technical assistance during the protein binding studies of L-dopa and 3-OMD and for his scientific advice.

Sonja Nick, Ruth Haas, and Markus Fassbender for the much appreciated friendship and scientific support.

Christine Operschall for her moral support, for motivating me in difficult times, and for the much appreciated friendship.

Jakob Maier for his encouragement and help, for all the delicious pasta lunches during our study days, and for the much appreciated friendship.

Lisa Maier for always being there when I needed support, for encouraging me in difficult times, and for the much appreciated friendship.

Tony Camen, who accompanied me during important years of my life, for his love.

A special thank-you to my parents, sister and friends for their love, infinite patience and endless encouragement and support; particularly my parents for their faith in me.

ACKNOWLEDGEMENTS	5
TABLE OF CONTENTS	7
LIST OF TABLES	12
LIST OF FIGURES	13
SUMMARY	17
GLOSSARY OF ABBREVIATIONS	21

CHAPTER 1

GENERAL INTRODUCTION	27
1.1 Parkinsonism	27
1.1.1 Clinical Features	27
1.1.2 Etiology	28
1.1.3 Pathological-Histological Features	29
1.1.4 Pathological-Neurochemical Features	29
1.1.5 Therapy.....	30
1.1.5.1 L-Dopa and Benserazide (Madopar®).....	31
1.2 Models and Modeling	33
1.2.1 Introduction	33
1.2.2 Modeling in Drug Development.....	34
1.2.3 Why Model Data and How to Go About It?.....	36
1.2.4 Definitions	37
1.2.5 Types of Models	38
1.2.5.1 Mechanistic Model versus Empirical Model	38
1.2.5.2 Mathematical Model versus Statistical Model.....	39
1.2.5.3 Descriptive Model versus Predictive Model.....	39
1.2.5.4 PK Model versus PD Model versus PKPD Model.....	39
1.2.5.5 Compartmental Model	40
1.2.6 Integration Algorithms	44
1.2.7 Methods Used for Curve Fitting (Optimization Methods).....	44
1.2.8 Weighting	46
1.2.9 Interpretation of the Results	47
1.2.9.1 Assessing the Goodness-of-fit	47
1.2.9.2 Discrimination between Rival Models.....	49
1.2.10 Individual and Population Analyses	50

1.3 Across Species Scaling	51
1.3.1 Introduction	51
1.3.2 Physiologically Based Models.....	51
1.3.3 Allometric Method	53
1.4 Methodologies to Describe and Understand PK Drug-Drug Interactions: Literature	
Review	56
1.4.1 Introduction	56
1.4.2 Underlying Mechanism of PK Drug-Drug Interactions.....	57
1.4.2.1 Absorption	58
1.4.2.2 Distribution	59
1.4.2.3 Metabolism	59
1.4.2.4 Excretion.....	61
1.4.3 Strategies and Methods to Determine Drug-Drug Interactions.....	61
1.4.3.1 In Vitro Models.....	62
1.4.3.2 Predicting In Vivo Drug-Drug Interactions from In Vitro Metabolic Data	65
1.4.3.3 Cocktail Strategy.....	65
1.4.3.4 Mechanism-Based PK Models.....	66
1.4.3.5 Population Approach	67
1.4.4 Summary	67
CHAPTER 2	
GENERAL OBJECTIVE AND OUTLINE OF THESIS	71
CHAPTER 3	
ASSESSMENT OF THE PHARMACOKINETIC INTERACTION OF L-DOPA AND BENSERAZIDE IN RATS: ANIMAL MODEL AND COMPARTMENTAL PK MODEL	75
3.1 Rationale	75
3.1.1 Rationale for Pharmacokinetic Study in Rats	75
3.1.2 Rationale for Pharmacokinetic Model	75
3.1.3 Rationale for Dose	76
3.2 Objective	76
3.3 Materials and Methods	76
3.3.1 Drugs and Chemicals.....	76
3.3.2 Animal Experiment.....	76
3.3.3 Drug Assay	77
3.3.4 Pharmacokinetic Analysis	78

3.3.4.1 Non-Compartmental Analysis	78
3.3.4.2 Compartmental Analysis.....	79
3.3.5 Statistical Analysis	84
3.3.6 Intravenous Data of Benserazide and Ro 04-5127	84
3.4 Results	84
3.4.1 Animal Experiment.....	84
3.4.2 Assay Performance of Drug Concentration Analysis	85
3.4.2.1 L-Dopa and its Metabolite 3-OMD.....	85
3.4.2.2 Benserazide and its Metabolite Ro 04-5127	85
3.4.3 Non-Compartmental PK Analysis of L-Dopa and its Metabolite 3-OMD	86
3.4.4 Non-Compartmental PK Analysis of Benserazide and its Metabolite Ro 04-5127.....	89
3.4.5 Compartmental PK Analysis of L-Dopa and its Metabolite 3-OMD	92
3.4.6 Compartmental PK Analysis of Benserazide and its Metabolite Ro 04-5127	94
3.5 Discussion.....	94
3.6 Conclusion	101

CHAPTER 4

PREDICTION OF HUMAN L-DOPA PHARMACOKINETICS AFTER L-DOPA TREATMENT WITH AND WITHOUT BENSERAZIDE FROM IN VIVO L-DOPA PHARMACOKINETICS IN RATS	105
4.1 Rationale	105
4.1.1 Rationale for Prediction of Human In Vivo Pharmacokinetics from In Vivo Pharmacokinetics in Rats	105
4.1.2 Rationale for Protein Binding Study.....	105
4.2 Objective	106
4.3 Materials and Methods.....	106
4.3.1 Assessment of Plasma Protein Binding of L-Dopa and 3-OMD in Rats and Humans	106
4.3.2 In Vivo Concentration-Time Data	108
4.3.3 Evaluation.....	109
4.3.3.1 PK Modeling and Simulation.....	109
4.3.3.2 Across Species Scaling	110
4.4 Results	110
4.4.1 Plasma Protein Binding of L-Dopa and 3-OMD in Rats and Humans	110
4.4.2 Across Species Scaling.....	111
4.5 Discussion.....	115

4.6 Conclusion	118
-----------------------------	------------

CHAPTER 5

NONLINEAR MIXED EFFECTS MODELING	121
5.1 Rationale	121
5.2 Objective	121
5.3 Materials and Methods	121
5.3.1 Experimental Data	122
5.3.2 Pharmacokinetic Analysis	122
5.3.2.1 Structural Pharmacokinetic Models	122
5.3.2.2 Statistical Models (Random Effects Models)	123
5.3.2.3 Model Selection Criteria	125
5.3.2.4 Integration and Optimization	125
5.3.3 Software.....	126
5.4 Results	126
5.4.1 L-Dopa/3-OMD after Administration of L-Dopa Alone	126
5.4.2 Benserazide/Ro 04-5127 after Administration of Benserazide Alone	129
5.4.3 Drug-Drug Interaction L-Dopa/Benserazide	132
5.4.4 Comparison of PK Parameters.....	134
5.5 Discussion.....	135
5.6 Conclusion	138

CHAPTER 6

PHYSIOLOGICALLY BASED PK MODELS FOR L-DOPA PHARMACOKINETICS WITH AND WITHOUT BENSERAZIDE INCLUDING LIVER CONCENTRATIONS AND ALLOWING FOR NONLINEAR KINETICS FOR THE ELIMINATION OF L-DOPA VIA THE AADC PATHWAY	141
6.1 Introduction.....	141
6.2 Basic L-Dopa/Benserazide Model (Part 1).....	146
6.2.1 Rationale.....	146
6.2.2 Objective	146
6.2.3 Materials and Methods	146
6.2.3.1 Experimental Data	146
6.2.3.2 Pharmacokinetic Model for L-Dopa and 3-OMD	147

6.2.4 Results	153
6.2.4.1 Well-Stirred Model	153
6.2.4.2 Parallel Tube Model.....	154
6.3 Benserazide/Ro 04-5127 Model (Part 2).....	156
6.3.1 Rationale.....	156
6.3.2 Objective	156
6.3.3 Materials and Methods	156
6.3.3.1 Experimental Data	156
6.3.3.2 Pharmacokinetic Model for Benserazide and Ro 04-5127.....	156
6.3.4 Results	160
6.4 Enhanced L-Dopa/Benserazide Model (Part 3).....	161
6.4.1 Rationale.....	161
6.4.2 Objective	162
6.4.3 Materials and Methods	162
6.4.3.1 Experimental Data	162
6.4.3.2 Pharmacokinetic Model for L-Dopa and 3-OMD.....	162
6.4.4 Results	165
6.5 Overall Discussion of Chapters 6.2 to 6.4	167
6.6 Overall Conclusion of Chapters 6.2 to 6.4	172
CHAPTER 7	
GENERAL CONCLUSIONS AND OUTLOOK.....	175
7.1 General Conclusions	175
7.2 Outlook.....	177
REFERENCE LIST	179
APPENDIX A: DEMOGRAPHIC DATA.....	193
A.1 Listings of Individual Demographic Data	193
APPENDIX B: BIOANALYTICAL DATA.....	195
B.1 Inter-Assay Precision from Quality Control Samples for L-Dopa in Rat Plasma and Human Plasma	195
B.2 Inter-Assay Precision from Quality Control Samples for 3-OMD in Rat Plasma and Human Plasma	197
B.3 Inter-Assay Precision from Quality Control Samples for Benserazide in Human Plasma	199
B.4 Inter-Assay Precision from Quality Control Samples for Ro 04-5127 in Human Plasma.....	199
B.5 L-Dopa and 3-OMD Assay: Chromatograms.....	200
B.6 Benserazide and Ro 04-5127 Assay: Chromatograms	202

APPENDIX C: PHARMACOKINETIC DATA.....	205
C.1 Listings of Individual Plasma Concentrations of L-Dopa and 3-OMD	205
C.2 Listings of Individual Plasma Concentrations of Benserazide and Ro 04-5127.....	207
C.3 Listings of Mean Plasma Concentrations of L-Dopa and 3-OMD	209
C.4 Listings of Mean Plasma Concentrations of Benserazide and Ro 04-5127.....	211
C.5 Listings of In Vitro Protein Binding Study Results.....	213
APPENDIX D: NONLINEAR MIXED EFFECTS MODELING	217
D.1 Results of NONMEM run doAP01_FOCEI.....	217
D.2 Results of NONMEM run bensAP13_FOCEI	218
D.3 Results of NONMEM run bedoAP06	219
APPENDIX E: REPARAMETERIZATION OF MICHAELIS-MENTEN EQUATION	221
CURRICULUM VITAE	223
PUBLICATIONS AND PRESENTATIONS	225

LIST OF TABLES

TABLE 1: Etiology of Parkinsonism.....	28
TABLE 2: Drug therapy in Parkinsonism.....	31
TABLE 3: Benefits of a model	36
TABLE 4: General approach to modeling	36
TABLE 5: Error types.....	46
TABLE 6: Allometric exponents	54
TABLE 7: List of events influencing the absorption of a drug.....	58
TABLE 8: Mechanisms of inhibition of enzymes.....	59
TABLE 9: Examples of predictions of in vivo drug-drug interactions based on in vitro data ^[137]	65
TABLE 10: Precision and bias of the plasma assay for L-dopa and 3-OMD according to quality control samples.....	85
TABLE 11: Precision and bias of the plasma assay for benserazide and its metabolite Ro 04-5127 according to quality control samples	86
TABLE 12: Pharmacokinetic parameters of L-dopa after treatment with L-dopa alone or with L-dopa/benserazide (non-compartmental analysis).....	88
TABLE 13: Pharmacokinetic parameters of 3-OMD after treatment with L-dopa alone or with L-dopa/benserazide (non-compartmental analysis).....	89
TABLE 14: Pharmacokinetic parameters of benserazide after treatment with benserazide alone or with L-dopa/benserazide (non-compartmental analysis).....	91
TABLE 15: Pharmacokinetic parameters of Ro 04-5127 after treatment with benserazide alone or with L-dopa/benserazide (non-compartmental analysis).....	92
TABLE 16: Pharmacokinetic parameters estimated by compartmental analysis.....	93

TABLE 17: Comparison of PK parameters of L-dopa and 3-OMD estimated by compartmental analysis (CA) and by standard non-compartmental analysis (NCA)	95
TABLE 18: Pharmacokinetic parameters of L-dopa and 3-OMD in rats and as predicted by allometry (Eq. 39) in humans	112
TABLE 19: Pharmacokinetic parameters of benserazide and Ro 04-5127 in rats and as predicted by allometry (Eq. 39) in humans	112
TABLE 20: Comparison of predicted PK parameters with PK parameters estimated by standard non-compartmental analysis (NCA) in humans	117
TABLE 21: Statistical models for residual error	124
TABLE 22: Estimation methods	126
TABLE 23: Population PK parameters, inter-individual variability and residual error for L-dopa and 3-OMD after L-dopa alone	127
TABLE 24: Population PK parameters, inter-individual variability and residual error for benserazide and Ro 04-5127 after benserazide alone	129
TABLE 25: Population PK parameters, inter-individual variability and residual error	132
TABLE 26: Comparison of PK parameters of L-dopa and 3-OMD after administration of L-dopa alone using two different methods for population PK analysis	134
TABLE 27: Comparison of PK parameters of benserazide and Ro 04-5127 after administration of benserazide alone using two different methods for population analysis	134
TABLE 28: Comparison of PK parameters after administration of L-dopa/benserazide using two different methods for population PK analysis	135
TABLE 29: Liver models	144
TABLE 30: Well-stirred model: Final parameter estimates	153
TABLE 31: Parallel tube model: Final parameter estimates	155
TABLE 32: Final parameter estimates	166
TABLE 33: Comparison of final parameter estimates	169
TABLE 34: Differences between PK models of Chapter 3 and Chapter 6.4	169
TABLE 35: Literature values for $K_{m_{AADC}}$	170
TABLE 36: Literature values for $V_{max_{AADC}}$	170

LIST OF FIGURES

FIGURE 1: Pathogenesis of Parkinson disease	29
FIGURE 2: Single Photon Emission Computerized Tomography [^{123}I] βCIT images from a patient with mild-early, moderate and severe Parkinson's disease and from an age-matched healthy subject. Levels of SPECT activity are color encoded from low (black) to high (yellow/white). Reprinted through the courtesy of the National Parkinson Foundation Inc. and J. Seibyl (Yale NeuroSPECT Center).	30
FIGURE 3: Metabolism of L-dopa and site of action of benserazide	32
FIGURE 4: Relationship between PK and PD	37
FIGURE 5: Schematic representation of a 1-compartment model after iv administration (I) and po administration (II)	40

FIGURE 6: Schematic representation of two different types of multi-compartment models (I: catenary system; II: mammillary system).....	42
FIGURE 7: Schematic representation of a 2-compartment mammillary model with elimination from the central compartment after iv administration (I) and po administration (II)	42
FIGURE 8: Schematic representation of a compartmental model for a drug and its metabolite.....	43
FIGURE 9: Schematic representation of least squares method.....	45
FIGURE 10: Relative residuals plotted versus time (I: Lack of fit due to inappropriate structural model; II: Lack of fit due to inappropriate weighting scheme).....	48
FIGURE 11: Model structure of a physiologically based pharmacokinetic model	52
FIGURE 12: Linear plot (I) and log-log plot (II) of allometric equation	54
FIGURE 13: Sites for PK drug-drug interactions.....	57
FIGURE 14: In vitro cytochrome P450 inhibition screening	64
FIGURE 15: Schematic representation of conceptual model to describe PK of L-dopa and 3-OMD.....	80
FIGURE 16: Schematic representation of conceptual model to describe PK of benserazide and Ro 04-5127	80
FIGURE 17: Average (\pm SD) plasma concentration-time profiles of L-dopa and 3-OMD after treatment with L-dopa alone (- Δ -) and after treatment with L-dopa/benserazide (- \blacksquare -).....	87
FIGURE 18: Average (\pm SD) plasma concentration-time profiles of benserazide and Ro 04-5127 after treatment with benserazide alone ¹ (- Δ -) and after treatment with L-dopa/benserazide (- \blacksquare -).....	90
FIGURE 19: Plasma concentration–time profile of Ro 04-5127 and the change of L-dopa clearance by AADC over time after oral administration of 80/20 mg/kg L-dopa/benserazide	93
FIGURE 20: Predicted and observed L-dopa and 3-OMD plasma concentrations after oral administration of 80 mg/kg L-dopa.....	94
FIGURE 21: Predicted and observed L-dopa and 3-OMD plasma concentrations after oral administration of 80/20 mg/kg L-dopa/benserazide	94
FIGURE 22: Schedule of assessment for 1 treatment period	108
FIGURE 23: Schematic representation of conceptual model describing the pharmacokinetics of L-dopa and 3-OMD with and without benserazide in humans.....	109
FIGURE 24: Fraction unbound of L-dopa and 3-OMD in human and rat plasma	111
FIGURE 25: Predicted and observed plasma concentration – time profiles of L-dopa and 3-OMD in humans after treatment with L-dopa alone	113
FIGURE 26: Predicted and observed plasma concentration – time profiles of L-dopa and 3-OMD in humans after treatment with L-dopa and benserazide	114
FIGURE 27: Comparison of protein binding results with literature data ^[190]	115
FIGURE 28: Predicted and observed plasma concentrations of L-dopa and 3-OMD after administration of L-dopa alone.....	128
FIGURE 29: Predicted and observed plasma concentrations of benserazide after intravenous and oral administration of benserazide	130
FIGURE 30: Predicted and observed plasma concentrations of Ro 04-5127 after intravenous and oral administration of benserazide	131

FIGURE 31: Predicted and observed plasma concentrations of L-dopa and 3-OMD after L-dopa/benserazide (L-dopa/benserazide model).....	133
FIGURE 32: Blood supply of the human liver.....	142
FIGURE 33: Organ clearance (panel A).....	142
FIGURE 34: Organ clearance (panel B).....	142
FIGURE 35: Organ clearance (panel C).....	142
FIGURE 36: Schematic representation of the well-stirred model (I) and the parallel tube model (II).....	145
FIGURE 37: Schematic representation of conceptual model.....	147
FIGURE 38: Well-stirred model: Predicted (—) and observed (*) plasma concentrations of L-dopa and 3-OMD after 80 mg/kg L-dopa.....	154
FIGURE 39: Well-stirred model: Predicted (—) and observed (*) plasma concentrations of L-dopa and 3-OMD after 80/20 mg/kg L-dopa/benserazide.....	154
FIGURE 40: Parallel tube model: Predicted (—) and observed (*) plasma concentrations of L-dopa and 3-OMD after 80 mg/kg L-dopa.....	155
FIGURE 41: Parallel tube model: Predicted (—) and observed (*) plasma concentrations of L-dopa and 3-OMD after 80/20 mg/kg L-dopa/benserazide.....	155
FIGURE 42: Schematic representation of conceptual model to describe pharmacokinetics of benserazide and Ro 04-5127 (I: physiological part of model; II: compartmental model).....	157
FIGURE 43: Predicted (—) and observed (Δ) plasma concentrations of benserazide and Ro 04-5127.....	161
FIGURE 44: Predicted concentrations of benserazide and Ro 04-5127 in the portal vein and the hepatic vein...	161
FIGURE 45: Schematic representation of conceptual model.....	163
FIGURE 46: Predicted (—) and observed (*) L-dopa and 3-OMD plasma concentrations after oral administration of 80 mg/kg L-dopa.....	166
FIGURE 47: Predicted (—) and observed (*) L-dopa and 3-OMD plasma concentrations after oral administration of 80/20 mg/kg L-dopa/benserazide.....	167

SUMMARY

Background

Over the last 20 years the use and acceptance of modeling and simulation in drug development has increased greatly. Not only the pharmaceutical industry and health authorities, but also financial analysts of PricewaterhouseCoopers believe that modeling and simulation play an increasingly important role in drug development, in particular towards a future electronic Research & Development (e-R&D) environment. Mathematical and statistical models are approaches to describe and summarize observations, to interpret data, to make predictions, and to support decisions. Data modeling enhances the learning steps throughout drug development and allows knowledge transfer and decision making at key transition points. Furthermore, modeling results can contribute directly to the information needed for the drug label. Another area in which modeling can provide helpful insight is that of pharmacokinetic (PK) drug-drug interactions. Mechanistically based PK models describe PK drug-drug interactions by a mathematical relationship taking into account the mechanism of interaction. The antiparkinsonian drug L-dopa, a dopamine precursor, is often administered together with an amino acid decarboxylase (AADC) inhibitor, e.g. benserazide, which inhibits peripheral dopamine formation. L-dopa/benserazide is an example of a therapeutically beneficial PK drug-drug interaction. Using L-dopa/benserazide data in rats and humans modeling was employed to describe the PK interaction between L-dopa and benserazide. Furthermore, modeling was combined with interspecies scaling techniques to predict the interaction in humans based on animal data.

Goals

The goals of the present thesis were to investigate whether PK relationships of varying complexity allow description and understanding of the mechanism of drug-drug interactions and whether the extrapolation from animal to human is facilitated by the use of PK models and parameters.

Methods and Results

This section provides a summary list of the main findings followed by a description of the methods and results of the four investigations which are presented in this thesis. The main findings were:

- * The L-dopa/benserazide compartmental model allowed a mechanism-based view of the L-dopa/benserazide interaction and supports the hypothesis that Ro 04-5127 is the primary active metabolite of benserazide.
- * This is the first investigation in which the PK of benserazide and Ro 04-5127 have been described by a compartmental model.
- * The PK model established in rats and combined with allometric scaling was found useful and successful in predicting and describing PK of L-dopa in humans after L-dopa treatment with and without benserazide.
- * The nonlinear mixed effects modeling approach provided comparable results to the naïve-pooled-data method and added information on the inter-individual variability.
- * A PK model was developed which predicts the liver concentrations of the interacting drugs and incorporates concentration dependent elimination of L-dopa via the AADC pathway.

The objective of the **first investigation** was to develop a model for the PK interaction of L-dopa and benserazide in rats, to better understand the use of these drugs in humans. An experiment was designed and performed to obtain L-dopa/benserazide data in rats. Male rats received a single oral dose of 80 mg/kg L-dopa or 20 mg/kg benserazide or 80/20 mg/kg L-dopa/benserazide. Blood was sampled and the plasma concentrations of L-dopa, its metabolite 3-O-methyldopa (3-OMD), benserazide and its metabolite Ro 04-5127 were determined by HPLC-electrochemical detection. The PK of L-dopa, 3-OMD, benserazide, and Ro 04-5127 were characterized by non-compartmental analysis and a compartmental model in which L-dopa clearance was the sum of the clearances mediated by AADC, catechol-O-methyltransferase, and other enzymes. In this model, Ro 04-5127 inhibited competitively the L-dopa clearance by AADC and affected the extent of absorption of L-dopa from the gut and extraction by the liver. The PK of benserazide and Ro 04-5127 were described with 2-compartment models, where the amount of Ro 04-5127 in plasma was the sum of metabolite formed systemically and presystemically. The population PK analysis was performed using the naïve-pooled data approach. The results show that the co-administration of L-dopa/benserazide resulted in a major increase in systemic exposure to L-dopa and 3-OMD caused by a decrease in L-dopa clearance. The compartmental model allowed an adequate description of the observed L-dopa and 3-OMD plasma concentrations in the

absence and presence of benserazide. The model-based analysis had advantages over the non-compartmental analysis because it gave insight into the mechanistic behavior of the interaction between L-dopa and benserazide such as describing the temporal change of inhibition and recovery of AADC.

The objective of the **second investigation** was to study the predictability of human L-dopa PK after L-dopa treatment with and without benserazide from *in vivo* PK in rats using PK modeling and allometric scaling of PK parameters. The PK parameters of L-dopa, its metabolite 3-OMD, benserazide and its active metabolite Ro 04-5127 were estimated by fitting the PK model described above to the observed rat data. The estimated parameters were scaled from rat to human allometrically using body weight with exponent 0.75 for clearance and 1.0 for volume terms. The model predictions were evaluated using results from a study in healthy volunteers who had received po 25 mg, 50 mg, 100 mg, or 200 mg benserazide t.i.d. for 14 days and a single oral dose of 250 mg L-dopa on day 13 of benserazide treatment. Expected human plasma concentrations of L-dopa and 3-OMD were simulated for each treatment using the allometrically scaled parameters and compared with the actually observed plasma concentrations. Over the dose range of 25 mg to 200 mg benserazide the predictions for L-dopa described the observed concentrations well. Only the predicted L-dopa concentrations at later time points (> 4 h) were overestimated compared to the L-dopa concentrations of the observed individual curves (bias < 100 % after 25 mg, 50 mg, 100 mg benserazide; bias < 190 % after 200 mg benserazide). The predicted 3-OMD concentration-time curves showed a flatter disposition phase and underestimated the actual C_{\max} . This could be explained by the poor prediction of the volume of distribution of 3-OMD in humans.

The objective of the **third investigation** was to study whether the approach of pooling the data leads to potential distortion of the model structure and parameter estimates. This was done by repeating the compartmental analysis of the L-dopa – benserazide rat data using nonlinear mixed effects modeling instead of the previously applied naïve-pooled-data method for the population PK analysis. The modeling was done stepwise. The model for L-dopa/3-OMD after treatment with L-dopa alone was first, followed by the model for benserazide/Ro 04-5127 after treatment with benserazide alone and then by the model describing the drug-drug interaction between L-dopa and benserazide. In the population analyses the first order (FO) and the first order conditional (FOCE) algorithms were used. The latter was always combined with the specification INTERACTION. For residual variability estimation three error models were tested, i.e. the additive error model, the proportional error model, and the combination of the two. To discriminate between the models the objective

function was used in combination with graphical tools for goodness-of-fit. The estimated parameters for L-dopa and 3-OMD after treatment with L-dopa alone and for benserazide and Ro 04-5127 after benserazide administration using nonlinear mixed effects modeling were comparable to those obtained with naïve pooling of data. The results of the drug-drug interaction model were inconclusive.

The objective of the **fourth investigation** was to develop a PK model which will estimate the liver concentrations of the interacting drugs L-dopa and benserazide using a liver model and which will allow for nonlinear kinetics for the elimination of L-dopa via the AADC pathway. The liver models used were the previously published well-stirred model and parallel tube model. Assuming that the interaction between L-dopa and benserazide takes place in the liver, liver concentrations would be more appropriate to describe the interaction process than plasma concentrations. The mathematical description of these models was complex, but feasible. Using the software ACSL the hurdle of solving implicit equations could be overcome. The available experimental data, however, was inadequate to estimate all parameters required by such complex models. Further experiments would be needed to provide additional information for the modeling. *In silico* trial simulation would be a useful approach to explore various study designs for such an additional *in vivo* experiment with the goal of finding the optimal study design which provides the data best suited to estimate the liver model parameters.

Conclusion

The present thesis demonstrates that PK relationships of varying complexity expressed in mathematical models permit the description and understanding of the mechanism of PK drug-drug interactions and that the extrapolation from rodents to human is facilitated by the use of PK models combined with allometric scaling.

Outlook

The L-dopa/benserazide model developed in this thesis was successfully used for rat data as well as for healthy human data. A potential further application would be to use it for patient data. Looking at drug development as a whole, it would be desirable to have a mechanism-based model throughout the development of an investigational drug. Especially for the development of drug combinations (e.g. L-dopa/benserazide, saquinavir/ritonavir) the model-based approach would be very valuable. On-going adaptation of the model would naturally be necessary as new information becomes available in the different stages of drug development.

GLOSSARY OF ABBREVIATIONS

A	Amount	$C_{\text{OMD},i}$	3-OMD concentration in systemic cpt, $i=b$ (treatment L-dopa), $i=c$ (treatment L-dopa/benserazide)
A_B	Amount benserazide in gut compartment	C_{Pi}	Concentration in initial plasma
$A_{\text{dopa},i}$	Amount L-dopa in gut cpt; $i=b$ (treatment L-dopa), $i=c$ (treatment L-dopa/benserazide)	C_{pv}	Portal vein concentration
A_e	Amount extracted	C_{pvB}	Portal vein concentration of benserazide
A_M	Amount Ro 04-5127 in gut compartment	$C_{\text{pvdopa},i}$	Portal vein concentration of L-dopa; $i=b$ (treatment L-dopa), $i=c$ (treatment L-dopa/benserazide)
AADC	Amino acid decarboxylase	C_{pvM}	Portal vein concentration of Ro 04-5127
ACSL	Advanced Continuous Simulation Language	C_{UF}	Concentration in ultrafiltrate
ADVAN6	Routine in PREDPP for implementing PK model, i.e. general nonlinear model	C_V	Concentration in venous blood
AGP	α_1 -acid glycoprotein	C_{1B}	Benserazide concentration of central compartment
AIC	Akaike Information Criterion	C_{1M}	Ro 04-5127 concentration of central compartment (inhibitor concentration)
AIDS	Acquired Immune Deficiency Syndrome	C_{2B}	Benserazide concentration of peripheral compartment
alb	Albumin	C_{2M}	Ro 04-5127 concentration of peripheral compartment
ATP	Adenosine triphosphate	\hat{C}	Predicted concentration
AUC	Area under the plasma concentration-time curve	\hat{C}_{last}	Last predicted concentration
$AUC_{0-\infty}$	Area under the plasma concentration-time curve from time zero to infinity	\hat{c}	Liver concentration in parallel tube model
AUC_M	Area under the plasma concentration-time curve of Ro 04-5127	$\hat{c}_{(I)}$	Liver concentration of inhibitor in parallel tube model
BLC	Below limit of calibration	CA	Compartmental analysis
BLQ	Below limit of quantification	CI	Confidence interval
BW	Body weight	CL	Clearance
C	Concentration	CL_{AADC}	L-dopa clearance via AADC
C_A	Concentration in arterial blood	CL_{AADC0}	L-dopa clearance via AADC (no inhibition)
C_B	Concentration of benserazide in systemic cpt	CL_B	Total benserazide clearance
$C_{\text{dopa},i}$	L-dopa concentration in systemic cpt; $i=b$ (treatment L-dopa), $i=c$ (treatment L-dopa/benserazide)	CL_{COMT}	L-dopa clearance via COMT
C_e	Concentration at enzyme site	CL_{dopa}	Total L-dopa clearance
C_{hv}	Hepatic vein concentration	CL_d	Intercompartmental clearance
Ch_{vB}	Hepatic vein concentration of benserazide	CL_{dB}	Intercompartmental clearance, benserazide
Ch_{vM}	Hepatic vein concentration of Ro 04-5127	CL_{dM}	Intercompartmental clearance, Ro 04-5127
$Ch_{\text{v}(I)}$	Hepatic vein concentration of inhibitor	CL_H	Hepatic clearance (used as general term) and hepatic clearance of L-dopa
C_{last}	Last observed concentration	$CL_{\text{H}(B)}$	Hepatic clearance of benserazide
C_{max}	Maximum plasma concentration	$CL_{\text{H}(M)}$	Hepatic clearance of Ro 04-5127
		$CL_{\text{H,tot}}$	Total hepatic clearance

$CL_{H,AADC}$	Hepatic clearance via AADC	F_c	Bioavailability of L-dopa after L-dopa/benserazide
$CL_{H,COMT}$	Hepatic clearance via COMT	F_B	Bioavailability of benserazide
CL_{int}	Intrinsic clearance	F_G	Gastrointestinal availability of L-dopa
$CL_{int(I)}$	Intrinsic clearance in the presence of an inhibitor	$F_{G(B)}$	Gastrointestinal availability of benserazide
$CL_{int,AADC}$	Intrinsic clearance via AADC	$F_{G(M)}$	Gastrointestinal availability of Ro 04-5127
$CL_{int,COMT0}$	Intrinsic clearance via COMT	F_H	Hepatic availability (used as general term) and hepatic availability of L-dopa
$CL_{int,OTHER}$	Intrinsic clearance via other pathways than AADC and COMT	$F_{H(B)}$	Hepatic availability of benserazide
$CL_{int,REST}$	Intrinsic clearance via other pathways than AADC	$F_{H(M)}$	Hepatic availability of Ro 04-5127
$CL_{int,tot}$	Total intrinsic clearance	F_M	Availability of Ro 04-5127 (% of benserazide dose)
$CL_{int,tot(I)}$	Total intrinsic clearance in the presence of an inhibitor	f	Fraction
CL_M	Total Ro 04-5127 clearance	f_{AADC}	Fraction metabolized by AADC
CL_{OMD}	3-OMD clearance	f_{COMT}	Fraction metabolized by COMT
$CL_{OMD,b}$	3-OMD clearance (L-dopa alone)	fe_B	Benserazide fraction excreted renally unchanged
$CL_{OMD,c}$	3-OMD clearance (L-dopa/benserazide)	fe_M	Ro 04-5127 fraction excreted renally unchanged
$CL_{OMD,i}$	3-OMD clearance; i=b (treatment L-dopa), i=c (treatment L-dopa/benserazide)	f_H	Hepatic fraction of total L- dopa clearance
CL_{Organ}	Organ clearance	fm	Fraction metabolized
CL_{REST}	L-dopa clearance via other elimination pathways	fm_B	Fraction of benserazide metabolized
$CL_{R(B)}$	Renal clearance of benserazide	fm_M	Fraction of Ro 04-5127 metabolized
$CL_{R(M)}$	Renal clearance of Ro 04-5127	fu	Fraction unbound
CL/F	Oral clearance	FDA	Food and Drug Administration (US Health Authorities)
COMT	Catechol-O-methyltransferase	FO	First order
Conc	Concentration	FOCE	First order conditional estimation
Cpt	Compartment	g	Gram
CV	Coefficient of variation	GI	Gastrointestinal tract
CYP450	Cytochrome P450	h	Hours
DOPAC	Dihydroxyphenylacetic acid	HIV	Human immunodeficiency virus
Dose_B	Benserazide dose	HPLC	High performance liquid chromatography
DV	Dependent variable (observed value)	HV	Healthy volunteer
e-R&D	Electronic research and development	HVA	Homovanillic acid
E_{max}	Maximum effect	IC₅₀	Concentration of inhibitor producing 50 % inhibition
EDTA	Calcium disodium edetate	IIV	Inter-individual variability
ELS	Extended least squares	IMPLC	Function in ACSL to solve implicit equations
ER	Extraction ratio	IPRED	Individual prediction (NONMEM)
ER_B	Extraction ratio of benserazide	IRLS	Iteratively reweighted least squares
ER_M	Extraction ratio of Ro 04-5127		
F	Bioavailability (used as general term) and bioavailability of L-dopa		
F_b	Bioavailability of L-dopa after L-dopa alone		

iv	Intravenous	N/A	Not assessed
k	Terminal rate constant	O	Objective function
ka	Absorption rate constant	OLS	Ordinary least squares
ka_b	Absorption rate constant of L-dopa (L-dopa alone)	3-OMD	3-O-methyl-dopa
ka_c	Absorption rate constant of L-dopa (L-dopa/benserazide)	P	Parameter
ka_i	Absorption rate constant of L-dopa; $i=b$ (treatment L-dopa), $i=c$ (treatment L-dopa/benserazide)	p	<i>stat.</i> Probability
ka_B	Absorption rate constant of benserazide	PBPK	Physiologically based pharmacokinetic
ka_M	Absorption rate constant of Ro 04-5127	PD	Pharmacodynamic(s)
ke_M	Elimination rate constant of Ro 04-5127	P-gp	P-glycoprotein
kg	Kilogram	PK	Pharmacokinetic(s)
ki	Inhibition constant	PKPD	Pharmacokinetic pharmacodynamic
K_m	Michaelis-Menten constant	po	Per os, oral
$K_{m_{AADC}}$	Michaelis-Menten constant of AADC	PRED	Population prediction (NONMEM)
L	Liter	PREDPP	Prediction for population pharmacokinetics (prediction subroutine for use with NONMEM)
LHS	Left-hand-side	Q	Hepatic blood flow
LNAA	Large neutral amino acid	R&D	Research and development
Log	Logarithm	RHS	Right-hand-side
M	Molar	Ro 04-5127	Trihydroxybenzylhydrazine
MAO	Monoamine oxidase	SD	Standard deviation
MAO-B	Monoamine oxidase type B	SE	Standard error
mg	Milligram	SPECT	Single photon emission computerized tomography
min	Minutes	SSR	Sum of squared residuals
mL	Milliliter	t.i.d.	Ter in diem, three times daily
MW	Molecular weight	T_{1/2}	Elimination half-life
MWCO	Molecular weight cut off	T_{max}	Time to maximum plasma concentration
N	<i>chem.</i> Normal	UDP	Uridine diphosphate
N	<i>stat.</i> Normal distribution	UGT	UDP-glucuronosyltransferase
N	Number	V	Volume of distribution (or metabolic rate depending on context (see below))
NaCl	Sodium chloride	V_{dopa}	Volume of distribution of L-dopa
NaF	Sodium fluoride	$V_{OMD,b}$	Volume of distribution of 3-OMD (L-dopa alone)
NAT	N-acetyltransferase	$V_{OMD,c}$	Volume of distribution of 3-OMD (L-dopa/benserazide)
NC	Not calculated		
NCA	Non-compartmental analysis		
NONMEM	Nonlinear mixed effects modeling		
NOP	No peak		
NPD	Naïve-pooled data		
NS	No sample		
NSP	No sample planned		

$V_{\text{OMD},i}$	Volume of distribution of 3-OMD; i=b (treatment L-dopa), i=c (treatment L-dopa/benserazide)
V_{SS}	Volume of distribution at steady state
V_1	Volume of central compartment
$V_{1\text{B}}$	Volume of central compartment, benserazide
$V_{1\text{M}}$	Volume of central compartment, Ro 04-5127
V_2	Volume of peripheral compartment
$V_{2\text{B}}$	Volume of peripheral compartment, benserazide
$V_{2\text{M}}$	Volume of peripheral compartment, Ro 04-5127
V/F	Oral volume of distribution
V	Metabolic rate (or volume of distribution depending on context (see above))
V^*	Estimated metabolic rate resulting from concentration C^*
V^*_{AADC}	For description see V^* , the subscript AADC shows that it is in context of the AADC kinetics
V_{max}	Maximum metabolic rate
V_{maxAADC}	Maximum metabolic rate of AADC
vs	Versus
W	Weight
WLS	Weighted least squares
WSSR	Sum of weighted squared residuals
Y	Observed data
\hat{Y}	Predicted data
β	Measure of degree of which the function deviates from linearity in concentration C
β_{AADC}	For description see β , the subscript AADC shows that it is in context of the AADC kinetics
ϵ	Residual random error
η	Inter-individual random error
θ	Parameter of structural model to be estimated (NONMEM notation)
μCi	Microcurie
μg	Microgram
μmol	Micromol
σ^2	Variance (used as general term) or variance of ϵ (NONMEM)
ω^2	Variance of η

Chapter 1

GENERAL INTRODUCTION

Chapter 1

GENERAL INTRODUCTION

The manuscript of the present thesis is divided in several chapters. Chapter 1 provides background information for a better understanding of the experimental chapters that follow the general introduction. This first chapter starts with a short introduction of the disease Parkinsonism. Then a review of several aspects of the modeling approach is presented followed by a brief description of methods for animal to human prediction. Chapter 1 will be concluded with a review on previously described pharmacokinetic drug-drug interactions. A summary of the goal and outline of the present thesis is given in Chapter 2 and leads into four experimental chapters (Chapters 3 to 6). The general conclusions and outlook complete the manuscript (Chapter 7).

1.1 PARKINSONISM

L-Dopa and benserazide, the two compounds chosen to investigate the hypotheses of the present thesis, are used for the treatment of the movement disorder Parkinsonism. The clinical features (Chapter 1.1.1), the etiology (Chapter 1.1.2), the pathological-histological features (Chapter 1.1.3), the pathological-neurochemical features (Chapter 1.1.4), and the therapy of Parkinsonism (Chapter 1.1.5) are described to provide the larger context in which L-dopa and benserazide are used. In Chapter 1.1.5.1 special attention is given to the combination therapy L-dopa/benserazide and its mechanism of action which forms the basis for the mathematical models in the experimental Chapters 3 to 6.

1.1.1 Clinical Features

Parkinsonism is a progressive neurodegenerative movement disorder characterized by clinical symptoms such as resting tremor, brady- and hypokinesia, muscular rigidity, and abnormalities in posture and gait. Besides these cardinal clinical symptoms, a decrease in respiratory movement, a deterioration of the control over extraocular muscles, a disturbance of the smooth muscles (dysphagia and drooling, constipation, dysuria or retention of urine), and psychiatric changes (depression and dementia) are observed. The patient suffers from a number of functional disabilities, which have a major impact on performing activities of daily living. These are inability to walk, a mask-like facial expression and impairment of speech, writing and eating. If Parkinsonism is not treated, the end stage of the disease is characterized

by a rigid akinetic state. Death is usually due to complications of immobility (e.g. pulmonary embolism, aspiration, hypostatic pneumonia). Morbidity from the disease has markedly reduced due to major advances in pharmacotherapy.^[1, 2]

1.1.2 Etiology

The etiology of Parkinsonism is diverse and partially unknown. On the basis of the cause of the disease a distinction is made between idiopathic Parkinsonism (~ 85 % of all cases^[3]) and secondary Parkinsonism.^[1, 4, 5] (Table 1)

TABLE 1: Etiology of Parkinsonism

Idiopathic Parkinsonism – cause of disease unknown	
Hypothesized causes are:	<ul style="list-style-type: none"> * aging * environmental factors * oxidative stress * autoimmunity * trauma * combination of genetic and environmental factors
Secondary Parkinsonism – cause of disease known	
Identified causes are:	<ul style="list-style-type: none"> * drugs¹ that deplete striatal dopamine (e.g. reserpine) or block striatal dopamine receptors (e.g. phenothiazine, butyrophenone, bulbocarpine) * toxins (e.g. 1-methyl-4-phenyl-1,2,3,6-tetrahydropyridine (MPTP), manganese, carbon monoxide, or carbon disulfide) * genetic predilection * infections (e.g. viral encephalitis) * structural lesions (e.g. micro-infarcts, tumors) * senile arteriosclerotic changes

¹ In the majority of cases drug-induced Parkinsonism is dose-dependent and reversible.

The pathogenesis of idiopathic Parkinsonism (Parkinson's disease) has been studied extensively and various hypothesis including aging, environmental factors, oxidative stress, autoimmunity, and trauma are under discussion as possible causes^[6]. Recent research showed that it might be due to genetic factors or a combination of genetic and environmental factors

[7, 8]. Idiopathic Parkinsonism occurs worldwide in all races. Males and females are affected almost equally [3, 9].

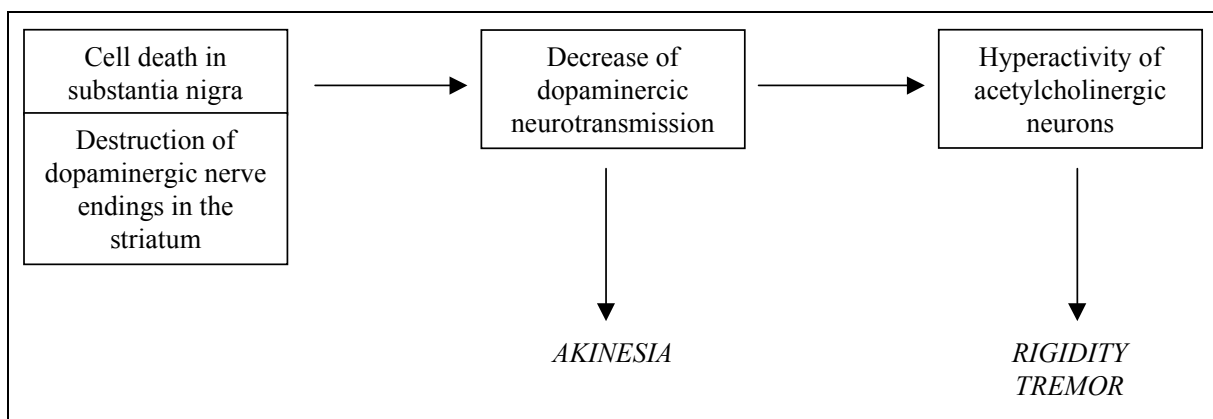
1.1.3 Pathological-Histological Features

In reversible drug-induced Parkinsonism there are no morphological changes, whereas in other types of Parkinsonism a degeneration of the nigrostriatal neurons is prominent [5]. Uitti and Calne [6] characterized the histological changes in idiopathic Parkinsonism as loss of neurons in the zona compacta of the substantia nigra and certain other pigmented nuclei, gliosis in these same regions, and an increase in neuronal inclusions called Lewy bodies [10]. However, Lewy bodies are non-specific markers for Parkinsonism. They occur also in healthy elderly persons as well as in several other neurological diseases (e.g. Hallervorder-Spatz disease) [10].

1.1.4 Pathological-Neurochemical Features

Neurochemically Parkinsonism is characterized by a deficiency of dopamine in brain areas that are part of the extrapyramidal motor system such as the striatum (i.e. caudate nucleus and putamen), the substantia nigra, and the globus pallidus [5]. The dopaminergic dysfunction is, in all cases other than drug-induced Parkinsonism, due to a degeneration of the nigrostriatal dopamine pathway originating in the substantia nigra and ending synaptically in the striatal regions. The loss of dopamine leads to a defective nigrostriatal dopaminergic transmission. Under normal conditions there is a functional balance between dopaminergic and acetylcholinergic activity. A decrease of dopaminergic activity as in Parkinsonism results in a functional hyperactivity of the striatal acetylcholinergic neurons (Figure 1).

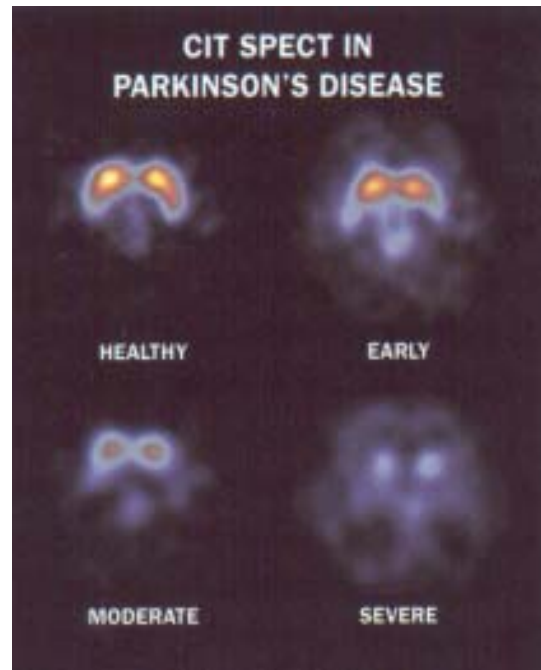
FIGURE 1: Pathogenesis of Parkinson disease



Adapted from Mutschler, Arzneimittelwirkungen, 1986 [11]

The loss of dopamine can be made visible by the technique of neurochemical brain imaging using a radioactive labeled marker (e.g. [^{123}I] βCIT (2 β -carboxymethoxy-3 β -(4-iodophenyl)tropane) which binds to dopamine reuptake sites on nigrostriatal terminals and provides an index of the integrity of nigrostriatal projections (Figure 2).

FIGURE 2: Single Photon Emission Computerized Tomography [^{123}I] βCIT images from a patient with mild-early, moderate and severe Parkinson's disease and from an age-matched healthy subject. Levels of SPECT activity are color encoded from low (black) to high (yellow/white). Reprinted through the courtesy of the National Parkinson Foundation Inc. and J. Seibyl (Yale NeuroSPECT Center).



The symptoms of Parkinsonism only become clinically overt if striatal dopamine is decreased by 60-80 % ^[12]. Lower degrees of dopamine loss are compensated by adaptive functional changes such as over-activity of the remaining dopamine neurons (i.e. dopamine synthesis \uparrow , dopamine release \uparrow) and increase in sensitivity of postsynaptic D₂ dopamine receptors to dopamine ^[13, 14].

1.1.5 Therapy

The drugs used to treat Parkinsonism have various mechanisms of action, e.g. they interfere either with the synthesis or the metabolism of dopamine, they act at the level of the synapses (reuptake inhibition, receptor stimulation), or they have an impact on the cholinergic system (Table 2).^[15]

An alternative to drug therapy, especially for patients not responding to available medication, is surgery (e.g. thalamotomy, thalamic stimulation, pallidotomy) ^[15]. Human and porcine transplants (brain grafting) are currently being investigated as potential therapeutic

interventions in patients with moderately advanced Parkinsonism ^[16-18]. This may be a new approach to treatment in the future.

TABLE 2: Drug therapy in Parkinsonism

Drug	Drug Category	Action
Bromocriptine Pergolide Pramipexole Ropinirole Apomorphine	Dopamine agonist	Stimulation of dopamine receptors (predominantly D ₂)
Selegiline	MAO-B inhibitor	Increase of dopamine levels by inhibition of dopamine metabolism (MAO-B inhibition) Methylselegiline (metabolite of selegiline) protects dopamine neurons
Trihexyphenidyl Benztropine	Anticholinergic	Anticholinergic activity
Amantadine	Dopamine reuptake inhibitor	Increase of dopamine levels by inhibition of dopamine reuptake
L-Dopa	Dopamine precursor	Increase of dopamine levels by supplying L-dopa
L-Dopa + Benserazide L-Dopa + Carbidopa	Dopamine precursor with AADC inhibitor	Increase of dopamine levels by supplying L-dopa and inhibition of L-dopa metabolism in the periphery (AADC inhibition)
Tolcapone Entacapone	COMT inhibitor	Increase of dopamine levels by inhibition of L-dopa metabolism (COMT inhibition)

1.1.5.1 L-Dopa and Benserazide (Madopar[®])

L-Dopa (L-3,4-dihydroxyphenylalanine), a dopamine precursor, is the most effective drug used for the treatment of Parkinsonism ^[19]. Dopamine itself is not suitable as treatment because it does not cross the blood-brain barrier and it is not active orally as a result of enzymatic degradation in the gut and first-pass metabolism ^[20]. In contrast to dopamine, L-dopa enters the brain where it is decarboxylated by amino acid decarboxylase (AADC) to dopamine. L-Dopa is rapidly absorbed, but systemic availability is reduced by competing metabolism, predominantly in the gut and the liver. The decarboxylation of L-dopa to dopamine by AADC is a major biotransformation pathway (69 %) for L-dopa ^[21]. A second, but less important pathway (10 %) is the O-methylation of L-dopa to 3-O-methyldopa

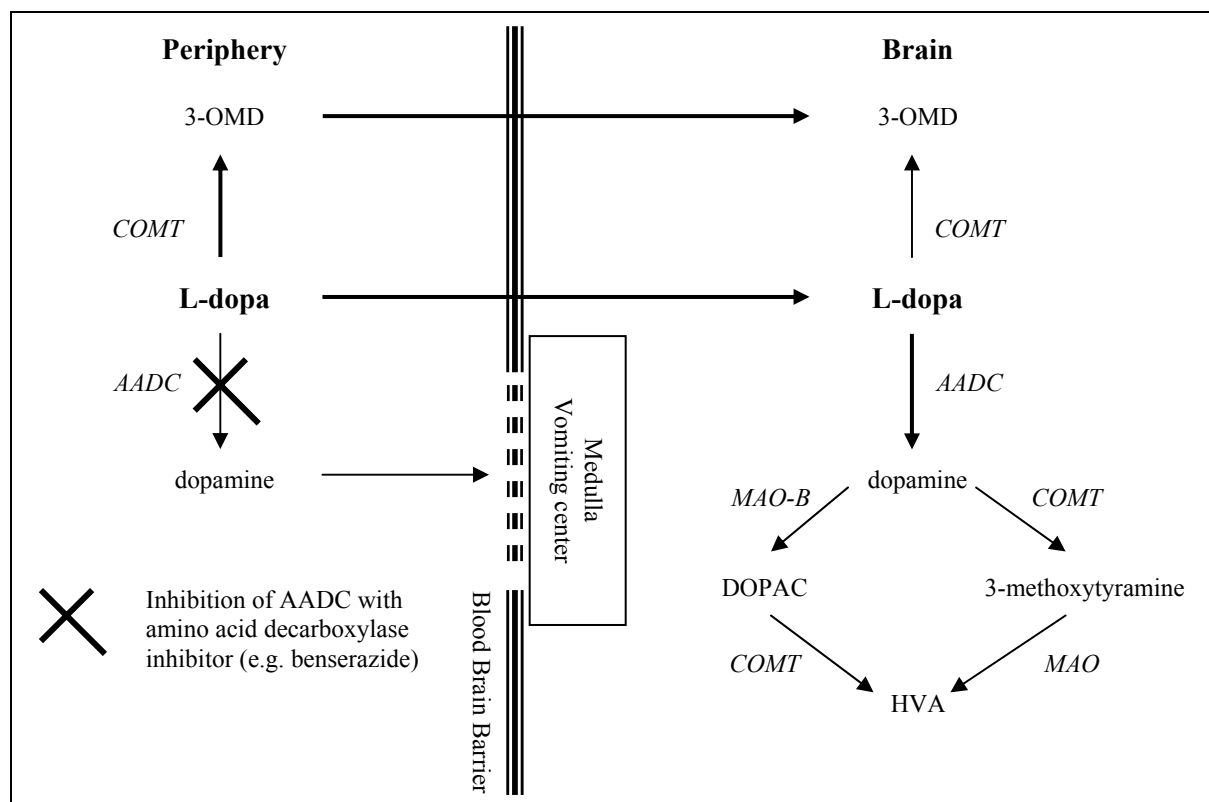
(3-OMD) by catechol-O-methyltransferase (COMT) ^[21]. Further pathways are transamination and oxidation ^[21]. Peripheral dopamine formation causes side effects (nausea and cardiac arrhythmias) ^[22]. Therefore, L-dopa is given together with a peripheral amino acid decarboxylase inhibitor such as benserazide or carbidopa.

Benserazide (seryl-trihydroxybenzylhydrazine) is mainly metabolized in the gut by splitting off of the serine residue to give its active metabolite Ro 04-5127 (trihydroxybenzylhydrazine), which inhibits L-dopa decarboxylation in the periphery. The inhibition of the amino acid decarboxylase by Ro 04-5127 appears to be pseudo-irreversible and competitive. ^[23, 24]

Madopar[®] (F. Hoffmann-La Roche Ltd) is the combination of L-dopa/benserazide in a ratio 1:4, which is available on the market for the treatment of Parkinsonism.

Figure 3 shows the metabolism of L-dopa in the periphery and the brain together with the site of action of benserazide.

FIGURE 3: Metabolism of L-dopa and site of action of benserazide



AADC: amino acid decarboxylase, **COMT:** catechol-O-methyltransferase, **DOPAC:** dihydrophenylacetic acid, **HVA:** homovanillic acid, **MAO:** monoamine oxidase, **MAO-B:** monoamine oxidase type B, **3-OMD:** 3-O-methyldopa

1.2 MODELS AND MODELING

“All models are wrong, but some are useful.”

George E. P. Box, statistician ^[25]

Modeling plays a central role in the present thesis. This chapter gives an overview starting with an introduction (Chapter 1.2.1), followed by a brief review of modeling in drug development (Chapter 1.2.2), reasons to model (Chapter 1.2.3), definitions (Chapter 1.2.4), and types of models (Chapter 1.2.5). The remaining chapters cover aspects regarding mathematics, statistics, and methodology of modeling such as integration algorithms used to solve differential equation (Chapter 1.2.6), mathematical methods for curve fitting (Chapter 1.2.7), weighting (Chapter 1.2.8), interpretation of results (Chapter 1.2.9), and individual/population approach (Chapter 1.2.10).

1.2.1 Introduction

The safe and effective use of a drug requires information on its pharmacokinetic and pharmacodynamic properties. The dosing regimen for most drugs in therapeutic use today has evolved from dose-effect relationship evaluations. However, there is strong evidence that a pharmacological effect correlates better with concentration than with dose. This leads to the target concentration strategy, where the focus is on the dose-concentration-effect relationship. Measurements of drug effects are interpreted in relation to achieved drug concentrations or exposure and not simply to the administered dose. The advantage of relating concentration rather than dose to effect is that pronounced variability due to pharmacokinetic differences can no longer perturb the exposure-effect relationship. Significant advances have been made in technologies to measure drug and metabolite concentrations in biological matrices and in the ability to quantify and understand drug effects. These scientific developments together with modeling techniques facilitate the application of the target concentration approach.

Scientists from academia, the pharmaceutical industry, and regulatory bodies (e.g. FDA) and financial analysts acknowledge the value and need of modeling in drug development.

1.2.2 Modeling in Drug Development

PricewaterhouseCoopers presented a first analysis ^[26] and a follow-up ^[27] of the current situation and the future trend in drug development (research and development (R&D)) within the pharmaceutical industry. Due to rapid changes within health care and within society, a need for new ways to handle drug development processes arises. Their conclusion was that information technology will be an increasingly important factor in enhancing the productivity throughout R&D via activities such as for example data handling, on-line information exchange, knowledge extraction and management, and computer assisted clinical trials. They foresee a need for a change from experimental R&D to electronic R&D (e-R&D). Modeling and simulation, as one of the rapidly emerging technologies, will play an important role in this change.

Over the last 20 years the use and acceptance of modeling in R&D has increased tremendously. This is reflected in numerous review publications on modeling in drug development written by scientists from the pharmaceutical industry, academia, and regulatory authorities ^[28-32]. But also in regulatory documents an increased presence of modeling is evidenced ^[33, 34]. Models describing pharmacokinetics and/or pharmacodynamics of a drug are applied at all stages of drug development.

In **preclinical research** animal experiments were designed in the past with emphasis on pharmacokinetics and rarely related concentration to effect. Commonly only dose-effect data was acquired. The allometric approach, and in recent years physiologically based pharmacokinetic (PBPK) modeling, were used to extrapolate pharmacokinetics from animals to humans. The collection of quantitative pharmacodynamic information only recently became more accepted in preclinical research ^[35]. Models for complex pharmacodynamic relationships found in non-human animals can be applied to similar processes in humans. Pharmacodynamic biomarkers developed and validated in non-human animals can be used throughout human studies. Causes of inter-individual variability in pharmacodynamics (e.g. underlying diseases) can sometimes be studied in non-human animals revealing crucial information for the treatment in humans ^[36-38]. Investigations showed that with the help of pharmacokinetic pharmacodynamic (PKPD) modeling, the relationship of systemic drug concentrations to pharmacodynamic endpoints in animals can facilitate and improve the clinical development process ^[39-41]. Due to the fact that the unbound plasma concentrations of a drug required to elicit a certain intensity of effect are often similar

in animals and humans, the knowledge of the dose-concentration-effect relationship in animals may give valuable indications of the likely steepness of the dose-effect curve in humans. PKPD modeling can also be used for toxicological evaluations. This would allow more accurate calculation of “no effect levels” once clinical data become available by incorporating interspecies differences in PKPD relationships. In toxicokinetics various models are used, including population pharmacokinetics, when sparse sampling is performed. An important aim of modeling in preclinical research is, of course, to support definition of a safe dose range for human use in Phase 1 investigations. PBPK modeling (Chapter 1.3.2) is frequently used for this.

In **clinical research** mathematical and/or statistical models are used throughout Phase 1 to Phase 4. The objective of Phase 1 is to characterize the basic properties of a new drug in humans in the expected therapeutic dose range (single and multiple dose pharmacokinetics, metabolic profile, bioavailability, PK drug-drug interaction studies, proof of concept studies). In this phase, PK models, PD models (e.g. modeling of (adverse-) effects), and in some cases, dependent on the available information, integrated PKPD models are used. The methodology to assess Phase 1 data is mostly a two-stage method involving individual parameter estimation followed by descriptive statistics. Recently, however, population (nonlinear mixed effects) modeling has also been applied successfully ^[42, 43]. The status of modeling in Phase 1 and the role it should play in the future was the topic of an expert meeting (COST B15¹) held in 2000 in Brussels. The outcome of this meeting was summarized in the publication “Role of modeling and simulation in Phase I drug development” ^[44]. In Phase 2, where studies are performed in patients to confirm that the expected therapeutic effect can be observed at well tolerated doses, integrated PKPD models can provide additional information to understand the concentration-effect relationship in the target population. In Phase 2 and 3 population modeling and computer assisted simulation of clinical trials (e.g. optimization of trial design and dosing) are successfully applied methods.

In conclusion, the application of integrated PKPD approaches in the drug development process leads to identification of dosing regimens for individual patients that optimize therapeutic outcome, allows knowledge transfer and decision-making at key transition points (e.g. from animals to humans or from healthy subjects to patients), and may help to save resources.

¹ Cost B15: Action sponsored by the European Community entitled “Modelling in drug development”

1.2.3 Why Model Data and How to Go About It?

Mathematical and/or statistical models are approaches to describe and summarize observations, to interpret data, to support decisions (e.g. CI from statistical model), and to make predictions (e.g. for unstudied conditions). They may facilitate extrapolation of parameters from animals to humans, from healthy subjects to patients, and from adults to children. Table 3 describes the benefits of modeling. In a broader sense, to model data enhances the learning curve throughout drug development. This can positively impact the information needed for the drug label or help plan the best design of a study (preclinical or clinical). Furthermore, PK/PD/statistical models, especially if they are entirely or partly mechanistic, can be looked at as knowledge store. Table 4 shows the steps during the modeling process.

TABLE 3: Benefits of a model

Modeling of data allows:	
*	to consolidate the collected data and knowledge.
*	to convert complex tabular data into a model description and meaningful parameter values.
*	to explore influence of underlying assumptions.
*	to explore the underlying mechanism.
*	to design future experiments cost-effectively and to maximize the likelihood of success.
*	to make predictions for studied and unstudied conditions. ^[45]

TABLE 4: General approach to modeling

Step	Activity
1	Design and perform experiment.
2	Collect and explore data.
3	Develop conceptual model and express the model mathematically.
4	Fit model to the data.
5	Evaluate fit to data.
6	If necessary, revise the model in step 3 and repeat the process until the model provides a satisfactory description of the data or perform new experiment (back to step 1) to gain more information.
7	Use the model.

Adapted from David W.A. Bourne, *Mathematical Modeling of Pharmaceutical Data*, 1995 ^[46]

Whenever possible, and if the objective of the modeling permits it, it is preferable to obtain some early understanding of the mechanism of action. This will permit the formulation of a model based on knowledge, i.e. a mechanistic model. Additionally sources of variability (e.g. inter-subject variability, intra-subject variability, inter-occasion variability, and residual error) have to be considered.

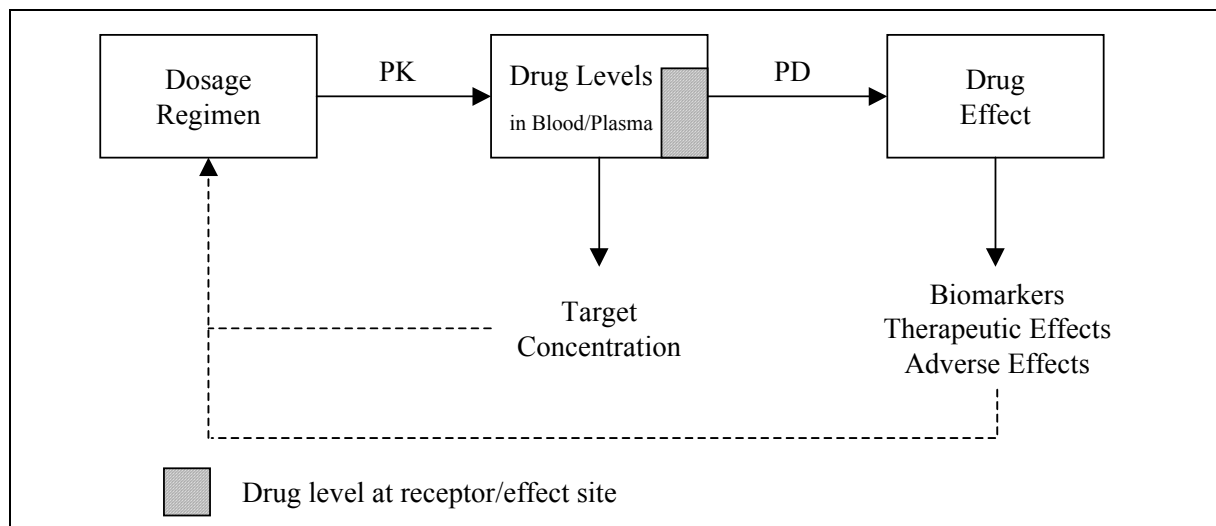
1.2.4 Definitions

Modeling is the use of a mathematical and/or statistical model to simulate or analyze data.

Pharmacokinetics (PK) can be expressed in simple words as what the body does to the drug. It describes the quantitative relationship between the administered dose and the concentration of drug in the body (e.g. plasma, tissue). This relationship is determined by physiological and biochemical processes such as absorption, distribution, metabolism, and excretion of a drug. (Figure 4)

Pharmacodynamics (PD) can be expressed in simple words as what the drug does to the body. It describes the quantitative relationship between drug concentrations in the body (e.g. plasma, tissue) and the size of the effect, where effects can be biomarkers, clinical outcomes, or toxic events (occurrence and/or duration of a drug-related adverse effect). (Figure 4)

FIGURE 4: Relationship between PK and PD



Constants, parameters and variables: In Eq. 1, y is the dependent variable (e.g. drug concentration in a PK model or drug effect in a PD model) and is a function of x , P , and c . X

is the independent variable (e.g. time in a PK model or drug concentration in a PD model). The other two terms are parameters (P) and constants (c).

$$\boxed{y = f(x, P, c)} \quad \text{Eq. 1}$$

A **constant** is defined as a value which remains fixed throughout the fitting process. In most cases this value is known either because it is fixed by the experiment itself (e.g. dose) or because it is known from a previous experiment or from the literature (e.g. hepatic blood flow); sometimes the value of the constant needs to be assumed.

A **parameter** is defined as a value, which is estimated by fitting the model to the data. For example, in a 1-compartmental model the parameters are clearance and volume of distribution.

1.2.5 Types of Models

Models can be classified in various ways:

- * mechanistic model versus empirical model
- * mathematical model versus statistical model
- * descriptive model versus predictive model
- * PK model versus PD model versus PKPD model
- * compartmental model

1.2.5.1 Mechanistic Model versus Empirical Model

Sheiner and Steimer^[31] define a **mechanistic model** as a model whose parameters correspond to physical or conceptual entities in the subject-matter domain, e.g. a model of drug distribution to an organ that is parameterized in organ blood flow, volume, and drug diffusivity. An **empirical model** is a non-mechanistic model^[31]. Empirical models are often applied if the biological system is complex and only little is known about its structural connectivity and underlying functional mechanisms. They have no biological relevance and are limited to describing the measured concentrations (e.g. 1-compartment PK model) or effects (e.g. E_{\max} model) using mathematical/statistical functions. However, empirical models may include some mechanistic assumptions leading to a seamless transition between pure empirical models and pure mechanistic models. The advantage of a mechanistic model over an empirical model is the possibility of making reliable predictions for unstudied conditions.

1.2.5.2 Mathematical Model versus Statistical Model

A **mathematical model** describes in a deterministic way the characteristics of the drug's pharmacokinetic and/or pharmacodynamic behavior, whereas a **statistical model** quantifies the uncertainty of information about that behavior using assumptions of the underlying distribution/probabilities. Mathematical models are often used in combination with statistical models.

1.2.5.3 Descriptive Model versus Predictive Model

A **descriptive model** can be applied a priori to a limited set of circumstances only (e.g. patient population, dose range, study design). By contrast a **predictive model** allows the prediction of outcomes under various, possibly even unstudied scenarios. ^[31]

1.2.5.4 PK Model versus PD Model versus PKPD Model

PK models describe the concentration-time profile of a drug. The currently used PK models can be divided into compartmental, physiological, and statistical models.

PD models are mathematical models relating the extent of the exposure of the drug to effect, where effects are measurements of biomarkers, therapeutic effect, or safety ^[44]. The most commonly used basic PD models in drug development are the linear effect-concentration model, the log-linear effect-concentration model, the E_{\max} model, and the sigmoid E_{\max} model. These models are applicable under steady-state conditions (i.e. the concentrations of the drug at the active site are constant (after long term infusions or multiple doses)).

Pharmacokinetic Pharmacodynamic (PKPD) models combine PK and PD and describe the relationship between the two for non steady-state conditions, i.e. after single doses as well as when time-dependent changes in PD parameters are present. Different subgroups of PKPD models are described in the literature.

- * Direct link model versus indirect link model ^[47, 48]
- * Direct response model ^[49, 50] versus indirect response model ^[51]
- * Empirical model versus mechanistic model ^[52]
- * Time variant model (modeling of tolerance ^[53] or sensitization ^[54])

A detailed discussion of specific PD models and PKPD models and their use is provided in Holford and Sheiner ^[47] and Meibohm and Derendorf ^[55].

1.2.5.5 Compartmental Model

The concept of the compartmental model described in great detail by Gibaldi and Perrier^[56] and Gabrielsson and Weiner^[57] is as follows. The body can be described as a number of well-stirred compartments. With exception of the PBPK models (Chapter 1.3.2) these compartments rarely have a physiologic or anatomic significance. There is input into compartments (e.g. absorption of drug), output (e.g. elimination of drug) or exchange between compartments (e.g. distribution of drug). The transfer processes are typically first-order, but this is not a requirement of the compartmental model. They may also be for example zero order or mixed order. The principle of mass balance applies to describe the rate of change of the drug amount in the compartment (mass balance equation, Eq. 2).

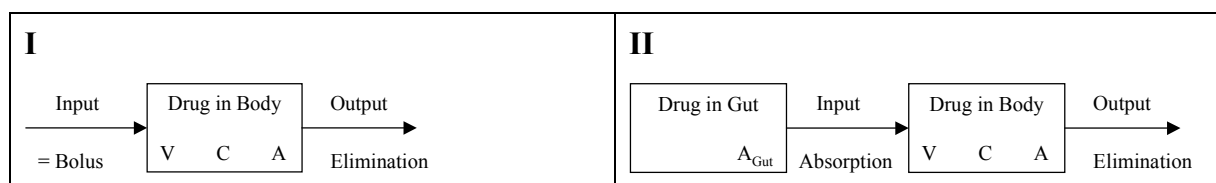
$$\boxed{\text{Rate of change} = \text{Rate in} - \text{Rate out}} \quad \text{Eq. 2}$$

Based on Eq. 2 the required differential equations can be derived to describe the mass balances for the compartments. These differential equations can then be readily integrated either analytically or numerically (Chapter 1.2.6).

The number of compartments needed is empirically determined from the data. Furthermore, the number of pharmacokinetic compartments reflects the number of exponential terms (e.g. biexponential equation = 2-compartment model).

Figure 5 shows a 1-compartment model, the simplest model, which represents the body as a single, kinetically homogenous unit. This model is useful for the pharmacokinetic analysis of drugs that distribute relatively rapidly throughout the body.

FIGURE 5: Schematic representation of a 1-compartment model after iv administration (I) and po administration (II)



A: amount, **C:** concentration, **V:** volume

Model I in Figure 5 can be mathematically defined by Eq. 3, with the initial condition $A(0) = \text{Dose}$.

$$\boxed{\frac{dA}{dt} = -k_{10} * A(t)}$$
 Eq. 3

k_{10} : elimination rate constant, $A(t)$: drug amount at time t

The rate of change of drug amount in the compartment can be expressed also in clearances instead of rate constants by substituting in Eq. 3 amount (A) by $C*V$ and thereafter $k_{10}*V$ by CL (Eq. 4). The initial condition for this differential equation is $C(0) = \text{Dose}/V$.

$$\boxed{V * \frac{dC}{dt} = -CL * C(t)}$$
 Eq. 4

V : volume of distribution, $C(t)$: concentration of drug at time t , CL : clearance

Because the differential equations used in this thesis are expressed in clearance terms all differential equations will from now on be given in terms of clearances and not rate constants (with exception of the absorption rate constant).

Model II in Figure 5 can be mathematically defined by Eq. 5 and Eq. 6, with the initial conditions $A_{Gut}(0) = F*\text{Dose}$ and $C(0) = 0$.

$$\boxed{\frac{dA_{Gut}}{dt} = -k_{01} * A_{Gut}(t)}$$
 Eq. 5

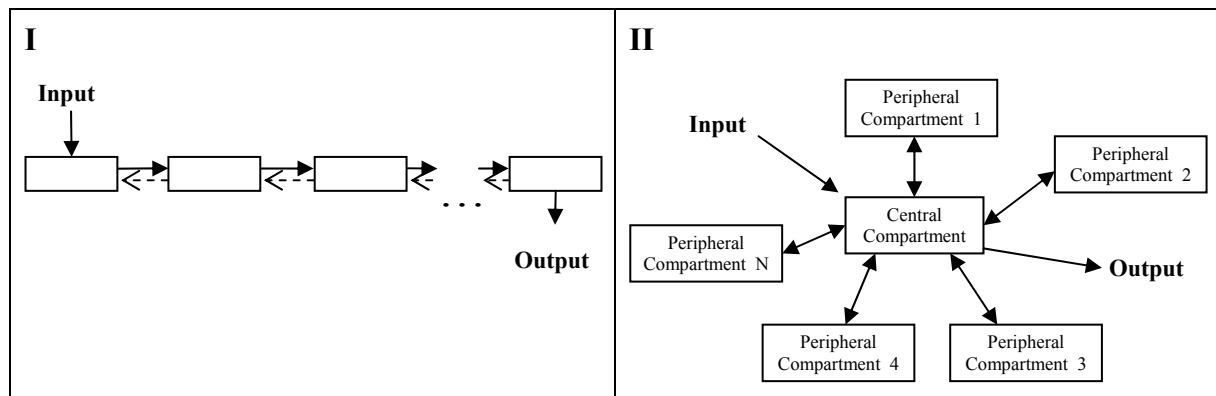
$$\boxed{V * \frac{dC}{dt} = k_{01} * A_{Gut}(t) - CL * C(t)}$$
 Eq. 6

A_{Gut} : drug amount in gut, k_{01} : absorption rate constant, V : volume of distribution, $C(t)$: concentration of drug at time t , CL : clearance, F : bioavailability

If the drug takes time to distribute into the tissues and reach equilibrium between plasma and tissues, a 1-compartment model may no longer be sufficient to describe the concentration-time profile of the drug, in which case more than one compartment is required in the model.

The multi-compartment model has additional compartments to allow for a description of the distribution and redistribution of the drug between the central compartment (blood and rapidly equilibrated organs) and the peripheral compartment (more slowly equilibrating tissues, which may either be poorly perfused or surrounded by protective membranes). There are two major topological families of compartmental models: the catenary and the mammillary type of model. The catenary model consists of a chain of interconnected compartments, while the mammillary model ^[58] is characterized by a central compartment interacting with a number of peripheral compartments (Figure 6).

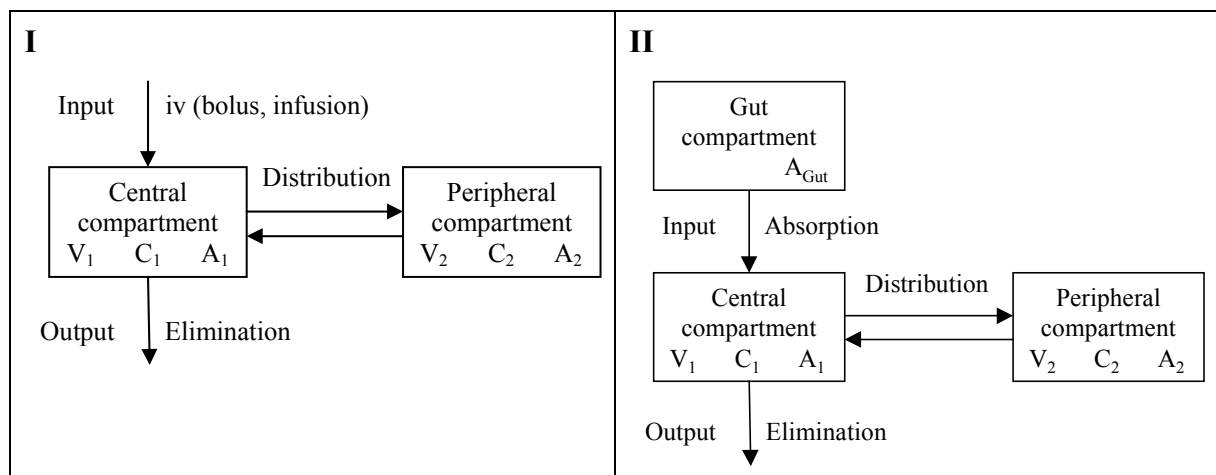
FIGURE 6: Schematic representation of two different types of multi-compartment models (I: catenary system; II: mammillary system)



Catenary system: Substance that flows from one compartment to another might never return to the original source or any compartment that it has passed, i.e. usually uni-directional flow.

Figure 7 shows a schematic representation of 2-compartment mammillary models with elimination from the central compartment. The effect of adding a second compartment to the model is to introduce a second exponential term into the predicted time course of the plasma concentration, so that it comprises a rapid and a slow phase.

FIGURE 7: Schematic representation of a 2-compartment mammillary model with elimination from the central compartment after iv administration (I) and po administration (II)



A: amount, **C:** concentration, **V:** volume

Model I in Figure 7 assuming a bolus input can be mathematically defined by Eq. 7 and Eq. 8, with the initial conditions $C_1(0) = \text{Dose}/V_1$ and $C_2(0) = 0$.

$$V_1 * \frac{dC_1}{dt} = -CL * C_1(t) - CLd * C_1(t) + CLd * C_2(t) \tag{Eq. 7}$$

$$V_2 * \frac{dC_2}{dt} = CLd * C_1(t) - CLd * C_2(t) \quad \text{Eq. 8}$$

V_1 : volume of distribution of central compartment, V_2 : volume of distribution of peripheral compartment, $C_1(t)$: concentration in central compartment at time t, $C_2(t)$: concentration in peripheral compartment at time t, CL : clearance, CLd : distribution clearance

Model II in Figure 7 can be mathematically defined by Eq. 9 to Eq. 11, with the initial conditions $A_{Gut}(0) = F * \text{Dose}$ and $C_1(0) = C_2(0) = 0$.

$$\frac{dA_{Gut}}{dt} = -k_{01} * A_{Gut}(t) \quad \text{Eq. 9}$$

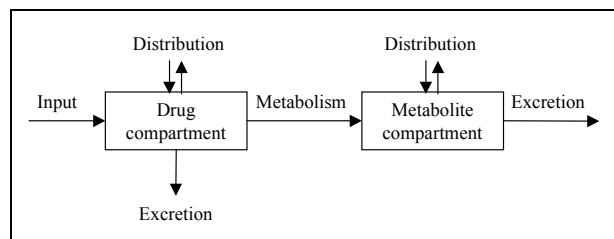
$$V_1 * \frac{dC_1}{dt} = k_{01} * A_{Gut}(t) - CL * C_1(t) - CLd * C_1(t) + CLd * C_2(t) \quad \text{Eq. 10}$$

$$V_2 * \frac{dC_2}{dt} = CLd * C_1(t) - CLd * C_2(t) \quad \text{Eq. 11}$$

$A_{Gut}(t)$: drug amount in gut at time t, k_{01} : absorption rate constant, V_1 : volume of distribution of central compartment, V_2 : volume of distribution of peripheral compartment, $C_1(t)$: concentration in central compartment at time t, $C_2(t)$: concentration in peripheral compartment at time t, CL : clearance, CLd : distribution clearance, F : bioavailability

The compartmental models described in this chapter up to now have covered the description of the absorption, elimination, and distribution of a drug. However, a compartmental model can also be used to describe the transformation (metabolism) of a drug (Figure 8). This can be of interest if the metabolite(s) of a drug are pharmacologically active or toxic, or because the metabolites give insight into sites of metabolism and possible reasons for changes in drug pharmacokinetics.

FIGURE 8: Schematic representation of a compartmental model for a drug and its metabolite



1.2.6 Integration Algorithms

As described above, PK compartmental models can be represented by differential equations, which are then solved analytically (e.g. by using Laplace transforms) or numerically. Numerical integration algorithms are:

- * Point-slope methods
- * Runge-Kutta methods (e.g. Runge-Kutta algorithm, Runge-Kutta-Fehlberg algorithm)
- * Multi-step methods (e.g. Adams-Moulton algorithm)
- * Methods for stiff systems (e.g. Gear algorithm)

The Runge-Kutta methods are suitable and efficient for the numerical integration of differential equations typically used in compartmental PK models. The Runge-Kutta algorithm is a fixed step, fixed order integration algorithm. The fourth order version is the most commonly used. A modification of the Runge-Kutta algorithm is the Runge-Kutta-Fehlberg algorithm, which has the advantage that it additionally determines the appropriate step size and is therefore a variable step, fixed order integration algorithm. If the model has a wide range in the values of the rate constants (or processes) used in the differential equations (stiffness index > 500) this is called a stiff system. In this case, integration methods such as the Gear algorithm are more suitable than non-stiff numerical integration algorithms.^[59]

1.2.7 Methods Used for Curve Fitting (Optimization Methods)

Curve fitting can be done using various mathematical techniques such as linear regression of transformed data, polynomial regression, cubic spline, or nonlinear regression. The first three methods show limitations with regard to their use in curve fitting of biological data^[60] and will not be discussed here further. By contrast, nonlinear regression is a powerful and suitable tool for fitting curves to data (e.g. concentration-time data) to determine the values of one or more parameters (e.g. pharmacokinetic parameters).

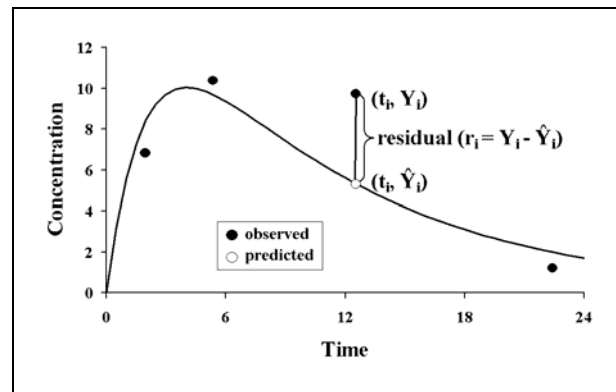
Nonlinear regression procedures use a variety of methods to determine the optimal values for a set of parameters given in a mathematical model, so that they describe the observed data best. Such methods are:

- * Method of maximum likelihood
- * Least squares method

The method of maximum likelihood ^[61] adjusts the values of the parameter(s) until they maximize the calculated probability of obtaining the given set of observed experimental data. The mathematical expression used to calculate the required probability is called the likelihood function and is a joint probability density function. For convenience, the logarithm of the likelihood function is used as the objective function. It is valid to do so since maximizing the logarithm of a function is equivalent to maximizing the function itself.

Nonlinear regression procedures, applying the least square method, estimate values of parameters that minimize the sum of the squared residuals. A residual ($Y_i - \hat{Y}_i$) is defined as the vertical difference between observed and predicted values (Figure 9).

FIGURE 9: Schematic representation of least squares method



Three of the most commonly used least squares methods are ordinary least squares (OLS, Eq. 12), weighted least squares (WLS, Eq. 13), and extended least squares (ELS, Eq. 14).

$$OLS \quad O_{OLS} = SSR = \sum_{i=1}^{i=n} [(Y_i - \hat{Y}_i)^2] \quad \text{Eq. 12}$$

$$WLS \quad O_{WLS} = WSSR = \sum_{i=1}^{i=n} [W_i (Y_i - \hat{Y}_i)^2] \quad \text{Eq. 13}$$

$$ELS \quad O_{ELS} = \sum_{i=1}^{i=n} [W_i (Y_i - \hat{Y}_i)^2 + \ln \text{var}(\hat{Y}_i)] \quad \text{Eq. 14}$$

O: objective function, **SSR**: sum of squared residuals, **WSSR**: sum of weighted squared residuals, **Y_i**: observed experimental data, **Ŷ_i**: predicted data (value of the curve), **W**: weight = 1/variance (see Chapter 1.2.8 below)

The extended least squares method ^[62] is a maximum likelihood procedure. A modification of WLS is the iteratively reweighted least squares (IRLS), where the weight is a function of the predicted value (\hat{Y}) and not the observed value (Y) as in WLS. Both IRLS and ELS are iterative procedures.

A nonlinear regression problem must be solved iteratively using algorithms such as the Marquardt method or the simplex method. The Marquardt method combines the advantages of two older algorithms, the method of steepest descent and the Gauss-Newton method. An alternative to the Marquardt method is the simplex method, which was refined by Nelder and Mead ^[63]. This method has the advantages over the Marquardt method of being less numerically intensive and rarely converging at a local minimum. It can also be used for discontinuous functions and is robust. However, it can be slower to converge than the Marquardt method.

1.2.8 Weighting

When analyzing pharmacokinetic and pharmacodynamic data, the variance of each observation may be different (e.g. in case of a large concentration range). To account for this it becomes important to use a suitable weighting scheme. The theoretically correct weight (W_i) to be assigned to the observed value is the reciprocal of the variance (standard deviation squared) of the observation (Eq. 15,^[64])

$$W_i = \frac{1}{\sigma_i^2}$$

Eq. 15

σ_i^2 : variance

Thus observations with large variances are assigned less weight than those with small variances when calculating the objective function. However, the true variance of an observation is seldom known and assumptions have to be made. One possible approach is to assume that the variance of the measurement is proportional to the observed value (Y) or the square of the observed value (Y^2). Another approach is to assume that the variance of the measurement is proportional to the predicted value (\hat{Y}) or the square of the predicted value (\hat{Y}^2). Table 5 lists different error types depending on the variance structure of the data.

TABLE 5: Error types

Error	Assumption
Constant absolute error	Variance is the same (= constant) for all observed values. Weights are set to a constant value (e.g. 1).
Poisson error	Variance is proportional to the mean of the predicted value.
Constant relative error	The coefficient of variation is constant over the range of observed values (proportional error).

If the applied model is correct, the contribution of the predicted value to the objective function is optimal.

1.2.9 Interpretation of the Results

Various diagnostic tools help to interpret the results of modeling and provide answers to the questions below.

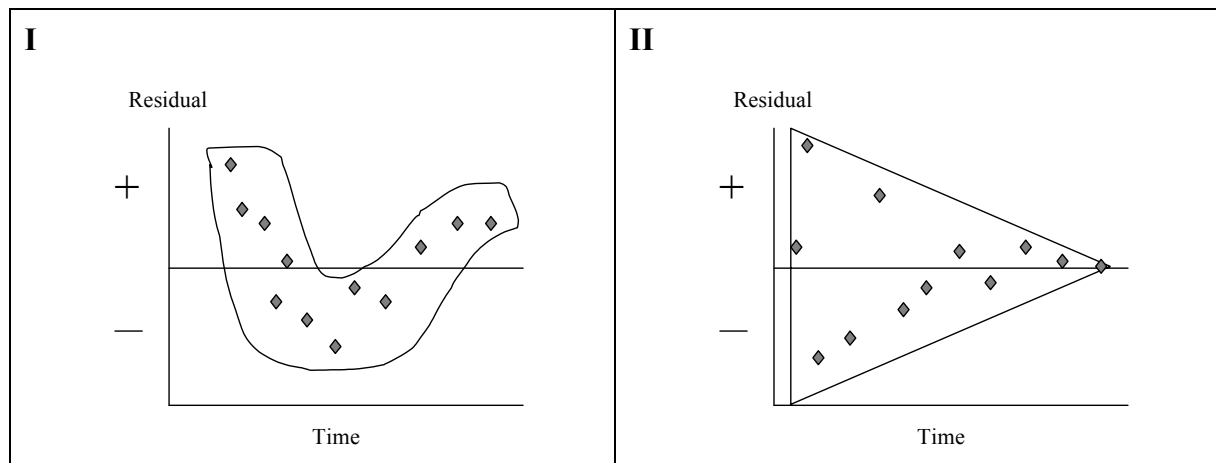
- * How well does the model describe the data?
- * Does this model fit the data better than an alternative model?
- * How big is the estimation error of the parameter estimates?
- * Does the model fit this set of data differently from another set of data?

1.2.9.1 Assessing the Goodness-of-fit

Graphical methods such as the plot of the fitted curve superimposed on the observed data, the predicted versus observed data plot, and residual plots are very useful in assessing the goodness-of-fit.^[60, 65]

Residuals should be plotted versus the independent variable (e.g. time) and the predicted dependent variable (e.g. concentration). Ideally the residuals are randomly scattered within a lower and upper horizontal band. There should be no outliers, i.e. data values, which were not fit well by the model, and runs, i.e. sequences of residuals having the same sign. If the residuals do not appear to be randomly distributed, the model or the weighting scheme may be incorrect. A U-shaped (or inverted U) pattern indicates problems with the structural model (Figure 10, I) whereas a cone shaped pattern points out problems with the error model (Figure 10, II). In the first case a 2-compartment model may be more suitable than the 1-compartment model. In the latter case the weighting scheme has to be changed.^[60, 65]

FIGURE 10: Relative residuals plotted versus time (I: Lack of fit due to inappropriate structural model; II: Lack of fit due to inappropriate weighting scheme)



Adapted from Gabrielsson and Weiner, Pharmacokinetic and Pharmacodynamic Data Analysis: Concepts and Applications, 2000 [66]

In addition to the graphical methods the following outputs are considered important in assessing the goodness-of-fit:

- * Objective function
- * Final parameter estimate, estimation error (SE, CV%), 95% confidence interval
- * Correlation matrix, variance-covariance matrix
- * Statement that convergence was achieved (no early termination)

The final parameters should ideally be estimated with high accuracy and precision. The precision of the parameter estimate can be determined by calculating the coefficient of variation, which is the standard error of the parameter (SE) divided by the parameter estimate (\hat{p}) (Eq. 16). The standard error of the parameter estimate is given by the square root of the k^{th} diagonal element of the variance-covariance matrix ($V_{k,k}$) (Eq. 17, Eq. 18).

$$CV\% = 100 * \frac{SE}{\hat{P}} \quad \text{Eq. 16}$$

$$SE = \sigma_{\hat{p}_k} = \sqrt{\sigma_{\hat{p}_k}^2} \quad \text{Eq. 17}$$

$$\sigma_{\hat{p}_k}^2 = V_{k,k} \quad \text{Eq. 18}$$

The variance-covariance matrix can be estimated from the inverse of the Hessian matrix. The confidence intervals represent boundaries of regions that have a given probability (commonly 95 %) of containing the true value of the estimated parameter. The univariate confidence

interval is calculated as the parameter plus and minus a t-value multiplied by the standard error of the parameter. The planar confidence interval is obtained from the tangent planes to the joint confidence ellipsoid of all the parameter estimates. It takes into account the correlation amongst the parameters, and will always be wider than the univariate limit. A further statistical method to obtain the confidence interval of parameters is bootstrapping^[67]. This is generally the preferred method, especially for non-linear regression when confidence intervals are often asymmetrical.

High values in CV% (> 20 %) or wide ranges in confidence intervals could indicate:

- * Too many or too few parameters in the selected model
- * Not enough data
- * Too much noise in the data
- * Data not collected at correct time

Two or more parameter estimates can be positively or negatively correlated or not correlated at all. The best case is that in which estimates of the parameters are totally uncorrelated. Parameter correlation is defined as a statistical dependence between two or more parameter estimates. As a result of this, any small change in one of the correlated parameters is compensated for by making an appropriate adjustment in the other while maintaining nearly identical values of the objective function. If parameters are highly correlated this may be due to insufficient information in the data to determine both parameters accurately and precisely.^[60, 65]

1.2.9.2 Discrimination between Rival Models

Statistical methods used for the discrimination between rival models are the F-test^[60], the Akaike Information Criterion (AIC)^[68, 69], and the Schwarz Criterion^[70]. The AIC was used in this thesis and will be discussed here in more detail. The AIC is estimated by Eq. 19 and takes into account the number of observations, WSSR, and the number of parameters in the model.

$$\boxed{AIC = N_{obs} * \ln(WSSR) + 2 * N_{par}} \quad \text{Eq. 19}$$

N_{obs} : number of observations, $WSSR$: sum of weighted squared residuals, N_{par} : number of parameters

The best model is that with the smallest value of AIC. Because the distribution of these values is unknown, it cannot be said how much smaller the value has to be in order to be statistically significantly better. Nonetheless, smaller is better. The AIC does not require nested models as

is the case for the F-test. However, models with different weighting schemes cannot be compared with this method. The same holds true for the Schwarz criterion.

1.2.10 Individual and Population Analyses

Methods to evaluate the data are individual analysis or population analysis. In data rich situations the model is fit to individual data (individual approach or individual modeling).

Population analysis methods are:

- * the naïve-pooled-data method
- * the naïve-averaging-data method
- * the two-stage method
- * the nonlinear mixed effects modeling method

In the present thesis the first two and the last method for population analysis were applied and will be discussed briefly. Naïve averaging of data and naïve-pooled-data are methods to pool the data. In the first case the data is averaged at each observation point and then a model is fit to these mean data. In the second case a model is fitted to all individual data observations simultaneously. Such methods can be used if the data density from individuals is not sufficient for analysis or the data are highly variable. A major drawback is the inability to describe between subject variability and to mask individually different behavior.^[71]

The population approach^[72], also called population modeling, is the analysis of pharmacokinetic and pharmacodynamic data using nonlinear mixed effects models. This technique may be applied to sparse or rich data or a combination of both^[44].

1.3 ACROSS SPECIES SCALING

In the present thesis the modeling approach will be combined with an across species scaling technique, specifically the allometric method. After a short introduction (Chapter 1.3.1) this chapter provides a description of the two different approaches used in across species scaling i.e. physiologically based models (Chapter 1.3.2) and allometric method (Chapter 1.3.3), with emphasis on the latter.

1.3.1 Introduction

Interspecies scaling has played an important role in drug development during the last 30 years. Pharmacokinetic characterization of a new drug has to be performed in at least two different animal species before entry into humans^[73]. There is a need to scale absorption, distribution, and elimination characteristics of such drugs from animals to humans^[74]. A survey showed that 80 % of the compounds withdrawn from drug development before 1985 failed because of inappropriate pharmacokinetics^[75]. Therefore, a good description of the pharmacokinetics in animals combined with appropriate scaling techniques to predict human pharmacokinetics is a step towards a successful drug development.

Interspecies pharmacokinetic scaling can be used:

- * to study the underlying similarities (or differences) in drug disposition among species.
- * to predict drug disposition in an untested species.
- * to design dosage regimens for experimental animal models.^[74]

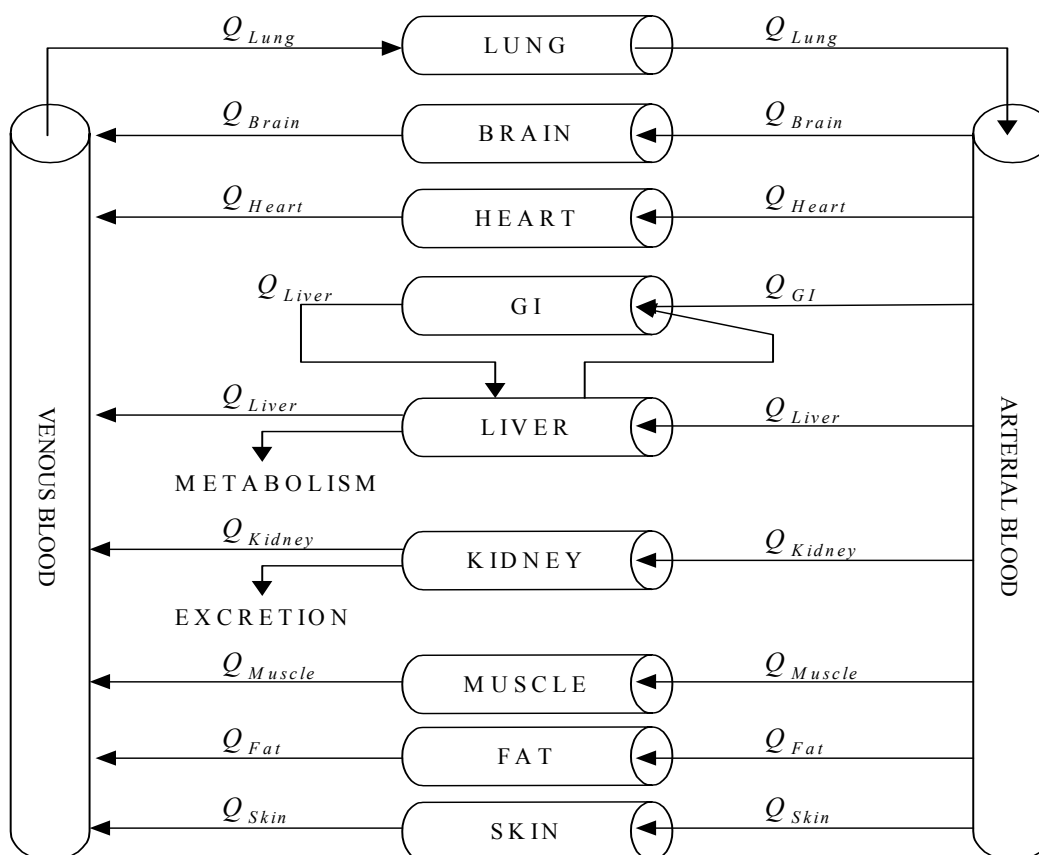
Interspecies scaling can be performed using two different approaches i.e. (1) physiologically based models or (2) allometric method.

1.3.2 Physiologically Based Models

In physiologically based pharmacokinetic (PBPK) models the body is not reduced to a simple series of compartments (Chapter 1.2.5.5), but is described in physiologically more meaningful terms. The different body organs and tissues are represented by their volumes and blood flows using a physiologic flow model (Figure 11). Thus the pharmacokinetics of the drug is characterized by parameters which are physiologically, anatomically, or biochemically meaningful. For each compartment (e.g. muscle, brain, lung) mass balance equations are

written using differential equations which are solved simultaneously. Once the PBPK model is defined for a drug in one animal species, predictions for humans can be obtained by substituting the values of the parameters of the test species with the values of corresponding parameters in humans, which are (1) taken from the literature, (2) estimated from *in vitro* tests, or (3) calculated by interspecies extrapolation.^[74, 76]

FIGURE 11: Model structure of a physiologically based pharmacokinetic model



Q: blood flow, **GI:** gastrointestinal tract

Although this method is highly complex and time consuming, it is becoming an increasingly popular and important tool for interspecies scaling in drug development. At two conferences in 1998, PBPK was acknowledged as an important technique for optimizing drug development^[77]. New software (e.g. ModelMaker, Cherwell Scientific Publishing Ltd, Oxford UK) and recent findings in this research area^[78, 79] facilitate and propagate the use of this method. Because the physiologically based modeling approach was not used for scaling across species in this thesis, this method will not be discussed here in more detail. References^[80-82] provide discussion of physiologically based models and their use in scaling across species.

1.3.3 Allometric Method

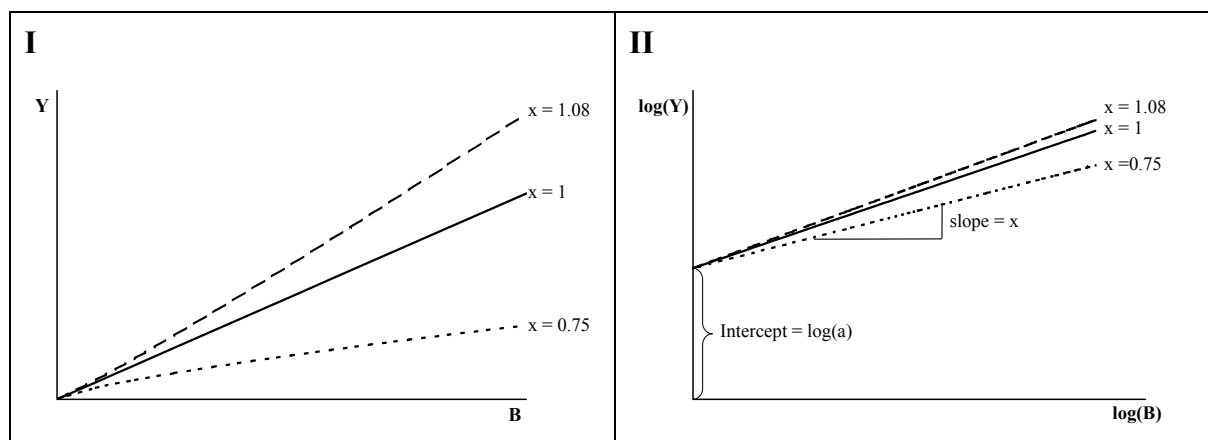
The allometric method is based on fundamental biological scaling relations which are characteristic of all organisms [83, 84]. Its advantages are that it is relatively simple to use, data analysis time is short, and it requires only blood (plasma, serum) concentration-time data, and knowledge about elimination pathways and extent of binding to blood components (e.g. proteins, red blood cells). Although there are drawbacks associated with its application [85-87] it has proven quite useful. Interspecies pharmacokinetic relationships are often remarkably well characterized by the allometric rule. Allometry literally means ‘by a different measure’ (allo = different, metry = measure) in contrast to isometry (iso = same, metry = measure) [88, 89]. While in isometric systems proportions remain the same (i.e. two bodies with the same proportion are isometric) they are altered in allometric systems, but to a particular rule. Thus the changes correlate for example with differences in size of the total organism or specific parts of it. [88] In nature we observe both, isometric scaling (e.g. shape (= volume) of the snail-shell) and allometric scaling (e.g. anatomic and physiological properties of land mammals). In order to apply scaling methods (e.g. allometric scaling) not only within species but also across species existence of a biological similarity between the species of interest has to be assumed. In the case of land mammals this assumption is widely accepted [74, 90, 91]. Their body weight ranges from the 3 g shrew to the 3000 kg elephant. In spite of this immense range of body weight, the anatomy, physiology, biochemistry, and cellular structure are similar and anatomic and physiological properties (e.g. metabolic rate, heart rate, blood flow, blood volume, skeletal mass) scale across mammalian species according to the allometric rule. As pharmacokinetic parameters such as clearance, volume of distribution, and half-life are based on those physiological properties it follows logically that this rule would also apply to them. This allometric relationship between body size and many anatomic, physiological, and pharmacokinetic variables can be described mathematically by Eq. 20 [92], known as the simple allometric equation,

$$Y = a * B^x \quad \text{Eq. 20}$$

where Y is the dependent variable (e.g. clearance, heart rate, skeletal mass), B is the independent variable (e.g. body weight) and a (= allometric coefficient) and x (= allometric exponent) are constants. Eq. 20 can be linearized (Eq. 21, Figure 12) by logarithmic transformation. Constant x becomes the slope of the line and constant a the antilog of the intercept. Estimates for a and x are commonly obtained by fitting a linear regression model to the log-transformed data (e.g. PK parameter versus body weight).

$$\log(Y) = x * \log(B) + \log(a)$$

Eq. 21

FIGURE 12: Linear plot (I) and log-log plot (II) of allometric equation

What is the meaning of the mathematical relationship described in Eq. 20? If the allometric exponent x is less than 1, a 100 % (2-fold) increase in body weight produces less than a 100 % increase in the dependent variable Y . The pharmacokinetic parameter clearance with an exponent of 0.75 falls into this category. With an exponent of 1 (e.g. blood volume, volume of distribution) a constant ratio exists between independent and dependent variable. Skeletal mass is an example where the exponent is greater than 1. Large land mammals have proportionally more of their body mass associated with bone than small ones. Table 6 lists the allometric exponents for a selection of variables, which are frequently used in biology and pharmacokinetics. These exponents are based on experiments and are widely accepted.

TABLE 6: Allometric exponents

Exponent	0.0	0.25	0.75	1.0	1.08
Dependent Variable	haematocrit	life span disposition half-life breath time heart beat time	metabolic rate clearance	blood volume volume of distribution	skeletal mass

Adapted from Gabrielsson and Weiner, Pharmacokinetic and Pharmacodynamic Data Analysis: Concepts and Applications, 2000 ^[66]

If the value for a parameter is known for one species, as well as the allometric exponent used to scale this parameter, then a parameter estimate can be obtained for another species applying

Eq. 22. This equation describes the relationship of a parameter across species (e.g. rat → human) taking into account their body weights,

$$P_{hu} = P_{rat} * \left(\frac{BW_{hu}}{BW_{rat}} \right)^x \quad \text{Eq. 22}$$

where P_{hu} is the parameter in humans, P_{rat} the parameter in rats, BW_{hu} the body weight of humans, BW_{rat} the body weight of rats, and x the allometric exponent. Eq. 22 is derived from Eq. 20.

Depending on the species the plasma protein binding can differ in general in a non allometric way. If this is the case, the unbound values of clearance and volume of distribution should be scaled.^[93]

Not for all drugs the clearance in humans can be predicted very well by applying the simple allometric equation (Eq. 20). In these cases different approaches are taken to modify the simple allometric equation and improve the prediction of clearance in humans such as:

- * Considering next to body weight also the maximum life-span potential ^[94].
- * Using a two-term power equation, which includes brain weight and body weight ^[95].
- * Using the product of clearance and brain weight ^[96, 97].
- * Combining *in vivo* preclinical data with *in vitro* metabolism data in animals and humans ^[87, 98].

1.4 METHODOLOGIES TO DESCRIBE AND UNDERSTAND PK DRUG-DRUG INTERACTIONS: LITERATURE REVIEW

The PK drug-drug interaction between L-dopa and benserazide was used together with modeling- and across species scaling techniques to investigate the hypotheses of the present thesis. PK drug-drug interactions are numerous, occur at different sites in the body, and several strategies and methods are available to determine them during drug development and post-marketing. This chapter gives an overview of all these aspects providing a broad background in which the interaction L-dopa/benserazide is set. There is an introduction (Chapter 1.4.1), followed by a description of mechanisms resulting in PK drug-drug interactions (Chapter 1.4.2) and strategies/methods to determine PK interactions (Chapter 1.4.3). A brief summary (Chapter 1.4.4) concludes the chapter on PK drug-drug interactions.

1.4.1 Introduction

A drug-drug interaction occurs when either the pharmacokinetics or the pharmacodynamics of one drug is changed by another drug. This can lead to diminished therapeutic effectiveness or adverse effects due to increased toxicity. However, interaction can also be an advantage if the beneficial effect is maximized as in the case of the drug combinations L-dopa-benserazide, saquinavir-ritonavir, and penicillin-probenecid.

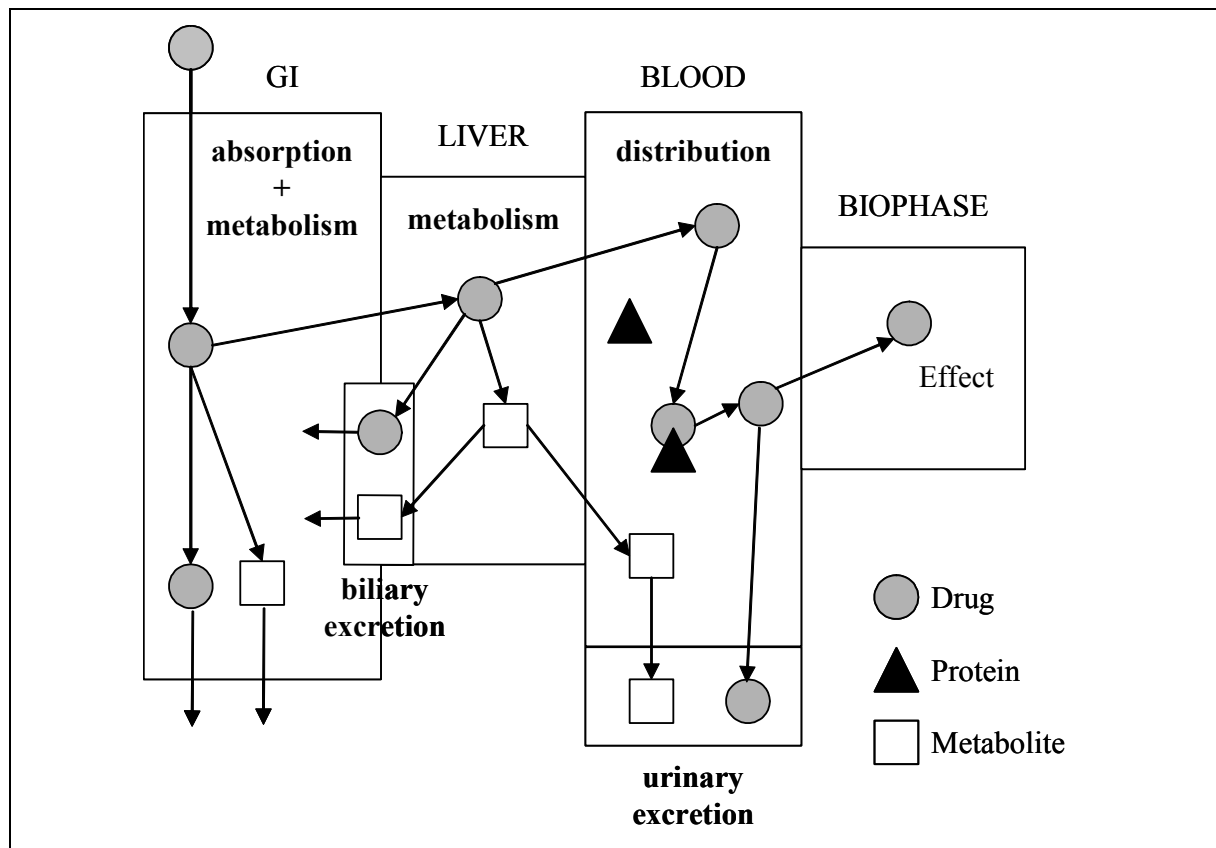
The significance of drug-drug interactions has played an increasing role in drug development over the last two decades^[99]. Reasons for this trend include an aging population receiving multiple drug therapy as well as the growing use of combination therapies in disease areas such as cardiovascular diseases, infections (e.g. AIDS), and cancer. Also, more and more drugs are mainly eliminated via active processes in the liver, i.e. biliary excretion and metabolism, rather than renal filtration of unchanged compound. General practitioners are often unfamiliar with the pharmacology and the interaction potential of the drugs on the market and the literature can sometimes be confusing. All these factors add to the risk of post-marketing drug-drug interactions. However, only a small number of occurring drug-drug interactions are clinically significant, and fewer still potentially disabling or life threatening. It is also known that the risk of clinical consequences is higher with some drug categories (e.g. anticoagulants, antihypertensive drugs^[100]) than with others. Most drug-drug interactions are predictable and preventable for example by adjusting the dose accordingly.

Due to advances in molecular biology, the use of *in vitro* models, and the availability of more sensitive analytical methods for the detection and characterization of metabolites, substantial progress, especially in the area of inhibition or induction of metabolizing enzymes, has been made towards understanding the mechanisms leading to many of the drug-drug interactions. There is rising awareness for the need to investigate drug-drug interactions in drug development to prevent undesirable post-marketing adverse effects such as seen with mibefradil. The calcium channel blocker mibefradil was withdrawn from the market due to its potential to cause fatal drug interactions by inhibiting the CYP3A4 mediated metabolism of certain drugs (e.g. simvastatin) ^[101, 102]. Pharmaceutical companies have applied rational strategies to address drug-drug interactions in drug development and regulatory authorities have provided guidelines on *in vitro* and *in vivo* investigation of drug-drug interactions ^[103-105].

1.4.2 Underlying Mechanism of PK Drug-Drug Interactions

PK drug-drug interactions can take place at the level of absorption, distribution, metabolism, and excretion (Figure 13).

FIGURE 13: Sites for PK drug-drug interactions



GI: gastrointestinal tract

Drug-drug interactions that alter the excretion of a drug, the systemic availability of a drug following oral administration, or the tissue distribution of drugs across membrane barriers are often linked to active transport processes by P-glycoprotein (P-gp) and organic ion transporters [106, 107]. The knowledge about P-gp and its role in drug-drug interactions has increased over the last years. P-gp, a member of the ATP binding cassette superfamily of transporters, is a membrane efflux protein. Like the other members of its family, it is responsible for the ATP-dependent transport of nutrients, peptides, organic ions, and toxins across a variety of cell membranes. P-gp is localized in numerous tissues such as liver, pancreas, kidney, colon, jejunum, adrenal glands, endothelial cells at the blood-brain barrier, placenta, and testis. The function of P-gp is to protect the organism against toxic, xenobiotic compounds by excreting them into the urine, bile, and the intestinal lumen, and by preventing their accumulation in critical organs such as brain and testis.[106, 108] Drugs can be substrates, inducers and/or inhibitors of P-gp. It was recently found that many CYP3A substrates are also substrates and/or inhibitors of P-gp.[109]

1.4.2.1 Absorption

The absorption (e.g. rate of absorption, fraction absorbed, first pass metabolism) of a drug can be altered by various events listed in Table 7, which in turn can all be caused by drug-drug interactions. Metoclopramide may affect the absorption of other drugs by either diminishing absorption from the stomach (e.g. digoxin) or enhance absorption from the small intestine (e.g. cyclosporine or paracetamol) [110].

TABLE 7: List of events influencing the absorption of a drug

- * pH effects on drug ionization and dissolution
 - * changes in gastrointestinal motility
 - * modification of gastric emptying rate
 - * formation of a complex, ion pair, or chelate
 - * interference with active transport (e.g. P-glycoprotein)
 - * disruption of lipid micelles
 - * changes in splanchnic blood flow
 - * toxic effects on gastrointestinal mucosa
 - * changes in volume, composition, and viscosity of secretions
 - * effects on mucosal and bacterial drug metabolism
-

1.4.2.2 Distribution

Plasma protein displacement interactions are drug-drug interactions altering the distribution of a drug. Displacement is the reduction in binding of a drug to a macromolecule, usually a protein, caused by competition of another drug for the common binding site(s). The result is a rise of the unbound fraction in plasma or tissue, or both. However, clinically significant drug-drug interactions due to displacement from protein binding are rarely significant and generally overestimated. Rolan et al. [111] have developed an algorithm to judge if a clinically significant interaction is likely or not. Only if the drug is (1) highly protein bound, (2) has a low volume of distribution and a high hepatic extraction ratio, (3) has a narrow therapeutic index and (4) is given intravenously does a clinically significant interaction become likely (e.g. intravenous dosing of lidocaine). [111, 112]

1.4.2.3 Metabolism

There is hepatic and extrahepatic (e.g. intestinal) metabolism. Drug metabolizing enzymes can be classified into enzymes responsible for changes in functional groups (Phase I; e.g. oxidation) and conjugation (Phase II). Phase I and II enzymes are grouped into families and subfamilies based on the structural homology of the enzymes. They can be inhibited and/or induced. Several different mechanisms of inhibition are known (Table 8).

TABLE 8: Mechanisms of inhibition of enzymes

Reversible inhibition	<ul style="list-style-type: none"> * competitive * noncompetitive * uncompetitive
Quasi-irreversible inhibition via Metabolic Intermediate Complexation	Metabolites form stable complexes with prosthetic haem of CYP450
Irreversible inhibition	Mechanism-based or suicide substrate (haem alkylation or covalent binding to apoprotein)

Phase I drug metabolizing enzymes include the flavin monooxygenases and the cytochrome P450 enzymes. The latter plays a pivotal role in the oxidation of drugs. The cytochromes P450 (CYP450) are a superfamily of haem-thiolate enzymes subdivided into families and subfamilies based on their degree of amino acid sequence homology [113]. CYP3A4 and the subfamily of CYP2C enzymes are quantitatively the most important. CYP3A4, CYP2D6, and the subfamily of CYP2C enzymes account for the major part of hepatic CYP-dependent drug metabolism. Multiple drug therapies will inevitably lead to a group of potentially competing

metabolic reactions. The majority of drug-drug interactions involve cytochromes P450 ^[114]. An example for a Phase I PK drug-drug interaction is ritonavir combined with saquinavir ^[115]. Ritonavir inhibits CYP3A4 ^[116], which is responsible for the metabolism of saquinavir. In this case the interaction is beneficial as the low and highly variable bioavailability of saquinavir could be improved by ritonavir.

Phase II reactions are for example glucuronidation, sulphation, and acetylation. The Phase II enzymes include UDP-glucuronosyltransferases (UGT), sulphotransferases, and N-acetyltransferases. The enzymes involved in Phase II reactions are less known than Phase I enzymes and research is ongoing to investigate their polymorphism, induction, and inhibition. The UGTs ^[117] consist of a superfamily of enzymes responsible for the conjugation of a large number of substrates (e.g. drugs containing amine functions such as amitriptyline) to form water-soluble glucuronides, which can be excreted. The human UGT enzyme family consists of two subfamilies (UGT-1 and UGT-2). Sulphotransferases are involved in the sulphation of drugs and endogenous compounds (e.g. drugs containing hydroxylgroups in phenols and aliphatic alcohols). N-acetyltransferases (NAT1 and NAT2) are needed for the N-acetylation of a many arylamines and hydrazines. ^[114] An example of a Phase II drug-drug reaction is valproate, which inhibits the glucuronidation of lorazepam decreasing the clearance of lorazepam ^[118].

Whilst the significance of hepatic metabolism has been recognized for some time, it has only recently been acknowledged that intestinal metabolism also makes a significant contribution. It is known that CYP3A4 is expressed in the gastrointestinal mucosa ^[119]. Also low levels of other cytochromes P450 (e.g. CYP1A1, CYP2C, and CYP2D6) and Phase II enzymes (e.g. UGT1A1, UGT1A6, UGT2B7, and sulphotranferases) have been detected ^[114]. There is consequently not only a hepatic but also an intestinal contribution to the overall first-pass extraction of orally administered drugs. Midazolam, a benzodiazepine, shows both gastrointestinal and hepatic CYP3A mediated metabolism, both contributing to the overall first-pass extraction ^[120].

There is also an important inter-individual and inter-ethnic variability in the capability of enzymes to metabolize drugs. The reasons for this include genetic factors (e.g. genetic polymorphism), non-genetic constitutional factors such as age (e.g. impaired liver function in elderly), nutritional state, and disease, or environmental factors such as climate, diet (e.g. grapefruit juice), and life style (e.g. smoking and alcohol habit). Genetic polymorphic enzymes within a population may differ with regard to their ability to metabolize drugs. This results in distinct subgroups within the population (e.g. bimodal distribution).

Subjects with deficient metabolism of a specific metabolic pathway are poor metabolizers compared to the “normal” extensive metabolizers.^[121] With regard to polymorphic enzymes the population can be classified into groups using methods such as phenotyping or genotyping. Examples for enzymes showing polymorphism are Phase I enzymes such as CYP2D6^[122, 123], CYP2C19^[124], and CYP2C9^[125] and Phase II enzymes such as N-acetyltransferases^[126]. Genetic polymorphism can complicate the drug-drug interaction picture.

1.4.2.4 Excretion

Hepatic transporters (e.g. P-gp) are involved in the biliary excretion of amphipathic organic cations, organic anions, conjugated bile acids, and phospholipids^[127, 128]. Drugs can be substrates, inducers and/or inhibitors of these transporters.

Renal excretion is dictated by glomerular filtration, active tubular secretion, and tubular reabsorption. Drug-drug interactions affecting active renal excretion can occur if there is a change in protein binding (glomerular filtration), an alteration in urinary pH and/or urinary flow rate (passive reabsorption), as well as by competition for active secretion in the renal tubule. Organic anion transporters, organic cation transporters, and P-gp are known transporters involved in the active tubular secretion of drugs^[129]. Their inhibition leads to a decrease in renal excretion of drugs such as penicillin (inhibitor: probenecid^[130]), methotrexate (inhibitor: non-steroidal anti-inflammatory drugs^[131]), and digoxin (inhibitor: quinidine^[132]). The tubular reabsorption of aspirin is reduced by antacid therapy through increase of urinary pH^[133].

1.4.3 Strategies and Methods to Determine Drug-Drug Interactions

The potential for drug-drug interactions is increased if one or both of the administered drugs are (1) dependent on a saturable transport system for absorption and/or excretion, (2) extensively protein-bound, (3) primarily metabolized via a single metabolic pathway, (4) capable of inhibiting or inducing metabolic enzymes, and/or (5) have a narrow therapeutic index.

Drug-drug interactions should be evaluated throughout drug development from candidate selection through preclinical development, clinical development to post-marketing, starting as early as possible. To obtain a knowledge-based understanding of the drug-drug interaction potential of an investigational drug in early drug development, it is important to

characterize the physicochemical properties, toxicokinetics, pharmacokinetics, and pharmacodynamics, to investigate the pathways of excretion, to determine the involved metabolic pathways and the corresponding enzymes, to characterize the metabolites (incl. their activity), and to determine the protein binding. This can be done using *in vitro* models (e.g. employing animal or human tissue) and *in vivo* studies in different animal species (e.g. rat, dog, and monkey). Positive results found *in vitro* (e.g. drug-drug interaction) are then extrapolated to an *in vivo* situation in humans, using methods such as PBPK modeling or allometric scaling (Chapter 1.3). Based on positive results from *in vitro* models, animal studies, and *in vitro* - *in vivo* predictions, the mechanistic clinical interaction studies can be planned to complement and confirm the preclinical findings. Besides these early mechanistic interaction studies in humans, where for example a cocktail approach (Chapter 1.4.3.3) can be applied, further clinical interaction studies are conducted. They are not based on *in vitro* findings but cover safety, regulatory or marketing aspects. These are interaction studies with drugs (e.g. anticoagulants, anticonvulsants, antiarrhythmics) that will be frequently co-medicated with the investigational drug and where a possibility of a clinically relevant interaction can be anticipated or interaction studies to obtain a statement in the label may be required.^[100] The following chapters describe different techniques for studying drug-drug interactions.

1.4.3.1 In Vitro Models

As a first step the metabolism of the test drug needs to be characterized. The human CYP450s involved in the metabolism of the test drug can be determined in human liver microsomes, hepatocytes, or recombinant enzymes using either selective chemical inhibitors for each major pathway or antibodies to specific CYP450s. Microsomes are a subcellular fraction of tissue obtained by high-speed centrifugation and contain all of the membrane-bound enzymes (including CYP450s). It is important to use microsomes from several donors to avoid false results due to microsomes that are deficient. Further, the incubating concentration of both inhibitor and substrate has to be selected with care.^[103, 114] Once the apparent metabolic pathway has been established using microsomes, recombinant enzymes provide a tool to confirm results identified in microsomes. Recombinant enzymes can be expressed in a variety of cells using cloned cDNAs for the common CYP450s^[134]. Intact liver systems (e.g. isolated hepatocytes, precision cut liver slices) provide the broadest picture for hepatic metabolism and are the methods of choice. The advantage over microsomes is that the cofactors are self-

sufficient and the natural orientation for linked enzymes is kept. The disadvantage is that the enzyme activities are only stable for a limited period.^[103, 114]

In order to describe the metabolism of the drug via an enzyme mathematically, the kinetic parameters, Michaelis-Menten constant (K_m) and maximum metabolic rate (V_{max}), are determined *in vitro*. K_m is defined as the drug concentration giving 50 % of V_{max} . Assuming Michaelis-Menten kinetics for the drug-enzyme kinetics, the metabolic rate (V) and the intrinsic clearance (CL_{int}) can be estimated using Eq. 23 to Eq. 25, respectively^[98]. The intrinsic clearance is a measure purely of enzyme activity.

$$V = \frac{V_{max} * C}{(K_m + C)} \quad \text{Eq. 23}$$

$$CL_{int} = \frac{V_{max}}{(K_m + C)} \quad \text{Eq. 24}$$

$$CL_{int} = \frac{V_{max}}{K_m} \quad \text{if } C \ll K_m \quad \text{Eq. 25}$$

V : metabolic rate, V_{max} : maximum metabolic rate, K_m : Michaelis-Menten constant, CL_{int} : intrinsic clearance, C : drug concentration at enzyme site

After having performed the *in vitro* tests to assess the metabolism of the drug, the following questions can be answered: (1) What are the metabolic pathways of the test drug and what is their relative importance? (2) Are polymorphic enzymes involved? (3) Is there a potential for inhibition of test drug metabolism by concomitant medication?

In a next step the effect of the test drug on other drugs can be assessed (e.g. inhibition and induction of metabolizing enzymes). The inhibitory effect of the test drug on common metabolic pathways can be determined by simultaneous incubation of the test drug with standard probe substrates (available for many CYP450 pathways) using human liver microsomes, hepatocytes, or recombinant enzymes.^[103, 114] Figure 14 shows an example for *in vitro* CYP450 inhibition screening. If the test drug inhibits one or more CYP450s the mechanism of inhibition (Table 8) should be determined together with the kinetic parameters characterizing the inhibition (e.g. k_i , IC_{50}). IC_{50} is the concentration of inhibitor producing 50 % inhibition whereas k_i is the dissociation constant of the enzyme-inhibitor complex and known as the inhibition constant^[135]. In the case of competitive inhibition, the rate of metabolism and the intrinsic clearance in presence of the inhibiting drug (V_I , $CL_{int(I)}$) can be

calculated by Eq. 26 to Eq. 28 ^[129]. The mathematical relationships of other types of enzyme inhibition are described by Ito et al. ^[129].

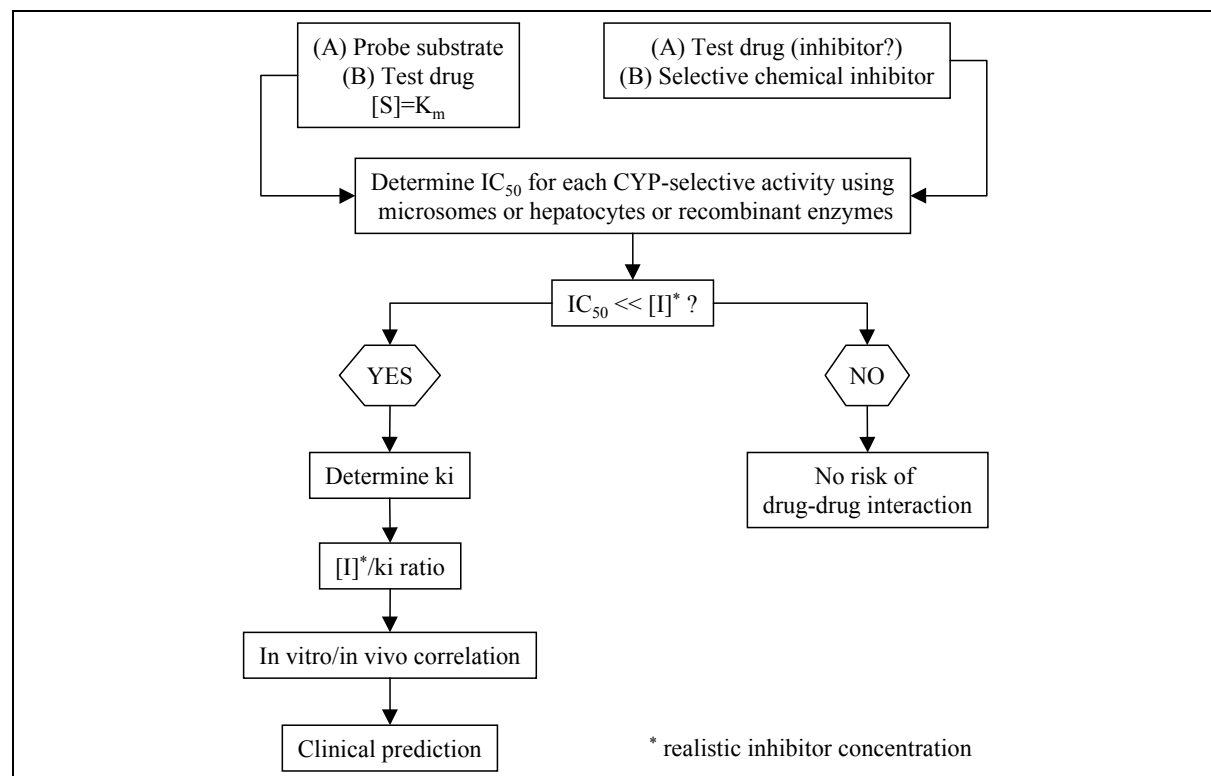
$$V_I = \frac{V_{\max} * C}{\left(C + K_m * \left(1 + \frac{I}{ki} \right) \right)} \quad \text{Eq. 26}$$

$$CL_{\text{int}(I)} = \frac{V_I}{C} = \frac{V_{\max}}{\left(C + K_m * \left(1 + \frac{I}{ki} \right) \right)} \quad \text{Eq. 27}$$

$$CL_{\text{int}(I)} = \frac{CL_{\text{int}}}{\left(1 + \left(\frac{I}{ki} \right) \right)} \quad \text{if } C \ll K_m \quad \text{Eq. 28}$$

$CL_{\text{int}(I)}$: intrinsic clearance of the drug in presence of the inhibiting drug, CL_{int} : intrinsic clearance of the drug in absence of the inhibiting drug, ki : inhibition constant, I : inhibitor concentration, V_{\max} : maximum metabolic rate, K_m : Michaelis-Menten constant, V_I : metabolic rate in presence of the inhibiting drug

FIGURE 14: In vitro cytochrome P450 inhibition screening



$[I]$: inhibitor concentration, IC_{50} : concentration of inhibitor producing 50% inhibition $[S]$: substrate concentration, ki : inhibition constant, K_m : Michaelis-Menten constant

Figure 14 shows two scenarios: **Scenario A** shows whether the test drug (A) has an inhibitory effect on another drug by using probe substrates (A). **Scenario B** shows whether the metabolic pathways of the test drug (B) are inhibited by other drugs by using selective chemical inhibitors (B).

A widely used *in vitro* model to study enzyme induction uses human hepatocytes. The induction of enzymes can also be easily characterized in animals. However, there are important differences between species, which limit the precision of extrapolations.^[103, 114]

To assess the potential of a displacement drug–drug interaction, the protein binding as well as *in vitro* protein binding displacement is determined^[136].

1.4.3.2 Predicting In Vivo Drug-Drug Interactions from In Vitro Metabolic Data

The ability to predict *in vivo* drug-drug interactions from preclinical data is becoming increasingly important in drug development^[137-139]. It is possible to predict metabolic interactions both qualitatively and quantitatively from *in vitro* data. However, not all predictions are successful. Table 9 lists examples from the literature where predictions came close to describing the *in vivo* situation and others which failed.

TABLE 9: Examples of predictions of in vivo drug-drug interactions based on in vitro data^[137]

	Inhibitor	Inhibited Drug	Enzyme
Successful examples	Sulphaphenazole Erythromycin	Tolbutamide Cyclosporine	CYP2C9 CYP3A4
Successful for the metabolic pathway, but unsuccessful for overall data	Quinidine Ketoconazole	Sparteine Terfenadine	CYP2D6 CYP3A4
Unsuccessful for metabolic pathway	Fluoxetine Ciprofloxacin	Imipramine Caffeine	CYP2D6 CYP1A2

The accuracy of such predictions is dependent on many factors. Does the metabolism follow Michaelis-Menten kinetics? How many different hepatic enzymes process a drug? Where are the metabolizing enzymes localized in the cell (cytosol or membrane)? What is the mechanism of enzyme inhibition (e.g. competitive, non-competitive, mechanism-based, metabolite intermediate complex)? What is the role of other eliminating organs in clearing the drug from the body? Are intestinal or hepatobiliary transporters involved? Is there intestinal metabolism?^[140] Moreover, the relative concentration of inhibitor and inhibited target at the site of interaction are usually unknown.

1.4.3.3 Cocktail Strategy

The cocktail strategy is the concomitant administration of multiple *in vivo* probes (= cocktail) to study simultaneously several drug metabolizing enzymes. An example for such a cocktail is

the Pittsburgh cocktail ^[141]. This is a five-drug cocktail containing caffeine, chlorzoxazone, dapson, debrisoquine, and mephenytoin as *in vivo* probes to determine simultaneously the activities of CYP1A2, CYP2E1, CYP3A, CYP2D6, and CYP2C19, respectively. Dapsone also provides an index of N-acetyltransferase activity. The cocktail strategy can be used to investigate drug metabolizing enzymes in healthy volunteers or in patients. In the latter population the effect of the disease state or the drug therapy on the activity of the enzyme(s) can be studied. Another field of application is PK drug-drug interactions. Useful information can be obtained on the selectivity, magnitude, and relevance of the effect(s) of the drug on one or more enzymes (e.g. inhibition or induction of cytochromes P450). To assess this, the cocktail is given alone and after dosing with test drug. Normally multiple dosing is applied until steady state concentrations are reached or the enzyme under investigation is induced. The change in the enzyme activity of the studied cytochromes P450 can then be determined. Based on the results, specific *in vivo* drug-drug interaction studies can be planned if necessary.^[141]

1.4.3.4 Mechanism-Based PK Models

In a specific *in vivo* drug-drug interaction study (e.g. warfarin + capecitabine) the PK parameters are estimated after single (warfarin alone) and after combined administration. The magnitude in the difference in the parameters (e.g. $AUC_{0-\infty}$, CL) then quantifies the drug-drug interaction. However, this information is not always sufficient. In some cases, it would be desirable to describe the specific mechanism of the drug-drug interaction and to develop general models for their description which can be used for a class of drugs. Mechanism-based PK models are an excellent tool to describe interactions quantitatively. In addition, they provide information on the type of inhibition, on enzymes and transporters involved, and on the site of inhibition. They are applied in various areas of drug-drug interactions. Two examples are given below to give a brief overview of work recently done in this field.

Ito et al. ^[142] developed a PK model for drug absorption addressing the metabolism by CYP3A4 inside the epithelial cells, the P-gp mediated efflux into the lumen, the intracellular diffusion from luminal side to basal side, and subsequent permeation through the basal membrane. Effects of inhibition of CYP3A4 and/or P-gp on the fraction absorbed were simulated for a hypothetical substrate for both CYP3A4 and P-gp. This modeling effort is a step towards understanding the drug absorption process and related drug-drug interactions.

Cyclophosphamide, a prodrug of the cytotoxic metabolite phosphoramidate mustard, is used in combination with thioTEPA in high-dose chemotherapy to treat cancer. The metabolism of cyclophosphamide shows autoinduction. Furthermore, thioTEPA inhibits CYP2B6, which is mainly responsible for the metabolism of cyclophosphamide to 4-hydroxycyclophosphamide, an intermediate step before the formation of phosphoramidate mustard. Huitema et al. [143] developed an integrated mechanism-based population PK model for cyclophosphamide and its metabolites describing the autoinduction as well as the drug-drug interaction with thioTEPA. The purpose of the modeling was to obtain greater insight into the metabolism of cyclophosphamide and form a basis for further optimization of treatment.

1.4.3.5 Population Approach

The population approach (Chapter 1.2.10) in Phase 2/3 clinical trials can be a valuable tool for screening for PK drug-drug interactions (e.g. [144]). The advantage of this approach is to highlight unsuspected interactions and to ensure absence of suspected interactions when the drug is given to large patient populations in Phase 2/3 clinical trials. However, the successful use of this approach to detect drug-drug interactions depends very much on the protocol inclusion criteria. It is important that there are enough patients taking the potentially interacting drug. The timing of test drug intake, of co-medication intake, and of blood sampling has to be recorded.

1.4.4 Summary

The review of PK drug-drug interactions in the literature reveals many different approaches to their detection. The methods range from qualitative to quantitative and from *in vitro* to *in vivo*. PK drug-drug interactions remain an issue throughout drug development and post-marketing. They are not only of scientific interest but their identification is also in the patient's interest (adverse effects ↓). Furthermore, there are economical aspects. The early detection of an undesired drug-drug interaction can be a no-go parameter for the development of the drug and saves costs and resources. Due to all these factors it becomes more and more imperative that quantitative methods replace qualitative methods where appropriate and that knowledge is gained on the mechanism of interaction. Two research areas recently have advanced to the stage at which they can address this need. On the one hand, today's *in vitro* models can identify the mechanism of interaction and the involved enzymes and/or transporters. On the other hand, the area of mathematical modeling is rapidly growing. PBPK

models are a tool to scale across species and bridge between *in vitro* and *in vivo* models. Mechanistically based PK models describe PK drug-drug interactions with a mathematical relationship taking into account the mechanism of interaction (e.g. type of inhibition, enzymes/transporters involved, site of inhibition). An additional plus of describing the interaction based on a model is that this approach allows simulations: Exploratory analyses can be performed to predict different scenarios such as effects upon multiple dosing or change in dose strength.

Chapter 2

GENERAL OBJECTIVE AND OUTLINE OF THESIS

Chapter 2

GENERAL OBJECTIVE AND OUTLINE OF THESIS

The objective of the work reported in this thesis was twofold: To investigate the modeling approach as a means of describing a PK drug-drug interaction and to assay combination of the modeling approach with interspecies scaling techniques as a means of predicting the interaction in humans on the basis of animal data. The following two hypotheses were investigated in this thesis:

- * Pharmacokinetic relationships of varying complexity expressed in mathematical models permit the description and understanding of the mechanism of PK drug-drug interactions.
- * The extrapolation from animal to human is facilitated by the use of parameters which are estimated using pharmacokinetic models.

To study the hypotheses two compounds, L-dopa and benserazide, were selected because there is a pharmacokinetic interaction between them: specifically, L-dopa concentrations are increased due to inhibition of L-dopa metabolism by the active metabolite of benserazide. L-dopa/benserazide is an example of a PK drug-drug interaction which has therapeutic benefits compared to L-dopa alone. Furthermore, with regard to L-dopa/benserazide there was already some preclinical and sufficient clinical data available in-house at F. Hoffmann-La Roche Ltd to test the hypotheses. This was considered an advantage, as not all data had to be generated by experiment, especially the human data. Finally, as described in the general introduction, L-dopa/benserazide are combined in a fixed ratio of 1:4 in Madopar[®] and are on the market in this form for the treatment of the movement disorder Parkinsonism. This severe disease affects about 4 million people worldwide ^[145]. It was considered valuable to study our hypotheses to gain knowledge to describe the PK interaction L-dopa/benserazide using a mechanistically based PK model and thus contributing to a better understanding of the Parkinson therapy L-dopa/benserazide.

Chapters 3 to 6 form the experimental part of the thesis. Each of these chapters is divided into a Rationale, Objective, Materials and Methods, Results, Discussion, and Conclusion part.

Not all required information on the drugs in question was already available. Chapter 3 describes (1) the single dose, parallel, pharmacokinetic study performed in rats in which blood samples were taken to assess the pharmacokinetics of L-dopa and benserazide,

(2) the analytical assays for L-dopa, 3-OMD, benserazide, and Ro 04-5127, and (3) the mathematical model developed to describe the PK drug-drug interaction L-dopa/benserazide.

Chapter 4 gives details on the *in vitro* plasma protein binding of L-dopa and 3-OMD performed in rats and humans. This information was needed for testing the predictability of human L-dopa pharmacokinetics after L-dopa treatment with and without benserazide from *in vivo* pharmacokinetics in rats using PK modeling and allometric scaling of PK parameters.

Chapter 5 deals with a methodological aspect of fitting a model to the data. In particular the question is posed whether the naïve-pooled-data approach used in Chapter 3 which combines PK data from different individual animals, thus ignoring inter-individual variability, provided correct results. A population PK analysis using nonlinear mixed effects modeling was performed to investigate this question.

In the last experimental chapter (Chapter 6) the issue as to whether the PK description of the interaction between L-dopa and benserazide could be substantially improved by using a model incorporating a mechanistic description for the function of the liver is investigated.

In the appendices raw data of the experimental work is listed starting with demographic data of the animal experiment in Appendix A, followed by bioanalytical data (inter-assay precision from quality control samples, representative chromatograms) in Appendix B, pharmacokinetic data (individual and mean plasma concentrations, results from protein binding study) in Appendix C, and results from nonlinear mixed effects modeling in Appendix D. Finally, the derivations for the reparameterization of the Michaelis-Menten equation applied in Chapter 6.2 are described in Appendix E.

Chapter 3

ASSESSMENT OF THE PHARMACOKINETIC INTERACTION OF L-DOPA AND BENSERAZIDE IN RATS: ANIMAL MODEL AND COMPARTMENTAL PK MODEL

Chapter 3

ASSESSMENT OF THE PHARMACOKINETIC INTERACTION OF L-DOPA AND BENSERAZIDE IN RATS: ANIMAL MODEL AND COMPARTMENTAL PK MODEL

3.1 RATIONALE

3.1.1 Rationale for Pharmacokinetic Study in Rats

Up to the time of our experiment described below no investigation had been done where both compounds, L-dopa and benserazide, were determined in rats after administration of these compounds individually and after combined L-dopa/benserazide. However, such data are necessary to establish and validate a PK model. Therefore, pharmacokinetic studies in rats were performed.

3.1.2 Rationale for Pharmacokinetic Model

In the literature the pharmacokinetics of L-dopa in rats after administration of L-dopa alone or L-dopa combined with a peripheral amino acid decarboxylase inhibitor was studied mainly using non-compartmental analysis^[146-152]. In some cases compartmental models were used to describe L-dopa disposition in non-humans. Sato et al.^[153] used a compartmental model to describe the pharmacokinetics of exogenous and endogenous L-dopa in rat plasma and striatum after iv administration of L-dopa. Bredberg et al.^[154] studied the pharmacokinetics of L-dopa in rats after L-dopa/carbidopa administration comparing different routes of administration. They fitted two different 2-compartment models to their L-dopa data; one with a first-order and the other with a mixed-order elimination. In two other publications^[146, 155] biexponential and triexponential models were fitted to L-dopa data. In all those cases the model described either the L-dopa pharmacokinetics after L-dopa alone or the L-dopa pharmacokinetics after the combination of L-dopa and an amino acid decarboxylase inhibitor without modeling the inhibition and the pharmacokinetics of the inhibitor. No attempt was made so far to mathematically describe the inhibition of L-dopa decarboxylation after benserazide administration and its effect on the pharmacokinetics of L-dopa and its metabolite 3-OMD in a mechanistic way.

3.1.3 Rationale for Dose

The oral doses of 20 mg/kg benserazide, 80 mg/kg L-dopa or 80/20 mg/kg L-dopa/benserazide used in the animal experiment described below were chosen because they were well tolerated in rats in previous experiments and the combination therapy has the same ratio as used in Madopar[®], i.e. 1:4.

3.2 OBJECTIVE

The objective of this study was to determine the plasma concentrations of L-dopa and its metabolite 3-OMD, and benserazide and its metabolite Ro 04-5127 in rats after oral treatment with L-dopa alone or benserazide alone or L-dopa/benserazide and to develop a model for the PK interaction of L-dopa and benserazide in rats with a view to better understand the use of these drugs in humans.

3.3 MATERIALS AND METHODS

3.3.1 Drugs and Chemicals

All chemicals used were of analytical grade. L-dopa and benserazide were provided by F. Hoffmann-La Roche Ltd. For administration L-dopa and benserazide were separately dissolved in 0.9 % NaCl (L-dopa 20 mg/mL, benserazide 10 mg/mL).

3.3.2 Animal Experiment

Twenty-one male albino rats (strain: Wistar/Füllinsdorf) weighing 262 g to 307 g and 3 male albino rats (strain: RoRo/Füllinsdorf) weighing 309 g to 323 g were used in this study. The age of the rats was 10 to 12 weeks. The individual demographic data of the rats is listed in Appendix A. The animals were allowed three days of acclimatization before entering the study. A single dose, parallel design with three treatments, 20 mg/kg (78 µmol/kg) benserazide po or 80 mg/kg (406 µmol/kg) L-dopa po or 80 mg/kg L-dopa + 20 mg/kg benserazide, was employed. Six rats (strain: Wistar/Füllinsdorf) were assigned to each treatment group. Another 3 rats (same strain) were included in the experiment for collecting predose samples. They did not receive treatment. In the treatment group where 80/20 mg/kg L-dopa/benserazide was given additional 3 rats (strain: RoRo/Füllinsdorf) were studied. These are also Wistar rats, which were bred at F. Hoffmann-La Roche Ltd. They were studied

additionally to compare the present data with former company studies where only RoRo rats had been used.

A catheter was implanted in the jugular vein for blood sampling two days before drug administration. Blood was collected for the determination of L-dopa, 3-OMD, benserazide, and Ro 04-5127. The blood sampling schedules were predose and 0.083, 0.17, 0.25, 0.5, 1, 2, 3, and 4 hours after benserazide treatment and predose and 0.083, 0.17, 0.25, 0.5, 1, 2, 3, 4, 6, 8, 10, and 24 hours after L-dopa treatment or L-dopa/benserazide treatment. All samples were stabilized by adding sodium metabisulfite immediately after blood collection (5 mg/mL blood) and a second time to each plasma sample (5 mg/mL plasma) immediately after centrifugation. The blood samples were centrifuged at 3500xg for 5 minutes and the plasma samples were kept at -80°C until drug assay. The samples containing benserazide and Ro 04-5127 were analyzed within 8 days, taking the compound's known instability into account ^[156]. This study was carried out in accordance with Art. 62 of the Swiss Federal Ordinance on the Protection of Animals.

3.3.3 Drug Assay

Two separate analytical methods were used to determine plasma concentrations of L-dopa and its metabolite 3-OMD on the one hand and benserazide and its metabolite Ro 04-5127 on the other, both using HPLC-electrochemical detection methodologies ^[157, 158]. The analytes together with added internal standards (alpha-ethyl-dopa for L-dopa/3-OMD, a methylated derivative of benserazide for benserazide/Ro 04-5127) were isolated from plasma by solid phase extraction using cation exchange cartridges (1mL/100mg SCX, Bondelut, Varian) in the L-dopa/3-OMD assay and aluminum oxide cartridges (1mL/100mg Alox-A, Bondelut, Varian) in the benserazide/Ro 04-5127 assay. Gradient elution and ion pair formation of the cationic compounds with anionic-pairing reagent at acidic pH was performed to separate the analytes from residual plasma constituents. A phosphate buffer (100 nM) / acetonitrile gradient containing 5 mM 1-octane-sulfonic acid and 0.5 mM EDTA was used as mobile phase. The analytes were quantified with amperometric detection.

The concentrations of the analytes were determined using a calibration curve calculated by linear least squares regression of peak height ratios (peak height of analyte / peak height of internal standard) versus nominal concentration. New curves were prepared with each batch of analytical samples. The weighting was $1/y^2$ (L-dopa and 3-OMD) and $1/x^2$ (benserazide and Ro 04-5127). The calibration samples were prepared from human plasma

(dialyzed for the L-dopa/3-OMD assay to remove endogenous L-dopa and 3-OMD (see Chapter 4.3.1 for dialysis method) and stabilized with 10 mg/mL sodium metabisulfite. The calibration range in this study generally was between 1 µg/L and 500 µg/L for L-dopa and 3-OMD and between 0.25 µg/L and 50 µg/L for benserazide and Ro 04-5127.

The quantification limits were determined by analyzing spiked plasma samples repeatedly over 5 days around the expected determination limit. The limit was then defined as 15 % below the lowest concentration, which could be determined with an inter-assay precision ≤ 20 % and a bias ≤ 15 %. The quantification limits for this study were defined as 0.85 µg/L (L-dopa and 3-OMD) and 0.20 µg/L (benserazide and Ro 04-5127). In the L-dopa/3-OMD assay quality control samples at two different appropriate concentrations were prepared with dialyzed plasma (human and rat) and stabilized with 10 mg/mL sodium metabisulfite. They were analyzed in duplicate with each assay batch (approx. 18 % to 43 % quality control samples referenced to the number of unknown samples). In the benserazide/Ro 04-5127 assay quality control samples at three different appropriate concentrations prepared from human stabilized plasma (10 mg/ml sodium metabisulfite) were analyzed in duplicate with each assay batch (approx. 19 % quality control samples referenced to the number of unknown samples). Results from unknown samples were accepted only if not more than 25 % of the quality control samples within each assay batch had a bias greater than 15 % (L-dopa, 3-OMD) or 20 % (benserazide, Ro 04-5127).

Data acquisition and processing was performed by means of a Hewlett-Packard Chemstation in connection with UNICHROM+ Version 1.3 ^[159].

3.3.4 Pharmacokinetic Analysis

The plasma concentration-time curves of L-dopa, 3-OMD, benserazide, and Ro 04-5127 were analyzed in two ways, namely by non-compartmental methods and by applying a compartmental model to the data to describe the PK interaction of L-dopa and benserazide. Visual inspection of the concentration-time profiles did not reveal any difference between the strains (Wistar, RoRo). To increase the data density for the modeling process the data of the RoRo rats were therefore included.

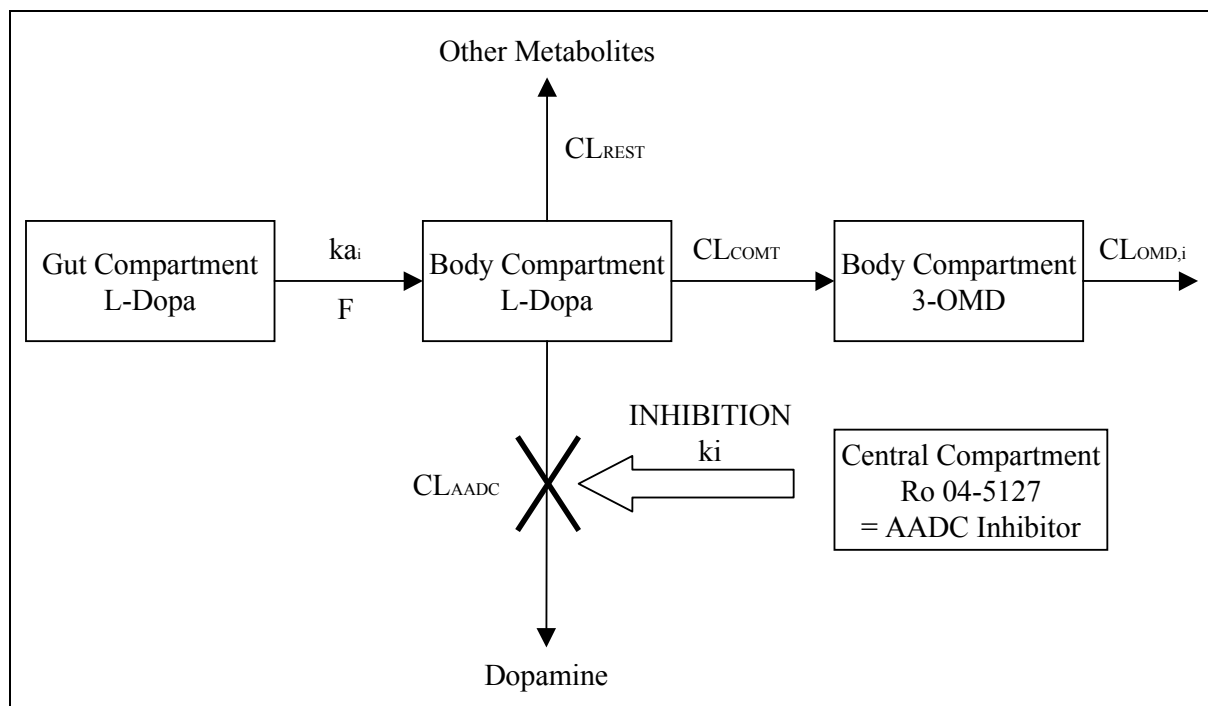
3.3.4.1 Non-Compartmental Analysis

For the non-compartmental analysis plasma concentration-time data were plotted first for visual inspection. The maximum plasma concentrations after a dose (C_{\max}) and the times of

their occurrence (T_{max}) were determined directly from the observed data. The beginning of the terminal log-linear phase was estimated by eye from log-linear plots and its slope, reflecting the terminal rate constant (k), calculated by log-linear regression analysis. The terminal half-life ($T_{1/2}$) was derived from $\ln(2)/k$. The absorption rate constant (k_a) was estimated by the method of residuals ^[160]. The areas under plasma concentration versus time curves from time zero to infinity ($AUC_{0-\infty}$) were obtained by applying the linear trapezoidal rule up to C_{max} and the logarithmic trapezoidal rule after C_{max} up to the last observed concentration (C_{last}) using actual sampling times. Extrapolation to time infinity (\hat{C}_{last}/k) was achieved using predicted concentrations at the last observation time point (\hat{C}_{last}) which were calculated from the regression line ^[161]. The oral clearance (CL/F) after a single oral dose was calculated by $dose/AUC_{0-\infty}$. Dividing CL/F by k gave an estimate of the oral volume of distribution (V/F). The non-compartmental analysis was performed using the software program WinNonlin 1.5 (Pharsight Corporation) for the calculation of the PK parameters.

3.3.4.2 Compartmental Analysis

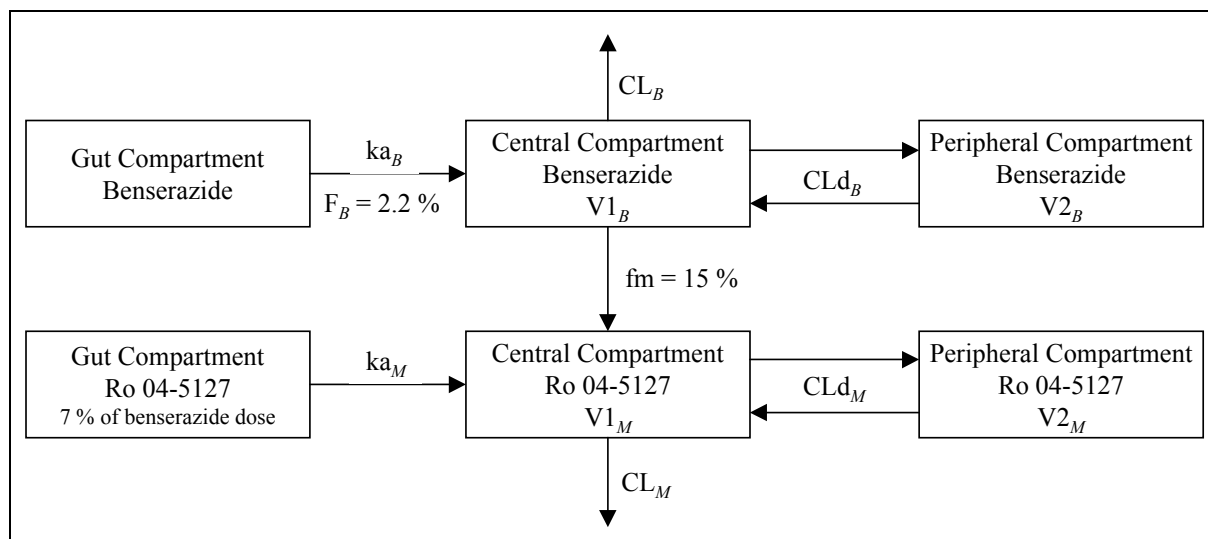
The pharmacokinetics of L-dopa and benserazide and their PK interaction is shown in Figure 15 and Figure 16.

FIGURE 15: Schematic representation of conceptual model to describe PK of L-dopa and 3-OMD

V_{dopa} , CL_{dopa} , $V_{\text{OMD},i}$, $CL_{\text{OMD},i}$, k_i are primary parameters, F , F_H , CL_H , CL_{AADC} , CL_{COMT} are secondary parameters, ka_i was calculated by NCA, Q (0.828 L/h/0.25kg) [162], f_{COMT} (10 %) [21], f_{AADC} (69 %) [21], f_H (13 %) [163], F_G after L-dopa alone (24 %) [155] are literature values and F_G after L-dopa/benserazide (100 %) is an assumption.

$ka_i = \text{eier } ka_b$ (treatment L-dopa) or ka_c (treatment L-dopa/benserazide), $CL_{\text{OMD},i} = \text{eier } CL_{\text{OMD},b}$ (treatment L-dopa) or $CL_{\text{OMD},c}$ (treatment L-dopa/benserazide),

For abbreviations in Figure 15 see text and glossary of abbreviations.

FIGURE 16: Schematic representation of conceptual model to describe PK of benserazide and Ro 04-5127

CL_B , V_{1B} , V_{2B} , CL_{d_B} , ka_B , V_{1M} , V_{2M} , CL_{d_M} , ka_M were primary parameters, CL_M was a secondary parameter (derived from $V_{1M} \cdot ke_M$), F_B (2.2 %) was derived from $AUC_{\text{oral}} \cdot D_{\text{iv}} / AUC_{\text{iv}} \cdot D_{\text{oral}}$, ke_M was an approximation from $\ln(2) / (T_{\text{max}}/3)$, and the fraction of benserazide metabolized to Ro 04-5127 ($fm = 15\%$) and fraction of Ro 04-5127 absorbed from the gut (7 %) were assumptions.

For abbreviations in Figure 16 see text and glossary of abbreviations.

L-dopa and its metabolite 3-OMD: For the compartmental analysis the pharmacokinetics of L-dopa and 3-OMD after 80 mg/kg L-dopa and 80/20 mg/kg L-dopa/benserazide were described by a 1-compartmental model (first-order absorption) where total L-dopa clearance (CL_{dopa}) was the sum of the clearances mediated by AADC, COMT and other elimination pathways (Eq. 29).

$$\boxed{CL_{\text{dopa}} = CL_{\text{AADC}} + CL_{\text{COMT}} + CL_{\text{REST}}} \quad \text{Eq. 29}$$

If L-dopa was administered alone the model was set up in accordance with literature information such that 69 %^[21] of L-dopa was metabolized by AADC (f_{AADC}), 10 %^[21] by COMT (f_{COMT}) and the rest, 21 %, by other enzymes. After administration of L-dopa together with benserazide those metabolic fractions were allowed to change in relation to the extent of inhibition. Ro 04-5127 was assumed to inhibit competitively^[23] the L-dopa clearance mediated by AADC (CL_{AADC}) and thereby to affect the total L-dopa clearance and the availability of L-dopa from the gut and across the liver. CL_{AADC} was estimated by Eq. 30 where $CL_{\text{AADC}0}$ was the L-dopa clearance via AADC with no inhibition, C_{IM} was the Ro 04-5127 concentration (inhibitor concentration) and k_i was the inhibition constant.

$$\boxed{CL_{\text{AADC}} = \frac{CL_{\text{AADC}0}}{\left(1 + \frac{C_{\text{IM}}}{k_i}\right)}} \quad \text{Eq. 30}$$

Therefore, the total L-dopa clearance varied after L-dopa/benserazide due to the changes in the AADC pathway (CL_{AADC}) caused by the inhibitor, whereas the total L-dopa clearance after L-dopa alone was kept at a constant value which was estimated as a primary parameter in the model.

The hepatic availability (F_{H}) was described by Eq. 31 where the hepatic extraction ratio (ratio of hepatic blood clearance of L-dopa (CL_{H}) to hepatic blood flow (Q ; 0.828 L/h/0.25kg^[162])) was subtracted from 1. The hepatic blood clearance of L-dopa was obtained from the product of the hepatically cleared fraction (f_{H}) and the total blood clearance of L-dopa (Eq. 32). Because the blood/plasma ratio of L-dopa was approximately 1.0^[163] the total plasma clearance of L-dopa, a primary parameter in the model, was set equal to the total blood clearance of L-dopa. The majority of L-dopa is metabolized extrahepatically ($1-f_{\text{H}}$) and the hepatic clearance of L-dopa was assumed to be 13 % of total body clearance^[163].

$$\boxed{F_{\text{H}} = 1 - \frac{CL_{\text{H}}}{Q}} \quad \text{Eq. 31}$$

$$\boxed{CL_H = f_H * CL_{dopa}} \quad \text{Eq. 32}$$

The gastrointestinal availability (F_G) was obtained from the literature (0.244^[155]) after administration of L-dopa alone and was assumed to be complete after combined administration of L-dopa/benserazide. The overall oral bioavailability of L-dopa (F) was estimated by $F_G * F_H$. A distinction was made between absorption parameters after L-dopa alone (ka_b , F_b) and absorption parameters after L-dopa/benserazide (ka_c , F_c). Based on initial modeling results the 3-OMD parameters, clearance and volume of distribution, were subsequently allowed to differ between the treatments L-dopa alone and L-dopa/benserazide ($CL_{OMD,b}$, $CL_{OMD,c}$, $V_{OMD,b}$, $V_{OMD,c}$). The mass balances for the compartments of L-dopa and 3-OMD were described by differential equations (Eq. 33 to Eq. 35).

$$\boxed{\frac{dA_{dopa,i}}{dt} = -ka_i * A_{dopa,i}(t)} \quad \text{Eq. 33}$$

$$\boxed{V_{dopa} * \frac{dC_{dopa,i}}{dt} = ka_i * A_{dopa,i}(t) * F_i - CL_{dopa} * C_{dopa,i}(t)} \quad \text{Eq. 34}$$

$$\boxed{V_{OMD,i} * \frac{dC_{OMD,i}}{dt} = CL_{COMT} * C_{dopa,i}(t) - CL_{OMD,i} * C_{OMD,i}(t)} \quad \text{Eq. 35}$$

$A_{dopa,i}$: amount L-dopa in gut compartment, $C_{dopa,i}$: L-dopa concentration in systemic compartment, $C_{OMD,i}$: 3-OMD concentration in systemic compartment (i = b (treatment L-dopa); i = c (treatment L-dopa/benserazide))

The data pooled per analyte was analyzed using the naïve-pooled-data approach. In a first step the L-dopa model was fitted simultaneously to the L-dopa and 3-OMD data after treatment with 80 mg/kg L-dopa. In a second step the model including inhibition of the AADC pathway was fitted simultaneously to the L-dopa and 3-OMD data after treatment with 80/20 mg/kg L-dopa/benserazide. Those parameters, which could be estimated in the first step, were fixed in the second step. The estimated primary parameters were the volume of distribution of L-dopa (V_{dopa}), the total clearance of L-dopa (CL_{dopa}) after L-dopa alone, the volume of distribution of 3-OMD after L-dopa alone ($V_{OMD,b}$) and after L-dopa/benserazide ($V_{OMD,c}$), the 3-OMD clearance after L-dopa alone ($CL_{OMD,b}$) and after L-dopa/benserazide ($CL_{OMD,c}$), and the inhibition constant (ki). The secondary parameters after treatment with L-dopa alone were the bioavailability of L-dopa (F), the hepatic availability of L-dopa (F_H), the hepatic clearance of L-dopa (CL_H), the L-dopa clearance by the AADC pathway, and the L-dopa clearance by the COMT pathway. The constants of the model were the L-dopa dose, the absorption rate constant of L-dopa after L-dopa alone (ka_b) and after L-dopa/benserazide (ka_c), the hepatic

blood flow, the L-dopa fraction metabolized by COMT after L-dopa alone (f_{COMT}), the L-dopa fraction metabolized by AADC after L-dopa alone (f_{AADC}), the hepatic fraction of L-dopa (f_{H}), and the gastrointestinal availability of L-dopa after L-dopa alone and after L-dopa/benserazide. The benserazide/Ro 04-5127 data were fitted separately and the estimated parameters for the benserazide/Ro 04-5127 pharmacokinetics were used as fixed parameters in the L-dopa model.

Benserazide and its metabolite Ro 04-5127: The pharmacokinetics of benserazide and Ro 04-5127 were described with 2-compartment models. After oral administration of benserazide the amount of Ro 04-5127 in plasma (central compartment) was assumed to be derived from the sum of metabolite formed systemically and presystemically. In order to model the pharmacokinetics of the metabolite Ro 04-5127 three further assumptions were necessary. The elimination of Ro 04-5127 was assumed to be the fastest process of all the first-order processes governing the pharmacokinetics of Ro 04-5127. Therefore, a rough approximation of the elimination rate constant (k_{EM}) was obtained from $\ln(2)/(T_{\text{max}}/3)$. The fraction of Ro 04-5127 absorbed from the gut was assumed to be 7%. The fraction of benserazide metabolized to Ro-04-5127 systemically, f_{M} , was assumed to be 15%.

The benserazide/Ro 04-5127 model was fitted simultaneously to the oral data of benserazide and Ro 04-5127 (pooled data from both treatments including benserazide) of the present study as well as intravenous data of benserazide and Ro 04-5127 from two previous studies ^[164, 165] (see Chapter 3.3.6). The estimated primary parameters in the benserazide/Ro 04-5127 model were the volumes of the central compartment ($V_{1\text{B}}$, $V_{1\text{M}}$), the volumes of the peripheral compartment ($V_{2\text{B}}$, $V_{2\text{M}}$), the intercompartmental clearances (CL_{dB} , CL_{dM}) and the absorption rate constants (k_{aB} , k_{aM}). The clearance for benserazide (CL_{B}) was a further primary parameter while for Ro 04-5127 it was derived from $V_{1\text{M}} \cdot k_{\text{EM}}$ (CL_{M}). The constants of the benserazide/Ro 04-5127 model were the benserazide dose, the bioavailability of benserazide, the fraction of Ro 04-5127 absorbed from the gut, the fraction of benserazide metabolized to Ro 04-5127, and the elimination rate constant of Ro 04-5127 (k_{EM}).

Weighting: The weighting was selected empirically from judging the goodness-of-fit. In the L-dopa model it was for both steps $1/Y^{0.25}$. The weighting was $1/\hat{Y}^2$ after intravenous administration of benserazide. Unit weighting was applied to model the data after oral administration of benserazide.

Integration and optimization: The integration algorithm was 4th-5th order Runge-Kutta with variable step size. The parameters were evaluated by nonlinear least squares estimation, using the simplex algorithm for minimizing the sum of squared residuals.

Hardware and software: The modeling analysis was performed on a Pentium Pro 200 Mhz (RAM 96 MB, HD 2 GB; Windows NT 4.0 SP3) computer using WinNonlin 1.5 (Pharsight Corporation).

3.3.5 Statistical Analysis

Descriptive statistics was performed to summarize the parameters. An unpaired Student's t-test was used to compare the pharmacokinetic parameters of L-dopa or 3-OMD between treatment with L-dopa alone and treatment with L-dopa/benserazide and to compare the pharmacokinetic parameters of benserazide or Ro 04-5127 between treatment with benserazide alone and treatment with L-dopa/benserazide. For this purpose all parameters were subjected to a logarithmic transformation [166]. The level of statistical significance was defined as $p < 0.05$. If no statistically significant difference was found between treatments a 95 % confidence interval for the true mean ratio (95 % CI) was calculated. The Student's t-test was not applicable for T_{\max} because it is a discrete variable.

3.3.6 Intravenous Data of Benserazide and Ro 04-5127

In the benserazide/Ro 04-5127 model intravenous data was incorporated from two previous studies [164, 165]. The data were obtained from five male rats (strain: RoRo/Füllinsdorf), which received intravenously 5 mg/kg (19 μ mol/kg) benserazide.

3.4 RESULTS

3.4.1 Animal Experiment

Rat a4 of treatment group 20 mg/kg benserazide and rat b6 of treatment group 80 mg/kg L-dopa died before dosing due to problems with the jugular vein catheter. They were not replaced. Therefore, only five rats were studied in those two treatment groups.

3.4.2 Assay Performance of Drug Concentration Analysis

3.4.2.1 L-Dopa and its Metabolite 3-OMD

The performance of the assay for L-dopa and its metabolite 3-OMD as determined from the analysis of daily quality control samples is listed in Table 10 and Appendix B (individual data). The inter-assay precision (coefficient of variation) of quality control samples ranged between 2.7 % and 11 % for L-dopa and between 2.6 % and 11 % for 3-OMD. There was no marked bias in the results from these quality control samples (bias: -3.8 % (N=18) to 7.9 % (N=18), L-dopa; -4.8 % (N=14) to 1.5 % (N=18), 3-OMD). All study samples were analyzed once. Typical chromatograms for L-dopa and 3-OMD in plasma samples are given in Appendix B.5.

TABLE 10: Precision and bias of the plasma assay for L-dopa and 3-OMD according to quality control samples

Analyte	Matrix	Nominal Conc. [µg/L]	N	Mean Conc. [µg/L]	Precision [%]	Bias [%]
L-Dopa	human plasma	9.77	11	10.5	5.8	7.5
	human plasma	9.27	18	10.0	4.6	7.9
	rat plasma	10.1	13	10.5	11	4.0
	rat plasma	9.76	18	10.3	4.6	5.5
	human plasma	195	10	197	4.0	1.0
	human plasma	208	18	201	3.0	-3.4
	rat plasma	203	10	205	5.7	0.99
	rat plasma	210	18	202	2.7	-3.8
3-OMD	human plasma	9.95	11	9.91	5.9	-0.40
	human plasma	9.80	14	9.33	11	-4.8
	rat plasma	9.28	13	9.32	10	0.43
	rat plasma	9.08	14	8.99	7.1	-0.99
	human plasma	197	10	192	3.1	-2.5
	human plasma	206	18	209	2.7	1.5
	rat plasma	193	10	191	2.6	-1.0
	rat plasma	208	18	209	2.6	0.48

Precision: defined as coefficient of variation (CV), **Bias:** defined as deviation between mean concentration and nominal concentration (expressed in % of nominal concentration).

3.4.2.2 Benserazide and its Metabolite Ro 04-5127

The performance of the assay for benserazide and its metabolite Ro 04-5127 as determined from the analysis of daily quality control samples is listed in Table 11 and Appendix B (individual data). The inter-assay precision (coefficient of variation) of quality control samples ranged between 6.5 % and 27 % for benserazide and between 5.8 % and 22 % for

Ro 04-5127. The bias for the quality control samples was -24 % (N=6) to -3.7 % (N=6) for benserazide and -14 % (N=6) to 1.3 % (N=6) for Ro 04-5127. The high coefficient of variation and bias were due to large deviations from the nominal concentration in one assay batch. The results of this assay batch were accepted because only its lowest quality control samples were affected and there was no assay material available for reanalysis. All study samples were analyzed once. Typical chromatograms for benserazide and Ro 04-5127 in plasma samples are given in Appendix B.6.

TABLE 11: Precision and bias of the plasma assay for benserazide and its metabolite Ro 04-5127 according to quality control samples

Analyte	Nominal Conc. [µg/L]	N	Mean Conc. [µg/L]	Precision [%]	Bias [%]
Benserazide	4.33	6	3.27	27	-24
	16.4	6	15.8	6.5	-3.7
	43.7	6	39.0	10	-11
Ro 04-5127	3.74	6	3.20	22	-14
	15.0	6	15.2	5.8	1.3
	45.0	6	39.2	11	-13

Precision: defined as coefficient of variation (CV), **Bias:** defined as deviation between mean concentration and nominal concentration (expressed in % of nominal concentration).

3.4.3 Non-Compartmental PK Analysis of L-Dopa and its Metabolite 3-OMD

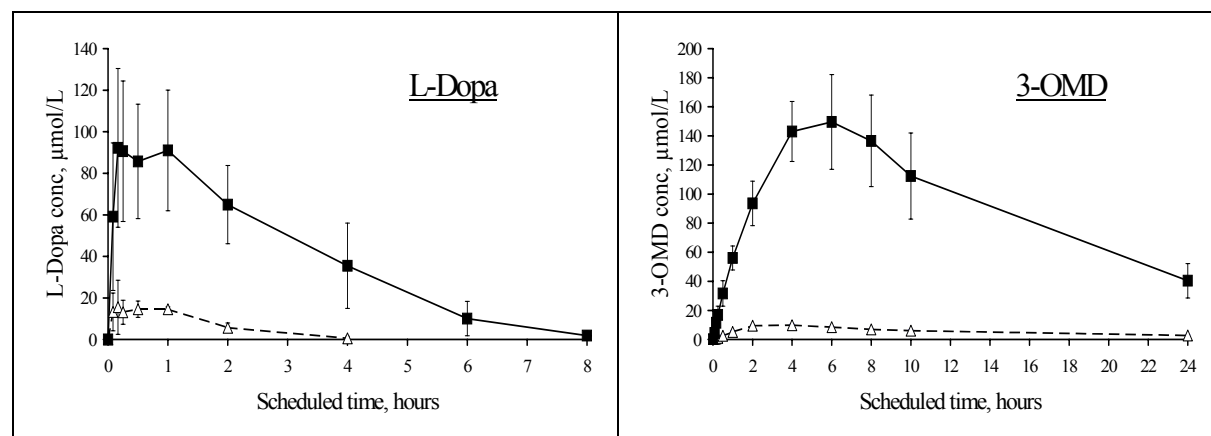
The individual plasma concentration-time data of L-dopa and 3-OMD following treatment with 80 mg/kg L-dopa or 80/20 mg/kg L-dopa/benserazide are displayed in Appendix C.1.

The 24-h sampling period was in all instances sufficient to describe the concentration-time curve of L-dopa and 3-OMD and to allow a reliable estimation of the terminal half-life in both treatment groups, 80 mg/kg L-dopa alone and 80/20 mg/kg L-dopa/benserazide. The terminal log-linear phase after treatment with 80 mg/kg L-dopa extended over 2 h to 3 h for L-dopa and over 18 h to 20 h for 3-OMD and its definition was in general defined based on three (L-dopa) and four (3-OMD) data points. The L-dopa pharmacokinetics of rat b4 after treatment with L-dopa alone did not follow a monophasic decline as in the other rats, but showed a biphasic decline. Therefore, its terminal half-life was not included in the statistical evaluation. The terminal log-linear phase after treatment with 80/20 mg/kg L-dopa/benserazide extended over 6 h to 8 h for L-dopa and over 16 h to 18 h for 3-OMD and its definition was in general defined based on four (L-dopa, 3-OMD) data

points. The 24-h L-dopa values of rat's c3, c8 and c9 after treatment with L-dopa/benserazide were around the limit of quantification. They were not used for the estimation of the terminal rate constant. The observation period after treatment with 80 mg/kg L-dopa covered in all cases more than 99 % of the total L-dopa $AUC_{0-\infty}$ (extrapolated part ≤ 0.6 %) and more than 69 % of the total 3-OMD $AUC_{0-\infty}$ (extrapolated part ≤ 31 %). The observation period after treatment with 80/20 mg/kg L-dopa/benserazide covered in all cases more than 98 % of the total L-dopa $AUC_{0-\infty}$ (extrapolated part ≤ 1.4 %) and more than 73 % of the of the total 3-OMD $AUC_{0-\infty}$ (extrapolated part ≤ 27 %). The absorption of L-dopa started rapidly in all rats, leading to a maximum concentration of L-dopa within 1 h after L-dopa dosing. The formation of the metabolite 3-OMD led to a maximum concentration of 3-OMD within 4 h after L-dopa administration and within 6 h after L-dopa/benserazide administration.

Average concentrations of L-dopa and 3-OMD at various time points after L-dopa dosing of each treatment are listed together with some descriptive statistics in Appendix C.3 and are shown in Figure 17. As deviations of actual from scheduled sampling times were minor, the average values given were not corrected for the differences in sampling times between rats.

FIGURE 17: Average (\pm SD) plasma concentration-time profiles of L-dopa and 3-OMD after treatment with L-dopa alone (- Δ -) and after treatment with L-dopa/benserazide (- \blacksquare -)



The average values of L-dopa and 3-OMD parameters are listed in Table 12 and Table 13. The L-dopa and 3-OMD pharmacokinetics were clearly different with and without benserazide. A statistically significant difference ($* p < 0.01$, $** p < 0.05$) was found for the L-dopa parameters $AUC_{0-\infty}^*$, C_{max}^* , CL/F^* , $T_{1/2}^*$, and k_a^{**} and for the 3-OMD parameters $AUC_{0-\infty}^*$, C_{max}^* , and $T_{1/2}^*$. The co-administration of 80/20 mg/kg L-dopa/benserazide resulted in an 11-fold increase in the L-dopa $AUC_{0-\infty}$ and a 6-fold increase in C_{max} of L-dopa. The oral clearance of L-dopa was 9-fold lower after treatment with L-dopa/benserazide than after

L-dopa alone. The half-life of L-dopa was prolonged by a factor 2 after L-dopa/benserazide treatment. There was a small difference in T_{\max} between the two treatment groups. However, in both cases the between-animal variability of T_{\max} was high. The absorption rate constant was higher after L-dopa alone than after L-dopa/benserazide. The effect of benserazide on the 3-OMD pharmacokinetics was a 15-fold increase in $AUC_{0-\infty}$ and C_{\max} of 3-OMD. The half-life of 3-OMD was shorter after treatment with L-dopa/benserazide than after L-dopa alone. There was a small increase in 3-OMD T_{\max} when L-dopa was given together with benserazide. The oral clearance of 3-OMD after 80 mg/kg L-dopa was 0.0563 ± 0.00556 L/h and the volume of distribution (V/F) was 0.945 ± 0.0759 L. The between-animal variability for the L-dopa parameters $AUC_{0-\infty}$, k_a , k , $T_{1/2}$, CL/F , and V/F was small after treatment with L-dopa alone. After combined treatment with L-dopa/benserazide the between-animal variability was not unexpectedly in most cases several times higher than after L-dopa alone.

TABLE 12: Pharmacokinetic parameters of L-dopa after treatment with L-dopa alone or with L-dopa/benserazide (non-compartmental analysis)

PK parameters of L-Dopa [Unit]		after L-Dopa	after L-Dopa/Benserazide
$AUC_{0-\infty}$ [h* μ mol/L]	Mean (CV%) Min – Max	27.9 (13%) 22.1-31.2	307 (27%) 216-482
C_{\max} [μ mol/L]	Mean (CV%) Min – Max	20.6 (53%) 13.2-38.8	115 (27%) 67.4-152
T_{\max} [h]	Median Min – Max	1.00 0.08-1.00	0.50 0.17-1.00
k_a [h ⁻¹]	Mean (CV%) Min – Max	2.11 (22%) 1.56-2.77	1.29 (60%) 0.55-3.25
k [h ⁻¹]	Mean (CV%) Min – Max	1.73 (7%) 1.60-1.90	0.887 (20%) 0.470-1.07
$T_{1/2}$ [h]	Mean (CV%) Min – Max	0.403 (7%) 0.365-0.433	0.824 (30%) 0.648-1.48
CL/F [L/h]	Mean (CV%) Min – Max	3.72 (14%) 3.20-4.59	0.397 (20%) 0.291-0.519
V/F [L]	Mean (CV%) Min – Max	2.22 (7%) 2.07-2.42	0.480 (43%) 0.301-0.952
N	-	5	9

Parameters for whole rats; no weight correction applied. N = 4 (for k , $T_{1/2}$, and V/F) after L-dopa alone.

TABLE 13: Pharmacokinetic parameters of 3-OMD after treatment with L-dopa alone or with L-dopa/benserazide (non-compartmental analysis)

PK Parameters of 3-OMD [Unit]		after L-Dopa	after L-Dopa/Benserazide
AUC _{0-∞} [h*μmol/L]	Mean (CV%) Min – Max	183 (12%) 161-217	2716 (24%) 1670-3550
C _{max} [μmol/L]	Mean (CV%) Min – Max	10.1 (6%) 9.11-10.6	154 (19%) 117-186
T _{max} [h]	Median Min – Max	4.03 2.05-4.08	6.00 4.00-6.00
k [h ⁻¹]	Mean (CV%) Min – Max	0.0602 (17%) 0.0496-0.0748	0.0748 (9%) 0.0624-0.0877
T _{1/2} [h]	Mean (CV%) Min – Max	11.8 (16%) 9.26-14.0	9.35 (10%) 7.90-11.1
CL/F [L/h]	Mean (CV%) Min – Max	0.0563 (10%) 0.0479-0.0621	-
V/F [L]	Mean (CV%) Min – Max	0.945 (8%) 0.830-1.01	-
N	-	5	9

Parameters for whole rats; no weight correction applied. CL/F and V/F after L-dopa were estimated assuming that the fraction metabolized to 3-OMD was 10 % [21]. CL/F and V/F after L-dopa/benserazide cannot be estimated, because the fraction metabolized changes with the degree of inhibition.

3.4.4 Non-Compartmental PK Analysis of Benserazide and its Metabolite Ro 04-5127

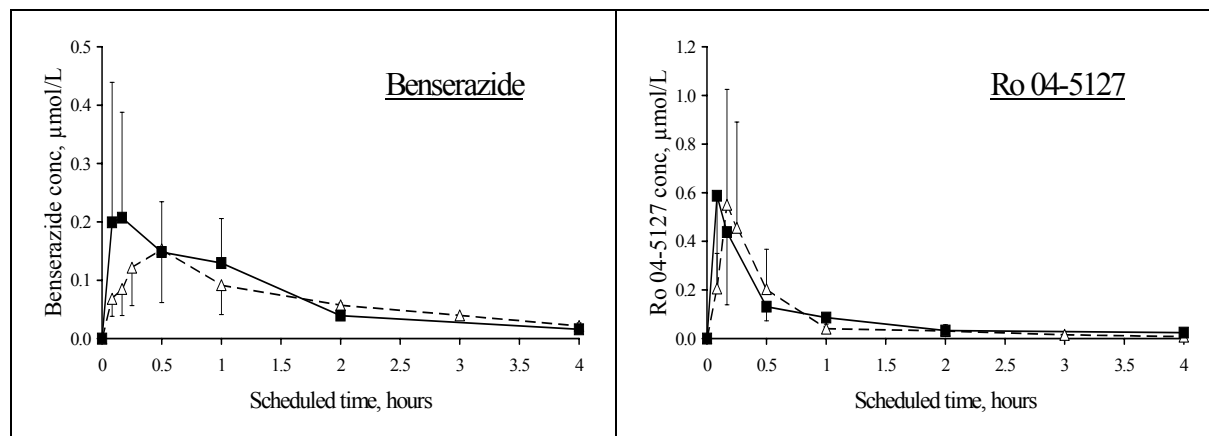
The individual plasma concentration-time data of benserazide and Ro 04-5127 following treatment with 20 mg/kg benserazide or 80/20 mg/kg L-dopa/benserazide are displayed in Appendix C.2.

The 4-h sampling period was in all instances sufficient to describe the concentration-time curve of benserazide and Ro 04-5127 and to allow a reliable estimation of the terminal half-life in both treatment groups, 20 mg/kg benserazide alone and 80/20 mg/kg L-dopa/benserazide. The terminal log-linear phase after treatment with 20 mg/kg benserazide extended over 2 h to 3 h for benserazide and 1 h to 3.75 h for Ro 04-5127 and its definition was in general based on 4 (benserazide) and 2 to 5 (Ro 04-5127) data points. The terminal log-linear phase after treatment with 80/20 mg/kg L-dopa/benserazide extended over 1 h to 3.8 h for benserazide and 0.5 h to 3.5 h for Ro 04-5127 and its definition was in general defined based on 2 to 5 (benserazide) and 2 to 3 (Ro 04-5127) data points. The observation period after treatment with 20 mg/kg benserazide covered in all cases more than 72 % of the total benserazide AUC_{0-∞} (extrapolated part ≤ 28 %) and in all but one case more than 91 % of

the total Ro 04-5127 $AUC_{0-\infty}$ (extrapolated part $\leq 9\%$). For rat a5 after treatment with benserazide alone the extrapolated part of the total Ro 04-5127 $AUC_{0-\infty}$ was 30%. The observation period after treatment with 80/20 mg/kg L-dopa/benserazide covered in all cases more than 76% of the total benserazide $AUC_{0-\infty}$ (extrapolated part $\leq 24\%$) and in all but one case more than 83% of the total Ro 04-5127 $AUC_{0-\infty}$ (extrapolated part $\leq 17\%$). For rat c9 after treatment with L-dopa/benserazide the extrapolated part of the total Ro 04-5127 $AUC_{0-\infty}$ was 30%. The absorption of benserazide was fast in all rats, with two exceptions, leading to a maximum benserazide concentration within 0.5 h after benserazide dosing. For two rats (a1 and c9) T_{max} was 2 h and 1 h, respectively. The formation of the metabolite Ro 04-5127 reached a maximum concentration of Ro 04-5127 within 0.27 h after administration of benserazide alone and within 0.5 h after L-dopa/benserazide administration.

Average concentrations of benserazide and Ro 04-5127 at various time points after benserazide dosing of each treatment are listed together with some descriptive statistics in Appendix C.4 and are shown in Figure 18. As deviations of actual from scheduled sampling times were minor the average values given were not corrected for the differences in sampling times between rats.

FIGURE 18: Average (\pm SD) plasma concentration-time profiles of benserazide and Ro 04-5127 after treatment with benserazide alone¹ (- Δ -) and after treatment with L-dopa/benserazide (- \blacksquare -)



¹ The 4-h value after treatment with benserazide alone was the average of 2 data points only.

The average values of benserazide and Ro 04-5127 parameters are listed in Table 14 and Table 15. The benserazide pharmacokinetics were similar with and without concomitantly administered L-dopa. No statistically significant difference ($p < 0.05$) was found for $AUC_{0-\infty}$ (and hence for CL/F), C_{max} , V/F between the treatments benserazide alone and L-dopa/benserazide. The observed mean ratio [(benserazide with L-dopa)/benserazide] for those parameters is presented together with the 95% CI in Table 14. The maximum

plasma benserazide concentration of rat c1 after L-dopa/benserazide was about five times higher than the other C_{max} values. This caused a high variability of C_{max} in the treatment group L-dopa/benserazide and an upward shift of the average value. The median of C_{max} and the median of $AUC_{0-\infty}$ were in both treatment groups similar confirming that the observed upwards shift of the average value was due to an individual extreme value. There was no relevant difference in $T_{1/2}$ and k between the two treatment groups. After treatment with L-dopa/benserazide T_{max} was shorter than after benserazide alone. However, the between-animal variability was in both groups very high. The pharmacokinetics of Ro 04-5127 were similar with and without L-dopa. No statistically significant difference ($p < 0.05$) was found for $AUC_{0-\infty}$, C_{max} , $T_{1/2}$, and k between the treatments benserazide alone and benserazide/L-dopa. The observed mean ratio [(benserazide with L-dopa)/benserazide] for those parameters is listed together with the 95 % CI in Table 15. T_{max} was similar between the two groups. However, the between-animal variability was high, especially after treatment with L-dopa/benserazide (CV 88 %).

TABLE 14: Pharmacokinetic parameters of benserazide after treatment with benserazide alone or with L-dopa/benserazide (non-compartmental analysis)

PK Parameters of Benserazide [Unit]		after Benserazide	after L-Dopa/Benserazide	Ratio ³ [95% CI]
$AUC_{0-\infty}$ [h* μ mol/L]	Mean (CV%)	0.297 (24%)	0.268 (49%)	0.85 [0.55; 1.32]
	Min – Max	0.224-0.413	0.161-0.569	
C_{max} [μ mol/L]	Mean (CV%)	0.161 (50%)	0.247 (90%)	1.38 [0.70; 2.73]
	Min – Max	0.0732-0.287	0.123-0.827	
T_{max} [h]	Median	0.50	0.17	-
	Min – Max	0.50-2.00	0.10-1.00	
k [h ⁻¹]	Mean (CV%)	0.567 (20%)	0.963 (38%)	-
	Min – Max	0.451-0.735	0.400-1.59	
$T_{1/2}$ [h]	Mean (CV%)	1.26 (19%)	0.842 (48%)	-
	Min – Max	0.943-1.54	0.436-1.73	
CL/F [L/h]	Mean (CV%)	70.8 (31%)	95.4 (36%)	1.31 [0.81; 2.12]
	Min – Max	48.0-95.1	39.7-144	
V/F [L]	Mean (CV%)	131 (39%)	110 (40%)	0.82 [0.44; 1.53]
	Min – Max	65.3-190	30.9-171	
N	-	5	8 ^{1,2}	-

¹ No data was available in the terminal phase for rat c9. Therefore, N was 8 for $AUC_{0-\infty}$, k , $T_{1/2}$, CL/F, and V/F.

² N = 9 for C_{max} and T_{max} .

³ Ratio (benserazide with L-dopa)/benserazide) was estimated from geometric means.

TABLE 15: Pharmacokinetic parameters of Ro 04-5127 after treatment with benserazide alone or with L-dopa/benserazide (non-compartmental analysis)

PK Parameters of Ro 04-5127 [Unit]		after Benserazide	after L-Dopa/Benserazide	Ratio ¹ [95% CI]
AUC _{0-∞} [h*μmol/L]	Mean (CV%) Min – Max	0.309 (42%) 0.171-0.502	0.321 (19%) 0.249-0.435	1.10 [0.78; 1.55]
C _{max} [μmol/L]	Mean (CV%) Min – Max	0.579 (79%) 0.143-1.15	0.621 (59%) 0.184-1.19	1.20 [0.47; 3.03]
T _{max} [h]	Median Min – Max	0.17 0.083-0.27	0.10 0.083-0.50	-
k [h ⁻¹]	Mean (CV%) Min – Max	0.525 (23%) 0.363-0.642	0.798 (42%) 0.275-1.25	1.40 [0.82; 2.41]
T _{1/2} [h]	Mean (CV%) Min – Max	1.38 (26%) 1.08-1.91	1.10 (60%) 0.553-2.52	0.71 [0.42; 1.22]
N	-	5	9	-

¹ Ratio ((benserazide with L-dopa)/benserazide) was estimated from geometric means.

3.4.5 Compartmental PK Analysis of L-Dopa and its Metabolite 3-OMD

The final parameter estimates of L-dopa and 3-OMD are listed in Table 16. After administration of L-dopa the hepatic availability of L-dopa was 87 %. Together with the literature value of the gastrointestinal availability of L-dopa (F_G : 24 %^[155]) this gave a bioavailability for L-dopa of 21 %. Further secondary parameters were the hepatic clearance of L-dopa (CL_H : 0.107 L/h), the L-dopa clearance by COMT (CL_{COMT} : 0.0823 L/h), and the L-dopa clearance by AADC (CL_{AADC} : 0.568 L/h). After administration of L-dopa together with benserazide the availability and clearance terms of L-dopa changed over time dependent on the time course of inhibitor Ro 04-5127. Figure 19 shows the plasma concentration-time profile of Ro 04-5127 and the temporal change of the L-dopa clearance by AADC after L-dopa/benserazide administration. The model fits to combined data sets of treatment with L-dopa and L-dopa/benserazide described the observed concentrations well (Figure 20 and Figure 21).

TABLE 16: Pharmacokinetic parameters estimated by compartmental analysis

Analyte	PK Parameter [Unit]	Treatment	Estimate	CV% ³
L-Dopa	V _{dopa} [L]	after L-dopa alone or L-dopa/benserazide	0.496	9
	CL _{dopa} [L/h]	after L-dopa alone	0.823	9
3-OMD	V _{OMD,b} [L]	after L-dopa alone	0.196	13
	V _{OMD,c} [L]	after L-dopa/benserazide	0.128	5
	CL _{OMD,b} [L/h]	after L-dopa alone	0.0120	27
	CL _{OMD,c} [L/h]	after L-dopa/benserazide	0.00895	11
Benserazide	CL _B [L/h]	after benserazide alone or L-dopa/benserazide	1.67	4
	V1 _B [L]		0.202	6
	V2 _B [L]		0.127	13
	CLd _B [L/h] ¹		0.0720	9
	ka _B [h ⁻¹]		0.940	27
Ro 04-5127	CL _M [L/h]	after benserazide alone or L-dopa/benserazide	4.29	11
	V1 _M [L]		0.0691	11
	V2 _M [L]		3.20	49
	CLd _M [L/h] ¹		1.06	5
	ka _M [h ⁻¹]		2.47	17
	ki [μmol/L] ²		0.00246	42

¹ intercompartmental clearance. ² inhibition constant. ³ CV% derived from asymptotic standard error of estimate.

FIGURE 19: Plasma concentration–time profile of Ro 04-5127 and the change of L-dopa clearance by AADC over time after oral administration of 80/20 mg/kg L-dopa/benserazide

The inset is an enlargement of the portion between 0 h and 1 h. L-dopa clearance by AADC at time zero (no inhibition) was defined as 69 % of the total L-dopa clearance. [21]

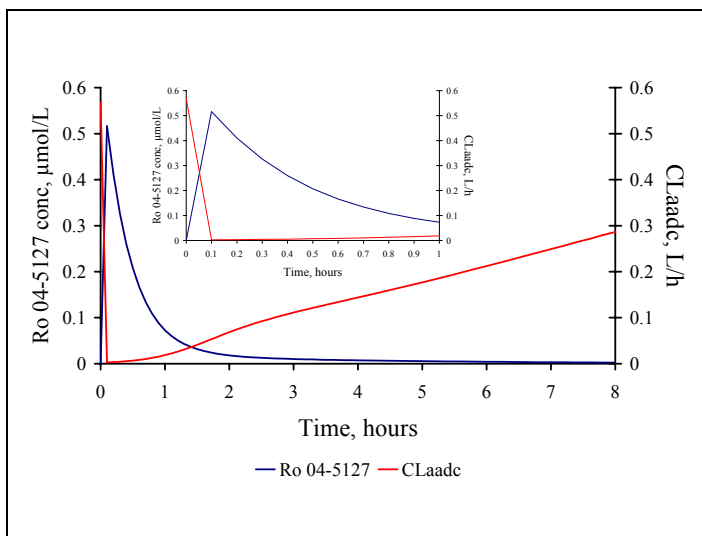


FIGURE 20: Predicted and observed L-dopa and 3-OMD plasma concentrations after oral administration of 80 mg/kg L-dopa

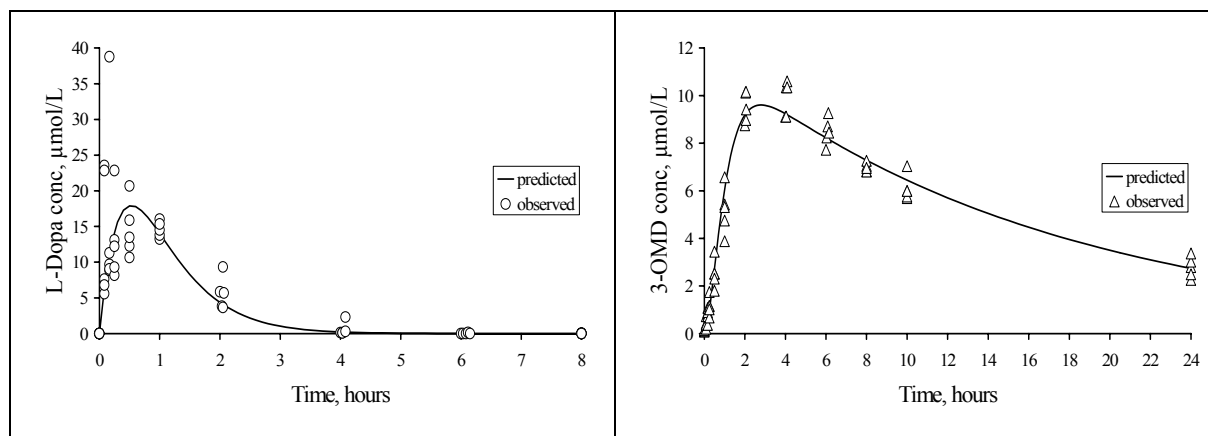
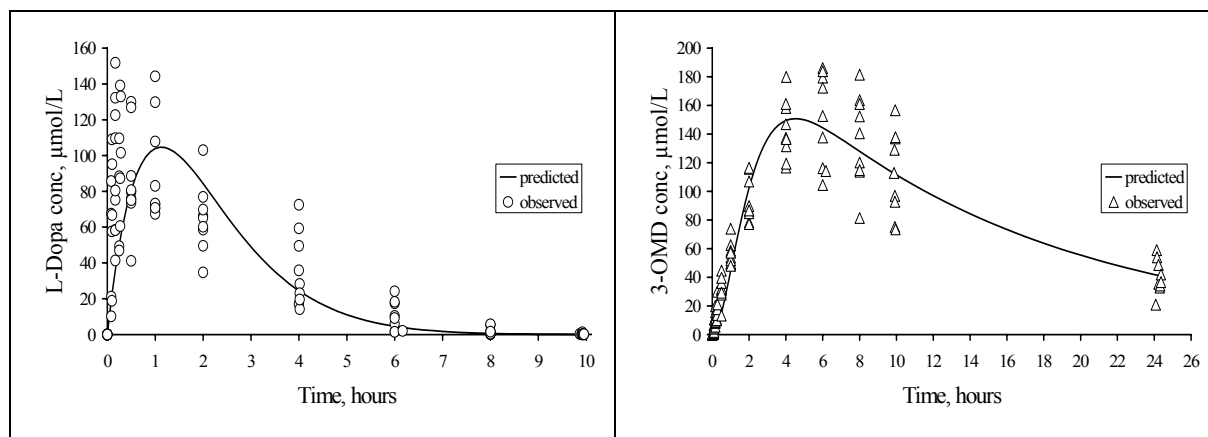


FIGURE 21: Predicted and observed L-dopa and 3-OMD plasma concentrations after oral administration of 80/20 mg/kg L-dopa/benserazide



3.4.6 Compartmental PK Analysis of Benserazide and its Metabolite Ro 04-5127

The final parameter estimates of benserazide and Ro 04-5127 are listed in Table 16. The fits to combined data sets of oral and intravenous data described the observed concentrations of benserazide and Ro 04-5127 well.

3.5 DISCUSSION

The mechanistic models formulated allowed to adequately describe the observed L-dopa and 3-OMD concentrations in absence and presence of benserazide. The adequacy of the model was corroborated by the fact that the parameter estimates of L-dopa and 3-OMD of the

compartmental analysis were similar to values obtained by non-compartmental analysis (Table 17).

TABLE 17: Comparison of PK parameters of L-dopa and 3-OMD estimated by compartmental analysis (CA) and by standard non-compartmental analysis (NCA)

Analyte	PK Parameter [Unit]	Estimate (NCA) ²	Estimate (CA) ^{1,2}
L-Dopa	V/F [L]	2.22	2.33
	CL/F [L/h]	3.72	3.88
	k [h ⁻¹] ³	1.73	1.66
3-OMD	V/F [L]	0.945	0.923
	CL/F [L/h]	0.0563	0.0563
	k [h ⁻¹] ³	0.0602	0.0611

¹ F = 0.212 (estimated from $F_G * F_H$). ² Calculations done with all significant figures. ³ k was estimated by linear regression analysis (NCA) and as a secondary parameter from CL/V (CA).

Furthermore, the model parameters were also in good agreement with values reported in the literature where available. The L-dopa volume of distribution and the L-dopa clearance of the present study expressed in units per kg body weight were V_{dopa} (1.98 L/kg) and CL_{dopa} (3.29 L/h/kg). Sato and co-workers^[153] estimated for L-dopa a volume of distribution ($V_{d\beta}$) of 1.79 L/kg and a clearance of 3.13 L/h/kg. Further L-dopa clearances reported in the literature were 4.46 L/h/kg^[155], 5.15 L/h/kg^[155], and 1.48 L/h^[163]. The bioavailability of L-dopa after L-dopa alone was estimated in the present study to be 21 %. This was in good accordance with work done by Iwamoto et al.^[155], where the bioavailability was 29 % for rats aged 9 weeks and 20 % for rats aged 11 weeks. The rats studied in the present study were between 10 and 12 weeks old.

In the compartmental model the bioavailability of L-dopa was the product of the gastrointestinal availability and the hepatic availability. The availability across the intestinal wall was introduced in addition to the hepatic availability because the gut wall contributes substantially to the overall first-pass effect of L-dopa^[155, 167, 168]. The gastric and intestinal walls are rich in AADC^[169-171]. This builds an efficient enzymatic barrier for the absorption of L-dopa. Although the liver has also high concentrations of AADC and quickly metabolizes L-dopa^[172], it seems to be a less important site of decarboxylation than the gut wall. Peripheral and hepatportal vein injections of L-dopa gave similar plasma concentrations^[163, 171, 173]. In addition, hepatectomy did not create major changes in the disposition of injected L-dopa^[174]. In the present study the gastrointestinal availability was 24 % and the hepatic

availability was 87 % after oral administration of L-dopa alone confirming that the gut is the major site of metabolism for L-dopa. After oral administration of L-dopa/benserazide the gastrointestinal availability was assumed to be 100 % while the hepatic availability changed dependent on the inhibition ($F_H \geq 87\%$).

The different magnitude of changes in L-dopa's oral clearance (9-fold) and half-life (2-fold) when the drug was given together with benserazide indicates that the change in CL/F is not only due to the decrease in systemic clearance of L-dopa when combined with benserazide, but also due to a change in the bioavailability of L-dopa. The fact that benserazide has a major effect on the bioavailability is also reflected in the almost 5-fold change in V/F between treatments. Benserazide affects gut wall AADC controlling the fraction absorbed while changes in systemic L-dopa clearance will be largely due to inhibition of AADC at sites other than the gut wall.

The absorption rate constant of L-dopa was higher after treatment with L-dopa alone than after L-dopa/benserazide. L-dopa is a large neutral amino acid (LNAA) and is absorbed via the saturable LNAA-system^[21, 22]. If L-dopa is administered together with benserazide, the metabolism of L-dopa to dopamine in the gut is inhibited. As a consequence higher amounts of L-dopa and 3-OMD, two competing substrates for the carrier^[21], are available for the transport than after administration of L-dopa alone. This competition determines the flux of each competing substrate across the membrane and may explain why we observed in the present study a slower absorption rate after L-dopa/benserazide than after L-dopa alone.

The between-animal variability was high for the L-dopa parameters C_{max} and T_{max} after L-dopa alone and for T_{max} and k_a after L-dopa/benserazide. Bredberg and co-workers^[154] made similar observations with regard to T_{max} and C_{max} after combined oral administration of L-dopa and carbidopa (another AADC inhibitor) and attributed this to factors influencing gastric emptying (e.g. diet, osmolality and pH of gastric content). They could show that the between-animal variability was significantly reduced after direct duodenal administration of L-dopa indicating that gastric emptying is an important source for this variability. These findings are in agreement with the marked inter-patient variability in T_{max} and C_{max} in humans after oral L-dopa administration^[175-179].

The terminal log-linear phase of 3-OMD after treatment with L-dopa alone and L-dopa/benserazide extended over 16 h to 20 h and was thus defined over less than 2 half-lives. Nevertheless, the elimination rate constant of 3-OMD could be estimated well by linear

regression; it was similar to the elimination rate constant obtained by compartmental analysis (Table 17) and from the literature ^[180].

Substantial effort was spent to fit models to the data after L-dopa alone and after L-dopa/benserazide keeping the 3-OMD clearance and the 3-OMD volume of distribution the same for both treatment groups. However, this resulted consistently in an underestimation of the 3-OMD plasma concentrations after L-dopa/benserazide and in a high estimation error for k_i . The fit became satisfactory only when allowing for different values for those two parameters in each treatment (the Akaike Information Criteria ^[68, 69] improved from 3868 to 3790). The fact that different values for clearance and volume of distribution had to be introduced for 3-OMD after treatment with L-dopa alone and with L-dopa/benserazide explains also the observed (using NCA) shorter half-life after L-dopa/benserazide and points to saturation in 3-OMD formation or elimination. In contrast to L-dopa, 3-OMD is a poor substrate for AADC ^[181]. Therefore, the possibility of benserazide inhibiting the metabolism of 3-OMD via AADC is judged to be small and does not explain the lower 3-OMD clearance after treatment with L-dopa/3-OMD.

In the present study the pharmacokinetics of benserazide and its metabolite Ro 04-5127 could be estimated in rats for the first time in some detail due to a newly available quantitative analytical method. The performance of the analytical assay (i.e. precision and bias) for benserazide and Ro 04-5127 as determined from quality control samples was better for the middle concentration than for the low and high concentrations for both analytes (Table 11). An explanation for this was not found.

Average curves of benserazide and its metabolite Ro 04-5127 look similar. However, this is an artifact of averaging concentrations. When plotting individual benserazide and associated Ro 04-5127 concentration-time profiles together, the metabolite peak was higher and occurred earlier than the benserazide peak. Furthermore, the metabolite Ro 04-5127 declined biphasically. This metabolite–parent compound pattern in the concentration-time profile is typical for drugs with a high extraction ratio where a substantial part of the parent compound is converted to metabolite during the absorption step ^[182, 183] and where the metabolite's elimination is formation-rate limited. In such a case, following an oral dose of drug the observed metabolite concentrations in plasma are the sum of metabolite concentrations from two sources: that formed during the absorption of the drug and that formed from absorbed drug. The decline of the metabolite formed during absorption is

determined by the elimination half-life of the metabolite, whereas the decline of metabolite formed from the absorbed drug is determined by the half-life of the drug, the rate limiting step. If most of the dose is converted to metabolite during the absorption of the drug the decline phase of the metabolite appears biphasic. This is the case for benserazide and its metabolite Ro 04-5127 where benserazide is substantially metabolized to Ro 04-5127 in the gut already. The terminal half-life of Ro 04-5127 (estimated by non-compartmental analysis) does not reflect the true elimination half-life of this metabolite.

The benserazide pharmacokinetics were described well by the benserazide/Ro 04-5127 model. The final benserazide parameters in the present study were in good agreement with values from a previous compartmental analysis. In that analysis intravenous data of benserazide of two previous studies ^[164, 165] had been fitted simultaneously to a standard 2-compartment model. The pharmacokinetic parameters of the present analysis compared to the previous analysis were CL_B : 1.67 L/h vs 1.62 L/h, V_{1B} : 0.202 L vs 0.186 L, V_{2B} : 0.127 L vs 0.115 L, and CL_{dB} : 0.0720 L/h vs 0.0685 L/h.

The benserazide parameters estimated by non-compartmental analysis were based on noisy data, where often only few points were available for parameter estimation. Still they were similar to estimates obtained by compartmental analysis where the data were pooled to increase the density of information (compartmental vs non-compartmental: CL/F : 76.0 L/h vs 70.8-95.4 L/h; F 2.2 % assumed for calculation of compartmental values).

The estimation of parameters for Ro 04-5127 was based on the four assumptions mentioned earlier (Chapter 3.3.4.2). Those assumptions did not influence the L-dopa/3-OMD parameters obtained. The benserazide/Ro 04-5127 model parameters adequately described the observed concentrations and were fixed when combining them with the L-dopa model. Knowledge on the fraction of benserazide metabolized to Ro 04-5127 resulted from the assumption that the total Ro 04-5127 blood clearance cannot be larger than the cardiac output in the rat (i.e. 110.4 ± 15.60 mL/min ^[184]). Thus the maximum value of f_m could be estimated from the total Ro 04-5127 clearance which was set to the cardiac output, the area under the plasma concentration-time curve of Ro 04-5127, and the benserazide dose. The f_m value used in our model, 15 %, was then arbitrarily chosen from the possible range 0-30 %. Further experiments will be needed to verify these assumptions and confirm the parameters estimated.

Benserazide is chemically a seryl-trihydroxybenzylhydrazine. In neutral, alkaline, or strongly acidic medium it is unstable ^[156]. In the body the seryl-moiety splits off enzymatically liberating trihydroxybenzylhydrazine (Ro 04-5127). In our compartmental model concentrations of Ro 04-5127 and not of benserazide itself were assumed to inhibit

AADC based on results by Burkard and co-workers [23]. The better fit with Ro 04-5127 as inhibitory moiety than with benserazide (the Akaike Information Criteria [68, 69] improved from 3793 to 3790) provides supportive evidence for this mechanism of action.

In the literature 2-compartment models are mostly found to describe the L-dopa pharmacokinetics. It is well known that L-dopa pharmacokinetics follow a biexponential decline after intravenous administration in rats, dogs and humans [19, 153-155, 173, 185]. The initial rapid decline of the L-dopa plasma concentration reflects its distribution from plasma to other tissues, primarily muscle [152, 186] as well as liver and kidney [187]. If L-dopa is administered orally the relatively rapid distribution phase is often masked by the simultaneous absorption of the drug [22, 151]. This was also seen in the present study where the initial distribution phase was not apparent after oral dosing. Therefore, a 1-compartment model was chosen to describe the L-dopa pharmacokinetics in the present study.

Given the study design of the present study, i.e. parallel treatment groups, and the limited data density, individual compartmental analysis was not a suitable option for modeling the drug-drug interaction between L-dopa and benserazide. It was decided to pool the data and to fit the model to all individual observations simultaneously (naïve-pooled-data approach). The disadvantage of pooling is a masking of the individual behavior and distortion of the model structure and parameter estimates. However, the profiles of individual animals given the same treatments had similar shapes and this encouraged the belief that pooling the data in order to explore model features that could not be defined by any one animal alone would not seriously affect our conclusions. This presumption was verified by performing a population PK analysis using nonlinear mixed effects modeling (see Chapter 5).

There are numerous descriptions of PK drug-drug interactions in the literature; they vary from qualitative versus quantitative and *in vitro* versus *in vivo* approaches. A PK drug-drug interaction can be described qualitatively. In this case the objective would be to answer the question of a possible occurrence of a PK drug-drug interaction with yes or no. However, this qualitative information is often not sufficient; there is frequently the need to quantify the PK drug-drug interaction. One approach to accomplish that is to estimate and compare PK parameters (e.g. $AUC_{0-\infty}$, C_{max}) of the investigational drug by non-compartmental analysis after separate administration with and without inhibitor. An alternative approach to quantify the interaction is to formulate a mathematical relationship describing the PK drug-drug

interaction taking into account the mechanism of the interaction (e.g. type of inhibition, enzymes involved, site of inhibition). In the present study both these quantitative approaches were applied. The non-compartmental analysis of drug-drug interaction did not necessitate knowledge about the mechanism of the interaction. Therefore, it was a useful tool to check for a potential bias any model could introduce and for initial quantification of the changes in $AUC_{0-\infty}$, C_{max} and CL/F caused by the interaction of L-dopa and benserazide. However, the limitation of this approach is that it gave no insight into the sequence and progression of events. Without applying a model the only conclusion from such considerations was that the decrease in CL/F led to higher exposure of L-dopa. In contrast, the compartmental model had the advantage of describing the temporal change of inhibition and the recovery of the enzyme. Thus a more explicit view could be gained of the events over time and of the cause for higher exposure of L-dopa and 3-OMD. PK parameters such as total L-dopa clearance, bioavailability of L-dopa, and fraction of L-dopa metabolized via COMT were allowed to change over time depending on the inhibitor concentration in plasma. The bioavailability of L-dopa increased from 21 % (L-dopa alone) to more than 87 % (L-dopa/benserazide). For some time after administration of benserazide the metabolic pathway via AADC was almost blocked after L-dopa/benserazide administration. The L-dopa clearance via AADC decreased within 5 minutes from 0.568 L/h to 0.00246 L/h and recovered only slowly over 24 hours (Figure 19). This had an influence on the total L-dopa clearance, which was reduced by 69 % within the first 5 minutes and recovered slowly over the next 24 hours. Those changes in bioavailability and total clearance resulted in a higher exposure of L-dopa. Due to the inhibition of the AADC pathway the fraction of L-dopa metabolized by COMT increased from 10 % to 31 % resulting in higher $AUC_{0-\infty}$ and C_{max} of 3-OMD. These temporal changes could not be described by non-compartmental analysis. Therefore, the PK drug-drug interaction described with modeling revealed more information about what happened when L-dopa and benserazide were administered together. Another advantage of describing the interaction with a model is that it allows simulations. Exploratory analyses can be performed to predict different scenarios such as consequences of multiple dosing or change in strength of dose. Modeling is a powerful tool to enhance the comprehension of the complex processes defining a PK drug-drug interaction and thus may also prove useful in drug development. However, the modeling approach requires a lot of information and, explicit assumptions on the drug behavior. Depending on the development stage of the drug this information is not always available. This could be a drawback for applying the modeling approach in early phases of drug development.

3.6 CONCLUSION

In conclusion, this study is the first investigation where the pharmacokinetics of benserazide and Ro 04-5127 have been described by a compartmental model facilitated by a newly developed analytical method to determine the chemically instable analytes. The L-dopa/benserazide model developed, based on the data collected, allowed a mechanism-based view of the PK interaction of L-dopa/benserazide and supports the hypothesis that Ro 04-5127 is the primary active principle of benserazide.

Chapter 4

PREDICTION OF HUMAN L-DOPA PHARMACOKINETICS AFTER L-DOPA TREATMENT WITH AND WITHOUT BENSERAZIDE FROM IN VIVO L-DOPA PHARMACOKINETICS IN RATS

Chapter 4

PREDICTION OF HUMAN L-DOPA PHARMACOKINETICS AFTER L-DOPA TREATMENT WITH AND WITHOUT BENSERAZIDE FROM IN VIVO L-DOPA PHARMACOKINETICS IN RATS

4.1 RATIONALE

4.1.1 Rationale for Prediction of Human In Vivo Pharmacokinetics from In Vivo Pharmacokinetics in Rats

In the field of drug-drug interactions the desirable objective is to be able to describe the drug-drug interaction quantitatively and to know if the interaction is likely to be of clinical relevance. As described in the introduction (Chapter 1.4) one way to achieve this is to use a mechanistic PK model. In a preclinical situation *in vivo* and/or *in vitro* data are used to build such a model. The results obtained from this modeling effort have then to be translated into the *in vivo* situation in humans using approaches such as the allometric method or PBPK models. A successful extrapolation of drug-drug interactions across species helps to plan safe and cost effective studies in humans. L-dopa with and without benserazide was chosen as an example to explore the power of mathematical modeling for interspecies PK scaling using the allometric approach.

4.1.2 Rationale for Protein Binding Study

An extrapolation of pharmacokinetic parameters of L-dopa and 3-OMD from rat to human is best based on unbound concentrations. The protein binding of L-dopa is known in humans [175, 188-190] and in dogs [191]. Also the protein binding of the metabolite 3-OMD had previously been determined in humans [188, 189] and in dogs [191]. However, no investigations have been performed so far to determine the plasma protein binding of L-dopa and its metabolite 3-OMD in rats. Therefore, the comparative *in vitro* binding of L-dopa and 3-OMD to plasma proteins in rats and humans was determined using the centrifugal ultrafiltration method.

4.2 OBJECTIVE

The objective was to investigate the predictability of human L-dopa pharmacokinetics after L-dopa treatment with and without benserazide from *in vivo* pharmacokinetics in rats using PK modeling, allometric scaling of PK parameters, and accounting for protein binding.

4.3 MATERIALS AND METHODS

4.3.1 Assessment of Plasma Protein Binding of L-Dopa and 3-OMD in Rats and Humans

Chemicals: To perform the experiment ^{14}C -labeled L-dopa (batch 50, code CFA439, Nycomed Amersham) and ^{14}C -labeled 3-OMD (Lot Nr. 19854B070.1DP, F. Hoffmann-La Roche Ltd) were used. The specific radioactivity of ^{14}C -labeled L-dopa was $50.8 \mu\text{Ci}/\text{mg}$ and the radiochemical purity was 98.9 %. The specific radioactivity of ^{14}C -labeled 3-OMD was $210 \mu\text{Ci}/\text{mg}$ and the radiochemical purity was 97.9 %. All other chemicals were of analytical grade.

Blood and plasma collection: Blood from healthy volunteers (HV) and from rats was collected following internal Roche guidelines ^[192], using EDTA as anticoagulant. As an additional stabilizer NaF was added to the blood. The plasma was pooled (human: dialyzed N = 1 HV, untreated N = 18 HV; rat: N = unknown)

Dialysis of blank plasma: Human plasma and rat plasma contain endogenous L-dopa and 3-OMD. Therefore, a batch of human plasma and a batch of rat plasma were dialyzed before use in order to remove endogenous L-dopa and 3-OMD. To dialyze the plasma 100 mL of plasma (rat or human) were placed into a tubular membrane (1 m in length, 25 mm flat width) which was washed before use with three portions of boiling water for about 10 minutes each. The tubular membrane was closed, was put into 5 L of 0.01 M phosphate buffer pH 7.5, and was stored for 16 hours at 4°C. After 8 hours the old buffer was replaced with new buffer to assure a quantitative removal of endogenous interferences.

Standard solutions: For the determination of the protein binding of L-dopa and 3-OMD the rat and human plasma samples (untreated or dialyzed) were spiked with ^{14}C -labeled drug (L-dopa or 3-OMD) to obtain concentrations ranging from $4 \mu\text{g}/\text{L}$ to $30000 \mu\text{g}/\text{L}$.

Centrifugal ultrafiltration: The determination of the *in vitro* binding of L-dopa and 3-OMD to plasma proteins was done by centrifugal ultrafiltration. The different plasma pools were brought where necessary to pH 7.3 with small amounts of 1N HCL, spiked with radiolabeled compound (^{14}C -labeled L-dopa or ^{14}C -labeled 3-OMD), covered with oxycarbon (only L-dopa samples) and equilibrated to 37°C for 15 minutes. This procedure was carried out in a fast sequential way to avoid a pH shift, which would occur over time. A 1.0 mL sample was subjected to centrifugal ultrafiltration in a micropartition system MPS (Centrifree[®], Order No. 4104, Amicon, Inc., Beverly, MA 01915 USA). The molecular weight cut off (MWCO) of the ultrafiltration membrane was 30000 Dalton. The sample was centrifuged for 9 minutes at 37°C with 1600xg in a fixed angle rotor centrifuge. The potential of non-specific adsorption of the free drug to the device, resulting in an overestimation of the binding, was measured by refiltering protein free ultrafiltrates containing ^{14}C -labeled drug and comparing the initial and final drug concentrations (recovery experiment).

Analytical methods: The concentration of ^{14}C -labeled drug (L-dopa or 3-OMD) was determined in ultrafiltrates (single determinations) and in plasma (duplicate determinations) by direct liquid scintillation counting.

The content of total protein and albumin in rat plasma and in human plasma and the content of α_1 -acid glycoprotein in human plasma were determined with the autoanalyzer Cobas[®] Mira (Roche Diagnostics System, F. Hoffmann-La Roche Ltd, Basel, Switzerland) by using the biuret method [193, 194], the modified bromcresol green method [195], and the immunoturbidimetric method [196].

Calculations: The unbound fraction of drug (f_u) and the percentages of unbound and bound drug were estimated by using Eq. 36 to Eq. 38 where C_{UF} and C_{Pi} were the concentrations in ultrafiltrate and in initial plasma, respectively.

$$\boxed{f_u = C_{UF} / C_{Pi}} \quad \text{Eq. 36}$$

$$\boxed{\%free = 100 * (C_{UF} / C_{Pi})} \quad \text{Eq. 37}$$

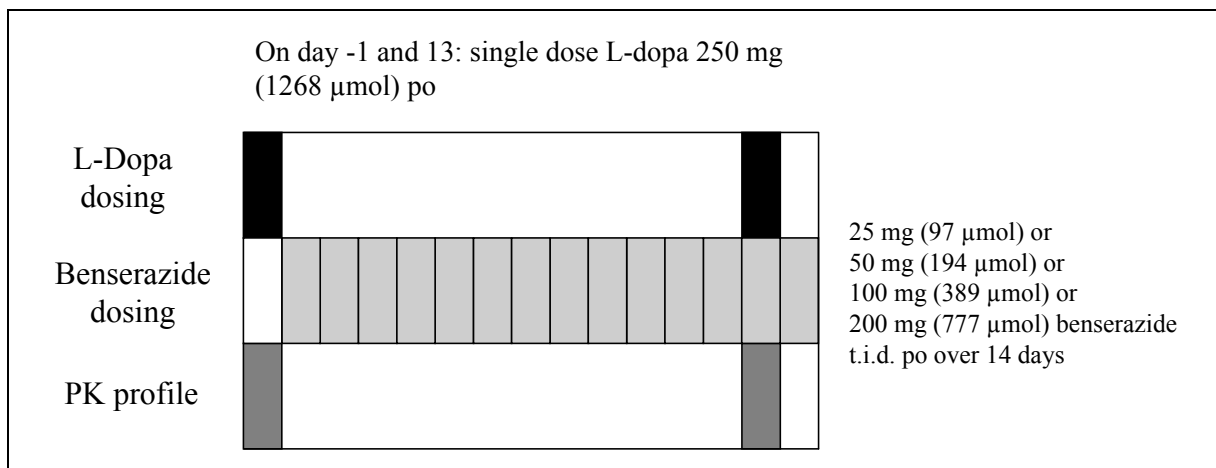
$$\boxed{\%bound = 100 - \%free} \quad \text{Eq. 38}$$

4.3.2 In Vivo Concentration-Time Data

Rat data: In a single dose parallel designed study male rats received the treatments, 20 mg/kg (78 $\mu\text{mol}/\text{kg}$) benserazide po or 80 mg/kg (406 $\mu\text{mol}/\text{kg}$) L-dopa po or 80 mg/kg L-dopa combined with 20 mg/kg benserazide po. Blood was collected for the determination of L-dopa, 3-OMD, benserazide, and Ro 04-5127. More details regarding this study are described in Chapter 3.3.2.

Human data: The usefulness of the developed PK model for predictions was evaluated using actual human concentration-time data of L-dopa and 3-OMD from a study performed at F. Hoffmann-La Roche Ltd [197]. The clinical study was an open label parallel group study in healthy male volunteers of 30-54 years of age (mean \pm SD: 42 ± 8 years) and having a body weight of 65-100 kg (mean \pm SD: 79 ± 10 kg). They were treated consecutively for periods of 14 days with benserazide at different dose levels. On days -1 and 13 of each period they received a single dose of 250 mg (1268 μmol) L-dopa. The data used in this evaluation included the benserazide doses 25 mg (97 μmol), 50 mg (194 μmol), 100 mg (389 μmol), and 200 mg (777 μmol). Blood was collected for the determination of L-dopa, 3-OMD, and 3,4-dihydroxyphenylacetic acid (DOPAC). The schedule of assessment of one treatment period is shown in Figure 22.

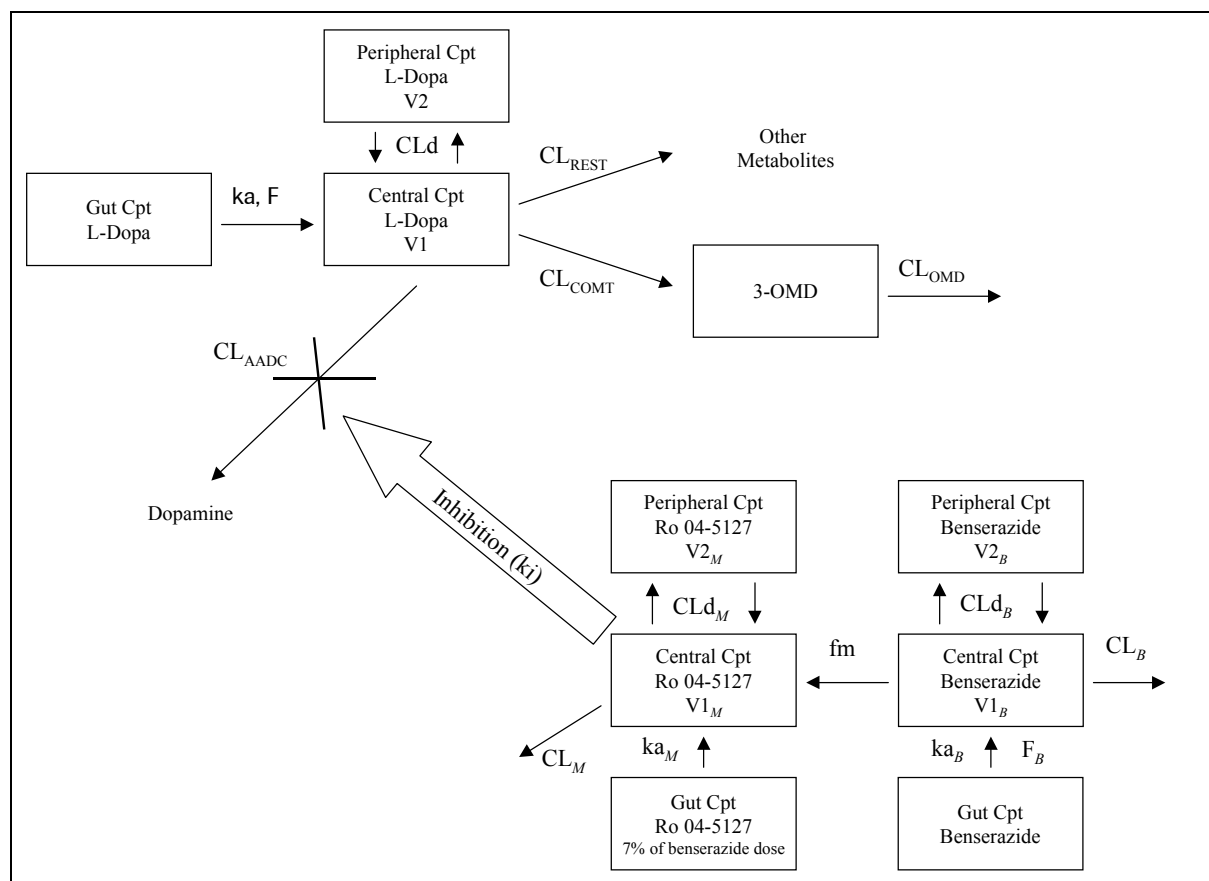
FIGURE 22: Schedule of assessment for 1 treatment period



4.3.3 Evaluation

4.3.3.1 PK Modeling and Simulation

FIGURE 23: Schematic representation of conceptual model describing the pharmacokinetics of L-dopa and 3-OMD with and without benserazide in humans



For abbreviations in Figure 23 see text and glossary of abbreviations.

The PK model shown in Figure 23 describes the PK interaction of L-dopa and benserazide in humans. This PK model was adapted from the PK model established in rats (Chapter 3) to account for differences in L-dopa PK between rats and humans. The only modification necessary was to change the 1-compartment model used for L-dopa in rats to a 2-compartment model for L-dopa in humans. L-dopa is known to follow in humans also after oral administration 2-compartment model characteristics [22], whereas in rats we observed after oral treatment 1-compartment model characteristics and only after iv treatment 2-compartment model characteristics.

The human PK parameters, used in the PK model (Figure 23), were derived from rat PK parameters using the allometric conversion shown in Eq. 39 (Chapter 4.3.3.2). All PK parameters in rats with exception of the 2-compartment model disposition parameters of L-dopa were obtained from the PK modeling described in Chapter 3. The L-dopa volume

terms (central and peripheral volume) and the intercompartmental clearance of L-dopa were obtained from an iv PK study in rats ^[153] from where 2-compartment disposition parameters could be derived.

The PK model was constructed in ModelMaker 3.0.4. (Cherwell Scientific, Ltd) to simulate expected human plasma concentrations of L-dopa and 3-OMD after L-dopa treatment with and without benserazide. The simulated concentrations were then compared with the actually observed concentrations.

4.3.3.2 Across Species Scaling

The estimated parameters were scaled from rat to human allometrically using Eq. 39.

$$P_{hu} = P_{rat} * \left(\frac{BW_{hu}}{BW_{rat}} \right)^a \quad \text{Eq. 39}$$

P_{hu}: PK parameter in humans, **P_{rat}**: PK parameter in rats, **BW_{hu}**: human body weight (79 kg), **BW_{rat}**: rat body weight (0.25 kg), **a**: exponent

The exponent, *a*, was 0.75 for clearance ^[198, 199] and 1.0 for volume terms ^[199]. Unbound clearance and unbound volume of distribution were used for interspecies scaling. The protein binding of L-dopa and 3-OMD in plasma was determined by centrifugal ultrafiltration. The protein binding of benserazide and Ro 04-5127 was not determined. However, due to the polarity of benserazide and Ro 04-5127 only a minor binding to plasma proteins is expected ^[200].

4.4 RESULTS

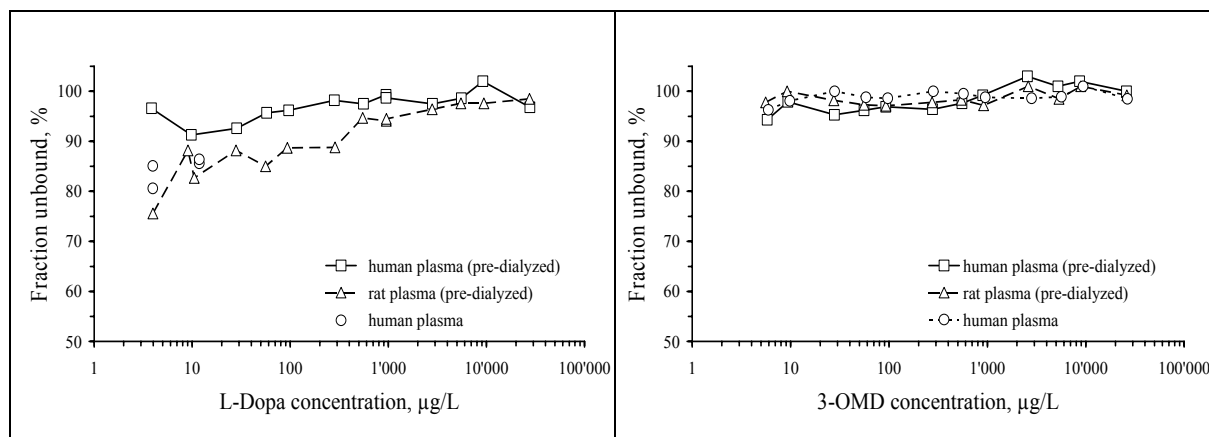
4.4.1 Plasma Protein Binding of L-Dopa and 3-OMD in Rats and Humans

Concentrations of total protein (tot. prot.), albumin (alb), and α_1 -acid glycoprotein (AGP) in the used plasma were within normal ranges (human dialyzed plasma: tot. prot. 59.7 g/L, alb 42.8 g/L, AGP 0.46 g/L; human plasma: tot. prot. 67.5 g/L, alb 49.9 g/L, AGP 0.64 g/L; rat dialyzed plasma: tot. prot. 48.8 g/L, alb 30.6 g/L).

Recovery experiments showed that the adsorption of L-dopa and 3-OMD to components of the ultrafiltration devices was negligible. The recovery was for L-dopa 96 % (CV 0.4 %, N=3) at a concentration of 35 μ g/L and for 3-OMD 98 % (CV 0.7 %, N=3) at a concentration of 14 μ g/L.

The results of the protein binding of L-dopa and 3-OMD in humans and rats are listed in Appendix C.5. Figure 24 shows the fraction unbound of L-dopa and 3-OMD in human and rat plasma over the studied concentration range of 4 $\mu\text{g/L}$ to 30000 $\mu\text{g/L}$.

FIGURE 24: Fraction unbound of L-dopa and 3-OMD in human and rat plasma



Overall the extent of binding of L-dopa and 3-OMD to human and rat plasma proteins was small. The protein binding of L-dopa in dialyzed human plasma was less than 9 % ($f_u > 0.91$) over the studied concentration range of 3.85 $\mu\text{g/L}$ to 27800 $\mu\text{g/L}$. In human plasma which was not dialyzed beforehand the extent of binding was with an average of 15.6 ± 2.6 % somewhat higher for the two studied concentration levels (3.97 $\mu\text{g/L}$ and 11.8 $\mu\text{g/L}$) than in dialyzed human plasma, but still in the low range. The protein binding of L-dopa in dialyzed rat plasma showed a concentration-dependent decrease of the binding starting at 24 % for low concentrations (3.98 $\mu\text{g/L}$) up to only 2 % for high concentrations (27500 $\mu\text{g/L}$).

The protein binding of 3-OMD in dialyzed human plasma was less than 6 % ($f_u > 0.94$) over the studied concentration of 5.79 $\mu\text{g/L}$ to 25900 $\mu\text{g/L}$, and in undialyzed human plasma less than 4 % ($f_u > 0.96$) over the studied concentration of 5.94 $\mu\text{g/L}$ to 26500 $\mu\text{g/L}$. The protein binding of 3-OMD in dialyzed rat plasma was less than 3 % ($f_u > 0.97$) over the studied concentration of 5.57 $\mu\text{g/L}$ to 26100 $\mu\text{g/L}$.

4.4.2 Across Species Scaling

The pharmacokinetic parameters for L-dopa, 3-OMD, benserazide, and Ro 04-5127 in rat, which were used for the allometric scaling, are listed in Table 18 and Table 19 together with the predicted pharmacokinetic parameters for humans.

TABLE 18: Pharmacokinetic parameters of L-dopa and 3-OMD in rats and as predicted by allometry (Eq. 39) in humans

Analyte	PK Parameter [Unit]	Treatment	Rat (BW 0.25 kg)	Human (BW 79 kg) predicted ^c
L-Dopa	V1 [L]	after L-dopa alone or L-dopa/benserazide	0.0522 ^b	16.5
	V2 [L]		0.222 ^b	70.0
	CL [L/h]		0.823	61.7
	CLd [L/h] ^a		0.884 ^b	66.3
	ka [h ⁻¹]	after L-dopa alone	2.11	2.11
	ka [h ⁻¹]	after L-dopa/benserazide	1.29	1.29
3-OMD	V [L]	after L-dopa alone	0.196	61.9
	V [L]	after L-dopa/benserazide	0.128	40.5
	CL [L/h]	after L-dopa alone	0.0120	0.897
	CL [L/h]	after L-dopa/benserazide	0.00895	0.671

^a intercompartmental clearance. ^b calculated using parameters reported by Sato et al. ^[153]. ^c calculations done with 4 significant figures.

TABLE 19: Pharmacokinetic parameters of benserazide and Ro 04-5127 in rats and as predicted by allometry (Eq. 39) in humans

Analyte	PK Parameter [Unit]	Treatment	Rat (BW 0.25 kg)	Human (BW 79 kg) predicted ^c
Benserazide	V1 _B [L]	after benserazide alone or L-dopa/benserazide	0.202	63.8
	V2 _B [L]		0.127	40.2
	CL _B [L/h]		1.67	125
	CLd _B [L/h] ^a		0.0720	5.39
	ka _B [h ⁻¹]		0.940	0.940
Ro 04-5127	V1 _M [L]	after benserazide alone or L-dopa/benserazide	0.0691	21.8
	V2 _M [L]		3.20	1012
	CL _M [L/h]		4.29	321
	CLd _M [L/h]		1.06	79.4
	ka _M [h ⁻¹]		2.47	2.47
Ro 04-5127	ki [μmol/L] ^b	after L-dopa/benserazide	0.00246	0.00246

^a intercompartmental clearance. ^b inhibition constant. ^c calculations done with 4 significant figures

Figure 25 and Figure 26 show the predicted (solid line) and observed (dashed lines) plasma concentration – time profiles of L-dopa and 3-OMD in humans after treatment with L-dopa with and without benserazide. The predictions of L-dopa in humans approximated the actually observed concentrations well after L-dopa (250 mg) and L-dopa (250 mg) + benserazide (25 mg – 200 mg). Only the predicted L-dopa concentrations at late time points were overestimated (see increasing deviation with increasing benserazide exposure in Figure 26) compared to the L-dopa concentrations of the observed individual curves (bias < 100 % after 25 mg, 50 mg, 100 mg benserazide; bias < 190 % after 200 mg benserazide). The predicted 3-OMD concentration-time curves showed a flatter disposition phase and underestimated the actual C_{max} . This was mainly due to the poor prediction of the volume of distribution of 3-OMD (V_{OMD}).

FIGURE 25: Predicted and observed plasma concentration – time profiles of L-dopa and 3-OMD in humans after treatment with L-dopa alone

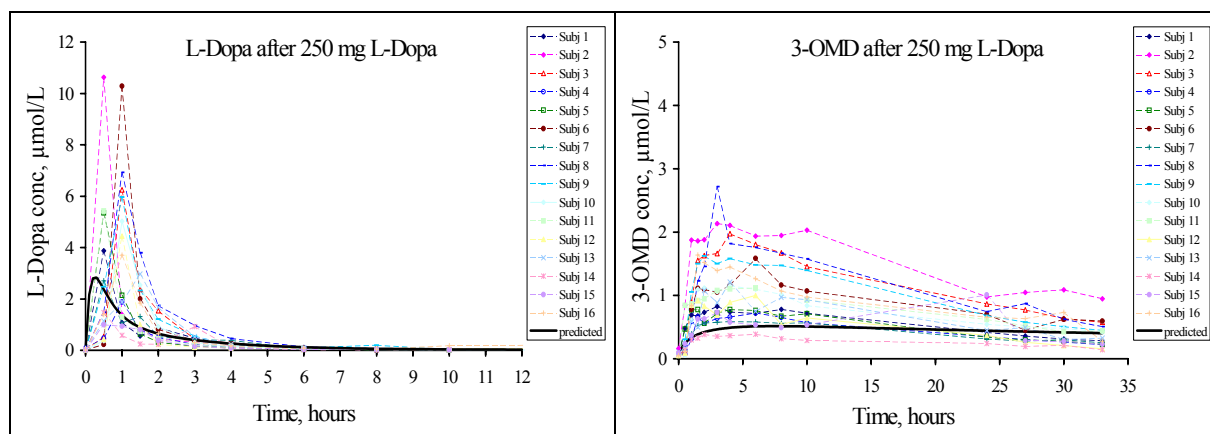
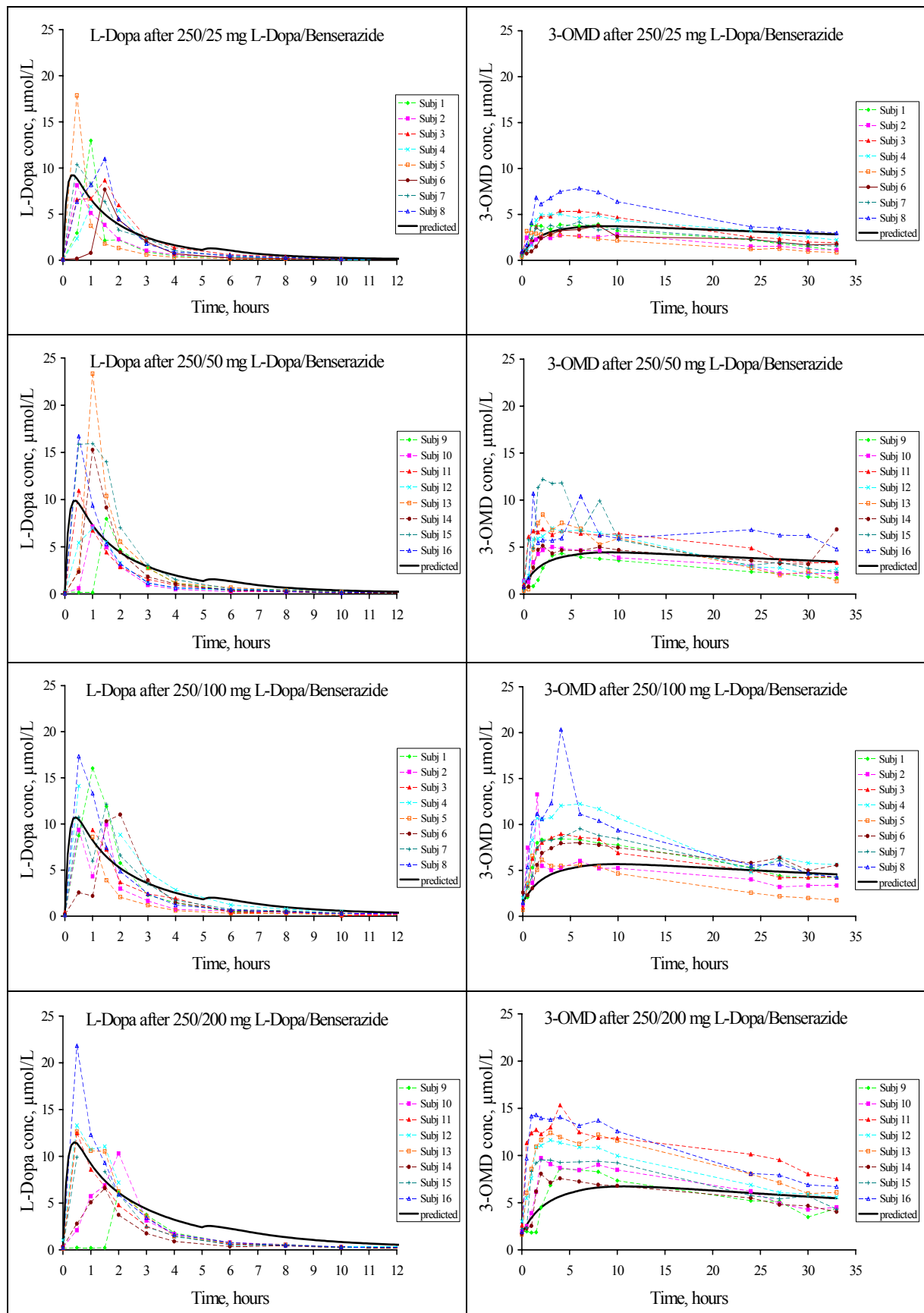


FIGURE 26: Predicted and observed plasma concentration – time profiles of L-dopa and 3-OMD in humans after treatment with L-dopa and benserazide



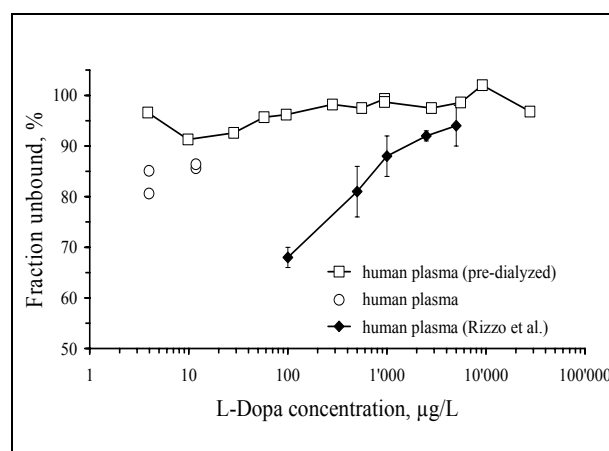
4.5 DISCUSSION

Protein binding of L-dopa and 3-OMD: Equilibrium dialysis and ultrafiltration are two *in vitro* methods, which are known to give accurate and precise assessments of the plasma protein binding provided due consideration is given to potential artifacts [136]. Due to the instability of L-dopa and 3-OMD in plasma [157], the ultrafiltration method was preferred over equilibrium dialysis. The only drawback of ultrafiltration is the potential for non-specific adsorption of free drug to the device resulting in an overestimation of the protein binding. However, recovery experiments showed that this was not the case for L-dopa and 3-OMD.

The concentration range chosen to study the protein binding of L-dopa and 3-OMD in rats and humans was 4-30000 $\mu\text{g/L}$. This covered the concentration range of L-dopa and 3-OMD observed in the study performed in rats, which was used to estimate the PK parameters in rats. This range also included the L-dopa and 3-OMD concentrations observed in the study performed in healthy volunteers, which was used to compare the predictions (maximum concentrations $< 25 \mu\text{mol/L}$ ($< 4930 \mu\text{g/L}$) for L-dopa and $< 21 \mu\text{mol/L}$ ($< 4436 \mu\text{g/L}$) for 3-OMD). A range of about 100-6000 $\mu\text{g/L}$ L-dopa is normally seen in patients with Parkinsonism receiving chronic treatment of L-dopa [177].

A concentration effect was seen for very low concentrations of L-dopa, with a resulting higher binding to protein. This effect was more pronounced in rat plasma than in human plasma. The protein binding results for L-dopa in human plasma of the present study are in good agreement with most sources in the literature [175, 189]. Compared to the values found in the present study Rizzo et al. [190] reported lower values for the fraction unbound of L-dopa in human plasma at low concentrations ($\leq 500 \mu\text{g/L}$) (Figure 27).

FIGURE 27: Comparison of protein binding results with literature data [190]



The discrepancy in the results shown in Figure 27 could be due to various reasons such as different sample handling, methodologies, analytical assays, or plasma. A hypothesis could be that the L-dopa binding to proteins is really higher at very low L-dopa concentrations (L-dopa < 500 $\mu\text{g/L}$ = < 2.5 $\mu\text{mol/L}$). This could mean that L-dopa binds to a specific protein at low concentrations other than albumin or α_1 -acid-glycoprotein. The molecular weight cut off (MWCO) of the ultrafiltration membrane used in the present experiment was 30000 Dalton. Rizzo et al. used a filter with a MWCO of 10000 Dalton. If this specific protein had a molecular weight between 10000 and 30000 Dalton it would not have been possible to detect the binding of L-dopa to this specific protein. However, in the range of therapeutic concentrations L-dopa was hardly bound in the present study as well as in the study performed by Rizzo et al.

3-OMD was almost completely unbound in human and rat plasma. This is in good agreement with protein binding data of 3-OMD in human plasma reported by Bennett et al. [189].

In the first run of the protein binding experiment the determinations for L-dopa were only done in dialyzed plasma. After comparing the results with those of Rizzo et al. it was decided to look also at untreated human plasma to investigate if dialysis might have had an influence, e.g. loss of proteins during dialysis through dilution or decomposition processes. For the 3-OMD *in vitro* protein binding study the untreated plasma was included from the beginning. This explains also why there is a full profile over the whole concentration for 3-OMD, but not so for L-dopa. L-Dopa bound a little more to protein in untreated human plasma compared to dialyzed human plasma. However, this effect was not seen with 3-OMD. Furthermore, the protein content was in the normal range for dialyzed plasma as well as for untreated plasma. This suggests that the dialysis process had no major impact on the protein binding results.

Dialysis was performed to remove endogenous L-dopa and 3-OMD from the plasma to prevent false results. However, given the low extent of binding it became clear from the results that the endogenous L-dopa and 3-OMD concentrations were too low to influence the protein binding results and therefore are negligible.

PK model /Across species scaling: The PK modeling coupled with allometric scaling of the rat PK parameters allowed us to predict the human L-dopa and 3-OMD plasma concentrations in absence and presence of benserazide. The fact that the predicted PK parameters of L-dopa and 3-OMD (with exception of 3-OMD V/F) were similar to values obtained by non-

compartmental analysis (Table 20) supported the approach to combine modeling with scaling techniques to predict human PK from rat. The only aberrant parameter was the volume term for 3-OMD: V/F observed in humans was about 40 % of the predicted one (Table 20).

TABLE 20: Comparison of predicted PK parameters with PK parameters estimated by standard non-compartmental analysis (NCA) in humans

Analyte	PK Parameter [Unit]	Human (BW 79 kg) predicted ^{f,g}	Human (BW 79 ± 10 kg) NCA ^h
L-Dopa	V/F [L]	738	722 ± 330
	CL/F [L/h]	291	283 ± 134
	T _{1/2} [h]	1.76	1.80 ± 0.354
3-OMD	V/F [L]	292	116 ± 65.8
	CL/F [L/h]	4.22	4.32 ± 1.80
	T _{1/2} [h]	48.0	18.3 ± 3.72

^f for comparison the predicted human PK parameters were divided by F. F was 0.212 (Chapter 3). ^g calculations done with all significant figures. ^h average ± SD

Furthermore, the predicted human PK parameters of L-dopa after administration of L-dopa alone were also in good agreement with values in the literature where reported. The predicted clearance of L-dopa in humans was 61.7 L/h. This was similar to L-dopa clearances reported in the literature which ranged between 45.9 L/h to 98.3 L/h^[185, 201, 202]. The predicted volume of distribution in humans was 16.5 L for V₁ and 70.0 L for V₂. The steady state volume of distribution (V_{SS}) that was estimated as the sum of V₁ and V₂, was therefore 86.5 L. This was in good accordance with V_{SS} values in the literature (66.7 L^[185], 115.5 L (young) and 130.4 L (elderly)^[202]). The predicted elimination half-life of L-dopa was 1.76 h and slightly higher than values found in the literature which ranged from 0.67 h^[185] to 1.33 h^[201].

The observed L-dopa plasma concentration-time data in humans showed a high inter-subject variability with regard to the L-dopa parameters C_{max} and T_{max} after L-dopa with and without benserazide. This is a well-known fact after oral administration of L-dopa and described in the literature^[175-179]. The variability in the absorption was not addressed in the PK model and in the predictions of human L-dopa PK. The absorption rate constant was a fixed value. Therefore, the predicted L-dopa concentrations did not describe the typical variability observed in the absorption phase, but gave only one possible solution.

The predicted 3-OMD concentration-time curves showed a flatter disposition phase and clearly underestimated actual C_{max}. While the oral clearance of 3-OMD was predicted

well (Table 20), the predicted 3-OMD elimination half-life was overestimated with a 3 times higher value than described in the literature ($T_{1/2} = 15 \text{ h}$ [203], and estimated by NCA ($T_{1/2} = 18 \text{ h}$, (Table 20)). The course of the plasma concentration-time curve of 3-OMD as well as the overestimation of the elimination half-life was mainly due to the poor prediction of the volume of distribution of 3-OMD (V_{OMD}). The predicted 3-OMD concentration-time profiles were improved, if the observed V_{OMD} was used instead of the predicted. A reason for this discrepancy between observed and predicted volume of distribution could be a species difference in protein binding or tissue binding. The first possibility was excluded based on the results of the protein binding study.

The set of parameters for Ro 04-5127 in rats gave an adequate description of the observations, but they are based on a multitude of assumptions described in Chapter 3.3.4.2 and discussed in Chapter 3.5. Whatever limitations apply to these assumptions will apply also to the parameters predicted for Ro 04-5127 in humans (Table 19).

The predictability of human L-dopa pharmacokinetics after L-dopa treatment with and without benserazide from *in vivo* pharmacokinetics in rats was investigated in a retrospective manner. The data in humans were already available at the time of the present predictions and thus could be used to evaluate the approach to combine PK modeling with allometric scaling. A prospective use of such methods predicting human pharmacokinetics from *in vivo* preclinical data is the ultimate goal to allow better planning of studies in humans. An advantage will be that exploratory analyses can be performed such as simulation of the PK at different doses. In the area of drug-drug interactions there is a need to quantify the interaction and to predict the situation in humans. Therefore, the successful modeling of the beneficial PK drug-drug interaction, L-dopa + benserazide, in rats and the prediction of human L-dopa pharmacokinetics based on this model is an encouraging contribution to achieve this goal.

4.6 CONCLUSION

L-dopa and 3-OMD are practically in an unbound state in human and rat plasma. The PK model established in rats combined with allometric scaling was found useful and successful in predicting and describing the L-dopa pharmacokinetics in humans after L-dopa treatment with and without benserazide.

Chapter 5

NONLINEAR MIXED EFFECTS MODELING

Chapter 5

NONLINEAR MIXED EFFECTS MODELING

5.1 RATIONALE

Given the parallel study design of the experiment in rats and the limited data density, individual compartmental analyses was not suitable for modeling the drug-drug interaction L-dopa/benserazide. In the model described in Chapter 3 the data was pooled and the model was fit to all individual observations simultaneously, i.e. by the naïve-pooled-data approach. The disadvantage of pooling is a masking of the individual behavior and potential distortion of the model structure and parameter estimates. However, the profiles of individual animals given the same treatments had similar shapes and this was considered to justify the view that pooling the data in order to explore model features that could not be defined by any one animal alone might not seriously affect conclusions. This presumption can be and was indeed verified by performing a population PK analysis using nonlinear mixed effects modeling.

5.2 OBJECTIVE

The objective was to investigate whether the naïve pooling of data as applied to define the PK of L-dopa/3-OMD with and without benserazide in rats (Chapter 3) had lead to potential distortion of the model structure and parameter estimates. This was done by repeating the compartmental analysis using nonlinear mixed effects modeling as a method for population analysis.

5.3 MATERIALS AND METHODS

The modeling was done in three steps using the software program NONMEM:

- * Step 1: Model L-dopa/3-OMD after administration of L-dopa alone.
- * Step 2: Model benserazide/Ro 04-5127 after administration of benserazide alone.
- * Step 3: Model the drug-drug interaction L-dopa/benserazide.

Each model was run with the two estimation methods, the first order method and the first order conditional estimation method (in combination with the specification: INTERACTION). For residual variability estimation three error models were tested, i.e. the additive error model, the proportional error model, and the combination of the two. In some instances it was necessary to fix random effects parameters. To discriminate between the

models the objective function was used in combination with graphical tools for goodness-of-fit.

5.3.1 Experimental Data

The data used for the nonlinear mixed effects analysis was exactly the same as used for the modeling in Chapter 3.

5.3.2 Pharmacokinetic Analysis

The population PK model employed in this analysis consists of three basic components:

- * The structural PK model component, which describes the plasma concentration-time profiles of L-dopa, 3-OMD, benserazide, or Ro 04-5127 in terms of PK parameters.
- * The inter-individual error model component, which describes the inter-individual variation in PK parameters.
- * The residual error model component, which describes the distribution of the error in the measured PK variable.

This population PK model did not include an inter-occasion variability component (i.e. a description of the variation of PK parameters within an individual) because each treatment was only studied once per animal. It also did not include a covariate model component (i.e. a description of the relationship between covariates (e.g. body weight) and PK parameters) because animals were of similar age and weight.

5.3.2.1 Structural Pharmacokinetic Models

In order to be able to compare the two population analysis methods, the PK models for L-dopa/3-OMD and benserazide/Ro 04-5127 were the same as described in Chapter 3. For further details such as conceptual models and equations see Chapter 3. The PK models described in Chapter 3 were implemented in the software NONMEM using the PREDPP subroutine ADVAN6.

The PK model for L-dopa/3-OMD after administration of L-dopa alone was parameterized using the volume of distribution of L-dopa (V_{dopa}), the clearance of L-dopa (CL_{dopa}), the volume of distribution of 3-OMD after L-dopa alone ($V_{\text{OMD,b}}$), and the clearance of 3-OMD after L-dopa alone ($CL_{\text{OMD,b}}$). The PK model for benserazide/Ro 04-5127 after administration of benserazide alone was parameterized using volume of distribution of the

central compartment ($V1_B$), volume of distribution of the peripheral compartment ($V2_B$), clearance (CL_B), intercompartmental clearance (CL_{d_B}), and absorption rate constant (ka_B) for benserazide, and volume of distribution of the central compartment ($V1_M$), volume of distribution of the peripheral compartment ($V2_M$), intercompartmental clearance (CL_{d_M}), and absorption rate constant (ka_M) for Ro 04-5127. The PK model describing the drug-drug interaction L-dopa/benserazide had, in addition to the above mentioned parameters, three newly introduced parameters, specifically: the inhibition constant (ki), volume of distribution of 3-OMD after L-dopa/benserazide ($V_{OMD,c}$), and clearance of 3-OMD after L-dopa/benserazide ($CL_{OMD,c}$). Only these three parameters were estimated. The other parameters were fixed to the values which were obtained with the PK model for L-dopa/3-OMD after administration of L-dopa alone and the PK model for benserazide/Ro 04-5127 after administration of benserazide alone. The reason for fixing the parameters was to have, in a first step, the same conditions as applied during the modeling in Chapter 3. In the event of successful modeling all parameters were to be estimated.

5.3.2.2 Statistical Models (Random Effects Models)

Model for inter-individual variability: The differences between individuals on a PK parameter are regarded as random quantities and were modeled in terms of random variables (η). Each η variable is assumed to have a mean equal to zero and a variance (ω^2) to be estimated. The inter-individual variability on the parameters was modeled by an exponential equation (Eq. 40),

$$\boxed{P_j = \theta * \exp(\eta_j)} \quad \eta_j \sim N(0, \omega^2) \quad \text{Eq. 40}$$

where θ is the population value for the parameter P , and P_j its value for the j^{th} individual. The magnitude of the inter-individual variability on a parameter is expressed as a coefficient of variation.

Models for residual variability (residual error): The differences between the observed plasma concentrations and the predicted plasma concentrations are regarded as random quantities and were modeled in terms of random variables (ϵ). Each ϵ variable is assumed to have a mean equal to zero and a variance (σ^2) to be estimated.

Three different error models were tested in NONMEM to model the residual variability:

1. The **additive error model**, where the variance is constant,

$$C_{ij} = \hat{C}_{ij} + \varepsilon_{ij} \quad \varepsilon_{ij} \sim N(0, \sigma^2) \quad \text{Eq. 41}$$

2. The **proportional error model** is also called the constant coefficient of variation error model, where the variance is proportional to the squared prediction,

$$C_{ij} = \hat{C}_{ij} * (1 + \varepsilon_{ij}) \quad \varepsilon_{ij} \sim N(0, \sigma^2) \quad \text{Eq. 42}$$

3. The **combination of additive and proportional error model**,

$$C_{ij} = \hat{C}_{ij} * (1 + \varepsilon_{1ij}) + \varepsilon_{2ij} \quad \varepsilon_{1ij} \sim N(0, \sigma_1^2) \quad \varepsilon_{2ij} \sim N(0, \sigma_2^2) \quad \text{Eq. 43}$$

where C_{ij} is the i^{th} value observed in the j^{th} individual, \hat{C}_{ij} is the i^{th} value predicted in the j^{th} individual using the PK model, and ε_{ij} , ε_{1ij} , ε_{2ij} are random variables which represent the discrepancy between C_{ij} and \hat{C}_{ij} . The magnitude of the residual variability is expressed as a standard deviation (unit: concentration) in the additive model and as a coefficient of variation in the proportional model.

Preliminary analyses looking at the objective function, the estimation error of the parameter estimates as well as the pattern of residuals showed that the residual variability was best described using the combined additive and proportional error model (Eq. 43). The statistical models for the residual error used in the final NONMEM runs are listed in Table 21.

TABLE 21: Statistical models for residual error

PK Model	Statistical model for residual error
L-Dopa/3-OMD after administration of L-dopa alone and L-Dopa/3-OMD after administration of L-dopa/benserazide (drug-drug interaction L-dopa/benserazide)	Proportional + additive error (Eq. 43). For L-dopa the additive error variance was fixed to 0.004311^2 which is the squared BLQ value of L-dopa in $\mu\text{mol/L}$. For 3-OMD the additive error variance was fixed to 0.004024^2 which is the squared BLQ value of 3-OMD in $\mu\text{mol/L}$.
Benserazide/Ro 04-5127 after administration of benserazide alone	Proportional + additive error (Eq. 43). For benserazide the additive error variance was fixed to 0.000777^2 which is the squared BLQ value of benserazide in $\mu\text{mol/L}$. For Ro 04-5127 the additive error variance was fixed to 0.001175^2 which is the squared BLQ value of Ro 04 5127 in $\mu\text{mol/L}$.

5.3.2.3 Model Selection Criteria

The structural models were combined with different residual error models and with different estimation methods, i.e. first order (FO) and first order with conditional estimation (FOCE), to identify the most appropriate mixed-effects model. Model selection as an important part of the data analysis process was performed using plots of weighted residuals, precision of the parameter estimate and comparison of the objective function values, which are part of the NONMEM output. The criteria for accepting the NONMEM model estimation as the final run include the following:

- * A successful minimization statement by the NONMEM program.
- * The number of significant digits should preferably be ≥ 3 for all θ 's (also a criterion for successful termination). If the number of significant digits is < 3 , reasons will be given for acceptance of the NONMEM run in the final report.
- * Estimates of θ 's should preferably not be close to a boundary.
- * The standard error of population parameters (θ , ω^2 , and σ^2) should preferably be less than the estimate itself.
- * The mean of individual η 's is supposed to be 0.
- * No unacceptable trends in the basic goodness of fit plots.

The goodness of fit plots are the following:

- * Predicted data versus observed data to check the quality of fit. Data will be predicted for the population (PRED, $\eta = 0$) and for each individual (IPRED, η).
- * Residuals versus time and versus predicted data (PRED and IPRED) to check within-individual structural model.

5.3.2.4 Integration and Optimization

The integration algorithm was a 4th order Runge–Kutta method. The fixed and random effects parameters for the population, i.e. θ , ω^2 , and σ^2 , were evaluated by minimizing the objective function (extended least squares) using first-order (FO) as well as first-order conditional estimation (FOCE) methods in NONMEM (Table 22). The FOCE algorithm was always used in combination with the specification INTERACTION. By doing so the dependence on η 's of the variance of the intra-individual random error was preserved in the computation of the objective function i.e. the η - ε interaction was taken into account.

TABLE 22: Estimation methods

Name of Algorithm	Coding \$ESTIMATION record	Description
FO (first order algorithm)	METHOD = 0 or ZERO	Always set η 's to 0 during the computation of the objective function.
FOCE (first order conditional estimation algorithm)	METHOD = 1 or CONDITIONAL	Use conditional estimates for the η 's during the computation of the objective function.

5.3.3 Software

Data analysis was performed by means of nonlinear mixed effects modeling using the software program NONMEM version V level 1.1 installed on the workstation Compaq Deskpro EN PIII 800 MHz. The Compaq's Visual Fortran Compiler V6.0 was used with the compiler options `op=/optimize:1 /fpe:0`. Data input and data retrieval (pre- and post-processing) was facilitated using specially developed SAS programs (SAS version 8.2 under Windows NT 4.0).

5.4 RESULTS

5.4.1 L-Dopa/3-OMD after Administration of L-Dopa Alone

The estimation method FOCE combined with the specification INTERACTION provided the best fit. The parameter estimates from this run are summarized in Table 23 and are listed in greater detail in Appendix D.1. The minimization was successful with an objective function of 94 (number of significant digits: 3.3). Figure 28 shows observed and predicted concentration versus time plots for L-dopa and 3-OMD. The prediction for the individual rats (IPRED) as well as the prediction for the population (PRED) is shown. The model fits described the observed data (DV) up to 6 hours well for L-dopa. For later time points it appears as if the predicted concentrations were underestimated. An explanation for this is detailed in the discussion (Chapter 5.4.4). The model fits described the observed data (DV) well for 3-OMD.

TABLE 23: Population PK parameters, inter-individual variability and residual error for L-dopa and 3-OMD after L-dopa alone

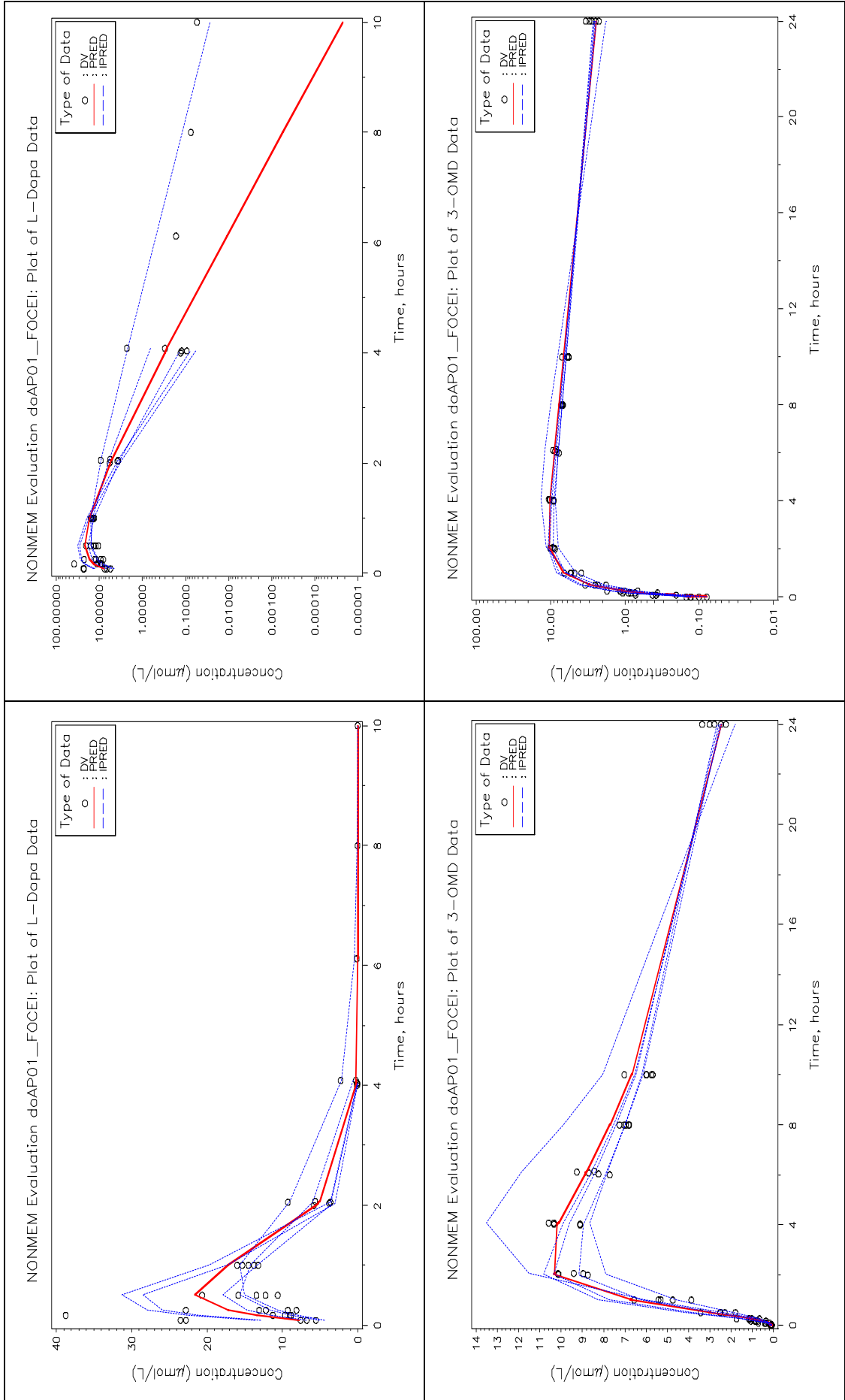
Analyte	PK Parameter [Unit]	Estimate	CV%	IIV [%]
L-Dopa	V_{dopa} [L]	0.426	26	52
	CL_{dopa} [L/h]	0.685	10	18
3-OMD	$V_{\text{OMD,b}}$ [L]	0.177	10	23
	$CL_{\text{OMD,b}}$ [L/h] *	0.0126	2	-

Additive residual error of L-dopa: 0.00436 $\mu\text{mol/L}$
 Proportional residual error of L-dopa: 46 %

Additive residual error of 3-OMD: 0.00400 $\mu\text{mol/L}$
 Proportional residual error of 3-OMD: 28 %

CV%: derived from asymptotic standard error of estimate, **IIV:** inter-individual variability, *: the estimated variance for η of $CL_{\text{OMD,b}}$ was very small and therefore was fixed in the final run to zero.

FIGURE 28: Predicted and observed plasma concentrations of L-dopa and 3-OMD after administration of L-dopa alone



5.4.2 Benserazide/Ro 04-5127 after Administration of Benserazide Alone

The estimation method FOCE combined with the specification INTERACTION provided the best fit. The parameter estimates from this run are summarized in Table 24 and are listed in greater detail in Appendix D.2. The minimization was successful with an objective function of -1355 (number of significant digits: 3.1). Figure 29 and Figure 30 show observed and predicted concentration versus time plots for benserazide and Ro 04-5127 after intravenous and oral administration of benserazide. The prediction for the individual rats (IPRED) as well as the prediction for the population (PRED) is shown. The model fits described the observed data (DV) well.

TABLE 24: Population PK parameters, inter-individual variability and residual error for benserazide and Ro 04-5127 after benserazide alone

Analyte	PK Parameter [Unit]	Estimate	CV%	IIV [%]
Benserazide	V _{1B} [L]	0.185	19	64
	V _{2B} [L] **	0.113	7	-
	CL _B [L/h]	1.55	8	31
	CLd _B [L/h] *	0.0691	9	-
	ka _B [h ⁻¹]	0.713	13	45
Ro 04-5127	V _{1M} [L]	0.0717	9	30
	V _{2M} [L]	1.93	90	70
	CLd _M [L/h] ***	1.25	76	-
	ka _M [h ⁻¹]	1.92	27	87

Additive residual error of benserazide: 0.000777 µmol/L

Proportional residual error of benserazide: 26 %

Additive residual error of Ro 04-5127: 0.001175 µmol/L

Proportional residual error of Ro 04-5127: 45 %

CV%: derived from asymptotic standard error of estimate, **IIV:** inter-individual variability, *: the variance for η of CLd_B was fixed to zero, **: the estimated variance for η of V_{2B} was very small and therefore was fixed in the final run to zero, ***: the variance for η of CLd_M was fixed to zero.

FIGURE 29: Predicted and observed plasma concentrations of benserazide after intravenous and oral administration of benserazide

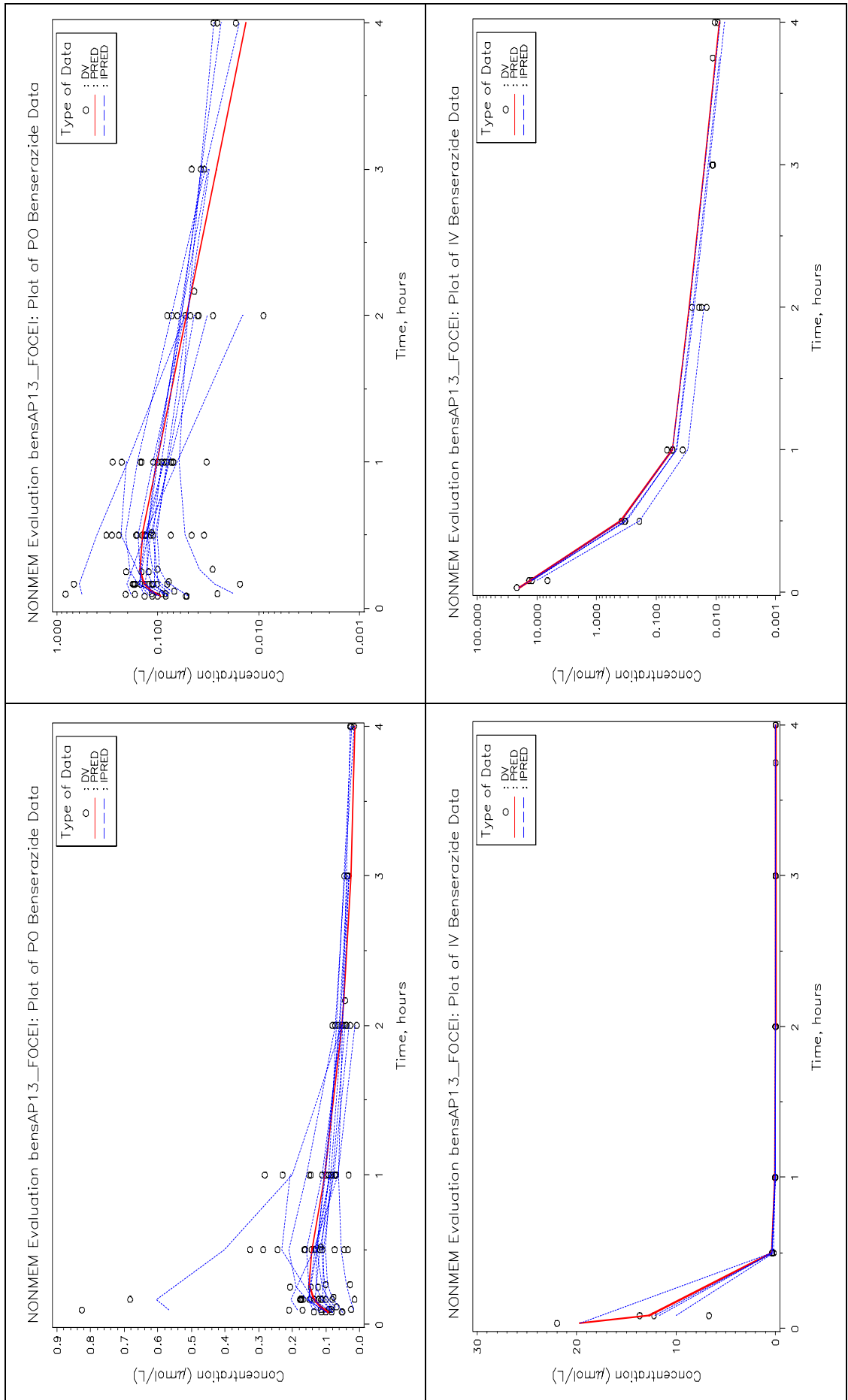
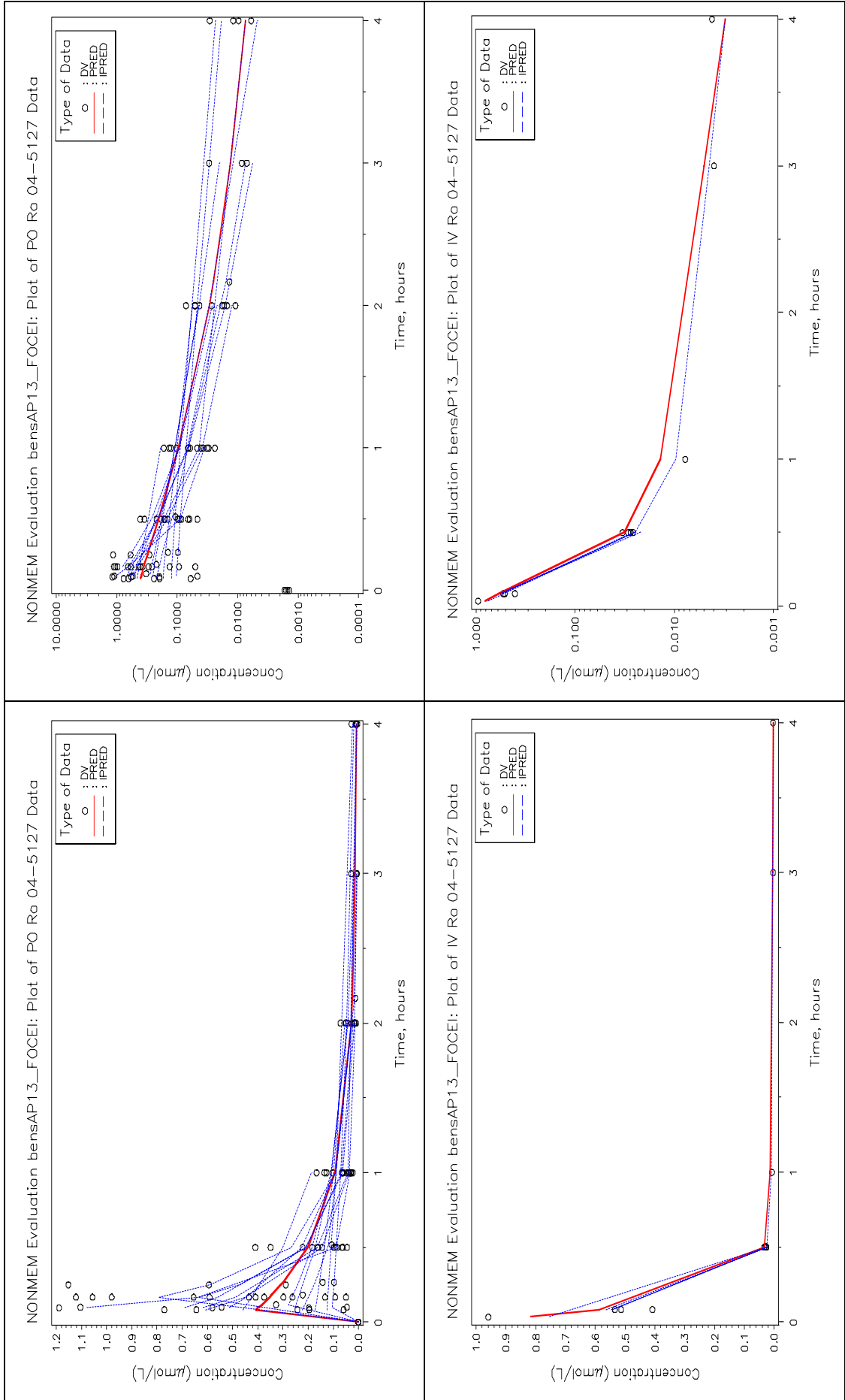


FIGURE 30: Predicted and observed plasma concentrations of Ro 04-5127 after intravenous and oral administration of benserazide



5.4.3 Drug-Drug Interaction L-Dopa/Benserazide

A number of NONMEM runs were set up for the model describing plasma concentrations of L-dopa and 3-OMD in presence of benserazide. However, none provided conclusive results. Non-convergence was the most frequent reason for lack of success. The run listed below shows an example of the various runs tested. The parameter estimates of this run are summarized in Table 25 and are listed in greater detail in Appendix D.3. There were estimation problems. While the minimization ran successfully with an objective function of 3392 (number of significant digits: 3.1), the covariance step aborted. Therefore, it was not possible to calculate the estimation error. Figure 31 shows observed and predicted concentration versus time plots for L-dopa and 3-OMD after treatment with L-dopa/benserazide. The prediction for the individual rats (IPRED) as well as the prediction for the population (PRED) are shown. The model fits described the observed data (DV) of L-dopa well whereas for 3-OMD the individual predictions as well as the population prediction were clearly overestimated.

TABLE 25: Population PK parameters, inter-individual variability and residual error

PK Parameter [Unit]	Estimate	CV%*	IIV [%]
$V_{\text{OMD},c}$ [L]	0.0363	-	23
$CL_{\text{OMD},c}$ [L/h] §	0.00591	-	-
k_i [$\mu\text{mol/L}$] #	0.000856	-	-

Additive residual error of L-dopa: 0.00436 $\mu\text{mol/L}$

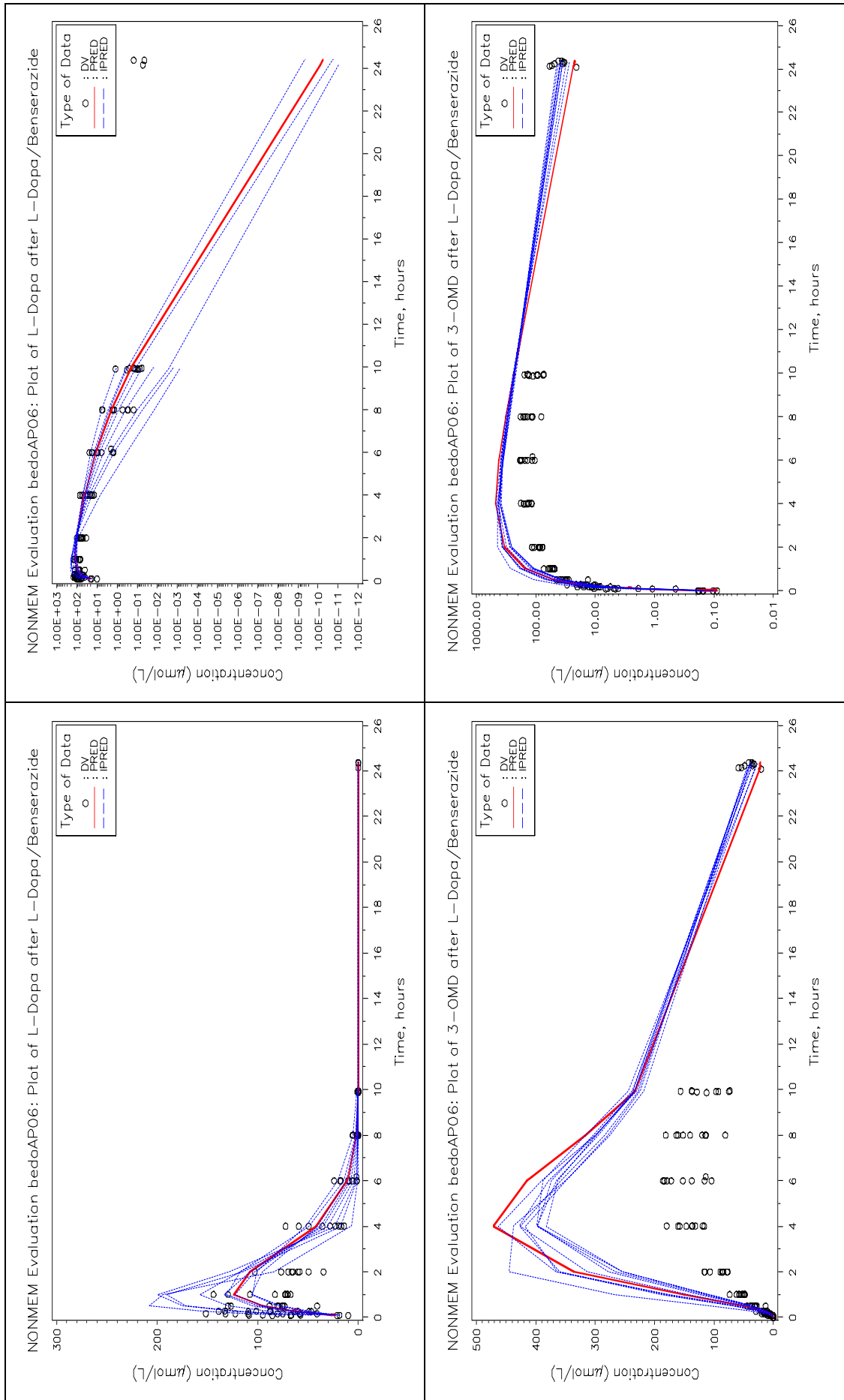
Proportional residual error of L-dopa: 88 %

Additive residual error of 3-OMD: 0.00400 $\mu\text{mol/L}$

Proportional residual error of 3-OMD: 63 %

CV%: derived from asymptotic standard error of estimate, **IIV:** inter-individual variability, *****: no estimation error could be estimated because the covariance step aborted, **§:** the estimated variance for η of $CL_{\text{OMD},c}$ was fixed to zero, **#:** the variance for η of k_i was fixed to zero.

FIGURE 31: Predicted and observed plasma concentrations of L-dopa and 3-OMD after L-dopa/benserazide and 3-OMD after L-dopa/benserazide model)



5.4.4 Comparison of PK Parameters

The final parameter estimates obtained by nonlinear mixed effects modeling were compared to those obtained in Chapter 3 where the naïve-pooled-data approach was applied. The parameter estimates for L-dopa, 3-OMD, benserazide, and Ro 04-5127 after treatment with L-dopa alone and benserazide alone were comparable (Table 26 and Table 27).

TABLE 26: Comparison of PK parameters of L-dopa and 3-OMD after administration of L-dopa alone using two different methods for population PK analysis

Analyte	PK Parameter [Unit]	Estimate (CV%)		Ratio
		NPD	NONMEM	NONMEM/NPD
L-Dopa	V_{dopa} [L]	0.496 (9 %)	0.426 (26 %)	0.86
	CL_{dopa} [L/h]	0.823 (9 %)	0.685 (10 %)	0.83
3-OMD	$V_{\text{OMD,b}}$ [L]	0.196 (13 %)	0.177 (10 %)	0.90
	$CL_{\text{OMD,b}}$ [L/h]	0.0120 (27 %)	0.0126 (2 %)	1.05

CV%: derived from asymptotic standard error of estimate, NPD: naïve-pooled data

TABLE 27: Comparison of PK parameters of benserazide and Ro 04-5127 after administration of benserazide alone using two different methods for population analysis

Analyte	PK Parameter [Unit]	Estimate (CV%)		Ratio
		NPD	NONMEM	NONMEM/NPD
Benserazide	CL_B [L/h]	1.67 (4 %)	1.55 (8 %)	0.93
	$V1_B$ [L]	0.202 (6 %)	0.185 (19 %)	0.92
	$V2_B$ [L]	0.127 (13 %)	0.113 (7 %)	0.89
	CL_{dB} [L/h]	0.0720 (9 %)	0.0691 (9 %)	0.96
	ka_B [h ⁻¹]	0.940 (27 %)	0.713 (13 %)	0.76
Ro 04-5127	CL_M [L/h]	4.29 (11 %)	NC	
	$V1_M$ [L]	0.0691 (11 %)	0.0717 (9 %)	1.04
	$V2_M$ [L]	3.20 (49 %)	1.93 (80 %)	0.60
	CL_{dM} [L/h]	1.06 (5 %)	1.25 (74 %)	1.18
	ka_M [h ⁻¹]	2.47 (17 %)	1.92 (28 %)	0.78

CV%: derived from asymptotic standard error of estimate, NC: not calculated, NPD: naïve-pooled data

The parameter estimates for the inhibition constant (k_i), the volume of distribution of 3-OMD after L-dopa/benserazide ($V_{\text{OMD,c}}$), and the 3-OMD clearance after L-dopa/benserazide

($CL_{\text{OMD},c}$) were 65 %, 72 %, and 34 % smaller compared to the results obtained with the naïve-pooled data approach (Table 28).

TABLE 28: Comparison of PK parameters after administration of L-dopa/benserazide using two different methods for population PK analysis

Analyte	PK Parameter [Unit]	Estimate (CV%)		Ratio
		NPD	NONMEM	NONMEM/NPD
3-OMD	$V_{\text{OMD},c}$ [L]	0.128 (5 %)	0.0363	0.28
	$CL_{\text{OMD},c}$ [L/h]	0.00895 (11 %)	0.00591	0.66
Ro 04-5127	k_i [$\mu\text{mol/L}$]	0.00246 (42 %)	0.000856	0.35

CV%: derived from asymptotic standard error of estimate, NPD: naïve-pooled data

5.5 DISCUSSION

The population PK analysis using nonlinear mixed effects modeling was successfully applied to describe the L-dopa/3-OMD PK after L-dopa alone and the benserazide/Ro 04-5127 PK after benserazide alone. The final parameter estimates for L-dopa, 3-OMD, benserazide, and Ro 04-5127 after L-dopa alone and benserazide alone obtained by nonlinear mixed effects modeling were comparable to those obtained in Chapter 3 where the naïve-pooled-data approach had been applied. While for treatment with L-dopa alone and benserazide alone, the respective models were fitted successfully to the data using nonlinear mixed effects modeling, the results from fitting the drug interaction model to L-dopa and 3-OMD data after treatment with combined L-dopa/benserazide were inconclusive. There were estimation problems, i.e. the covariance step aborted and no covariance matrix and correlation matrix could be estimated. Moreover, the predicted concentrations of 3-OMD (individual and population) after L-dopa/benserazide treatment were overestimated considerably. The parameter estimates for the inhibition constant, the volume of distribution of 3-OMD after L-dopa/benserazide, and the 3-OMD clearance after L-dopa/benserazide differed from the results obtained with the naïve-pooled data approach. Because the estimation error could not be estimated, no statement about the precision of these parameters can be made.

By performing a population PK analysis using nonlinear mixed effects modeling an alternative methodology for modeling the data was explored. Due to the data situation, individual compartmental analysis was never an option to model the drug-drug interaction between L-dopa and benserazide. This left population approaches such as naïve-pooled-data

(Chapter 3), naïve averaging of data (Chapter 6) or, as described in this chapter, the nonlinear mixed effects modeling. The first two population methods have the disadvantage that the individual behavior may be masked or that there may be a potential distortion of the model structure or the parameter estimates. The results from the nonlinear mixed effects modeling showed that, in the case of the L-dopa model and the benserazide model, the results obtained with the naïve-pooled-data approach were comparable with those from the nonlinear mixed effects modeling. This is partly due to the fact that the profiles of individual animals given the same treatments were similar. In fact, the same issues (e.g. overparameterization) became evident independent of the population method applied and were largely a consequence of the complexity of the models which was not supported in all respects by the data.

In the PK model for benserazide/Ro 04-5127 NONMEM was not fully capable of estimating all the random variables. The solution to this was to fix the variance parameters stepwise until NONMEM minimized successfully. The parameters were sorted according to magnitude for inter-subject variability which was $CL > V1 > V2 > CLd$. Based on this, the decision was taken to fix the variances of η to zero for those fixed parameters (θ) where the smallest inter-individual variability was expected, i.e. for the intercompartmental clearance of benserazide (CLd_B) and for the distribution clearance of Ro 04-5127 (CLd_M). With these two variances fixed to zero a successful NONMEM run was obtained.

From looking at the semi-logarithmic plot of L-dopa after treatment with L-dopa alone, it appears as if the predicted concentrations are underestimated in the terminal phase from 6 hours onwards. However, this is not the case. The limit of quantification for L-dopa was 0.85 $\mu\text{g/L}$ (0.00431 $\mu\text{mol/L}$). Six hours after dosing there was only one animal (rat b4) left with measurable L-dopa concentrations. For all the other animals the L-dopa concentrations were below limit of quantification. Therefore, the predicted L-dopa concentrations reflect the information in the data, namely, that around 6 hours the concentration falls below limit of quantification.

Three different error models were tested to model the residual variability. These were the additive error model, the proportional error model as well as the combination of both. The combination of the additive and the proportional error model provided the best fits. This is not surprising as, with concentration data varying over more than 1 log where the lowest

concentrations are near the limit of the assay, as is the case for the present data, this error model is frequently found to be the best.

The additive error model is best when the range of the drug is not more than 1 log. The data used for the modeling, however, ranged over more than 1 log.

The proportional error model is suitable for concentrations varying over more than 1 log. However, with this model the residual error variance approaches zero for low concentrations. This error model is therefore inappropriate for data including low concentrations which is the case for the experimental data used for the modeling in this thesis.

By combining the proportional error model with the additive error model the large concentration range, as well as very small values close the limit of the assay, can be addressed successfully.

This chapter deals with the comparison of two methods for population PK analyses. The naïve-pooled-data approach was implemented in the software WinNonlin using the weighted least squares method to find the optimal set of parameter values to describe the observed data best, whereas the nonlinear mixed effects modeling implemented in the software NONMEM used extended least squares for optimization. The difference in estimation methods made it difficult to compare the objective functions between the two approaches to determine population PK.

The naïve-pooled-data method is a pooling method with the advantage that all the data can be used while allowing flexible modeling using independent variables. However, a drawback is that this method does not permit to consider any aspect of random inter-individual or residual variability. Furthermore, if there is a high diversity in the data to be fitted, e.g. the concentration-time profiles, the estimated population parameters may not be representative for the individual data. There is also the possibility that the model established with naïve pooling of data is wrong. In such a situation it is contemplated using the two-stage method or even better nonlinear mixed effects modeling.

The advantage of nonlinear mixed effects modeling is to obtain additional information on the inter-individual variability as well as on the residual variability. Using posthoc estimation methods it is also possible to estimate the parameters for each individual. The estimation of the inter-individual variability is less important if the number of individuals is small, as was the case for the data used for the modeling in this thesis, but gains importance in large Phase 2/3 trials. The disadvantages of nonlinear mixed effects modeling implemented in NONMEM are that the handling of this program is complex compared to modeling in

WinNonlin. With regard to the PK models presented in this chapter, NONMEM was more susceptible to non-convergence, i.e. termination of minimization, and abortion at the covariance step. Furthermore, the run times were very long. These findings are not unexpected as more parameters are estimated when applying nonlinear mixed effects modeling compared to the naïve-pooled-data approach.

5.6 CONCLUSION

The population PK analysis using nonlinear mixed effects modeling described in this chapter showed that population PK parameters obtained with nonlinear mixed effects modeling were comparable to those obtained with the naïve-pooled-data approach for the L-dopa model and the benserazide model. Taking the approach of nonlinear mixed effect modeling provided in addition valuable information on the inter-individual variability. This information was not obtainable with the naïve-pooled-data method.

Chapter 6

PHYSIOLOGICALLY BASED PK MODELS FOR L-DOPA PHARMACOKINETICS WITH AND WITHOUT BENSERAZIDE INCLUDING LIVER CONCENTRATIONS AND ALLOWING FOR NONLINEAR KINETICS FOR THE ELIMINATION OF L-DOPA VIA THE AADC PATHWAY

Chapter 6

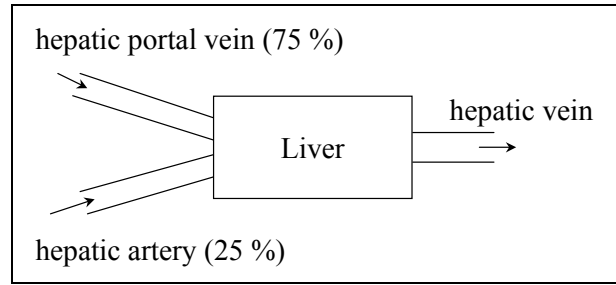
PHYSIOLOGICALLY BASED PK MODELS FOR L-DOPA PHARMACOKINETICS WITH AND WITHOUT BENSERAZIDE INCLUDING LIVER CONCENTRATIONS AND ALLOWING FOR NONLINEAR KINETICS FOR THE ELIMINATION OF L-DOPA VIA THE AADC PATHWAY

The liver plays an important role in the disposition of L-dopa and in the definition of the magnitude of an interaction between L-dopa and benserazide. In this chapter the incorporation of liver concentrations in the modeling efforts was explored. Three subchapters describing sequential steps in the modeling process follow a short introduction in Chapter 6.1. In Chapter 6.2 a basic L-dopa/benserazide model was constructed with the objective of exploring ways to apply a liver model, based on information about previous use of liver models in the literature. The work presented in Chapters 6.3 and 6.4 was performed later and benefited from more insight gained regarding the PK model for L-dopa/benserazide. In summary, this chapter gives an introduction to the use of liver models and provides an overview of the endeavor to model the PK drug-drug interaction L-dopa/benserazide by taking into account liver concentrations and allowing for nonlinear kinetics for the elimination of L-dopa via AADC.

6.1 INTRODUCTION

The liver is the central organ of intermediate metabolism in the body. This organ performs important functions such as detoxification, inactivation, and elimination of endogenous and exogenous compounds. Furthermore, bile is formed in the liver and secreted directly into the duodenum after food intake or into the gallbladder in-between food intake. Bile provides the main excretory pathway for toxic metabolites, cholesterol, and lipid waste products and is needed to facilitate digestion and absorption of dietary fats. The liver is also part of the reticulo-endothelial system and thus has functions in defense and as a filter system of the body. Up to 75 % of the blood flowing to the liver is supplied by the portal vein and up to 25 % by the hepatic artery. The blood in the portal vein is oxygen-poor blood coming from the gastrointestinal tract (e.g. stomach, small intestine, part of the large intestine, pancreas, and spleen). The blood of the hepatic artery and the portal vein reaches the hepatic vein via the capillaries of the liver (i.e. the sinusoids). (Figure 32) ^[204, 205]

FIGURE 32: Blood supply of the human liver



The clearance of any eliminating organ (e.g. liver) is defined as the volume of the perfusing medium (e.g. blood) that is effectively cleared of a drug by that organ per unit time ^[206]. For drugs mainly eliminated via the liver, the hepatic clearance becomes important. In Figure 33 to Figure 35 the concept of organ clearance is presented schematically. ^[207]

FIGURE 33: Organ clearance (panel A)

The extraction rate can be described using the mass balance equation.

$$\frac{dA_e}{dt} = Q * C_A - Q * C_V = Q(C_A - C_V)$$

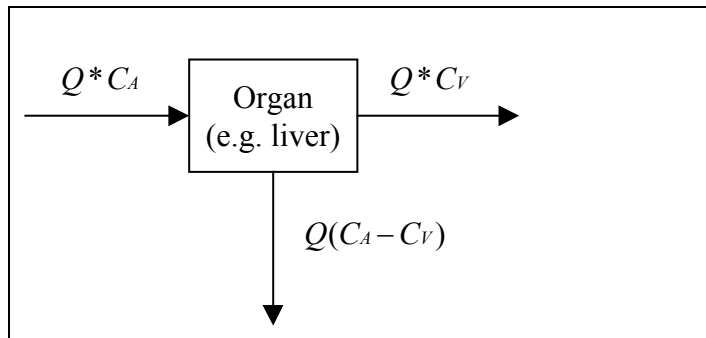


FIGURE 34: Organ clearance (panel B)

Same as in panel A, but normalized for input rate ($Q * C_A$).

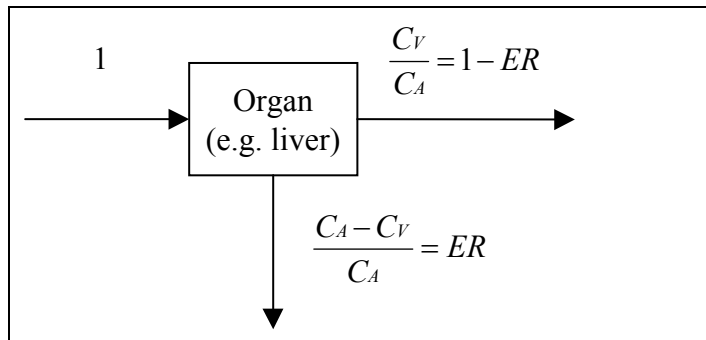
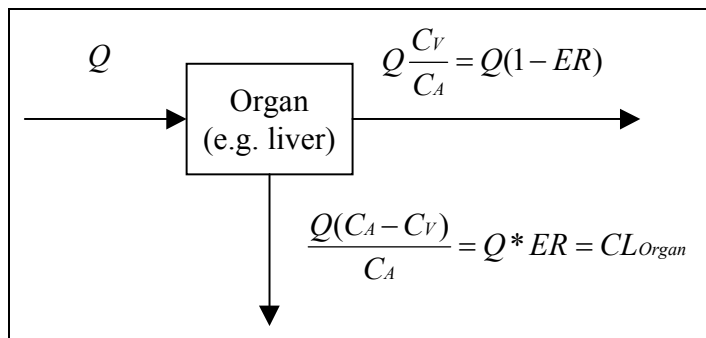


FIGURE 35: Organ clearance (panel C)

Same as in panel A, but normalized for C_A .



A_e : amount extracted, C_A : concentration in arterial blood, C_V : concentration in venous blood, CL_{Organ} : organ clearance, ER : extraction ratio, Q : hepatic blood flow

In the case where the liver is the eliminating organ, the organ clearance is named hepatic clearance (CL_H), Q is the hepatic blood flow and ER is the hepatic extraction ratio. The hepatic clearance and the hepatic extraction ratio are then calculated using Eq. 44 and Eq. 45, respectively.

$$\boxed{CL_H = Q * ER} \quad \text{Eq. 44}$$

$$\boxed{ER = \frac{CL_H}{Q}} \quad \text{Eq. 45}$$

The liver has a unique location between the gastrointestinal tract and the general circulation and receives the majority of blood supply perfusing the gastrointestinal tract. Besides essential nutrients for the body this blood also contains orally administered and absorbed drugs. Thus the concentration of drug on the first passage through the liver can be significantly reduced by presystemic hepatic elimination, so decreasing the drug's oral availability to the systemic circulation. This is called hepatic first-pass effect and is calculated by Eq. 46 where F_H is the hepatic availability. ^[208]

$$\boxed{F_H = 1 - ER} \quad \text{Eq. 46}$$

For drugs that are highly extracted by the liver, the first-pass effect becomes significant (e.g. for propranolol ^[209]). The liver is assumed to be the major site of first-pass metabolism of a drug administered orally, but there can be also other sites such as for example the gastrointestinal tract or the lungs. Therefore, the first-pass elimination occurs when a drug is metabolized between the site of administration and the site of sampling for measurement of drug concentration. ^[208]

The factors that influence hepatic clearance include hepatic blood flow, the fraction unbound (f_u), and the intrinsic clearance (CL_{int}) ^[210]. The intrinsic clearance (Eq. 47) is the clearance that would be observed in the absence of blood flow and protein binding restrictions.

$$\boxed{CL_{int} = \frac{V_{max}}{K_m + C_e}} \quad \text{Eq. 47}$$

The concentration of the drug at the enzyme site (C_e) in the liver cannot be determined practically. Therefore, mathematical models, "liver models", were developed by various authors, which describe this concentration and the quantitative relationship between hepatic clearance, blood flow, fraction unbound, and intrinsic clearance. Several possible liver models

are listed in Table 29 from very simple models such as the naïve engineer model to more complex models such as the dispersion model.

TABLE 29: Liver models

-
- * the naïve engineer model ^[211]
 - * the well-stirred model (or venous equilibration model) ^[206, 211, 212]
 - * the parallel tube model (or undistributed sinusoidal perfusion model) ^[206, 211, 212]
 - * the distributed sinusoidal perfusion model ^[212-214]
 - * the dispersion model ^[212, 215, 216]
-

All these liver models assume (1) that there is thorough mixing between hepatic portal blood and hepatic arterial blood before drug enters the liver, (2) that only unbound drug can traverse membranes, (3) that there is no diffusional barrier between the drug in the blood and the enzyme within the hepatocyte, (4) that the rate of drug elimination is a function of the unbound drug concentration and (5) there is a homogenous distribution of enzymes within the liver ^[98, 206]. The well-stirred model and the parallel tube model were used to describe the L-dopa/benserazide pharmacokinetics and will be presented here in more detail.

The **well-stirred model** (Figure 36, I) assumes that all hepatocytes are exposed to the same concentration of drug. It also assumes that the liver can be considered as a single well-stirred container, in which the drug is distributed rapidly, and the drug concentration in the efferent venous blood is in equilibrium with the drug concentration in the liver. Therefore, the concentration available to the metabolizing enzyme is equal to the unbound drug concentration in hepatic venous blood. The well-stirred model defines the hepatic clearance, the intrinsic clearance and the concentration in the hepatic vein (C_{hv}) using Eq. 48 to Eq. 50. ^[206, 212]

$$\boxed{CL_H = \frac{Q * CL_{int} * fu}{(Q + CL_{int} * fu)}} \quad \text{Eq. 48}$$

$$\boxed{CL_{int} = \frac{V_{max}}{(K_m + C_{hv})}} \quad \text{Eq. 49}$$

$$\boxed{C_{hv} = C_{pv} * (1 - ER) = C_{pv} * \left(1 - \frac{CL_H}{Q}\right) = \frac{C_{pv} * Q}{(Q + CL_{int} * fu)}} \quad \text{Eq. 50}$$

The **parallel tube model** (Figure 36, II) allows the drug concentration to fall as the blood flows through the hepatic sinusoids due to continuous removal of the drug by the liver. The liver is mimicked as a series of equivalent tubes with constant enzyme activity along the length of each tube. The drug concentration decreases along the length of the tube. The average concentration available to the metabolizing enzyme, the liver concentration (\hat{c}), is the logarithmic mean of the portal vein concentration and the hepatic vein concentration. In the parallel tube model the hepatic clearance, the intrinsic clearance, and the liver concentration are described by Eq. 51 to Eq. 53. ^[206, 212]

$$CL_H = Q * \left(1 - e^{-\frac{CL_{int} * fu}{Q}} \right) \quad \text{Eq. 51}$$

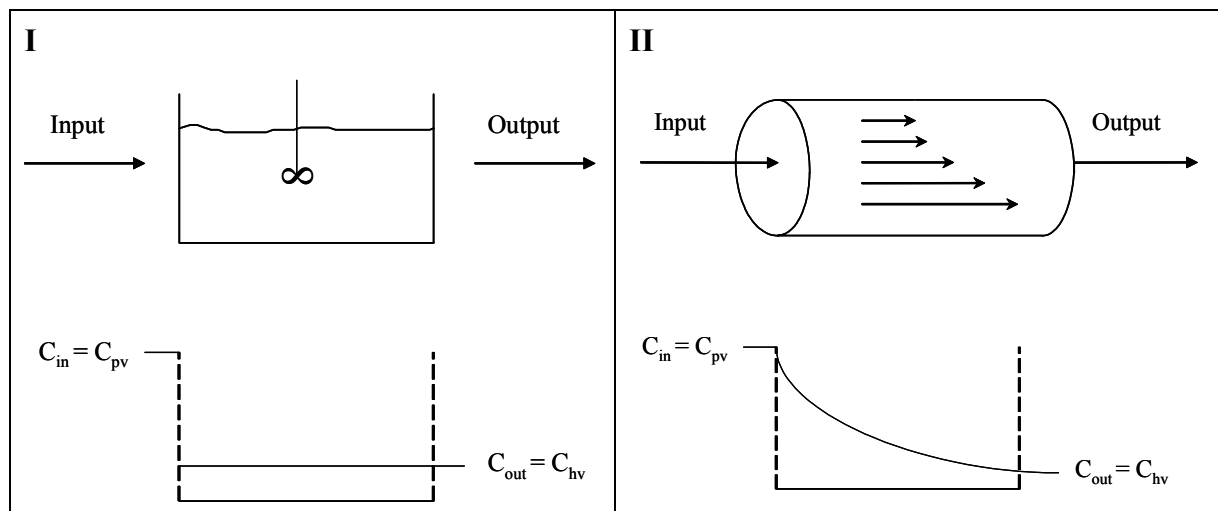
$$CL_{int} = \frac{V_{max}}{(K_m + \hat{c})} \quad \text{Eq. 52}$$

$$\hat{c} = \frac{(C_{pv} - C_{hv})}{\ln(C_{pv} / C_{hv})} \quad \text{Eq. 53}$$

The hepatic vein concentration is defined in the parallel tube model by Eq. 54. ^[206]

$$C_{hv} = C_{pv} * (1 - ER) = C_{pv} * \left(1 - \frac{CL_H}{Q} \right) = C_{pv} * \left(1 - \left(1 - e^{-\frac{CL_{int} * fu}{Q}} \right) \right) = C_{pv} * e^{-\frac{CL_{int} * fu}{Q}} \quad \text{Eq. 54}$$

FIGURE 36: Schematic representation of the well-stirred model (I) and the parallel tube model (II)



Hardware and software: The modeling analysis presented in this chapter was performed on a Pentium Pro 200 Mhz (RAM 96 MB, HD 2 GB; Windows NT 4,0 SP3) computer using the software ACSL (Advanced Continuous Simulation Language) by Mitchell and Gauthier Associates (MGA) Inc.. This software was chosen as it allows solving complex mathematical equations such as implicit functions² employed in the liver models described below.

6.2 BASIC L-DOPA/BENSERAZIDE MODEL (PART 1)

6.2.1 Rationale

In the PK model for L-dopa/benserazide described in Chapter 3, the PK drug-drug interaction was driven by the plasma concentrations of the interacting drugs. Assuming that the majority of the interaction takes place in the liver, liver concentrations would be more appropriate to describe the interaction processes than plasma concentrations. Furthermore, due to higher concentrations of the drugs in the liver than in plasma, particularly during the absorption phase, nonlinear elimination processes can be expected. Therefore, a PK model was developed to estimate the liver concentrations of the interacting drugs using a liver model and allowing for nonlinear kinetics for the elimination of L-dopa via the AADC pathway. The parameter changing with degree of inhibition was the intrinsic clearance; this had therefore to be estimated explicitly in the models.

6.2.2 Objective

The objective was to establish a PK model for L-dopa/benserazide including a liver model, which allows for nonlinear kinetics for the elimination of L-dopa via the AADC pathway and describes the liver concentrations of L-dopa and the inhibitor benserazide.

6.2.3 Materials and Methods

6.2.3.1 Experimental Data

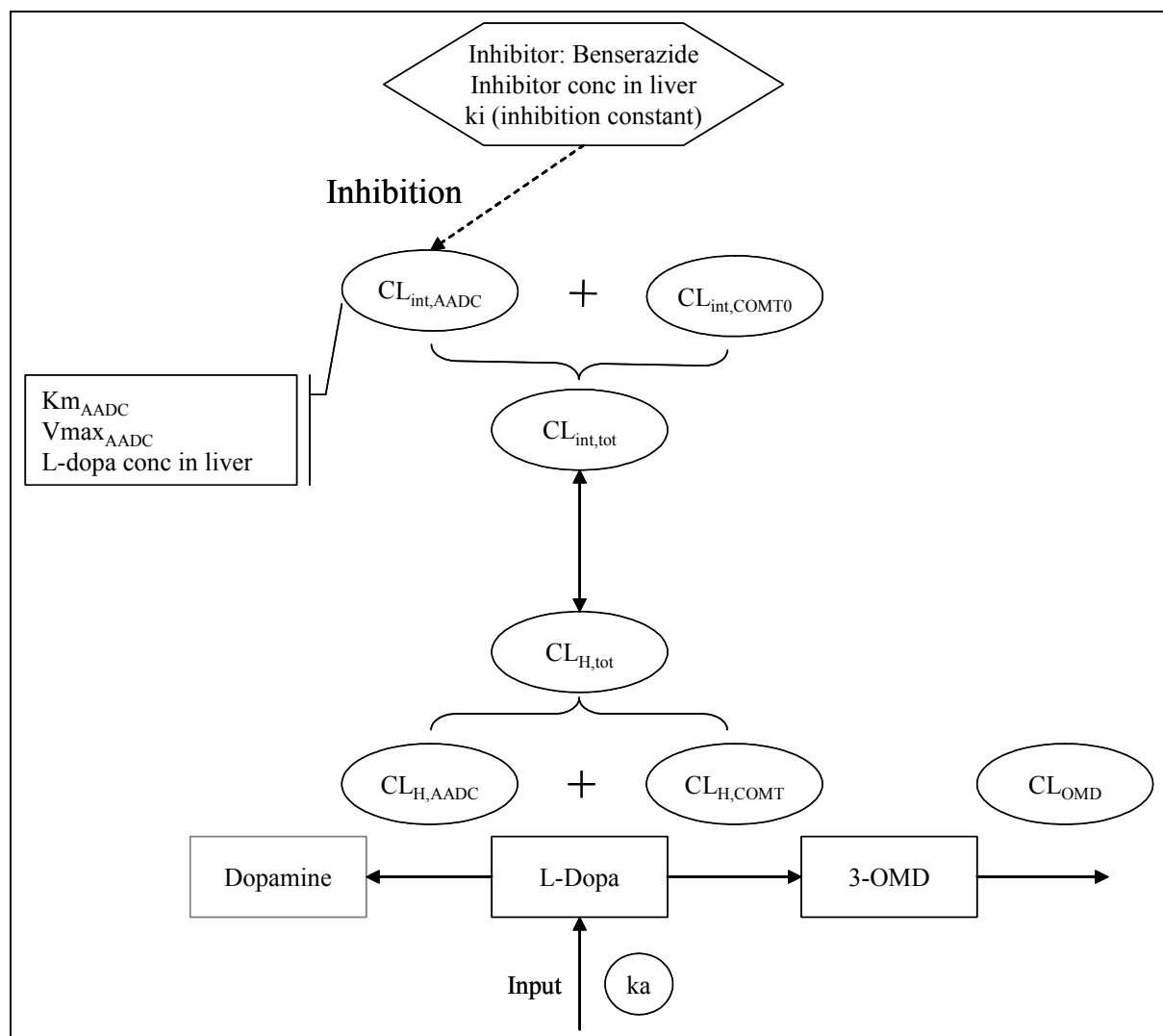
The plasma concentrations of L-dopa and its metabolite 3-OMD, which were used for the fitting, were taken from the animal experiment in rats described in Chapter 3.

² An implicit function is a function in which the dependent variable is not isolated on one side of the equation in comparison to an explicit function in which the dependent variable can be written explicitly in terms of the independent variable.

6.2.3.2 Pharmacokinetic Model for L-Dopa and 3-OMD

The conceptual model for the pharmacokinetics of L-dopa and its metabolite 3-OMD containing liver and plasma concentrations as well as the inhibition of the L-dopa metabolism by benserazide in the liver is shown in Figure 37.

FIGURE 37: Schematic representation of conceptual model



For abbreviations in Figure 37 see text and glossary of abbreviations.

The mass balances for the L-dopa compartment and the 3-OMD compartment were described by differential equations (Eq. 55 to Eq. 57).

$$\frac{dA_{dopa,i}}{dt} = -ka * A_{dopa,i}(t) \quad \text{Eq. 55}$$

$$V_{dopa} * \frac{dC_{dopa,i}}{dt} = ka * A_{dopa,i}(t) * F_i - CL_{H,tot} * C_{dopa,i}(t) \quad \text{Eq. 56}$$

$$V_{OMD} * \frac{dC_{OMD,i}}{dt} = CL_{H,COMT} * C_{dopa,i}(t) - CL_{OMD} * C_{OMD,i}(t) \quad \text{Eq. 57}$$

$A_{dopa,i}$: amount L-dopa in gut compartment, $C_{dopa,i}$: L-dopa concentration in systemic compartment, $C_{OMD,i}$: 3-OMD concentration in systemic compartment (i = b (treatment L-dopa); i = c (treatment L-dopa/benserazide))

The bioavailability (F) and the hepatic extraction ratio (ER) of L-dopa were calculated by Eq. 58 and Eq. 59, respectively.

$$F = 1 - ER \quad \text{Eq. 58}$$

$$ER = \frac{CL_{H,tot}}{Q} \quad \text{Eq. 59}$$

The portal vein concentration of L-dopa was calculated by Eq. 60

$$Cpv_{dopa,i} = C_{dopa,i} + \frac{A_{dopa,i} * ka}{Q} \quad \text{Eq. 60}$$

$A_{dopa,i}$: amount L-dopa in gut compartment, $C_{dopa,i}$: L-dopa concentration in systemic compartment, $Cpv_{dopa,i}$: portal vein concentration of L-dopa (i = b (treatment L-dopa); i = c (treatment L-dopa/benserazide))

The total hepatic clearance of L-dopa, the total intrinsic clearance, as well as the hepatic vein concentration of L-dopa differed depending on whether the well stirred model or the parallel tube model was applied. The specific equations for each liver model are listed below under “Equations for well-stirred model” and “Equations for parallel tube model”.

The pharmacokinetics of benserazide was described with a 1-compartment model. The concentrations of benserazide in the portal and hepatic vein were calculated by Eq. 61 and Eq. 62. The extraction ratio of benserazide was set to 0.98 ($ER_B = 1 - F_B$; $F_B = 2.2\%$ Figure 16).

$$Cpv_B = C_B + \frac{A_B * ka_B}{Q} \quad \text{Eq. 61}$$

$$Chv_B = Cpv_B * (1 - ER_B) \quad \text{Eq. 62}$$

A_B : amount benserazide in gut compartment, C_B : benserazide concentration in systemic compartment, Chv_B : hepatic vein concentration of benserazide, Cpv_B : portal vein concentration of benserazide, ER_B : extraction ratio of benserazide, ka_B : absorption rate constant of benserazide, Q : hepatic blood flow

Equations for well-stirred model: Based on Eq. 48 the total hepatic clearance of L-dopa was calculated using the hepatic blood flow, the total intrinsic clearance of L-dopa and the fraction unbound of L-dopa that was set to 1. The total intrinsic clearance is defined as the sum of intrinsic clearances of individual pathways. ^[212] In the case of L-dopa, the total intrinsic clearance was described as the sum of the intrinsic clearances of AADC and COMT (Eq. 63). Michaelis-Menten kinetics was used to allow for nonlinear kinetics for the AADC pathway. The concentration in the hepatic vein, C_{hv} , in Eq. 63 was replaced by Eq. 50 and the fraction unbound, f_u , was set to 1 to obtain Eq. 64.

$$CL_{int,tot} = CL_{int,AADC} + CL_{int,COMT0} = \frac{V \max_{AADC}}{(Km_{AADC} + C_{hv})} + CL_{int,COMT0} \quad \text{Eq. 63}$$

$$CL_{int,tot} = \frac{V \max_{AADC}}{\left(Km_{AADC} + \left(\frac{C_{pv} * Q}{(Q + CL_{int,tot})} \right) \right)} + CL_{int,COMT0} \quad \text{Eq. 64}$$

C_{hv} : hepatic vein concentration of L-dopa, C_{pv} : portal vein concentration of L-dopa, $CL_{int,AADC}$: intrinsic clearance via AADC, $CL_{int,COMT0}$: intrinsic clearance via COMT, $CL_{int,tot}$: total intrinsic clearance, Km_{AADC} : Michaelis-Menten constant of AADC, $V\max_{AADC}$: maximum metabolic rate of AADC, Q : hepatic blood flow

In order to solve Eq. 64 for $CL_{int,tot}$ the equation was rewritten (Eq. 65 to Eq. 70) to obtain a quadratic equation which could be solved for $CL_{int,tot}$ algebraically. For this Eq. 64 was rewritten as Eq. 65.

$$x = \frac{a}{\left(b + \left(\frac{c * d}{(d + x)} \right) \right)} + e \quad \text{Eq. 65}$$

a: $V\max_{AADC}$, **b:** Km_{AADC} , **c:** C_{pv} , **d:** Q , **e:** $CL_{int,COMT0}$, **x:** $CL_{int,tot}$

Eq. 65 was solved for x. Term b in Eq. 65 was written as fraction $b(d+X)/(d+X)$. (Eq. 66 and Eq. 67)

$$x = \frac{a}{\frac{b * (d + x) + c * d}{(d + x)}} + e \quad \text{Eq. 66}$$

$$x = \frac{a * (d + x)}{b * (d + x) + c * d} + e \quad \text{Eq. 67}$$

The brackets in nominator and denominator of Eq. 67 were removed.

$$x = \frac{a*d + a*x}{b*d + b*x + c*d} + e \quad \text{Eq. 68}$$

The term e of Eq. 68 was multiplied with the term in the denominator on the right-hand-side (RHS) and the term in denominator was taken on the left-hand-side (LHS).

$$x*(b*d + b*x + c*d) = a*d + a*x + e*(b*d + b*x + c*d) \quad \text{Eq. 69}$$

The brackets on RHS and LHS of Eq. 69 were removed and the variables sorted to obtain the quadratic Eq. 70.

$$b*x^2 + x*(c*d + b*d - a - e*b) - (a*d + e*b*d + e*c*d) = 0 \quad \text{Eq. 70}$$

Because only the positive solution was of interest, the quadratic equation was solved for x using the algebraic solution as described in Eq. 71.

$$x = -\frac{g}{(2*i)} + \sqrt{\left(\frac{g}{(2*i)}\right)^2 - \frac{h}{i}} \quad \text{Eq. 71}$$

$$i = b$$

$$g = c*d + b*d - a - e*b$$

$$h = -(a*d + e*b*d + e*c*d)$$

In the case where L-dopa was co-administered with benserazide, the total intrinsic clearance of L-dopa, assuming competitive inhibition was defined by Eq. 72. The hepatic vein concentration, C_{hv} , was replaced by Eq. 50 (fraction unbound in Eq. 50 was set to 1) to obtain Eq. 73.

$$CL_{int,tot(I)} = \frac{V \max_{AADC}}{\left(Km_{AADC} * \left(1 + \frac{C_{hv(I)}}{ki} \right) + C_{hv} \right)} + CL_{int,COMT0} \quad \text{Eq. 72}$$

$$CL_{int,tot(I)} = \frac{V \max_{AADC}}{\left(Km_{AADC} * \left(1 + \frac{C_{hv(I)}}{ki} \right) + \left(\frac{C_{pv} * Q}{(Q + CL_{int,tot(I)})} \right) \right)} + CL_{int,COMT0} \quad \text{Eq. 73}$$

C_{hv} : hepatic vein concentration of L-dopa, $C_{hv(I)}$: hepatic vein concentration of inhibitor, C_{pv} : portal vein concentration of L-dopa, $CL_{int,AADC}$: intrinsic clearance via AADC, $CL_{int,COMT0}$: intrinsic clearance via COMT, $CL_{int,tot(I)}$: total intrinsic clearance in the presence of an inhibitor, ki : inhibition constant, Km_{AADC} : Michaelis-Menten constant of AADC, $Vmax_{AADC}$: maximum metabolic rate of AADC, Q : hepatic blood flow

In order to solve Eq. 73 for $CL_{int,tot(I)}$ the equation was rewritten (Eq. 74 to Eq. 75) to obtain a quadratic equation which could be solved for $CL_{int,tot(I)}$ algebraically. For this Eq. 73 was written as Eq. 74.

$$x = \frac{a}{\left(b * \left(1 + \frac{v}{w} \right) + \left(\frac{c * d}{(d + x)} \right) \right)} + e \quad \text{Eq. 74}$$

a: $Vmax_{AADC}$, **b:** Km_{AADC} , **c:** C_{pv} , **d:** Q , **e:** $CL_{int,COMT0}$, **v:** C_{hv} of inhibitor, **w:** ki , **x:** $CL_{int,tot(I)}$

The term $1+(v/w)$ in Eq. 74 was substituted by the variable u and the equation was solved for x as described above to obtain the quadratic Eq. 75.

$$b * u * x^2 + x * (c * d + b * u * d - a - e * b * u) - (a * d + e * b * u * d + e * c * d) = 0 \quad \text{Eq. 75}$$

Only the positive solution for x was of interest. Therefore, the quadratic equation was solved for x using the algebraic solution as described in Eq. 76.

$$x = -\frac{g}{(2 * j)} + \sqrt{\left(\frac{k}{(2 * j)} \right)^2 - \frac{l}{j}} \quad \text{Eq. 76}$$

$$j = b * u$$

$$k = c * d + b * u * d - a - e * b * u$$

$$l = -(a * d + e * b * u * d + e * c * d)$$

Equations for parallel tube model: The total hepatic clearance of L-dopa was estimated by Eq. 51 using the hepatic blood flow, the total intrinsic clearance of L-dopa, and the fraction unbound that was set to 1. As in the well-stirred model, the total intrinsic clearance of L-dopa was the sum of the intrinsic clearances of AADC and COMT, with the difference that the liver concentration was not the hepatic vein concentration, but the logarithmic mean of the portal vein concentration and the hepatic vein concentration, \hat{c} (Eq. 77).

$$CL_{int,tot} = CL_{int,AADC} + CL_{int,COMT0} = \frac{V \max_{AADC}}{(Km_{AADC} + \hat{c})} + CL_{int,COMT0} \quad \text{Eq. 77}$$

\hat{c} : liver concentration of L-dopa, $CL_{int,AADC}$: intrinsic clearance via AADC, $CL_{int,COMT0}$: intrinsic clearance via COMT, $CL_{int,tot}$: total intrinsic clearance, Km_{AADC} : Michaelis-Menten constant of AADC, $Vmax_{AADC}$: maximum metabolic rate of AADC

In Eq. 77 the concentration \hat{c} was replaced by Eq. 53 using Eq. 54 to calculate the hepatic vein concentration. The fraction unbound, fu , was set to 1.

If L-dopa was combined with benserazide, the total intrinsic clearance of L-dopa, assuming competitive inhibition, was then defined by Eq. 78.

$$CL_{\text{int,tot}(I)} = \frac{V \max_{AADC}}{\left(Km_{AADC} * \left(1 + \frac{\hat{c}_{(I)}}{ki} \right) + \hat{c} \right)} + CL_{\text{int,COMT}0} \quad \text{Eq. 78}$$

\hat{c} : liver concentration of L-dopa, $\hat{c}_{(I)}$: liver concentration of inhibitor, $CL_{\text{int,AADC}}$: intrinsic clearance via AADC, $CL_{\text{int,COMT}0}$: intrinsic clearance via COMT, $CL_{\text{int,tot}(I)}$: total intrinsic clearance in the presence of an inhibitor, ki : inhibition constant, Km_{AADC} : Michaelis-Menten constant of AADC, $V\max_{AADC}$: maximum metabolic rate of AADC

Eq. 77 and Eq. 78 are implicit functions and were solved numerically for the total intrinsic clearance (with and without inhibition) using the ACSL function IMPLC. The algebraic constraints were defined by subtracting in Eq. 77 and Eq. 78 the RHS from the LHS evaluating to a residual. The residual was kept close to zero.

Reparameterization of Michaelis-Menten equation: This was based on a publication by Bachman et al. ^[217] in which the authors reparameterized the sigmoid E_{\max} model for the use with truncated PKPD data. The same concept was applied to the Michaelis-Menten equation. For detailed derivation of the equation see Appendix E. The consequence of this reparameterization is that the two parameters K_m and V_{\max} are not estimated directly, but derived from the newly introduced parameters β and V^* .

Weighting: The Optimize option in ACSL Math allows choice between absolute error, which is translated into a value of 0 for the weighting parameter also called the heteroscedasticity parameter, and relative error, which is given the value 2. It is also possible to fix any value between 0 and 2. In addition, ACSL Optimize has the option of estimating the optimal value for the weighting parameter. This option was chosen to fit the model to the data.

Integration and optimization: The integration algorithm used was Runge-Kutta-Fehlberg with a variable step size and a fixed order (i.e. 5th order). The step size was limited such that it could not exceed 0.01. The model was fitted to the average L-dopa and 3-OMD plasma concentrations with and without benserazide simultaneously, using the approach of naïve averaging of data. The parameters were evaluated by maximum likelihood estimation, using as optimization algorithm, the Generalized Reduced Gradient ^[218], for maximizing the log likelihood function.

For the parallel tube model the starting point for the iterative root finding method (to solve Eq. 77 and Eq. 78) was set to a slightly higher value than zero, i.e. to 0.01. This ensured that the intrinsic clearance never became zero during the solving of the implicit equation.

6.2.4 Results

6.2.4.1 Well-Stirred Model

The L-dopa plasma concentrations predicted after treatment with L-dopa alone were underestimated, whereas the predicted 3-OMD plasma concentrations were close to the observed mean data (Figure 38). The predicted plasma concentrations of L-dopa and 3-OMD described the average observed data relatively well in the group where L-dopa and benserazide were administered together (Figure 39). The final parameter estimates are listed in Table 30. The estimation error could not be calculated for the parameters β_{AADC} , V_{AADC}^* , absorption rate constant of L-dopa (k_a), and inhibition constant (k_i). The clearance of 3-OMD (CL_{OMD}), the volume of distribution of L-dopa and 3-OMD (V_{dopa} , V_{OMD}) were estimated reasonably well. The parameters Km_{AADC} and $Vmax_{AADC}$ were 1869 $\mu\text{mol/L}$ and 14517 $\mu\text{mol/h}$, respectively. The objective function expressed as log likelihood function was -310.

TABLE 30: Well-stirred model: Final parameter estimates

Analyte	Treatment	PK Parameter [Unit]	Estimate	CV%
L-Dopa	after L-dopa alone or L-dopa/benserazide	V_{dopa} [L/kg]	3.83	3
		k_a [h^{-1}]	13.5	NC
		β_{AADC}	0.910	NC
		V_{AADC}^* [$\mu\text{mol/h}$]	6915	NC
3-OMD	after L-dopa alone or L-dopa/benserazide	V_{OMD} [L/kg]	0.327	3
		CL_{OMD} [L/h/kg]	0.0246	4
Benserazide	after L-dopa/benserazide	k_i [$\mu\text{g/L}$]	0.0145	NC

CV%: derived from asymptotic standard error of estimate, NC: not calculated, due to estimation problems of standard error

FIGURE 38: Well-stirred model: Predicted (—) and observed (*) plasma concentrations of L-dopa and 3-OMD after 80 mg/kg L-dopa

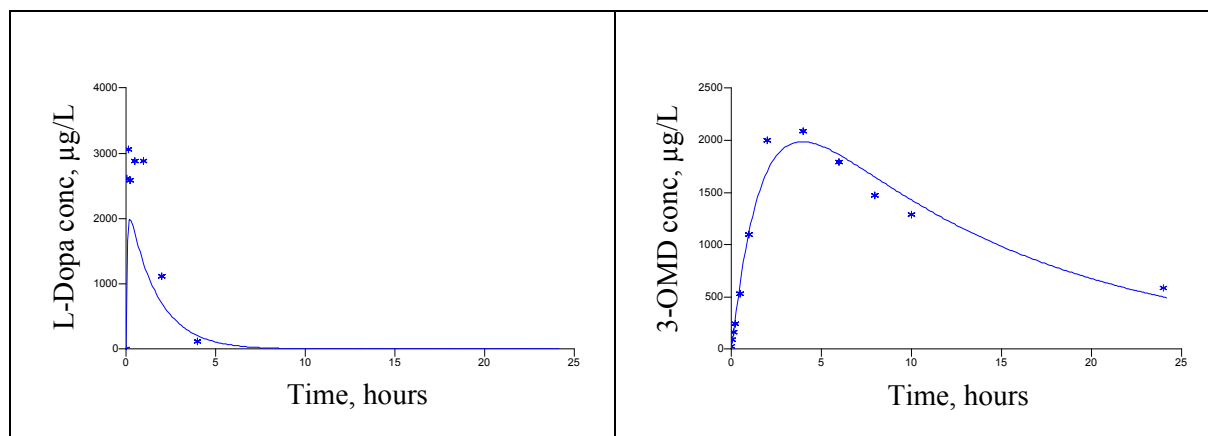
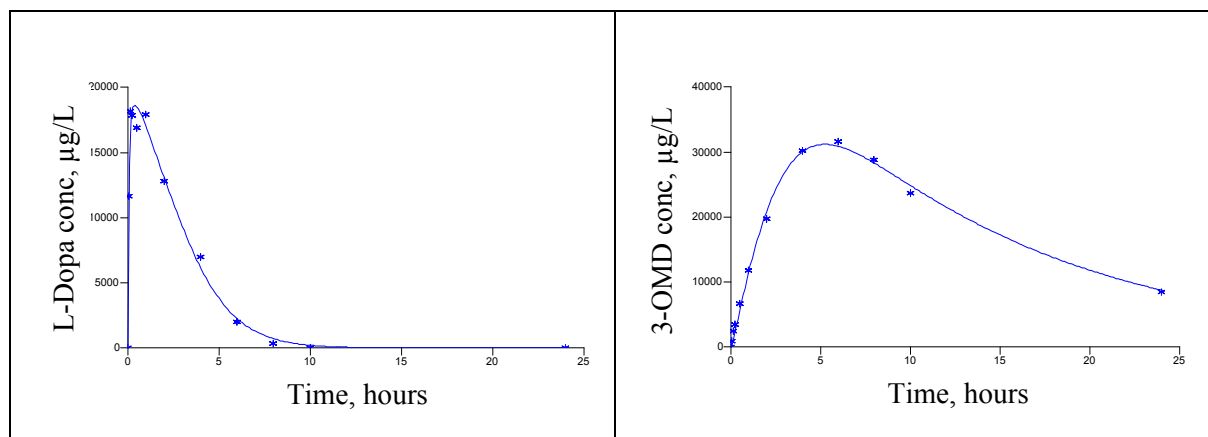


FIGURE 39: Well-stirred model: Predicted (—) and observed (*) plasma concentrations of L-dopa and 3-OMD after 80/20 mg/kg L-dopa/benserazide



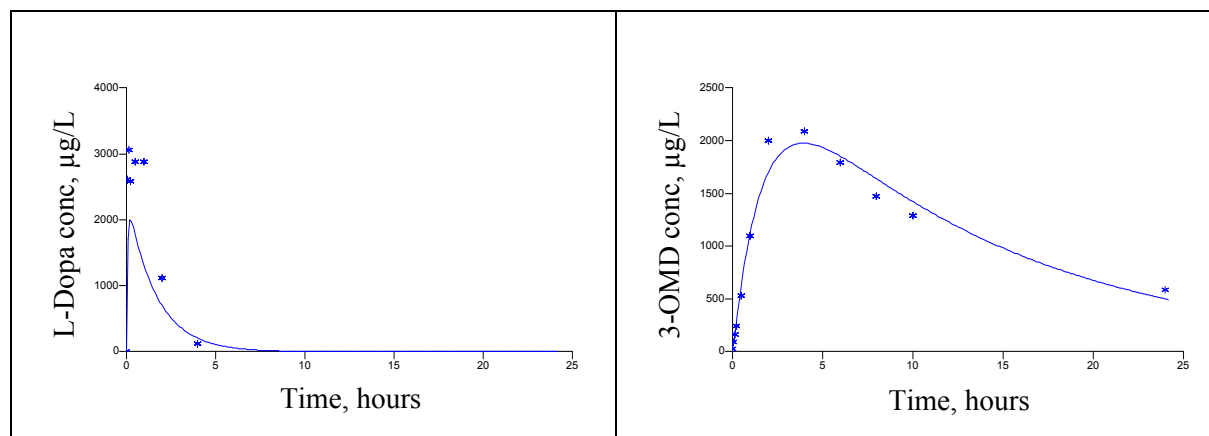
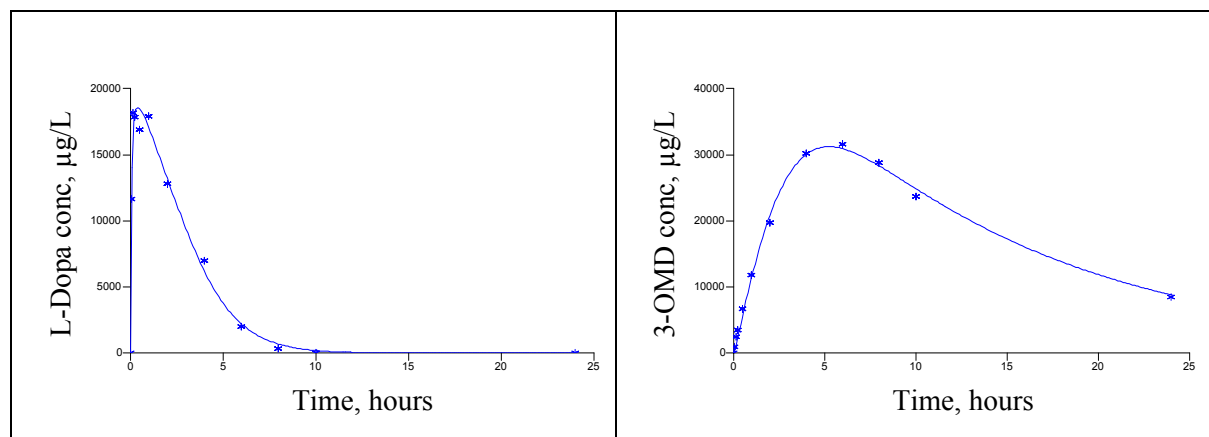
6.2.4.2 Parallel Tube Model

In the group receiving L-dopa alone the predicted L-dopa concentrations were underestimated, whereas the predicted 3-OMD plasma concentrations were close to the observed mean data (Figure 40). The predicted plasma concentrations of L-dopa and 3-OMD described the average observed data relatively well in the group receiving L-dopa and benserazide administered together (Figure 41). The final parameter estimates are listed in Table 31. They were reasonable. However, the estimation error for β_{AADC} was high. The two parameters β_{AADC} and V_{AADC}^* were highly correlated ($r = -0.998$). The parameters Km_{AADC} and $Vmax_{AADC}$ were 6438 $\mu\text{mol/L}$ and 13321 $\mu\text{mol/h}$, respectively. The objective function expressed as log likelihood function was -309.

TABLE 31: Parallel tube model: Final parameter estimates

Analyte	Treatment	PK Parameter [Unit]	Estimate	CV%
L-Dopa	after L-dopa alone or L-dopa/benserazide	V_{dopa} [L/kg]	3.84	3
		k_a [h^{-1}]	13.4	12
		β_{AADC}	0.295	212
		V_{AADC}^* [$\mu\text{mol/h}$]	3035	37
3-OMD	after L-dopa alone or L-dopa/benserazide	V_{OMD} [L/kg]	0.331	4
		CL_{OMD} [L/h/kg]	0.0247	5
Benserazide	after L-dopa/benserazide	k_i [$\mu\text{g/L}$]	0.942	20

CV%: derived from asymptotic standard error of estimate

FIGURE 40: Parallel tube model: Predicted (—) and observed (*) plasma concentrations of L-dopa and 3-OMD after 80 mg/kg L-dopa**FIGURE 41: Parallel tube model: Predicted (—) and observed (*) plasma concentrations of L-dopa and 3-OMD after 80/20 mg/kg L-dopa/benserazide**

6.3 BENSERAZIDE/RO 04-5127 MODEL (PART 2)

6.3.1 Rationale

For the purposes of simplification, the L-dopa/benserazide model described in Chapter 6.2 characterized only the benserazide liver concentrations which acted as inhibitor of AADC. However, from the literature and the PK model described in Chapter 3 it is known that the situation is more complex. The metabolite of benserazide, Ro 04-5127, is already formed to a major extent in the gut and inhibits AADC. Therefore, the possibility of establishing a PK model to describe the liver concentrations of the metabolite Ro 04-5127 was investigated. This was done using information from the literature as far as reported and the benserazide/Ro 04-5127 data collected in the animal experiment of Chapter 3.

6.3.2 Objective

The objective was to develop a PK model for benserazide and its metabolite Ro 04-5127 including liver concentrations of Ro 04-5127.

6.3.3 Materials and Methods

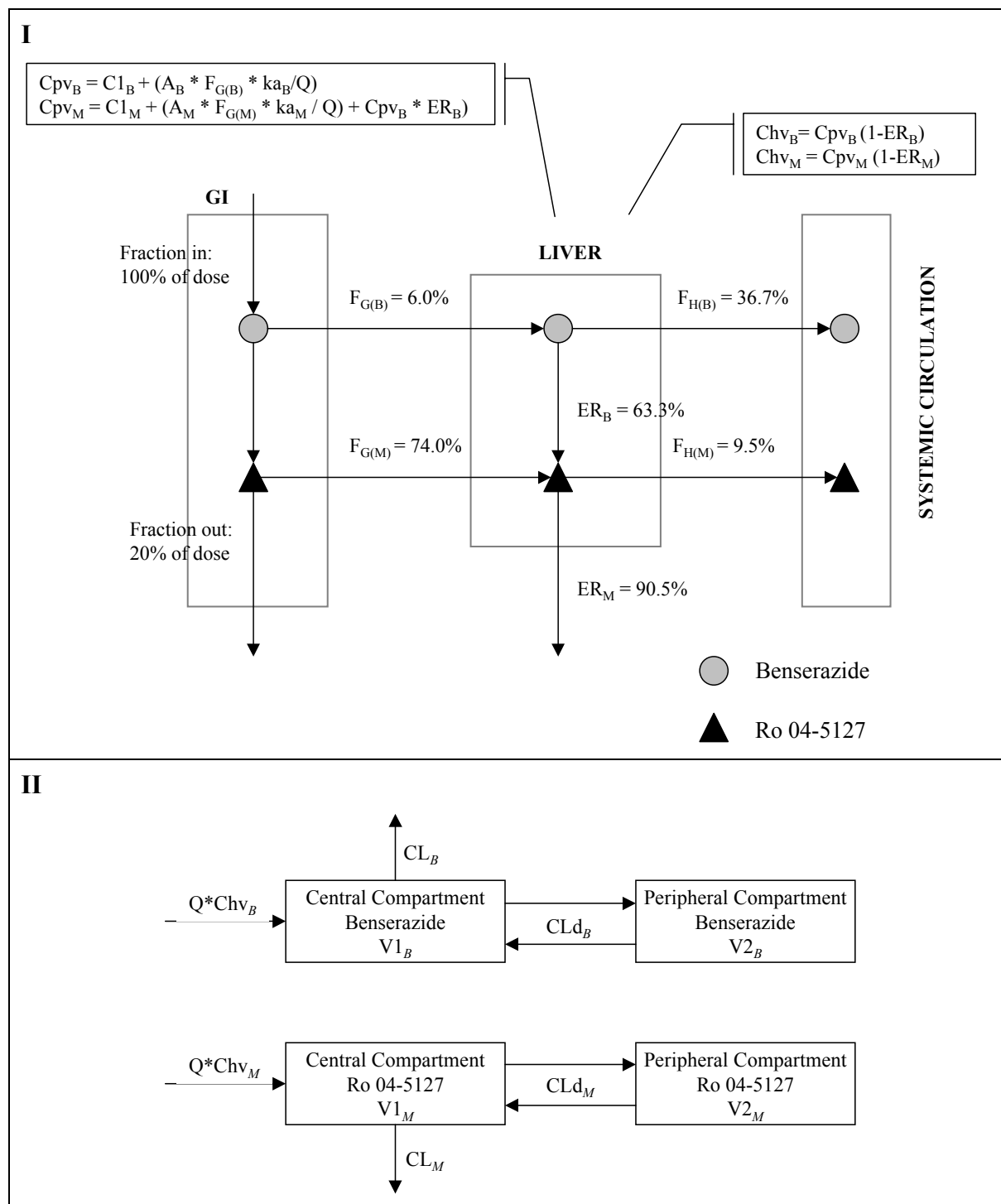
6.3.3.1 Experimental Data

The plasma concentrations of benserazide and its metabolite Ro 04-5127, which were used to evaluate the model, were taken from the animal experiment in rats described in Chapter 3.

6.3.3.2 Pharmacokinetic Model for Benserazide and Ro 04-5127

The conceptual model of the pharmacokinetics of benserazide and its metabolite Ro 04-5127 is shown in Figure 42. In contrast to the PK benserazide/Ro 04-5127 model described in Chapter 3, the metabolic formation of Ro 04-5127 takes place in the gut and the liver.

FIGURE 42: Schematic representation of conceptual model to describe pharmacokinetics of benserazide and Ro 04-5127 (I: physiological part of model; II: compartmental model)



The values for CL_B , $V1_B$, $V2_B$, CLd_B , ka_B , CL_M , $V1_M$, $V2_M$, CLd_M , ka_M were taken from PK model described in Chapter 3, Q (0.828 L/h/0.25kg)^[162] and $F_{G(B)}$ (6%)^[156] are literature values, $F_{G(M)}$ (74%) is calculated based on values reported in literature and assumptions (see below), $F_{H(B)}$ (37%) and $F_{H(M)}$ (9%) are calculated by Eq. 79, and ER_B (63%) and ER_M (91%) are calculated by Eq. 80.

For abbreviations in Figure 42 see text and glossary of abbreviations.

Benserazide: The bioavailability of benserazide (F_B) was estimated to be 2.2 % (Figure 16). The bioavailability of benserazide is the product of gastrointestinal availability ($F_{G(B)}$) and hepatic availability ($F_{H(B)}$). In the literature^[156] it is reported that less than 6 % of benserazide was found unchanged in the portal blood. Based on this, the assumption was made that the gastrointestinal availability was 6 %. The hepatic availability of benserazide can then be calculated using Eq. 79 and was 37 %. The hepatic extraction ratio of benserazide (ER_B) was estimated to be 63 % (Eq. 80).

$$F_{H(B)} = \frac{F_B}{F_{G(B)}} \quad \text{Eq. 79}$$

$$ER_B = 1 - F_{H(B)} \quad \text{Eq. 80}$$

The total clearance of benserazide (CL_B) was 1.672 L/h (Table 16). The hepatic clearance ($CL_{H(B)}$) was calculated using Eq. 81 and was 0.5244 L/h. Subtracting the hepatic clearance from the total clearance we obtained the renal clearance of benserazide ($CL_{R(B)}$, Eq. 82) as 1.148 L/h. The fraction excreted unchanged in urine (fe_B : 0.6864) and the fraction metabolized (fm_B : 0.3136) were estimated using Eq. 83 and Eq. 84.

$$CL_{H(B)} = ER_B * Q \quad \text{Eq. 81}$$

$$CL_{R(B)} = CL_B - CL_{H(B)} \quad \text{Eq. 82}$$

$$fe_B = \frac{CL_{R(B)}}{CL_B} \quad \text{Eq. 83}$$

$$fm_B = \frac{CL_{H(B)}}{CL_B} \quad \text{Eq. 84}$$

Because less than 6 % of benserazide was found unchanged in portal blood, 6 % was the upper limit for $F_{G(B)}$. Therefore, it was decided to define a range for $F_{G(B)}$. The hepatic availability, $F_{H(B)}$, cannot exceed 1. Based on this, the smallest possible value for $F_{G(B)}$ is 0.022. This results in a range of 2.2 % to 6 % for $F_{G(B)}$, of 0 to 0.63 for ER_B , and of 0 to 0.3 for fm_B .

The concentrations of benserazide in the portal vein and in the hepatic vein were calculated by Eq. 85 and Eq. 86, respectively.

$$\boxed{Cpv_B = C1_B + \frac{(A_B * F_{G(B)} * ka_B)}{Q}} \quad \text{Eq. 85}$$

$$\boxed{Chv_B = Cpv_B(1 - ER_B)} \quad \text{Eq. 86 = Eq. 62}$$

A_B: amount benserazide in gut compartment, **C1_B**: benserazide concentration of central compartment, **Chv_B**: hepatic vein concentration of benserazide, **Cpv_B**: portal vein concentration of benserazide, **ER_B**: extraction ratio of benserazide **F_{G(B)}**: gastrointestinal availability of benserazide, **ka_B**: absorption rate constant of benserazide, **Q**: hepatic blood flow

The mass balances for the central and peripheral compartment of benserazide were described by differential equations (Eq. 87 and Eq. 88)

$$\boxed{V1_B * \frac{dC1_B}{dt} = Q * Chv_B + CLd_B * C2_B(t) - CLd_B * C1_B(t) - CL_B * C1_B(t)} \quad \text{Eq. 87}$$

$$\boxed{V2_B * \frac{dC2_B}{dt} = CLd_B * C1_B(t) - CLd_B * C2_B(t)} \quad \text{Eq. 88}$$

C1_B: benserazide concentration of central compartment, **C2_B**: benserazide concentration of peripheral compartment

Ro 04-5127: Of the administered benserazide dose, 6 % is absorbed unchanged into the portal vein and 20 % is not absorbed and excreted via feces^[156]. This leaves 74 % of the benserazide dose, which was assumed to be metabolized in the gut to Ro 04-5127. If the gastrointestinal availability of Ro 04-5127 (**F_{G(M)}**) is 74 % and the total availability of Ro 04-5127 (**F_M**) is 7 % (Figure 16), then the hepatic availability and the hepatic extraction ratio are 9 % and 91 %, respectively. The total clearance of Ro 04-5127 (**CL_M**) was estimated to be 4.287 L/h (Table 16), the hepatic clearance (**CL_{H(M)}**) 0.7497 L/h, the renal clearance (**CL_{R(M)}**) 3.537 L/h, the fraction excreted renally unchanged (**fe_M**) 0.8251, and the fraction metabolized (**fm_M**) 0.1749. All these parameters were calculated applying the same equations described for benserazide above.

The concentrations of Ro 04-5127 in the portal vein and in the hepatic vein were calculated by Eq. 89 and Eq. 90, respectively.

$$\boxed{Cpv_M = C1_M + \frac{(A_M * F_{G(M)} * ka_M)}{Q} + Cpv_B * ER_B} \quad \text{Eq. 89}$$

$$\boxed{Chv_M = Cpv_M(1 - ER_M)} \quad \text{Eq. 90}$$

A_M: amount Ro 04-5127 in gut compartment, **C1_M**: Ro 04-5127 concentration of central compartment, **Chv_M**: hepatic vein concentration of Ro 04-5127, **Cpv_B**: portal vein concentration of benserazide, **Cpv_M**: portal vein concentration of

Ro 04-5127, ER_B : extraction ratio of benserazide, ER_M : extraction ratio of Ro 04-5127, $F_{G(M)}$: gastrointestinal availability of Ro 04-5127, ka_M : absorption rate constant of Ro 04-5127, Q : hepatic blood flow

The mass balances for the central and peripheral compartment of Ro 04-5127 were described by differential equations (Eq. 91 and Eq. 92)

$$V1_M * \frac{dC1_M}{dt} = Q * Chv_M + CLd_M * C2_M(t) - CLd_M * C1_M(t) - CL_M * C1_M(t) \quad \text{Eq. 91}$$

$$V2_M * \frac{dC2_M}{dt} = CLd_M * C1_M(t) - CLd_M * C2_M(t) \quad \text{Eq. 92}$$

$C1_M$: Ro 04-5127 concentration of central compartment, $C2_M$: Ro 04-5127 concentration of peripheral compartment

Based on this PK model the plasma concentrations, the concentrations in the portal vein, and the concentrations in the hepatic vein of benserazide and Ro 04-5127 were calculated and the plasma concentrations of benserazide and Ro 04-5127 were compared with observed individual data obtained in the animal experiment (Chapter 3). In this case the PK model was not fitted to the benserazide and Ro 04-5127 data.

Integration: The integration algorithm was Runge-Kutta-Fehlberg with a variable step size and a fixed order (i.e. 5th order). The step size was defined such that it could not exceed 0.01.

6.3.4 Results

The calculated plasma concentrations of benserazide and its metabolite Ro 04-5127 described the observed individual concentrations well (Figure 43). The liver concentrations of benserazide and Ro 04-5127 in the portal vein and the hepatic vein are shown in Figure 44.

FIGURE 43: Predicted (—) and observed (Δ) plasma concentrations of benserazide and Ro 04-5127

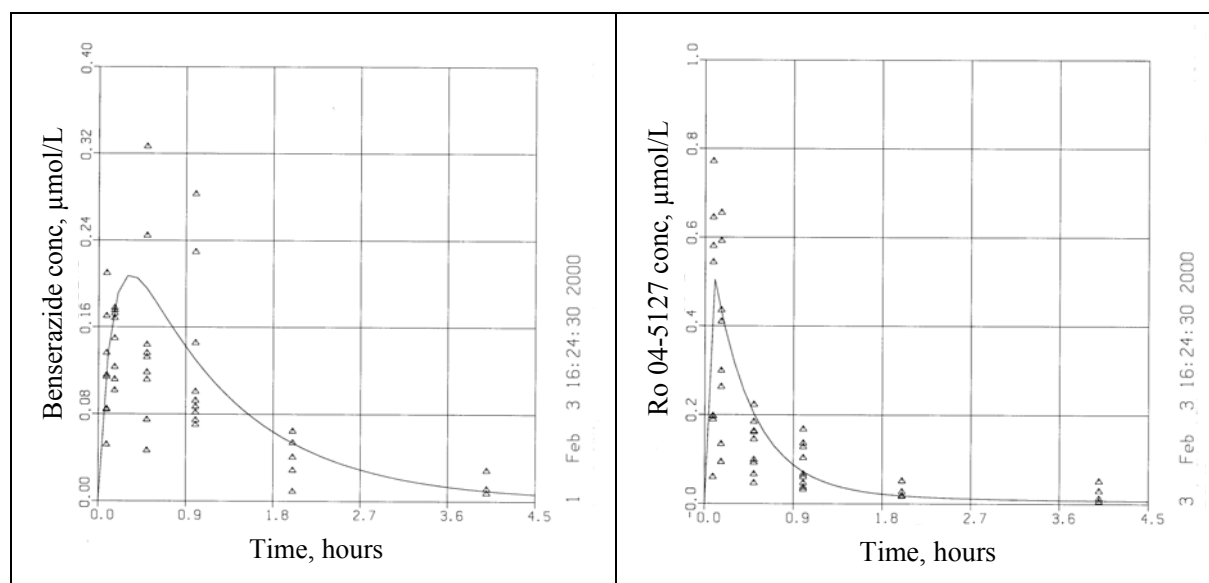
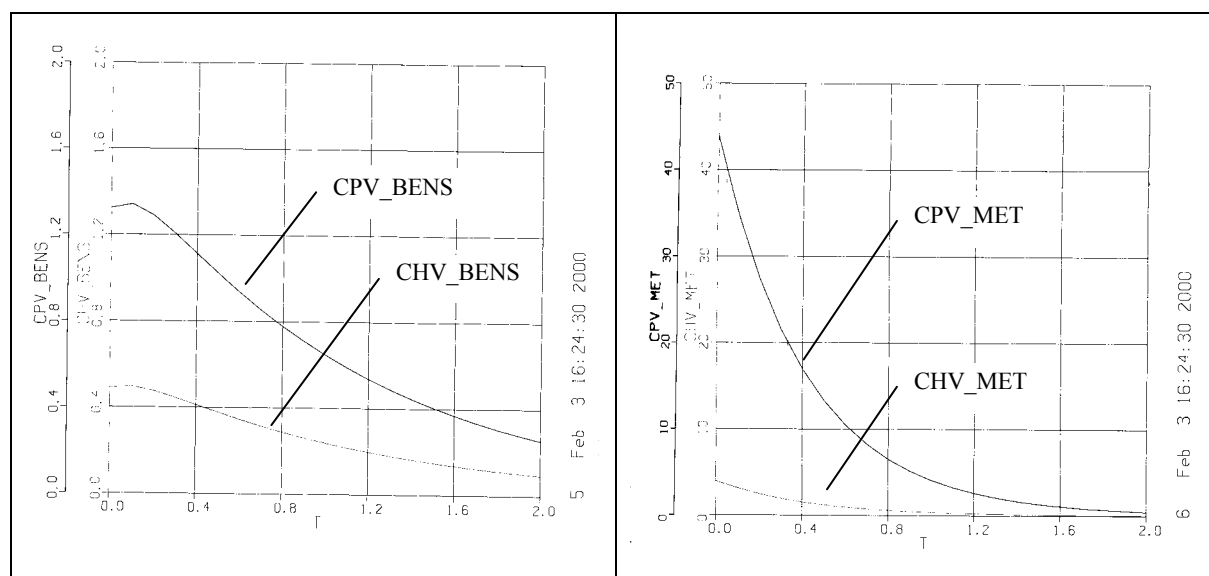


FIGURE 44: Predicted concentrations of benserazide and Ro 04-5127 in the portal vein and the hepatic vein



CPV_BENS: benserazide concentration in portal vein ($\mu\text{mol/L}$), **CHV_BENS:** benserazide concentration in hepatic vein ($\mu\text{mol/L}$), **CPV_MET:** Ro 04-5127 concentration in portal vein, **CHV_MET:** Ro 04-5127 concentration in hepatic vein, **T:** time (hours)

6.4 ENHANCED L-DOPA/BENSERAZIDE MODEL (PART 3)

6.4.1 Rationale

As described in Chapter 6.3.1 the metabolite of benserazide (Ro 04-5127) and not benserazide itself plays the role of the inhibitor. Therefore, the basic PK model L-dopa/benserazide

described in Chapter 6.2 was developed further. Knowledge gained throughout the modeling work with L-dopa and benserazide was taken into account as well as the benserazide/Ro 04-5127 model described in Chapter 6.3. The latter allowed the calculation of Ro 04-5127 liver concentrations.

6.4.2 Objective

The objective was to enhance the basic L-dopa/benserazide model described in Chapter 6.2 by:

- * using the benserazide/Ro 04-5127 model from Chapter 6.3
- * choosing as liver model the parallel tube model, and
- * allowing for different values for the absorption rate constant of L-dopa, the volume of distribution of 3-OMD, and the clearance of 3-OMD depending on the administered treatment i.e. L-dopa alone or L-dopa/benserazide.

6.4.3 Materials and Methods

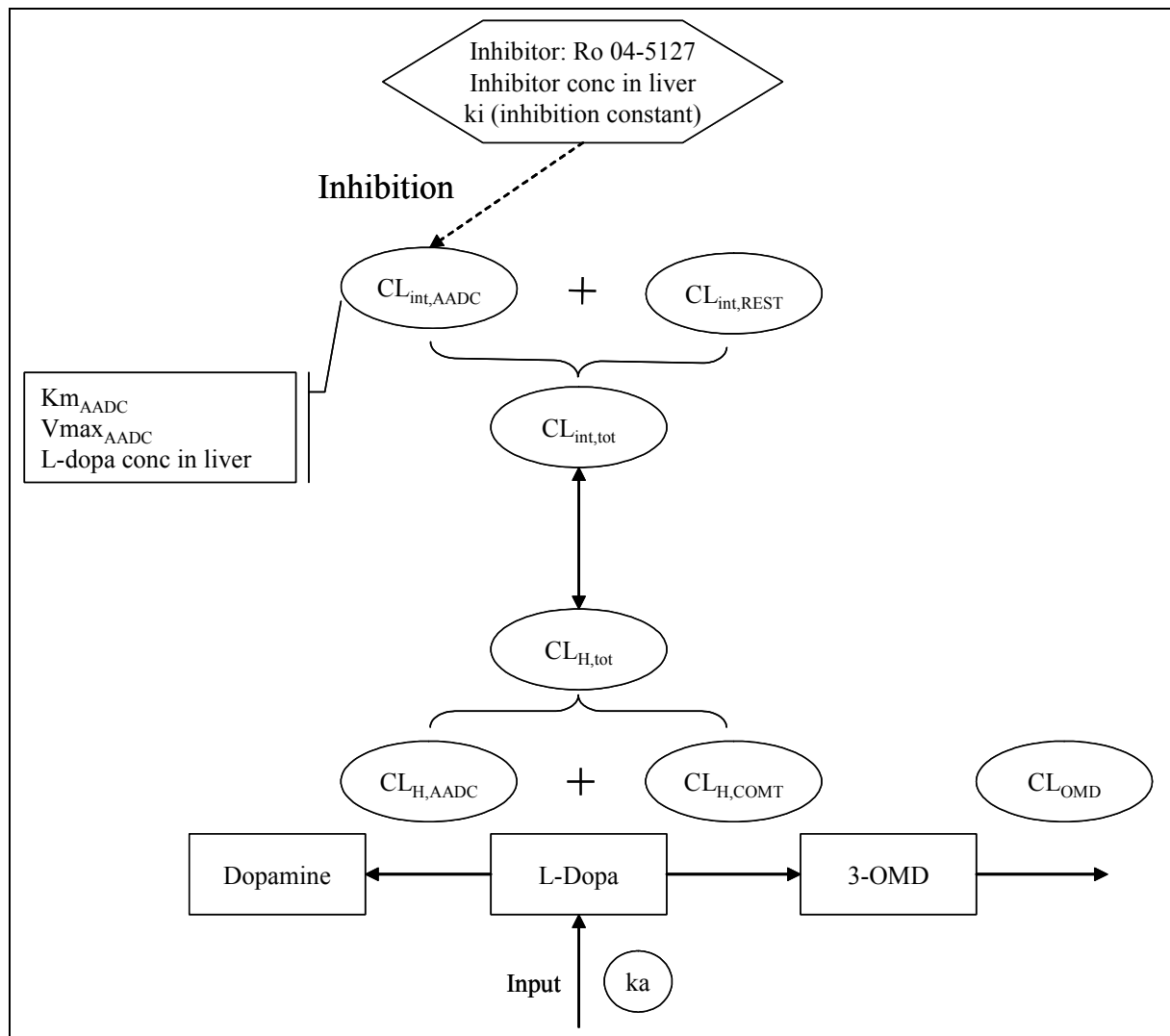
6.4.3.1 Experimental Data

The plasma concentrations of L-dopa and 3-OMD which were used for the fitting were taken from the animal experiment in rats described in Chapter 3.

6.4.3.2 Pharmacokinetic Model for L-Dopa and 3-OMD

The conceptual model for the pharmacokinetics of L-dopa and its metabolite 3-OMD containing liver and plasma concentrations as well as the inhibition of the L-dopa metabolism by Ro 04-5127 in the liver is shown in Figure 45.

FIGURE 45: Schematic representation of conceptual model



For abbreviations in Figure 45 see text and glossary of abbreviations.

The same parameters were estimated as in the model described in Chapter 3 (i.e. without the liver model) plus three new parameters i.e. $V_{max_{AADC}}$, $K_{m_{AADC}}$, $CL_{int,REST}$. There were two different absorption rate constants for L-dopa required; both were estimated. K_{a_b} was the absorption rate constant after treatment with L-dopa alone and k_{a_c} was the absorption rate constant after treatment with L-dopa/benserazide. In addition there were two different volumes of distributions and clearances for 3-OMD, depending on whether L-dopa was given alone or together with benserazide. The liver model adopted the conditions of the parallel tube model. The total intrinsic clearance of L-dopa was the sum of intrinsic clearance mediated by AADC and the intrinsic clearance mediated by other enzymes. In the presence of the inhibitor the intrinsic clearance of L-dopa via the AADC pathway was inhibited competitively by the liver concentration of Ro 04-5127.

The mass balances for the L-dopa compartment and the 3-OMD compartment were described by differential equations (Eq. 93 to Eq. 95).

$$\frac{dA_{dopa,i}}{dt} = -ka_i * A_{dopa,i}(t) \quad \text{Eq. 93}$$

$$V_{dopa} * \frac{dC_{dopa,i}}{dt} = Q * C_{hv} - CL_{H,tot} * C_{dopa,i}(t) \quad \text{Eq. 94}$$

$$V_{OMD,i} * \frac{dC_{OMD,i}}{dt} = CL_{H,COMT} * C_{dopa,i}(t) - CL_{OMD,i} * C_{OMD,i}(t) \quad \text{Eq. 95}$$

$A_{dopa,i}$: amount L-dopa in gut compartment, $C_{dopa,i}$: L-dopa concentration in systemic compartment, $C_{OMD,i}$: 3-OMD concentration in systemic compartment (i = b (treatment L-dopa); i = c (treatment L-dopa/benserazide))

The bioavailability (F) and the hepatic extraction ratio (ER) of L-dopa were calculated by Eq. 58 and Eq. 64, respectively. The total hepatic clearance of L-dopa as well as the total intrinsic clearance were based on the parallel tube model as liver model and are listed below under “Equations for parallel tube model”.

Equations for parallel tube model: The total hepatic clearance of L-dopa was estimated by Eq. 51 using the hepatic blood flow, the total intrinsic clearance of L-dopa, and the fraction unbound that was set to 1. The total intrinsic clearance of L-dopa was the sum of the intrinsic clearances mediated by AADC, COMT, and OTHER elimination pathways. The intrinsic clearances of COMT and via OTHER elimination pathways were taken together as $CL_{int,REST}$. The liver concentration (\hat{c}) was the logarithmic mean of the portal vein concentration and the hepatic vein concentration. (Eq. 96)

$$CL_{int,tot} = CL_{int,AADC} + CL_{int,COMT0} + CL_{int,OTHER} = CL_{int,AADC} + CL_{int,REST} = \frac{V \max_{AADC}}{(Km_{AADC} + \hat{c})} + CL_{int,REST} \quad \text{Eq. 96}$$

\hat{c} : liver concentration of L-dopa, $CL_{int,AADC}$: intrinsic clearance via AADC, $CL_{int,COMT0}$: intrinsic clearance via COMT, $CL_{int,OTHER}$: intrinsic clearances via pathways other than AADC and COMT, $CL_{int,REST}$: intrinsic clearances via pathways other than AADC, $CL_{int,tot}$: total intrinsic clearance, Km_{AADC} : Michaelis-Menten constant of AADC, $V\max_{AADC}$: maximum metabolic rate of AADC

In Eq. 96 the concentration \hat{c} was replaced by Eq. 53 using Eq. 54 to calculate the hepatic vein concentration. The fraction unbound, f_u , was set to 1.

If L-dopa was combined with benserazide, the total intrinsic clearance of L-dopa, assuming competitive inhibition, was then defined by Eq. 97.

$$CL_{\text{int,tot}(I)} = \frac{V \max_{AADC}}{\left(Km_{AADC} * \left(1 + \frac{\hat{c}(I)}{ki} \right) + \hat{c} \right)} + CL_{\text{int,REST}} \quad \text{Eq. 97}$$

\hat{c} : liver concentration of L-dopa, $\hat{c}(I)$: liver concentration of inhibitor, $CL_{\text{int,REST}}$: intrinsic clearances via pathways other than AADC, $CL_{\text{int,tot}(I)}$: total intrinsic clearance in the presence of the inhibitor, ki : inhibition constant, Km_{AADC} : Michaelis-Menten constant of AADC, $V\max_{AADC}$: maximum metabolic rate of AADC

Eq. 96 and Eq. 97 are implicit functions and were solved numerically for the total intrinsic clearance (with and without inhibition) as described for Eq. 77 and Eq. 78.

Weighting: In ACSL Optimize the option for the optimizer to find the best value for the weighting parameter was chosen.

Integration and optimization: The integration algorithm used was Runge-Kutta-Fehlberg with a variable step size and a fixed order (i.e. 5th order). The step size was defined such that it could not exceed 0.01. The model was fitted to the average L-dopa and 3-OMD plasma concentrations with and without benserazide simultaneously, using the approach of naïve averaging of data. The parameters were evaluated by maximum likelihood estimation, using as optimization algorithm, the Generalized Reduced Gradient ^[218], for maximizing the log likelihood function.

6.4.4 Results

After treatment with L-dopa alone the predicted C_{max} of L-dopa was overestimated, whereas the predicted 3-OMD plasma concentrations described the observed mean data well (Figure 46). In the group in which L-dopa was combined with benserazide the predicted plasma concentrations of both L-dopa and 3-OMD were comparable with the observed mean data (Figure 47). The final parameter estimates are listed in Table 32. The objective function expressed as log likelihood function was -75 .

TABLE 32: Final parameter estimates

Analyte	Treatment	PK Parameter [Unit]	Estimate	CV%
L-Dopa	after L-dopa alone	ka_b [h^{-1}]	2.89	17
	after L-dopa/benserazide	ka_c [h^{-1}]	12.9	13
	after L-dopa alone or L-dopa/benserazide	V_{dopa} [L]	0.450	5
		$CL_{int,REST}$ [L/h]	0.675	2
		Km_{AADC} [$\mu\text{mol/L}$]	715	117
	$Vmax_{AADC}$ [$\mu\text{mol/h}$]	584	109	
3-OMD	after L-dopa alone	$CL_{OMD,b}$ [L/h]	0.0292	11
		$V_{OMD,b}$ [L]	0.459	9
	after L-dopa/benserazide	$CL_{OMD,c}$ [L/h]	0.0174	5
		$V_{OMD,c}$ [L]	0.225	3
Ro 04-5127	after L-dopa/benserazide	ki [$\mu\text{mol/L}$]	0.00245	44

CV%: derived from asymptotic standard error of estimate

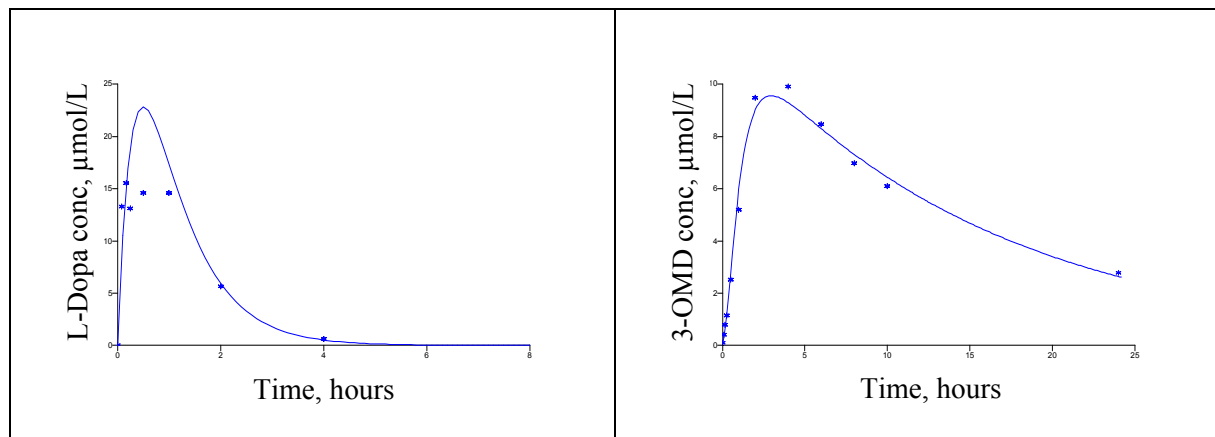
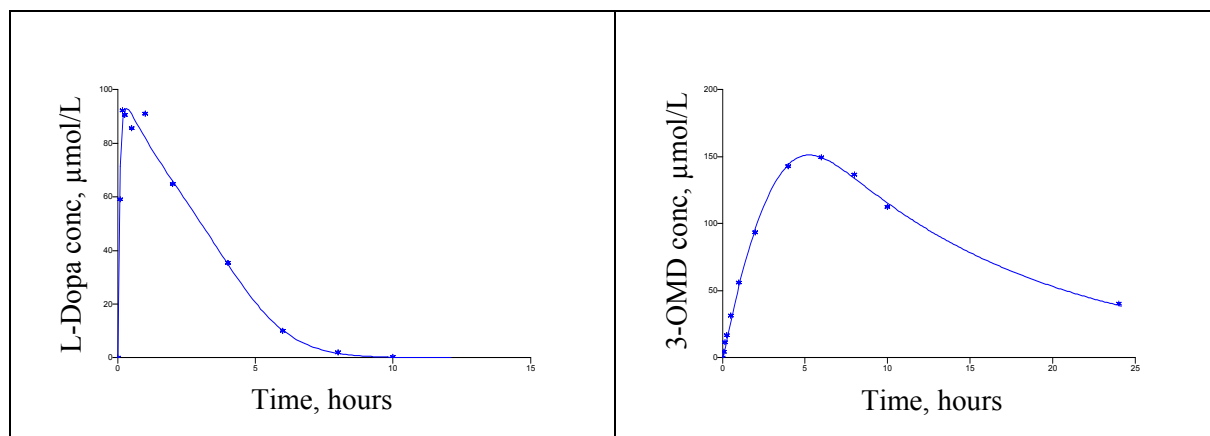
FIGURE 46: Predicted (—) and observed (*) L-dopa and 3-OMD plasma concentrations after oral administration of 80 mg/kg L-dopa

FIGURE 47: Predicted (—) and observed (*) L-dopa and 3-OMD plasma concentrations after oral administration of 80/20 mg/kg L-dopa/benserazide



6.5 OVERALL DISCUSSION OF CHAPTERS 6.2 TO 6.4

Modeling of the PK drug-drug interaction between L-dopa and benserazide at the level of the liver posed several difficulties which are described below and demonstrated the limitations and difficulties inherent in modeling a complex process.

In **Chapter 6.2** liver models, such as the well-stirred model and the parallel tube model, were implemented mathematically to describe the L-dopa/benserazide interaction in the liver and the modeling results were compared.

Most of the parameters, i.e. the absorption rate constant of L-dopa, the volume of distribution of L-dopa and 3-OMD and the clearance of 3-OMD, were very similar between the two models. The inhibition constant was 0.942 $\mu\text{g/L}$ for the parallel tube model, whereas the inhibition constant for the well-stirred model was 60 times smaller i.e. 0.0145 $\mu\text{g/L}$. The two parameters β_{AADC} and V_{AADC}^* are not comparable because they relate to different concentrations C^* . The Michaelis-Menten constant of AADC, K_{mAADC} , was 6438 $\mu\text{mol/L}$ for the parallel tube model and 1869 $\mu\text{mol/L}$ for the well-stirred model. The maximum rate of metabolism of AADC, V_{maxAADC} , was 13321 $\mu\text{mol/h}$ for the parallel tube model and 14517 $\mu\text{mol/h}$ for the well-stirred model. However, the parameter estimates for the well-stirred model need to be interpreted with caution due to uncertainty in their estimation.

Both liver models could be fitted to the average observed values in spite of their complex mathematical relationships (i.e implicit function). However, the results did not permit discrimination between the two models nor a precise determination of K_{mAADC} and V_{maxAADC} . The plasma concentrations of L-dopa and 3-OMD were insufficiently informative

to support such complex models. This manifested itself in high correlations between parameters as well as high estimation errors of the final parameter estimates. Furthermore, in the well-stirred model, V_{AADC}^* was an insensitive parameter; the final estimate was the same as the initial estimate. In both models, if the concentration C^* was changed, the estimates for $K_{m_{AADC}}$ and $V_{max_{AADC}}$ changed, indicating the uncertainty in these parameter estimates.

The initial concept was to run the models with the classical Michaelis-Menten parameterization in a second step using the computed values for $K_{m_{AADC}}$ and $V_{max_{AADC}}$ from the reparameterized model as initial estimates. However, the results were not usable and are not reported here.

In both models, the liver concentrations of benserazide drove the inhibition. This is a simplification, as it is known that the metabolite Ro 04-5127 is the actual inhibitor. In spite of this simplification as well as the questionable results, this work provided experience in implementing liver models into the L-dopa/benserazide situation and how to overcome mathematical and programming issues. This ultimately helped to develop the final model described in Chapter 6.4.

In **Chapter 6.3** a PK model for benserazide and its metabolite Ro 04-5127 is described. This PK model was developed to calculate the liver concentrations of Ro 04-5127 which is formed to a major extent in the gut and inhibits the enzyme AADC. The data situation combined with the high complexity of the model did not permit fitting of the model to the observed plasma concentrations of benserazide and Ro 04-5127. However, based on information reported in the literature and the knowledge gained in Chapter 3 of this thesis, it was possible to develop a PK model which calculated the plasma concentrations of benserazide and Ro 04-5127 well. The formulation of the benserazide/Ro 04-5127 model was an important step towards establishment of the enhanced PK model L-dopa/benserazide described in Chapter 6.4.

In **Chapter 6.4** an enhanced PK model for L-dopa/benserazide was developed in which the liver model was represented by parallel tubes and the liver concentrations of Ro 04-5127 were inhibiting AADC. The parallel tube model was chosen as liver model, since the optimization process was in general more stable than for the well-stirred model, although the latter is the simpler model of the two. The estimated PK parameters obtained with this fit were not in all instances comparable to those obtained in Chapter 3 by compartmental and non-compartmental analyses. The estimated absorption rate after L-dopa was comparable to that calculated with the residual method (fit vs residual method: 2.89 h^{-1} vs 2.11 h^{-1}), whereas after

L-dopa/benserazide k_a was 10 times higher than calculated with the residual method (fit vs residual method: 12.9 h^{-1} vs 1.29 h^{-1}). Assuming a saturable process for the absorption of L-dopa one would expect that the absorption rate constant after L-dopa/benserazide was smaller than after L-dopa alone, as higher L-dopa concentrations are reached. The final parameter estimates of the 3-OMD volumes of distribution and of the 3-OMD clearances differed from the final estimates obtained with the compartmental model described in Chapter 3, which did not include a liver model (Table 33). The volume of distribution of L-dopa was similar (Table 33).

TABLE 33: Comparison of final parameter estimates

PK Parameters [Unit]	Final Parameter Estimate	
	<i>Compartmental analysis without liver model</i>	<i>Compartmental analysis with liver model</i>
$V_{\text{OMD},b}$ [L]	0.196	0.459
$V_{\text{OMD},c}$ [L]	0.128	0.225
$CL_{\text{OMD},b}$ [L/h]	0.0120	0.0293
$CL_{\text{OMD},c}$ [L/h]	0.00895	0.0174
V_{dopa} [L]	0.496	0.450

However, the comparison between the PK parameters of Chapter 6.4 and the one described in Chapter 3 needs to be interpreted with caution as there are differences between the two PK models (Table 34).

TABLE 34: Differences between PK models of Chapter 3 and Chapter 6.4

	Compartmental PK model of Chapter 3	PK model of Chapter 6.4
Inhibitor concentration	Plasma concentration of Ro 04-5127	Liver concentration of Ro 04-5127
Bioavailability of L-dopa	$F = F_G * F_H$	$F = F_H$
Optimization	Naïve pooling of data	Naïve averaging of data

The Michaelis-Menten constant of AADC, $K_{m\text{AADC}}$, was estimated to be $6438 \mu\text{mol/L}$ for the parallel tube model in Chapter 6.2 and $715 \mu\text{mol/L}$ for the parallel tube model described in Chapter 6.4. The K_m -values described in the literature varied over a great range, depending on the localization of the enzyme and the assay conditions, such as e.g., protein concentration (Table 35). This made it difficult to draw conclusions from comparison of the estimates.

TABLE 35: Literature values for $K_{m_{AADC}}$

Enzyme	Substrate	Cells	$K_{m_{AADC}}$	Reference
AADC	L-dopa	human antrum human jejunum human brain	95 $\mu\text{mol/L}$ 600 $\mu\text{mol/L}$ 414 $\mu\text{mol/L}$	[219]
AADC	L-dopa	-	500 to 50000 $\mu\text{mol/L}$	[220]
AADC	L-dopa	AADC purified from beef adrenal tissue	540 $\mu\text{mol/L}$	[221]
AADC	L-dopa	AADC from guinea-pig kidney extracts	530 $\mu\text{mol/L}$	[222]
AADC	L-dopa	AADC purified from hog kidney	190 $\mu\text{mol/L}$	[223]
AADC	L-dopa	homogenates of isolated renal tubules of rat	3580 $\mu\text{mol/L}$	[224]
AADC	L-dopa	rat hypothalamic slices	131 $\mu\text{mol/L}$	[225]

The comparison of the estimated V_{\max} -values using liver models and the V_{\max} -values in the literature is even more difficult due the fact that the experimentally determined V_{\max} -values are given in units concentration / amount protein (Table 36).

TABLE 36: Literature values for $V_{\max_{AADC}}$

Enzyme	Substrate	Cells	$V_{\max_{AADC}}$	Reference
AADC	L-dopa	homogenates of isolated renal tubules of rat	0.305 $\mu\text{mol/h/mg protein}$	[224]
AADC	L-dopa	rat hypothalamic slices	0.0073 $\mu\text{mol/h/mg protein}$	[225]
AADC	L-dopa	human jejunum	0.198 $\mu\text{mol/h/mg protein}$	[219]

It was not possible to compare the estimated values for the inhibition constant to literature data, as this value has not been reported. The *in vitro* value for the k_i of Ro 04-5127 has never been determined.

For practical reasons the software ACSL was chosen in preference to WinNonlin and NONMEM, because this software provides a documented and integrated function for solving implicit equations, i.e. IMPLC. This device was necessary in order to solve the equations used in the models of this chapter.

The models were fitted to the average L-dopa and 3-OMD plasma concentrations (naïve averaging of data). Given the use of ACSL to fit this kind of structural model (containing implicit equations) and the limitations of the experimental data, neither individual fitting nor population methods, i.e. naïve-pooled-data or mixed effects modeling, were suitable for application.

A reparameterization of the Michaelis-Menten equation was considered in the PK models described in Chapter 6.2. It is known that the parameters of the Michaelis-Menten equation are poorly estimated when the range of the available data is limited to $< 0.95 V_{\max}$. Through reparameterization the concentration C^* is chosen within the range of the observed data, and therefore the parameters V^* and β are more precisely estimated than the parameters K_m and V_{\max} of the standard parameterization. However, the reparameterization did not improve the precision of the parameter estimates and therefore was abandoned again for the model described in Chapter 6.4.

In all models for the purpose of simplification assumptions were necessary. The plasma concentrations were used interchangeably with blood concentrations assuming a blood/plasma partition ratio of 1. The bioavailability was assumed to be reduced by hepatic first-pass metabolism only, thus ignoring the possibility of gut wall metabolism. The total clearance of L-dopa was considered only to be hepatic, neglecting any renal contribution.

With all this in mind, the models can describe the observed L-dopa and 3-OMD plasma concentrations. However, these models are clearly a simplification of the true processes; their full support by experimental data would require much more information than was available from the limited experiments performed. Such experimental data could include an in-vivo experiment in which various doses of L-dopa are given to characterize the nonlinear kinetics for the elimination of L-dopa via AADC or an animal experiment in which liver concentrations of L-dopa, 3-OMD, benserazide, and Ro 04-5127 are measured assaying liver homogenates at different time points after dosing.

Before performing a further study in rats, however, one could also contemplate applying *in silico* trial simulation^[226] to explore various candidate study designs, e.g. employing various dosing regimens, with the objective of selecting a study design permitting estimation of $V_{\max AADC}$ and $K_{m AADC}$ with greater accuracy and precision than was possible with the data from the current study design (see Chapter 3). This would have the advantage of providing useful advance information for a rational planning and successful outcome of an

in vivo experiment in rats. In addition, other objectives such as the influence of various analysis models (e.g. first order versus Michaelis-Menten) could be evaluated with the trial simulation technique.

In summary, the obtained parameter estimates especially k_i , $K_{m_{AADC}}$, and $V_{max_{AADC}}$ are questionable, because the experimental data available for the fit were not found to support the estimation of the parameters of these complex models. Although a variety of data evaluation approaches and models were explored, they could not overcome the deficiencies inherent in the available data. The work presented here gives clear indications on the type of information which is missing for a comprehensive mechanistic understanding and what would be needed to close the gap.

6.6 OVERALL CONCLUSION OF CHAPTERS 6.2 TO 6.4

The work presented in this chapter was an attempt to model a highly complex system. Despite best efforts to fit a coherent PK model taking liver concentrations into account to earlier derived *in vivo* experimental data the results were unsatisfactory. This was due to the lack of information, in particular kinetic data, derivable from the earlier experimental work and other sources adequately meeting the demands of the modeling methods available.

Chapter 7

GENERAL CONCLUSIONS AND OUTLOOK

Chapter 7

GENERAL CONCLUSIONS AND OUTLOOK

Throughout recorded history it has been a human desire to explore and understand the environment. Within the natural sciences, including the science of pharmacology, the process begins with the observation of a phenomenon, for example an event or relationship, requiring analysis and description. Precise measurement and the numerical evaluation and expression of a phenomenon under investigation are crucial to its interpretation and understanding. In the disciplines of pharmacokinetics and pharmacodynamics the application of mathematical models provides key means for the numerical expression of a given observed phenomenon. They provide a greater understanding of the mechanistic relationships of pharmacological processes. Mathematical and computer sciences have accordingly become prime tools in pharmacology and for the past few years have been employed throughout preclinical and clinical drug development.

7.1 GENERAL CONCLUSIONS

The present thesis demonstrates that pharmacokinetic relationships of varying complexity expressed in mathematical models permit the description and understanding of the mechanism of PK drug-drug interactions and that the extrapolation from animal to human subjects is facilitated by the use of parameters which are estimated using pharmacokinetic models.

This is demonstrated in that the L-dopa/benserazide compartmental model established in rats permitted a mechanism-based view of the interaction between L-dopa and benserazide and supported the hypothesis that Ro 04-5127 is the primary active metabolite of benserazide. This pharmacokinetic model combined with allometric scaling of parameter estimates for rats was found useful and successful in predicting and describing the L-dopa pharmacokinetics in humans after L-dopa treatment with and without benserazide.

The L-dopa/benserazide compartmental model established in rats was not validated with a second dataset. However, the parameter estimates obtained with this model were compared to literature data (rat data and human data (after allometric scaling)) and they were in good accord. Furthermore, in order to exclude a potential distortion of the model structure or the parameter estimates due to the employed naïve-pooled-data approach, the population PK

analysis was repeated using nonlinear mixed effects modeling. This showed that the population parameters obtained with nonlinear mixed effects modeling were comparable to the population parameters obtained by pooling the data for L-dopa/3-OMD after L-dopa alone and for benserazide/Ro-5127 after benserazide alone. The interaction between L-dopa and benserazide was too complex to be modeled by this approach.

The pharmacokinetics of benserazide and its metabolite Ro 04-5127 have been described for the first time by a compartmental model.

Finally, liver models such as the well-stirred model and the parallel tube model were studied for their use to describe the drug-drug interaction between L-dopa and benserazide at the level of the liver. This was an attempt to model a highly complex system. In doing so, despite extensive effort to succeed within the limits of what can be learnt from the existing data and the modeling methods available, it was very difficult to fit a coherent PK model, which takes liver concentrations into account, to the data.

The investigation of the two hypotheses, using L-dopa and benserazide as model compounds for the pharmacokinetic interaction, covers not only preclinical as well as clinical data but also uses a variety of software to obtain the answers. The software programs WinNonlin, ModelMaker, ACSL, and NONMEM together with SAS were applied depending on their strengths. WinNonlin is widely used in the pharmacokinetic community, is easy to work with, but is not suitable for complex mathematical functions (e.g. implicit function), quick simulations or nonlinear mixed effect modeling. For this one would use ACSL, ModelMaker, and NONMEM, respectively. The model for describing an interaction such as that between L-dopa and benserazide was not available in the software library of any of these softwares but had to be programmed in the respective software language. In conclusion, it can be said that at present there is no one single software suitable for all issues and, depending on the software and the model task, skill-flexibility is required. Most pharma industries have responded to this difficulty by setting up dedicated departments for modeling and simulation.

The work presented in this thesis was made possible by integrating techniques and know-how from a variety of disciplines such as pharmacology, mathematics, informatics (programming), and bioanalytics. It was through the interplay of all four sciences that a deeper understanding of the interaction between L-dopa and benserazide was attained. In the future such

interdisciplinary work in drug development will become increasingly important and will be the key to success.

7.2 OUTLOOK

The purpose of this thesis has been the investigation of modeling approaches to describe the PK drug-drug interaction between L-dopa and benserazide in the rat and combining them with interspecies scaling techniques to predict the interaction in humans based on rat data. The L-dopa/benserazide model was used for rat data as well as for healthy human data. A potential further application would be to use the model for patient data. Moreover, it would be capable of adaptation to include PD measurements and also to take into account underlying disease progress.

Mechanism-based modeling was not used during the development of Madopar[®] (co-formulation of L-dopa and benserazide) in the sixties. It was, however, adopted in the more recent development program for saquinavir (Invirase[®], Fortovase[®]) for treatment of HIV infected patients. In this latter case mechanism-based mathematical modeling was successfully applied and provided a description of the main findings on saquinavir exposure, including the influence of controllable factors such as formulation, food, and combinations with drugs such as ritonavir or nelfinavir. The saquinavir model was useful for identifying gaps and guiding the direction of preclinical and clinical investigations. Regarding the drug combination saquinavir/ritonavir it provided key findings for the choice of investigational doses for the two drugs. One could contemplate that, had such mechanism-based modeling been available during the development of Madopar[®], it would have brought comparable benefit as was seen for saquinavir. Thus a model such as that presented here might have helped investigation of the optimal dose combination for L-dopa and benserazide. Moreover, the present model might also be further developed to study the interaction between L-dopa/benserazide and a COMT inhibitor such as tolcapone or entacapone or be adaptable to other compounds exhibiting interaction with a second drug similar to that of L-dopa with benserazide. Thus the model-based approach could be especially applicable in the development of combination drug therapy as demonstrated with saquinavir/ritonavir.

Looking at drug development as a whole, it would be desirable to have a mechanism-based model throughout the development of an investigational drug, i.e. the model would be applied first to animal data, then to healthy human data and subsequently to patient data. One could also contemplate application in specific patient populations such as

liver or renal impaired patients. On-going adaptation would naturally be necessary, i.e. the model would develop to take into account information newly available in the different stages of drug development. Another area of use in drug development would be to apply the model established for a lead compound to any follow-up compound, thus enhancing knowledge transfer.

* * * * *

Research, in particular drug research, is frequently driven by current concepts of what is rational and logical. Thus the search for novel solutions or deeper insight may be seen as proceeding primarily via application of a logical sequence of studies or steps. However, the contribution to be made by intuition, logic's equally important counterpart, should not be overlooked and the need for flexibility should not be forgotten.

“The intellect has little to do on the road of discovery. There comes a leap in consciousness, call it intuition or what you will, and the solution comes to you and you don't know how or why.”

Albert Einstein (1879-1955)

REFERENCE LIST

1. D. B. Calne. Parkinsonism. Clinical and neuropharmacologic aspects. *Postgraduate Medicine* 64: 82-88 (1978).
2. J. M. Cedarbaum and L. S. Schleifer. Drugs for Parkinson's disease, spasticity, and acute muscle spasms. In A. Goodman-Gilman, T. W. Rall, A. S. Nies and P. Taylor, *Goodman and Gilman's the pharmacological basis of therapeutics*, Pergamon Press, New York, 1990 pp. 463-484.
3. A. H. Rajput, K. P. Offord, C. M. Beard and L. T. Kurland. Epidemiology of parkinsonism: incidence, classification, and mortality. *Annals of Neurology* 16: 278-282 (1984).
4. O. Hornykiewicz. The pathochemical perspectives of Parkinson's disease. An attempt at a neurochemical definition. *Functional Neurology* 3: 379-391 (1988).
5. O. Hornykiewicz. Parkinson's disease: from brain homogenate to treatment. *Federation Proceedings* 32: 183-190 (1973).
6. R. J. Uitti and D. B. Calne. Pathogenesis of idiopathic parkinsonism. *European Neurology* 33: 6-23 (1993).
7. K. Gwinn-Hardy. Genetics of Parkinsonism. *Movement Disorders* 17: 645-656 (2002).
8. Z. Huang, F. R. De la Fuente and A. J. Stoessl. Etiology of Parkinson's disease. *The Canadian Journal of Neurological Sciences* 30: S10-S18 (2003).
9. B. S. Schoenberg, D. W. Anderson and A. F. Haerer. Prevalence of Parkinson's disease in the biracial population of Copiah County, Mississippi. *Neurology* 35: 841-845 (1985).
10. L. S. Forno. Pathology of parkinson's disease: The importance of the substantia nigra and Lewy bodies. In G. M. Stern, *Parkinson's disease*, Johns Hopkins Press, Baltimore, 1990 pp. 185-238.
11. E. Mutschler. *Arzneimittelwirkungen, Lehrbuch der Pharmakologie und Toxikologie*, Wissenschaftliche Verlagsgesellschaft mbH, Stuttgart, 1986.
12. H. Bernheimer, W. Birkmayer, O. Hornykiewicz, K. Jellinger and F. Seitelberger. Brain dopamine and the syndromes of Parkinson and Huntington. Clinical, morphological and neurochemical correlations. *Journal of the Neurological Sciences* 20: 415-455 (1973).
13. O. Hornykiewicz and S. J. Kish. Biochemical pathophysiology of Parkinson's disease. *Advances in Neurology* 45: 19-34 (1987).
14. O. Hornykiewicz. Biochemical aspects of Parkinson's disease. *Neurology* 51: S2-S9 (1998).
15. J. Jankovic. New and emerging therapies for Parkinson disease. *Archives of Neurology* 56: 785-790 (1999).
16. A. Björklund, S. B. Dunnett, P. Brundin, A. J. Stoessl, C. R. Freed, R. E. Breeze, M. Levivier, et al. Neural transplantation for the treatment of Parkinson's disease. *Lancet Neurology* 2: 437-445 (2003).
17. S. Polgar, M. E. Morris, S. Reilly, B. Bilney and P. R. Sanberg. Reconstructive neurosurgery for Parkinson's disease: a systematic review and preliminary meta-analysis. *Brain Research Bulletin* 60: 1-24 (2003).

18. R. A. Hauser, T. B. Freeman, B. J. Snow, M. Nauert, L. Gauger, J. H. Kordower and C. W. Olanow. Long-term evaluation of bilateral fetal nigral transplantation in Parkinson disease. *Archives of Neurology* 56: 179-187 (1999).
19. G. F. Wooten. Pharmacokinetics of levodopa. In C. D. Marsden and S. Faka, *Movement disorders*, Butterworths, 1984 pp. 231-240.
20. Monograph Dopamine Hydrochloride. In K. Parfitt, *Martindale*, The Pharmaceutical Press, London, 2003.
21. J. G. Nutt and J. H. Fellman. Pharmacokinetics of levodopa. *Clinical Neuropharmacology* 7: 35-49 (1984).
22. J. G. Nutt. Pharmacokinetics of levodopa. In W. C. Koller, *Handbook of Parkinson's Disease*, Marcel Dekker Inc, New York - Basel, 1987 pp. 339-354.
23. W. Burkard, K. Gey and A. Pletscher. Inhibition of decarboxylase of aromatic amino acids by 2,3,4-trihydroxybenzylhydrazine and its seryl derivative. *Archives of Biochemistry and Biophysics* 107: 187-196 (1964).
24. Monograph Benserazide Hydrochloride. In K. Parfitt, *Martindale*, The Pharmaceutical Press, London, 2003.
25. G. E. P. Box. Robustness in the strategy of scientific model building. In R. L. Launer and G. N. Wilkinson, *Robustness in statistics*, Academic Press, New York, 1979 pp. 202.
26. PricewaterhouseCoopers. Pharma 2005 - Silicon Rally: The race to e-R&D. 1-21 (1999).
27. PricewaterhouseCoopers. Pharma 2010 - The threshold of innovation. 1-52 (2002).
28. B. G. Reigner, P. E. O. Williams, J. H. Patel, J. L. Steimer, C. Peck and P. van Brummelen. An evaluation of the integration of pharmacokinetic and pharmacodynamic principles in clinical drug development: Experience within Hoffmann La Roche. *Clinical Pharmacokinetics* 33: 142-152 (1997).
29. D. D. Breimer and M. Danhof. Relevance of the application of pharmacokinetic-pharmacodynamic modelling concepts in drug development. The "wooden shoe" paradigm. *Clinical Pharmacokinetics* 32: 259-267 (1997).
30. S. G. Machado, R. Miller and C. Hu. A regulatory perspective on pharmacokinetic / pharmacodynamic modelling. *Statistical Methods in Medical Research* 8: 217-245 (1999).
31. L. B. Sheiner and J. L. Steimer. Pharmacokinetic / pharmacodynamic modeling in drug development. *Annual Review of Pharmacology and Toxicology* 40: 67-95 (2000).
32. L. P. Balant and M. Gex Fabry. Modelling during drug development. *European Journal of Pharmaceutics and Biopharmaceutics* 50: 13-26 (2000).
33. ICH, 1997. ICH consensus guideline on general considerations for clinical trials. CPMP/ICH/291/95. (1997).
34. CDER: Guidance for industry: population pharmacokinetics. <http://www.fda.gov/cder/guidance/index.htm> (1999).
35. M. Danhof, J. W. Mandema, A. Hoogerkamp and R. A. Mathôt. Pharmacokinetic-pharmacodynamic modelling in pre-clinical investigations: principles and perspectives. *European Journal of Drug Metabolism and Pharmacokinetics* 18: 41-47 (1993).

36. G. Levy. Variability in animal and human pharmacodynamic studies. In M. Rowland, L. B. Sheiner and J. L. Steimer, *Variability in drug therapy: description, estimation and control*, Raven Press, New York, 1985 pp. 125-138.
37. P. M. Klockowski and G. Levy. Kinetics of drug action in disease states. XXIII: Effect of acute hypovolemia on the pharmacodynamics of phenobarbital in rats. *Journal of Pharmaceutical Sciences* 77: 365-366 (1988).
38. I. M. Ramzan and G. Levy. Kinetics of drug action in disease states. XVIII. Effect of experimental renal failure on the pharmacodynamics of theophylline- induced seizures in rats. *The Journal of Pharmacology and Experimental Therapeutics* 240: 584-588 (1987).
39. G. Levy. The case for preclinical pharmacodynamics. In A. Yacobi, J. P. Skelly, V. P. Shah and L. Z. Benet, *Integration of pharmacokinetics, pharmacodynamics and toxicokinetics in rational drug development*, Plenum Press, New York, 1993 pp. 7-13.
40. J. M. Collins, C. K. Grieshaber and B. A. Chabner. Pharmacologically guided phase I clinical trials based upon preclinical drug development. *Journal of the National Cancer Institute* 82: 1321-1326 (1990).
41. C. C. Peck, W. H. Barr, L. Z. Benet, J. Collins, R. E. Desjardins, D. E. Furst, J. G. Harter, et al. Opportunities for integration of pharmacokinetics, pharmacodynamics, and toxicokinetics in rational drug development. *Pharmaceutical Research* 9: 826-833 (1992).
42. R. C. Schoemaker and A. F. Cohen. Estimating impossible curves using NONMEM. *British Journal of Clinical Pharmacology* 42: 283-290 (1996).
43. P. O. Gisleskog, D. Hermann, M. Hammarlund Udenaes and M. O. Karlsson. The pharmacokinetic modelling of GI198745 (dutasteride), a compound with parallel linear and nonlinear elimination. *British Journal of Clinical Pharmacology* 47: 53-58 (1999).
44. L. Aarons, M. O. Karlsson, F. Mentré, F. Rombout, J. L. Steimer and A. van Peer. Role of modelling and simulation in Phase I drug development. *European Journal of Pharmaceutical Sciences* 13: 115-122 (2001).
45. D. W. A. Bourne. Why model the data. In *Mathematical modeling of pharmacokinetic data*, Technomic Publishing Company Inc., Lancaster - Basel, 1995 pp. 1-8.
46. D. W. A. Bourne. *Mathematical modeling of pharmacokinetic data*, Technomic Publishing Company Inc., Lancaster - Basel, 1995.
47. N. H. G. Holford and L. B. Sheiner. Understanding the dose-effect relationship: clinical application of pharmacokinetic-pharmacodynamic models. *Clinical Pharmacokinetics* 6: 429-453 (1981).
48. W. A. Colburn. Simultaneous pharmacokinetic and pharmacodynamic modeling. *Journal of Pharmacokinetics and Biopharmaceutics* 9: 367-388 (1981).
49. H. Derendorf, H. Möllmann, M. Krieg, S. Tunn, C. Möllmann, J. Barth and H. J. Röthig. Pharmacodynamics of methylprednisolone phosphate after single intravenous administration to healthy volunteers. *Pharmaceutical Research* 8: 263-268 (1991).
50. H. G. Schaefer, R. Heinig, G. Ahr, H. Adelman, W. Tetzloff and J. Kuhlmann. Pharmacokinetic-pharmacodynamic modelling as a tool to evaluate the clinical relevance of a drug-food interaction for a nisoldipine controlled-release dosage form. *European Journal of Clinical Pharmacology* 51: 473-480 (1997).

51. W. J. Jusko and H. C. Ko. Physiologic indirect response models characterize diverse types of pharmacodynamic effects. *Clinical Pharmacology and Therapeutics* 56: 406-419 (1994).
52. H. Derendorf, G. Hochhaus, H. Möllmann, J. Barth, M. Krieg, S. Tunn and C. Möllmann. Receptor-based pharmacokinetic-pharmacodynamic analysis of corticosteroids. *Journal of Clinical Pharmacology* 33: 115-123 (1993).
53. M. Wakelkamp, G. Alván, J. Gabrielsson and G. Paintaud. Pharmacodynamic modeling of furosemide tolerance after multiple intravenous administration. *Clinical Pharmacology and Therapeutics* 60: 75-88 (1996).
54. M. R. Gastonguay and S. L. Schwartz. The use of multiple doses and pharmacodynamic system analysis to distinguish between dispositional delays and time-variant pharmacodynamics. *Pharmaceutical Research* 11: 1825-1828 (1994).
55. B. Meibohm and H. Derendorf. Basic concepts of pharmacokinetic / pharmacodynamic (PK/PD) modelling. *International Journal of Clinical Pharmacology and Therapeutics* 35: 401-413 (1997).
56. M. Gibaldi and D. Perrier. One-compartment model; Multicompartment model. In J. Swarbrick, *Pharmacokinetics*, Marcel Dekker Inc., New York - Basel, 1982 pp. 1-111.
57. J. Gabrielsson and D. Weiner. Pharmacokinetic concepts. In *Pharmacokinetic and Pharmacodynamic Data Analysis: Concepts and Applications*, Swedish Pharmaceutical Press, Stockholm, Sweden, 2000 pp. 45-174.
58. K. Godfrey. *Compartmental models and their application*, Academic Press, London, 1983.
59. D. W. A. Bourne. Simulation of data. In *Mathematical modeling of pharmacokinetic data*, Technomic Publishing Company Inc., Lancaster - Basel, 1995 pp. 35-55.
60. H. J. Motulsky and L. A. Ransnas. Fitting curves to data using nonlinear regression: a practical and nonmathematical review. *The FASEB Journal* 1: 365-374 (1987).
61. D. R. Cox and D. V. Hinkley. Maximum likelihood estimates. In *Theoretical Statistics*, Chapman & Hall, London, 1974 pp. 283-310.
62. C. C. Peck, S. L. Beal, L. B. Sheiner and A. I. Nichols. Extended least squares nonlinear regression: a possible solution to the "choice of weights" problem in analysis of individual pharmacokinetic data. *Journal of Pharmacokinetics and Biopharmaceutics* 12: 545-558 (1984).
63. J. A. Nelder and R. Mead. A simplex method for function minimization. *The Computer Journal* 7: 308-313 (1965).
64. N. R. Draper and H. Smith. *Applied regression analysis*, John Wiley & Sons, New York, 1981.
65. J. Gabrielsson and D. Weiner. Assessing the goodness-of-fit. In *Pharmacokinetic and Pharmacodynamic Data Analysis: Concepts and Applications*, Swedish Pharmaceutical Press, Stockholm, Sweden, 2000 pp. 300-314.
66. J. Gabrielsson and D. Weiner. *Pharmacokinetic and Pharmacodynamic Data Analysis: Concepts and Applications*, Swedish Pharmaceutical Press, Stockholm, Sweden, 2000.
67. T. J. DiCiccio and B. Efron. Bootstrap confidence intervals. *Statistical Science* 11: 189-212 (1996).
68. K. Yamaoka, T. Nakagawa and T. Uno. Application of Akaike's information criterion (AIC) in the evaluation of linear pharmacokinetic equations. *Journal of Pharmacokinetics and Biopharmaceutics* 6: 165-175 (1978).

-
69. H. Akaike. A new look at the statistical model identification. *IEEE Transactions on Automatic Control* 19: 716-723 (1974).
70. G. Schwarz. Estimating the dimension of a model. *The Annals of Statistics* 6: 461-464 (1978).
71. J. Gabrielsson and D. Weiner. Modeling strategies. In *Pharmacokinetic and Pharmacodynamic Data Analysis: Concepts and Applications*, Swedish Pharmaceutical Press, Stockholm, Sweden, 2000 pp. 261-327.
72. J. L. Steimer, S. Vozeh, A. Racine-Poon, N. Holford and R. O'Neill. The population approach: Rationale, methods, and applications in clinical pharmacology and drug development. In P. G. Welling and L. P. Balant, *Handbook of experimental pharmacology, pharmacokinetics of drugs*, Springer Verlag, Berlin-Heidelberg, 1994 pp. 405-451.
73. ICH Harmonised Tripartite Guideline (M3(M)) "Maintenance of the ICH guideline on non-clinical safety studies for the conduct of human clinical trials for pharmaceuticals".
74. J. Mordenti. Man versus beast: pharmacokinetic scaling in mammals. *Journal of Pharmaceutical Sciences* 75: 1028-1040 (1986).
75. R. A. Prentis, Y. Lis and S. R. Walker. Pharmaceutical innovation by the seven UK-owned pharmaceutical companies (1964-1985). *British Journal of Clinical Pharmacology* 25: 387-396 (1988).
76. D. W. A. Bourne. Physiologically based models. In *Mathematical modeling of pharmacokinetic data*, Technomic Publishing Company Inc., Lancaster - Basel, 1995 pp. 30-33.
77. L. J. Lesko, M. Rowland, C. C. Peck and T. F. Blaschke. Optimizing the science of drug development: opportunities for better candidate selection and accelerated evaluation in humans. *Pharmaceutical Research* 17: 1335-1344 (2000).
78. P. Poulin and F. P. Theil. A priori prediction of tissue:plasma partition coefficients of drugs to facilitate the use of physiologically-based pharmacokinetic models in drug discovery. *Journal of Pharmaceutical Sciences* 89: 16-35 (2000).
79. P. Poulin, K. Schoenlein and F. P. Theil. Prediction of adipose tissue: plasma partition coefficients for structurally unrelated drugs. *Journal of Pharmaceutical Sciences* 90: 436-447 (2001).
80. R. Kawai, D. Mathew, C. Tanaka and M. Rowland. Physiologically based pharmacokinetics of cyclosporine A: extension to tissue distribution kinetics in rats and scale-up to human. *Journal of Pharmacology and Experimental Therapeutics* 287: 457-468 (1998).
81. R. E. Oliver, A. F. Jones and M. Rowland. A whole-body physiologically based pharmacokinetic model incorporating dispersion concepts: Short and long time characteristics. *Journal of Pharmacokinetics and Pharmacodynamics* 28: 27-55 (2001).
82. B. Peng, J. Andrews, I. Nestorov, B. Brennan, P. Nicklin and M. Rowland. Tissue distribution and physiologically based pharmacokinetics of antisense phosphorothioate oligonucleotide ISIS 1082 in rat. *Antisense and Nucleic Acid Drug Development* 11: 15-27 (2001).
83. G. B. West, J. H. Brown and B. J. Enquist. A general model for the origin of allometric scaling laws in biology. *Science* 276: 122-126 (1997).
84. G. B. West, J. H. Brown and B. J. Enquist. The fourth dimension of life: Fractal geometry and allometric scaling of organisms. *Science* 284: 1677-1679 (1999).
85. J. Prothero. Methodological aspects of scaling in biology. *Journal of Theoretical Biology* 118: 259-286 (1986).

86. R. J. Smith. Allometric scaling in comparative biology: problems of concept and method. *The American Journal of Physiology* 246: R152-R160 (1984).
87. T. Lave, P. Coassolo and B. Reigner. Prediction of hepatic metabolic clearance based on interspecies allometric scaling techniques and in vitro-in vivo correlations. *Clinical Pharmacokinetics* 36: 211-231 (1999).
88. S. J. Gould. Allometry and size in ontogeny and phylogeny. *Biological reviews of the Cambridge Philosophical Society* 41: 587-640 (1966).
89. T. A. McMahon. Allometry and biomechanics: Limb bones in adult ungulates. *The American Naturalist* 109: 547-563 (1975).
90. R. L. Dedrick. Animal scale-up. *Journal of Pharmacokinetics and Biopharmaceutics* 1: 435-461 (1973).
91. J. Mordenti. Pharmacokinetic scale-up: accurate prediction of human pharmacokinetic profiles from animal data. *Journal of Pharmaceutical Sciences* 74: 1097-1099 (1985).
92. E. F. Adolph. Quantitative relations in the physiological constitutions of mammals. *Science* 109: 579-585 (1949).
93. W. L. Hayton. Pharmacokinetic parameters for interspecies scaling using allometric techniques. *Health Physics* 57 Suppl 1: 159-164 (1989).
94. H. Boxenbaum. Interspecies pharmacokinetic scaling and the evolutionary-comparative paradigm. *Drug Metabolism Reviews* 15: 1071-1121 (1984).
95. H. Boxenbaum and J. B. Fertig. Scaling of antipyrine intrinsic clearance of unbound drug in 15 mammalian species. *European Journal of Drug Metabolism and Pharmacokinetics* 9: 177-183 (1984).
96. I. Mahmood and J. D. Balian. Interspecies scaling: predicting clearance of drugs in humans. Three different approaches. *Xenobiotica* 26: 887-895 (1996).
97. I. Mahmood and J. D. Balian. Interspecies scaling: predicting pharmacokinetic parameters of antiepileptic drugs in humans from animals with special emphasis on clearance. *Journal of Pharmaceutical Sciences* 85: 411-414 (1996).
98. J. B. Houston. Utility of in vitro drug metabolism data in predicting in vivo metabolic clearance. *Biochemical Pharmacology* 47: 1469-1479 (1994).
99. P. J. Marroum, R. S. Uppoor, T. Parmelee, F. Ajayi, A. Burnett, R. Yuan, R. Svadjian, et al. In vivo drug-drug interaction studies--a survey of all new molecular entities approved from 1987 to 1997. *Clinical Pharmacology and Therapeutics* 68: 280-285 (2000).
100. J. Kuhlmann and W. Muck. Clinical-pharmacological strategies to assess drug interaction potential during drug development. *Drug Safety* 24: 715-725 (2001).
101. D. Schmassmann-Suhjar, R. Bullingham, R. Gasser, J. Schmutz and W. E. Haefeli. Rhabdomyolysis due to interaction of simvastatin with mibefradil. *Lancet* 351: 1929-1930 (1998).
102. Roche, FDA announce new drug-interaction warnings for mibefradil. *American Journal of Health System Pharmacy* 55: 210 (1998).
103. CDER: Guidance for industry: drug metabolism / drug interactions in the drug development process: studies in vitro. <http://www.fda.gov/cder/guidance/index.htm>. (1997).

104. CDER: Guidance for industry: in vivo drug metabolism / drug interaction studies: study design, data analysis, and recommendations for dosing and labeling in the drug development process: studies in vitro. <http://www.fda.gov/cder/guidance/index.htm> (1999).
105. CPMP: Note for guidance on the investigation of drug interactions, EWP/560/95. <http://www.emea.eu.int/>. (1998).
106. D. K. Yu. The contribution of P-glycoprotein to pharmacokinetic drug-drug interactions. *Journal of Clinical Pharmacology* 39: 1203-1211 (1999).
107. D. K. Meijer, G. J. Hooiveld, A. H. Schinkel, J. E. van Montfoort, M. Haas, D. de- Zeeuw, F. Moolenaar, et al. Transport mechanisms for cationic drugs and proteins in kidney, liver and intestine: implication for drug interactions and cell-specific drug delivery. *Nephrology Dialysis Transplantation* 14: 1-3 (1999).
108. M. Verschraagen, C. H. Koks, J. H. Schellens and J. H. Beijnen. P-glycoprotein system as a determinant of drug interactions: the case of digoxin-verapamil. *Pharmacological Research* 40: 301-306 (1999).
109. V. J. Wacher, C. Y. Wu and L. Z. Benet. Overlapping substrate specificities and tissue distribution of cytochrome P450 3A and P-glycoprotein: implications for drug delivery and activity in cancer chemotherapy. *Molecular Carcinogenesis* 13: 129-134 (1995).
110. Monograph Metoclopramide Hydrochloride. In K. Parfitt, *Martindale*, The Pharmaceutical Press, London, 2003.
111. P. E. Rolan. Plasma protein binding displacement interactions--why are they still regarded as clinically important? *British Journal of Clinical Pharmacology* 37: 125-128 (1994).
112. L. Z. Benet and B. Hoener. Changes in plasma protein binding have little clinical relevance. *Clinical Pharmacology and Therapeutics* 71: 115-121 (2002).
113. F. J. Gonzalez. The molecular biology of cytochrome P450s. *Pharmacological Reviews* 40: 243-288 (1988).
114. R. J. Weaver. Assessment of drug-drug interactions: concepts and approaches. *Xenobiotica* 31: 499-538 (2001).
115. N. Buss, P. Snell, J. Bock, A. Hsu and K. Jorga. Saquinavir and ritonavir pharmacokinetics following combined ritonavir and saquinavir (soft gelatin capsules) administration. *British Journal of Clinical Pharmacology* 52: 255-264 (2001).
116. G. N. Kumar, A. D. Rodrigues, A. M. Buko and J. F. Denissen. Cytochrome P450-mediated metabolism of the HIV-1 protease inhibitor ritonavir (ABT-538) in human liver microsomes. *The Journal of Pharmacology and Experimental Therapeutics* 277: 423-431 (1996).
117. B. Burchell and M. W. Coughtrie. UDP-glucuronosyltransferases. *Pharmacology and Therapeutics* 43: 261-289 (1989).
118. E. E. Samara, R. G. Granneman, G. F. Witt and J. H. Cavanaugh. Effect of valproate on the pharmacokinetics and pharmacodynamics of lorazepam. *Journal of Clinical Pharmacology* 37: 442-450 (1997).
119. I. de Waziers, P. H. Cugnenc, C. S. Yang, J. P. Leroux and P. H. Beaune. Cytochrome P 450 isoenzymes, epoxide hydrolase and glutathione transferases in rat and human hepatic and extrahepatic tissues. *The Journal of Pharmacology and Experimental Therapeutics* 253: 387-394 (1990).

120. K. E. Thummel, O. S. D, M. F. Paine, D. D. Shen, K. L. Kunze, J. D. Perkins and G. R. Wilkinson. Oral first-pass elimination of midazolam involves both gastrointestinal and hepatic CYP3A-mediated metabolism. *Clinical Pharmacology and Therapeutics* 59: 491-502 (1996).
121. U. A. Meyer. Genetic polymorphisms of drug metabolism. *Fundamental and Clinical Pharmacology* 4: 595-615 (1990).
122. F. Broly, A. Gaedigk, M. Heim, M. Eichelbaum, K. Morike and U. A. Meyer. Debrisoquine/sparteine hydroxylation genotype and phenotype: analysis of common mutations and alleles of CYP2D6 in a European population. *DNA and Cell Biology* 10: 545-558 (1991).
123. F. J. Gonzalez and U. A. Meyer. Molecular genetics of the debrisoquin-sparteine polymorphism. *Clinical Pharmacology and Therapeutics* 50: 233-238 (1991).
124. D. A. Flockhart. Drug interactions and the cytochrome P450 system. The role of cytochrome P450 2C19. *Clinical Pharmacokinetics* 29: 45-52 (1995).
125. J. O. Miners and D. J. Birkett. Cytochrome P4502C9: an enzyme of major importance in human drug metabolism. *British Journal of Clinical Pharmacology* 45: 525-538 (1998).
126. S. P. Spielberg. N-acetyltransferases: pharmacogenetics and clinical consequences of polymorphic drug metabolism. *Journal of Pharmacokinetics and Biopharmaceutics* 24: 509-519 (1996).
127. H. Kusuhara, H. Suzuki and Y. Sugiyama. The role of P-glycoprotein and canalicular multispecific organic anion transporter in the hepatobiliary excretion of drugs. *Journal of Pharmaceutical Sciences* 87: 1025-1040 (1998).
128. V. Lecreur, A. Courtois, L. Payen, L. Verhnet, A. Guillouzo and O. Fardel. Expression and regulation of hepatic drug and bile acid transporters. *Toxicology* 153: 203-219 (2000).
129. K. Ito, T. Iwatsubo, S. Kanamitsu, K. Ueda, H. Suzuki and Y. Sugiyama. Prediction of pharmacokinetic alterations caused by drug-drug interactions: Metabolic interaction in the liver. *Pharmacological Reviews* 50: 387-411 (1998).
130. W. C. Hunter. Oral administration of procaine penicilin with and without benemid p-(di-n-propylsulphamyl) benzoic acid. *Lancet* 261: 104-106 (1951).
131. P. Statkevich, D. J. Fournier and K. R. Sweeney. Characterization of methotrexate elimination and interaction with indomethacin and flurbiprofen in the isolated perfused rat kidney. *The Journal of Pharmacology and Experimental Therapeutics* 265: 1118-1124 (1993).
132. Y. Tanigawara, N. Okamura, M. Hirai, M. Yasuhara, K. Ueda, N. Kioka, T. Komano, et al. Transport of digoxin by human P-glycoprotein expressed in a porcine kidney epithelial cell line (LLC-PK1). *The Journal of Pharmacology and Experimental Therapeutics* 263: 840-845 (1992).
133. J. O. Miners. Drug interactions involving aspirin (acetylsalicylic acid) and salicylic acid. *Clinical Pharmacokinetics* 17: 327-344 (1989).
134. F. P. Guengerich. In vitro techniques for studying drug metabolism. *Journal of Pharmacokinetics and Biopharmaceutics* 24: 521-533 (1996).
135. Y. Cheng and W. H. Prusoff. Relationship between the inhibition constant (K_i) and the concentration of inhibitor which causes 50 per cent inhibition (I_{50}) of an enzymatic reaction. *Biochemical Pharmacology* 22: 3099-3108 (1973).
136. J. H. Lin and A. Y. Lu. Role of pharmacokinetics and metabolism in drug discovery and development. *Pharmacological Reviews* 49: 403-449 (1997).

137. K. Ito, T. Iwatsubo, S. Kanamitsu, Y. Nakajima and Y. Sugiyama. Quantitative prediction of in vivo drug clearance and drug interactions from in vitro data on metabolism, together with binding and transport. *Annual Review of Pharmacology and Toxicology* 38: 461-499 (1998).
138. B. Davit, K. Reynolds, R. Yuan, F. Ajayi, D. Conner, E. Fadiran, B. Gillespie, et al. FDA evaluations using in vitro metabolism to predict and interpret in vivo metabolic drug-drug interactions: impact on labeling. *Journal* 39: 899-910 (1999).
139. R. J. Bertz and G. R. Granneman. Use of in vitro and in vivo data to estimate the likelihood of metabolic pharmacokinetic interactions. *Clinical Pharmacokinetics* 32: 210-258 (1997).
140. K. A. Bachmann and R. Ghosh. The use of in vitro methods to predict in vivo pharmacokinetics and drug interactions. *Current Drug Metabolism* 2: 299-314 (2001).
141. R. F. Frye, G. R. Matzke, A. Adedoyin, J. A. Porter and R. A. Branch. Validation of the five-drug "Pittsburgh cocktail" approach for assessment of selective regulation of drug-metabolizing enzymes. *Clinical Pharmacology and Therapeutics* 62: 365-376 (1997).
142. K. Ito, H. Kusuhara and Y. Sugiyama. Effects of intestinal CYP3A4 and P-glycoprotein on oral drug absorption--theoretical approach. *Pharmaceutical Research* 16: 225-231 (1999).
143. A. D. R. Huitema, R. A. A. Mathot, M. M. Tibben, S. Rodenhuis and J. H. Beijnen. A mechanism-based pharmacokinetic model for the cytochrome P450 drug-drug interaction between cyclophosphamide and thioTEPA and the autoinduction of cyclophosphamide. *Journal of Pharmacokinetics and Pharmacodynamics* 28: 211-230 (2001).
144. E. Yukawa. Population-based investigations of drug relative clearance using nonlinear mixed-effect modelling from information generated during the routine clinical care of patients. *Journal of Clinical Pharmacy and Therapeutics* 24: 103-113 (1999).
145. Parkinson's disease - a unique survey launched, Press Release WHO/71. <http://www.who.int/> (1998).
146. H. J. Doller, J. D. Connor, D. R. Lock, R. S. Sloviter, B. H. Dvorchik and E. S. Vesell. Levodopa pharmacokinetics: alterations after benserazide, a decarboxylase inhibitor. *Drug Metabolism and Disposition* 6: 164-168 (1978).
147. P. S. Leppert, M. Cortese and J. A. Fix. The effects of carbidopa dose and time and route of administration on systemic L-dopa levels in rats. *Pharmaceutical Research* 5: 587-591 (1988).
148. S. Rose, P. Jenner and C. D. Marsden. Chronic administration does not alter the pharmacokinetic profile of L-dopa in the rat. *Journal of Pharmacy and Pharmacology* 45: 725-730 (1993).
149. L. K. Cheng and H. L. Fung. Dose-dependent pharmacokinetics of laevodopa and its metabolites in the rat. *Xenobiotica* 6: 237-248 (1976).
150. N. D. Huebert, M. G. Palfreyman and K. D. Haegle. A comparison of the effects of reversible and irreversible inhibitors of aromatic L-amino acid decarboxylase on the half-life and other pharmacokinetic parameters of oral L-3,4-dihydroxyphenylalanine. *Drug Metabolism and Disposition* 11: 195-200 (1983).
151. S. Rose, P. Jenner and C. D. Marsden. Peripheral pharmacokinetic handling and metabolism of L-dopa in the rat: the effect of route of administration and carbidopa pretreatment. *Journal of Pharmacy and Pharmacology* 43: 325-330 (1991).
152. S. Rose, P. Jenner and C. D. Marsden. The effect of carbidopa on plasma and muscle levels of L-dopa, dopamine, and their metabolites following L-dopa administration to rats. *Movement Disorders* 3: 117-125 (1988).

153. S. Sato, T. Koitabishi and A. Koshiro. Pharmacokinetic and pharmacodynamic studies of L-dopa in rats. I. pharmacokinetic analysis of L-dopa in rat plasma and striatum. *Biological and Pharmaceutical Bulletin* 17: 1616-1621 (1994).
154. E. Bredberg, H. Lennernaes and L. K. Paalzow. A study of the pharmacokinetics of levodopa in the rat following different routes of administration. *Pharmaceutical Research* 11: 549-555 (1994).
155. K. Iwamoto, J. Watanabe, M. Yamada, F. Atsumi and T. Matsushita. Effect of age on gastrointestinal and hepatic first-pass effects of levodopa in rats. *Journal of Pharmacy and Pharmacology* 39: 421-425 (1987).
156. D. E. Schwartz and R. Brandt. Pharmacokinetic and metabolic studies of the decarboxylase inhibitor benserazide in animals and man. *Arzneimittelforschung* 28: 302-307 (1978).
157. M. Schleimer and G. Fischer. Determination of endogenous L-dopa and 3-O-methyldopa together with carbidopa or benserazide and (2,3,4-Trihydroxybenzyl)hydrazine in human plasma using solid phase extraction and HPLC with electrochemical detection. *Data on file*, F. Hoffmann-La Roche Ltd., Basel; 1996.
158. M. Schleimer and G. Fischer. Determination of benserazide (Ro 04-4602) and (2,3,4-Trihydroxybenzyl)hydrazine (Ro 04-5127) in human, dog and rat plasma using HPLC with electrochemical detection. *Data on file*, F. Hoffmann-La Roche Ltd., Basel; 1996.
159. U. Timm and K. Fuchs. Concept and specification of LIMS for pharmacokinetic studies. *Laboratory Automation and Information Management* 32: 7-22 (1996).
160. M. Gibaldi and D. Perrier. Method of residuals. In J. Swarbrick, *Pharmacokinetics*, Marcel Dekker Inc., New York - Basel, 1982 pp. 433-444.
161. S. Riegelman and P. Collier. The application of statistical moment theory to the evaluation of in vivo dissolution time and absorption time. *Journal of Pharmacokinetics and Biopharmaceutics* 8: 509-534 (1980).
162. B. Davies and T. Morris. Physiological parameters in laboratory animals and humans. *Pharmaceutical Research* 10: 1093-1095 (1993).
163. P. T. Mearrick, G. G. Graham and D. N. Wade. The role of the liver in the clearance of l-dopa from plasma. *Journal of Pharmacokinetics and Biopharmaceutics* 3: 13-23 (1975).
164. M. Schmitt, M. Schleimer and G. Fischer. Effect of tolcapone on benserazide (Ro 04-4602) plasma levels in rats. *Data on file*, F. Hoffmann-La Roche Ltd., Basel; 1996.
165. M. Schmitt, M. Schleimer, G. Fischer, M. S. Gruyer and P. Schrag. Benserazide exposure in rats and dogs after oral administration. *Data on file*, F. Hoffmann-La Roche Ltd., Basel; 1997.
166. L. F. Lacey, O. N. Keene, J. F. Pritchard and A. Bye. Common noncompartmental pharmacokinetic variables: are they normally or log-normally distributed? *Journal of Biopharmaceutical Statistics* 7: 171-178 (1997).
167. L. Landsberg, M. B. Berardino, J. Stoff and J. B. Young. Further studies on catechol uptake and metabolism in rat small bowel in vivo: (1) a quantitatively significant process with distinctive structural specifications; and (2) the formation of a dopamine glucuronide reservoir after chronic L-dopa feeding. *Biochemical Pharmacology* 27: 1365-1371 (1978).
168. L. Landsberg, M. B. Berardino and P. Silva. Metabolism of 3-H-L-dopa by the rat gut in vivo-evidence for glucuronide conjugation. *Biochemical Pharmacology* 24: 1167-1174 (1975).

-
169. L. Rivera Calimlim, C. A. Dujovne, J. P. Morgan, L. Lasagna and J. R. Bianchine. Absorption and metabolism of L-dopa by the human stomach. *European Journal of Clinical Investigation* 1: 313-320 (1971).
170. L. Rivera Calimlim, J. P. Morgan, C. A. Dujovne, J. R. Bianchine and L. Lasagna. L-3,4-dihydroxyphenylalanine metabolism by the gut in vitro. *Biochemical Pharmacology* 20: 3051-3057 (1971).
171. K. Sasahara, T. Nitani, T. Habara, T. Kojima, Y. Kawahara, T. Morioka and E. Nakajima. Dosage form design for improvement of bioavailability of levodopa IV: Possible causes of low bioavailability of oral levodopa in dogs. *Journal of Pharmaceutical Sciences* 70: 730-733 (1981).
172. G. M. Tyce. Metabolism of 3,4-dihydroxyphenylalanine by isolated perfused rat liver. *Biochemical Pharmacology* 20: 3447-3462 (1971).
173. S. Cotler, A. Holazo, H. G. Boxenbaum and S. A. Kaplan. Influence of route of administration on physiological availability of levodopa in dogs. *Journal of Pharmaceutical Sciences* 65: 822-827 (1976).
174. G. M. Tyce and C. A. Owen. Administration of L-3,4-dihydroxyphenylalanine to rats after complete hepatectomy-II. Excretion of metabolites. *Biochemical Pharmacology* 28: 3279-3284 (1979).
175. H. Hinterberger and C. J. Andrews. Catecholamine metabolism during oral administration of levodopa. *Archives of Neurology* 26: 245-252 (1972).
176. W. B. Abrams, C. B. Coutinho, A. S. Leon and H. E. Spiegel. Absorption and metabolism of levodopa. *The Journal of the American Medical Association* 218: 1912-1914 (1971).
177. E. S. Tolosa, W. E. Martin, H. P. Cohen and R. L. Jacobson. Patterns of clinical response and plasma dopa levels in Parkinson's disease. *Neurology* 25: 177-183 (1975).
178. D. N. Wade, P. T. Mearrick, D. J. Birkett and J. Morris. Variability of L-dopa absorption in man. *Australian and New Zealand Journal of Medicine* 4: 138-143 (1974).
179. M. A. Evans, E. J. Triggs, G. A. Broe and N. Saines. Systemic activity of orally administered L-dopa in the elderly Parkinson patient. *European Journal of Clinical Pharmacology* 17: 215-221 (1980).
180. G. Bartholini, I. Kuruma and A. Pletscher. Distribution and metabolism of L-3-O-methyldopa in rats. *British Journal of Pharmacology* 40: 461-467 (1970).
181. R. Ferrini and A. Glässer. In vitro decarboxylation of new phenylalanine derivatives. *Biochemical Pharmacology* 13: 798 (1964).
182. M. Rowland and T. N. Tozer. Metabolite kinetics. In *Clinical pharmacokinetics: Concepts and applications*, Lea & Febiger, Philadelphia - London, 1989 pp. 347-375.
183. T. Walle, T. C. Fagan, E. C. Conradi, U. K. Walle and T. E. Gaffney. Presystemic and systemic glucuronidation of propranolol. *Clinical Pharmacology and Therapeutics* 26: 167-172 (1979).
184. R. P. Brown, M. D. Delp, S. L. Lindstedt, L. R. Rhomberg and R. P. Beliles. Physiological parameter values for physiologically based pharmacokinetic models. *Toxicology and Industrial Health* 13: 407-484 (1997).
185. K. Sasahara, T. Nitani, T. Habara, T. Morioka and E. Nakajima. Dosage form design for improvement of bioavailability of levodopa II: bioavailability of marketed levodopa preparations in dogs and parkinsonian patients. *Journal of Pharmaceutical Sciences* 69: 261-265 (1980).

186. J. A. Romero, L. D. Lytle, L. A. Ordonez and R. J. Wurtman. Effects of L-dopa administration on the concentrations of dopa, dopamine and norepinephrine in various rat tissues. *Journal of Pharmacology and Experimental Therapeutics* 184: 67-72 (1973).
187. G. A. Lyles. Effects of L-DOPA administration upon monoamine oxidase activity in rat tissues. *Life Sciences* 22: 603-609 (1978).
188. G. V. Melzi d Eril and V. Rizzo. Determination of free DOPA and 3-O-methyl-DOPA in human plasma by high-performance liquid chromatography with electrochemical detection. *Journal of Chromatography* 553: 265-269 (1991).
189. J. P. Bennett, Jr., M. Turk and E. Landow. Continuous oral administration of L-dihydroxyphenylalanine (L-DOPA) solution to patients with advanced Parkinson's disease. *Clinical Neuropharmacology* 12: 285-292 (1989).
190. V. Rizzo, M. Memmi, R. Moratti, G. Melzi d' Eril and E. Perucca. Concentrations of L-dopa in plasma and plasma ultrafiltrates. *Journal of Pharmaceutical and Biomedical Analysis* 14: 1043-1046 (1996).
191. S. Sarre, D. Deleu, K. Van Belle, G. Ebinger and Y. Michotte. Quantitative microdialysis for studying the in vivo L-DOPA kinetics in blood and skeletal muscle of the dog. *Pharmaceutical Research* 12: 746-750 (1995).
192. R. Brandt and J. Meyer. Guidelines for protein binding. LP-007; May 3, 1994.
193. B. T. Doumas, D. D. Bayse, R. J. Carter, T. Peters, Jr. and R. Schaffer. A candidate reference method for determination of total protein in serum. I. Development and validation. *Clinical Chemistry* 27: 1642-1650 (1981).
194. B. T. Doumas, D. D. Bayse, K. Borner, R. J. Carter, F. Elevitch, C. C. Garber, R. A. Graby, et al. A candidate reference method for determination of total protein in serum. II. Test for transferability. *Clinical Chemistry* 27: 1651-1654 (1981).
195. B. T. Doumas, W. A. Watson and H. G. Biggs. Albumin standards and the measurement of serum albumin with bromocresol green. *Clinica Chimica Acta* 31: 87-96 (1971).
196. N. W. Tietz. Clinical guide to laboratory tests. In WB Saunders, Philadelphia, 1995 pp. 8-9.
197. J. Dingemanse, C. H. Kleinbloesem, G. Zurcher, N. D. Wood and C. Crevoisier. Pharmacodynamics of benserazide assessed by its effects on endogenous and exogenous levodopa pharmacokinetics. *British Journal of Clinical Pharmacology* 44: 41-48 (1997).
198. N. H. G. Holford. A size standard for pharmacokinetics. *Clinical Pharmacokinetics* 30: 329-332 (1996).
199. J. Gabrielsson and D. Weiner. Interspecies scaling. In *Pharmacokinetic and Pharmacodynamic Data Analysis: Concepts and Applications*, Swedish Pharmaceutical Press, Stockholm, Sweden, 2000 pp. 153-174.
200. D. E. Schwartz and R. Brandt. Pharmacokinetics and metabolism of the decarboxylase inhibitor benserazide (Ro 04-4602) in animals and man. *Data on file*, Hoffmann-La Roche Ltd., Basel; 1975.
201. J. G. Nutt, W. R. Woodward and J. L. Anderson. The effect of carbidopa on the pharmacokinetics of intravenously administered levodopa: the mechanism of action in the treatment of parkinsonism. *Annals of Neurology* 18: 537-543 (1985).

-
202. D. R. Robertson, N. D. Wood, H. Everest, K. Monks, D. G. Waller, A. G. Renwick and C. F. George. The effect of age on the pharmacokinetics of levodopa administered alone and in the presence of carbidopa. *British Journal of Clinical Pharmacology* 28: 61-69 (1989).
203. N. S. Sharpless, M. D. Muentner, G. M. Tyce and C. A. Owen, Jr. 3-methoxy-4-hydroxyphenylalanine (3-O-methyldopa) in plasma during oral L-dopa therapy of patients with Parkinson's disease. *Clinica Chimica Acta* 37: 359-369 (1972).
204. D. Sasse, U. M. Spornitz and I. P. Maly. Liver architecture. *Enzyme* 46: 8-32 (1992).
205. J. K. Corless and H. M. Middleton, 3rd. Normal liver function. A basis for understanding hepatic disease. *Archives of Internal Medicine* 143: 2291-2294 (1983).
206. K. S. Pang and M. Rowland. Hepatic clearance of drugs. I. Theoretical considerations of a "well-stirred" model and a "parallel tube" model. Influence of hepatic blood flow, plasma and blood cell binding, and the hepatocellular enzymatic activity on hepatic drug clearance. *Journal of Pharmacokinetics and Biopharmaceutics* 5: 625-653 (1977).
207. M. Rowland and T. N. Tozer. Elimination. In *Clinical pharmacokinetics: Concepts and applications*, Lea & Febiger, Philadelphia - London, 1989 pp. 148-176.
208. S. M. Pond and T. N. Tozer. First-pass elimination. Basic concepts and clinical consequences. *Clinical Pharmacokinetics* 9: 1-25 (1984).
209. D. G. Shand and R. E. Rangno. The disposition of propranolol. I. Elimination during oral absorption in man. *Pharmacology* 7: 159-168 (1972).
210. G. R. Wilkinson and D. G. Shand. A physiological approach to hepatic drug clearance. *Clinical Pharmacology and Therapeutics* 18: 377-390 (1975).
211. N. H. G. Holford. Complex PK/PD models - an alcoholic experience. *International Journal of Clinical Pharmacology and Therapeutics* 35: 465-468 (1997).
212. G. R. Wilkinson. Clearance approaches in pharmacology. *Pharmacological Reviews* 39: 1-47 (1987).
213. L. Bass and S. Keiding. Physiologically based models and strategic experiments in hepatic pharmacology. *Biochemical Pharmacology* 37: 1425-1431 (1988).
214. L. Bass, P. Robinson and A. J. Bracken. Hepatic elimination of flowing substrates: the distributed model. *Journal of Theoretical Biology* 72: 161-184 (1978).
215. M. S. Roberts and M. Rowland. A dispersion model of hepatic elimination: 1. Formulation of the model and bolus considerations. *Journal of Pharmacokinetics and Biopharmaceutics* 14: 227-260 (1986).
216. M. S. Roberts and M. Rowland. Correlation between in-vitro microsomal enzyme activity and whole organ hepatic elimination kinetics: analysis with a dispersion model. *The Journal of Pharmacy and Pharmacology* 38: 177-181 (1986).
217. W. J. Bachman and W. R. Gillespie. "Truncated sigmoid Emax models": A reparameterization of the sigmoid Emax model for use with truncated PK/PD data. *Clinical Pharmacology and Therapeutics* 63: 199 (1998).
218. Optimization algorithms. In *ACSL Optimize, User's guide for windows*, Mitchell and Gauthier Associates (MGA) Inc., Concord MA 01742 USA, 1997 pp. 99-103.

219. E. Schultz. L-dopa as substrate for human duodenal catechol-O-methyltransferase and aromatic L-amino acid decarboxylase. *Biomedical Chromatography* 4: 242-244 (1990).
220. A. Pletscher, K. Gey and W. Burkard. Inhibitors of monoaminooxidase and decarboxylase of aromatic amino acids. In *Handbook of experimental pharmacology*, 1965 pp. 594-735.
221. J. H. Fellman. Purification and properties of adrenal L-dopa decarboxylase. *Enzymologia* 20: 366-376 (1959).
222. H. F. Schott and W. G. Clark. Dopa decarboxylase inhibition through the interaction of coenzyme and substrate. *The Journal of Biological Chemistry* 196: 449-462 (1952).
223. J. G. Christenson, W. Dairman and S. Udenfriend. Preparation and properties of a homogeneous aromatic L-amino acid decarboxylase from hog kidney. *Archives of Biochemistry and Biophysics* 141: 156-367 (1970).
224. M. Pestana, M. A. Vieira Coelho, O. P. Pinto do, M. H. Fernandes and P. Soares da Silva. Assessment of renal dopaminergic system activity during cyclosporine A administration in the rat. *British Journal of Pharmacology* 115: 1349-1358 (1995).
225. Y. Goshima, S. Nakamura and Y. Misu. L-dopa facilitates the release of endogenous norepinephrine and dopamine via presynaptic beta 1- and beta 2-adrenoceptors under essentially complete inhibition of L-aromatic amino acid decarboxylase in rat hypothalamic slices. *Japanese Journal of Pharmacology* 53: 47-56 (1990).
226. H. C. Kimko and S. B. Duffull. *Simulation for designing clinical trials: A pharmacokinetic-pharmacodynamic modeling perspective*, Marcel Dekker Inc., New York - Basel, 2003.

Appendix A: DEMOGRAPHIC DATA

A.1 Listings of Individual Demographic Data

A.1.1 Demographic data of rats used in treatment group 20 mg/kg L-dopa

Rat ID	Name code	String	Age [weeks]	Gender	Body weight before operation [g]	Body weight before experiment [g]
a1	Rat J171/97	Wistar/Füllinsdorf	10-12	Male	296	262
a2	Rat J172/97	Wistar/Füllinsdorf	10-12	Male	286	256
a3	Rat J173/97	Wistar/Füllinsdorf	10-12	Male	270	239
a4	Rat J174/97	Wistar/Füllinsdorf	10-12	Male	291	N/A
a5	Rat J175/97	Wistar/Füllinsdorf	10-12	Male	282	250
a6	Rat J176/97	Wistar/Füllinsdorf	10-12	Male	303	267

N/A: not assessed, rat a4 died due to problems with jugular vein catheter.

A.1.2 Demographic data of rats used in treatment group 80 mg/kg benserazide

Rat ID	Name code	String	Age [weeks]	Gender	Body weight before operation [g]	Body weight before experiment [g]
b1	Rat J177/97	Wistar/Füllinsdorf	10-12	Male	298	263
b2	Rat J178/97	Wistar/Füllinsdorf	10-12	Male	286	256
b3	Rat J179/97	Wistar/Füllinsdorf	10-12	Male	281	252
b4	Rat J180/97	Wistar/Füllinsdorf	10-12	Male	275	244
b5	Rat J181/97	Wistar/Füllinsdorf	10-12	Male	292	260
b6	Rat J182/97	Wistar/Füllinsdorf	10-12	Male	287	N/A

N/A: not assessed, rat b6 died due to problems with jugular vein catheter.

A.1.3 Demographic data of rats used in treatment group 80/20 mg/kg L-dopa/benserazide

Rat ID	Name code	String	Age [weeks]	Gender	Body weight before operation [g]	Body weight before experiment [g]
c1	Rat J184/97	Wistar/Füllinsdorf	10-12	Male	307	286
c2	Rat J185/97	Wistar/Füllinsdorf	10-12	Male	302	271
c3	Rat J186/97	Wistar/Füllinsdorf	10-12	Male	285	264
c4	Rat J187/97	Wistar/Füllinsdorf	10-12	Male	278	263
c5	Rat J188/97	Wistar/Füllinsdorf	10-12	Male	296	271
c6	Rat J189/97	Wistar/Füllinsdorf	10-12	Male	290	271
c7	Rat J193/97	RoRo/Füllinsdorf	10-12	Male	318	299
c8	Rat J194/97	RoRo/Füllinsdorf	10-12	Male	309	290
c9	Rat J195/97	RoRo/Füllinsdorf	10-12	Male	323	308

A.1.4 Demographic data of rats used for collection of predose samples

Rat ID	Name code	String	Age [weeks]	Gender	Body weight before operation [g]	Body weight before experiment [g]
d1	Rat J190/97	Wistar/Füllinsdorf	10-12	Male	N/A	262
d2	Rat J191/97	Wistar/Füllinsdorf	10-12	Male	N/A	284
d3	Rat J192/97	Wistar/Füllinsdorf	10-12	Male	N/A	284

N/A: not assessed, rats d1 to d3 were not operated.

Appendix B: BIOANALYTICAL DATA

B.1 Inter-Assay Precision from Quality Control Samples for L-Dopa in Rat Plasma and Human Plasma

B.1.1 L-Dopa plasma concentrations of quality control samples Q01 to Q04

Assay batch number	Q01 9.77 µg/L* human plasma	Q02 195 µg/L* human plasma	Q03 10.1 µg/L* rat plasma	Q04 203 µg/L* rat plasma
1P220597	10.3 10.5	198 203	10.8 9.52	202 196
1P270597	9.90 10.3	206 200	13.4 9.89	214 216
1P290597	10.7 10.3	198 207	10.4 9.77	197 222
1P020697	11.9 10.6	192 189	10.8 9.87	184 208
1P040697	10.3 10.8	185 187	9.97 10.7	199 215
1P230697	9.48	-	12.2 9.81	-
1P250697	-	-	9.81	-
Mean [µg/L]	10.5	197	10.5	205
SD [µg/L]	0.604	7.87	1.12	11.7
CV %	5.8	4.0	11	5.7
Bias %	7.5	1.0	4.0	0.99
N	11	10	13	10

*: nominal concentration; N: number of observations used for descriptive statistics. **Bias**: defined as deviation between mean concentration and nominal concentration (expressed in % of nominal concentration).

B.1.2 L-Dopa plasma concentrations of quality control samples Q11 to Q14

Assay batch number	Q11 9.27 µg/L* human plasma	Q12 208 µg/L* human plasma	Q13 9.76 µg/L* rat plasma	Q14 210 µg/L* rat plasma
1P230697	9.62 11.2	189 193	11.1 9.13	194 191
1P250697	9.59 9.60	191 201	10.5 9.78	201 203
1P270697	10.3 11.1	195 198	11.1 10.6	194 195
1P300697	10.1 9.94	205 197	10.2 10.4	201 207
1P020797	9.82 9.77	201 204	10.7 10.2	201 206
1P030797	9.81 9.58	196 205	10.0 9.96	201 205
2P160797	10.1 10.3	210 208	10.1 10.3	210 207
2P170797	9.99 10.2	207 202	9.96 9.94	207 207
1P240797	10.0 9.73	205 205	10.3 10.4	205 207
Mean [µg/L]	10.0	201	10.3	202
SD [µg/L]	0.467	6.10	0.467	5.55
CV %	4.6	3.0	4.6	2.7
Bias %	7.9	-3.4	5.5	-3.8
N	18	18	18	18

*: nominal concentration; **N**: number of observations used for descriptive statistics. **Bias**: defined as deviation between mean concentration and nominal concentration (expressed in % of nominal concentration).

B.2 Inter-Assay Precision from Quality Control Samples for 3-OMD in Rat Plasma and Human Plasma

B.2.1 3-OMD plasma concentrations of quality control samples Q01 to Q04

Assay batch number	Q01 9.95 µg/L* human plasma	Q02 197 µg/L* human plasma	Q03 9.28 µg/L* rat plasma	Q04 193 µg/L* rat plasma
1P220597	10.4 9.91	189 187	9.32 8.37	186 188
1P270597	9.24 9.19	192 196	8.81 8.24	194 194
1P290597	10.2 9.68	201 196	9.66 8.84	195 186
1P020697	10.4 9.91	196 198	9.46 9.63	189 199
1P040697	9.68 9.33	185 183	11.6 10.0	183 193
1P230697	11.1	-	7.97	-
1P250697	-	-	9.94 9.29	-
Mean [µg/L]	9.91	192	9.32	191
SD [µg/L]	0.582	6.04	0.942	5.03
CV %	5.9	3.1	10	2.6
Bias %	-0.40	-2.5	0.43	-1.0
N	11	10	13	10

*: nominal concentration; N: number of observations used for descriptive statistics. **Bias:** defined as deviation between mean concentration and nominal concentration (expressed in % of nominal concentration).

B.2.2 3-OMD plasma concentrations of quality control samples Q11 to Q14

Assay batch number	Q11 9.80 µg/L* human plasma	Q12 206 µg/L* human plasma	Q13 9.08 µg/L* rat plasma	Q14 208 µg/L* rat plasma
1P230697	-	206 201	-	202 192
1P250697	-	204 196	-	208 206
1P270697	9.89 9.71	209 208	9.73 9.24	204 209
1P300697	9.09 8.68	220 212	9.20 8.31	212 212
1P020797	8.21 8.45	211 212	8.64 8.68	213 212
1P030797	8.14 8.16	214 214	8.36 8.34	212 214
2P160797	9.80 10.0	205 204	9.44 9.71	208 208
2P170797	10.5 9.88	215 212	9.63 9.92	211 210
1P240797	11.5 8.66	212 211	8.04 8.55	214 212
Mean [µg/L]	9.33	209	8.99	209
SD [µg/L]	1.01	5.73	0.635	5.37
CV %	11	2.7	7.1	2.6
Bias %	-4.8	1.5	-0.99	0.48
N	14	18	14	18

*: nominal concentration; **N**: number of observations used for descriptive statistics. **Bias**: defined as deviation between mean concentration and nominal concentration (expressed in % of nominal concentration).

B.3 Inter-Assay Precision from Quality Control Samples for Benserazide in Human Plasma

B.3.1 Benserazide plasma concentrations of quality control samples Q31 to Q33

Assay batch number	Q31 4.33 µg/L* human plasma	Q32 16.4 µg/L* human plasma	Q33 43.7 µg/L* human plasma
1P080497	3.82 3.93	14.5 16.0	38.9 42.9
2P090497	3.71 3.90	14.7 17.0	42.6 32.0
1P100497	2.26 2.01	15.6 16.7	40.0 37.8
Mean [µg/L]	3.27	15.8	39.0
SD [µg/L]	0.887	1.02	3.99
CV %	27	6.5	10
Bias %	-24	-3.7	-11
N	6	6	6

*: nominal concentration; **N**: number of observations used for descriptive statistics. **Bias**: defined as deviation between mean concentration and nominal concentration (expressed in % of nominal concentration).

B.4 Inter-Assay Precision from Quality Control Samples for Ro 04-5127 in Human Plasma

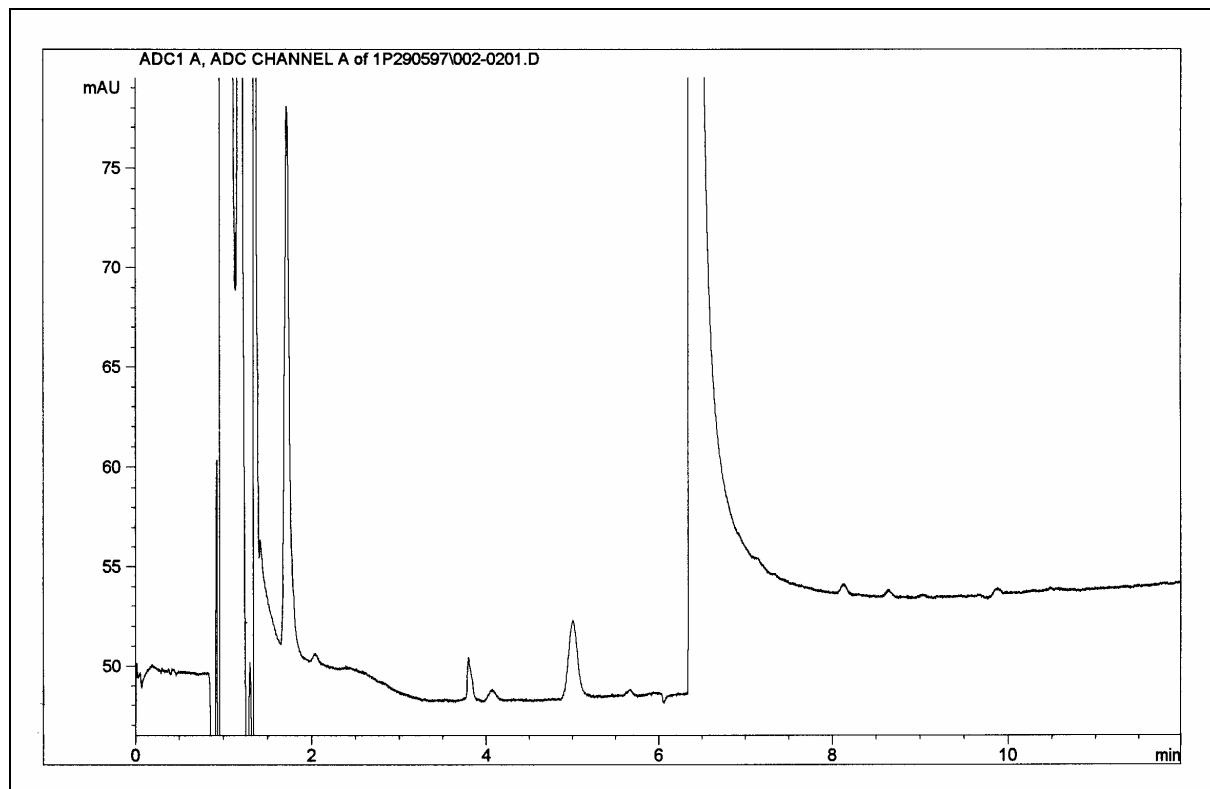
B.4.1 Ro 04-5127 plasma concentrations of quality control samples Q31 to Q33

Assay batch number	Q31 3.74 µg/L* human plasma	Q32 15.0 µg/L* human plasma	Q33 45.0 µg/L* human plasma
1P080497	3.68 3.52	13.9 15.4	40.1 43.5
2P090497	3.54 3.82	14.7 16.4	42.6 31.9
1P100497	2.47 2.15	15.1 15.9	38.8 38.4
Mean [µg/L]	3.20	15.2	39.2
SD [µg/L]	0.703	0.885	4.12
CV %	22	5.8	11
Bias %	-14	1.3	-13
N	6	6	6

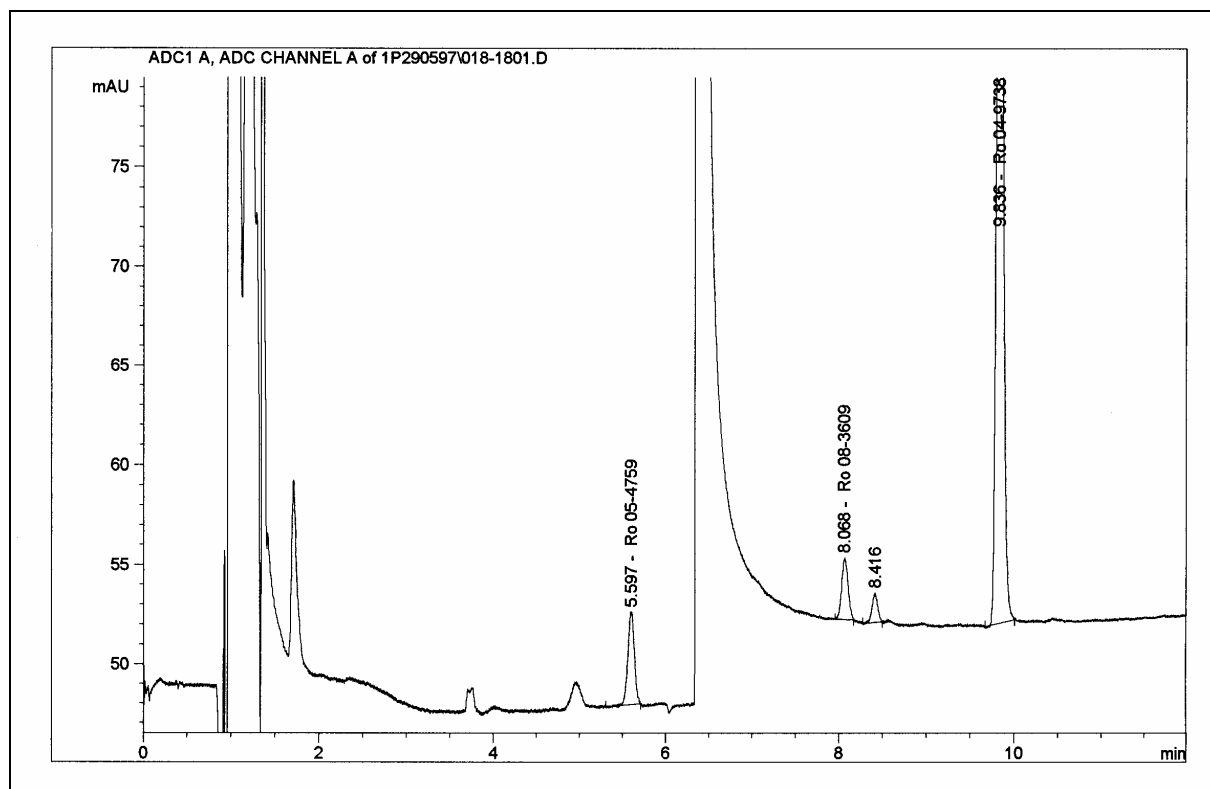
*: nominal concentration; **N**: number of observations used for descriptive statistics. **Bias**: defined as deviation between mean concentration and nominal concentration (expressed in % of nominal concentration).

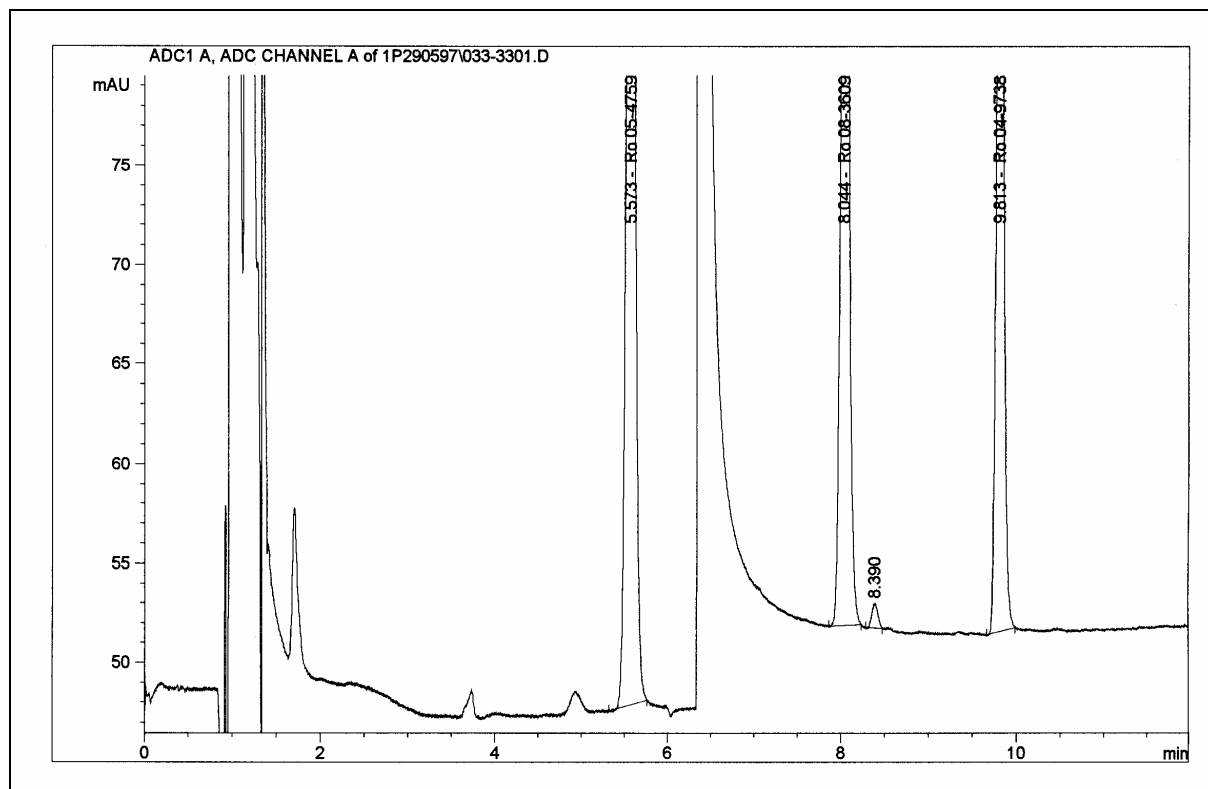
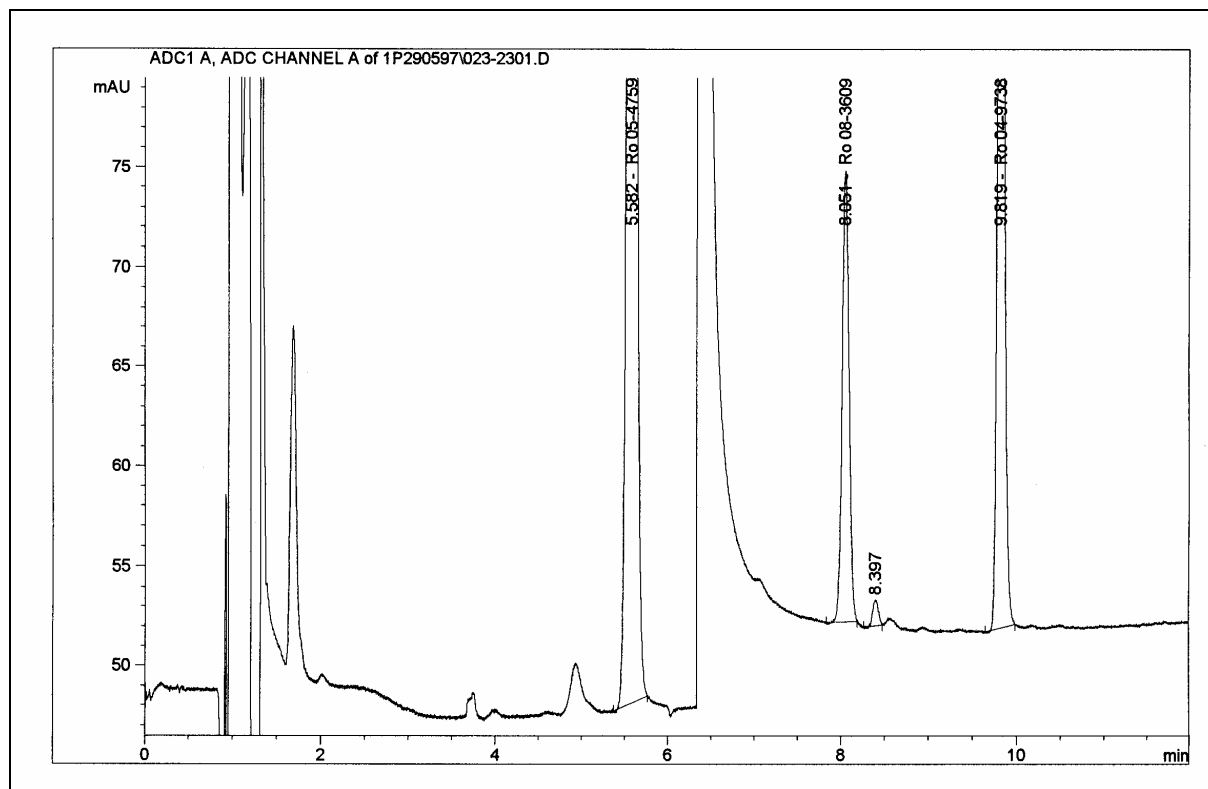
B.5 L-Dopa and 3-OMD Assay: Chromatograms

B.5.1 Chromatogram of blank human plasma



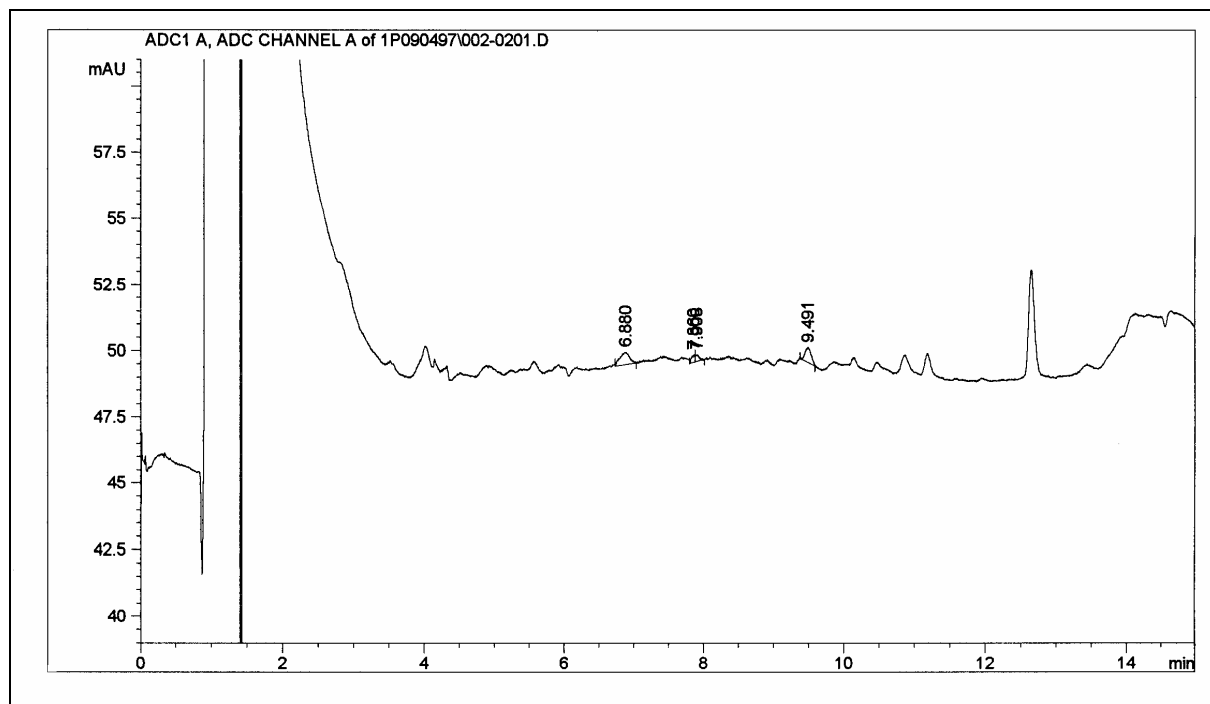
B.5.2 Chromatogram of human blank plasma spiked with additional 9.77 µg/L L-dopa (Ro 05-4759) and 9.95 µg/L 3-OMD (Ro 08-3609)



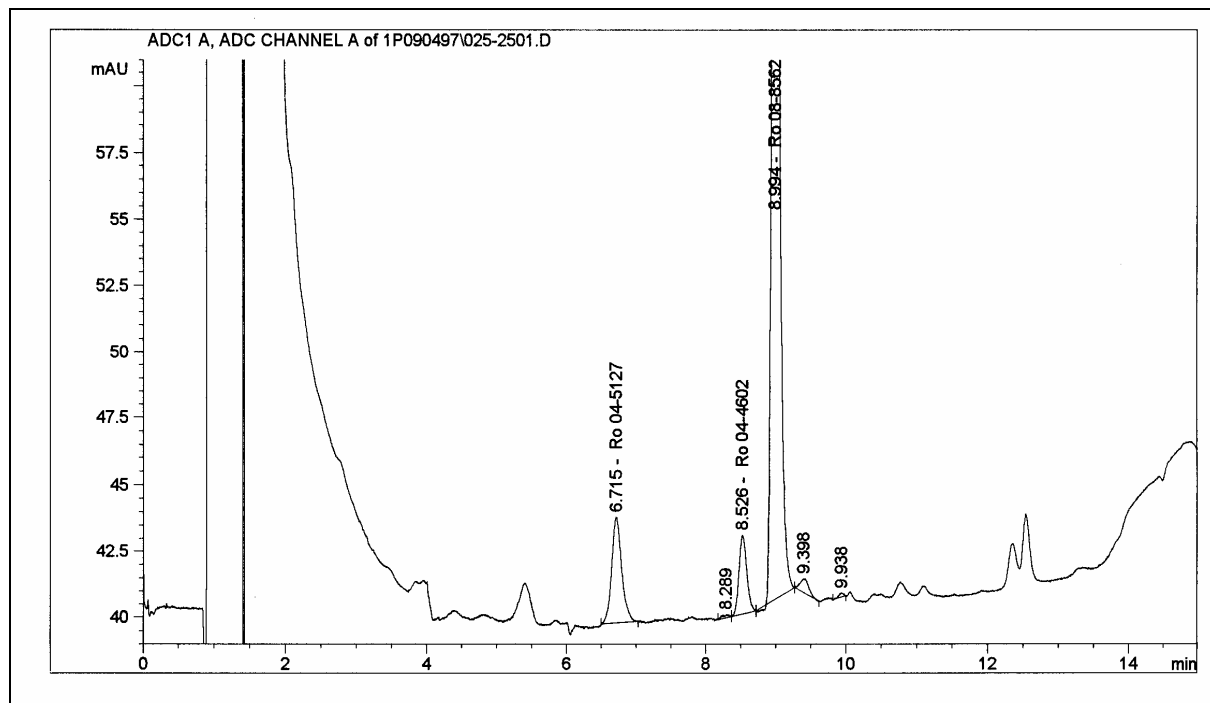
B.5.3 Chromatogram of human blank plasma spiked with additional 195 µg/L L-dopa (Ro 05-4759) and 197 µg/L 3-OMD (Ro 08-3609)**B.5.4 Chromatogram of plasma from rat B3 0.5 h after an oral dose of 80 mg/kg L-dopa**

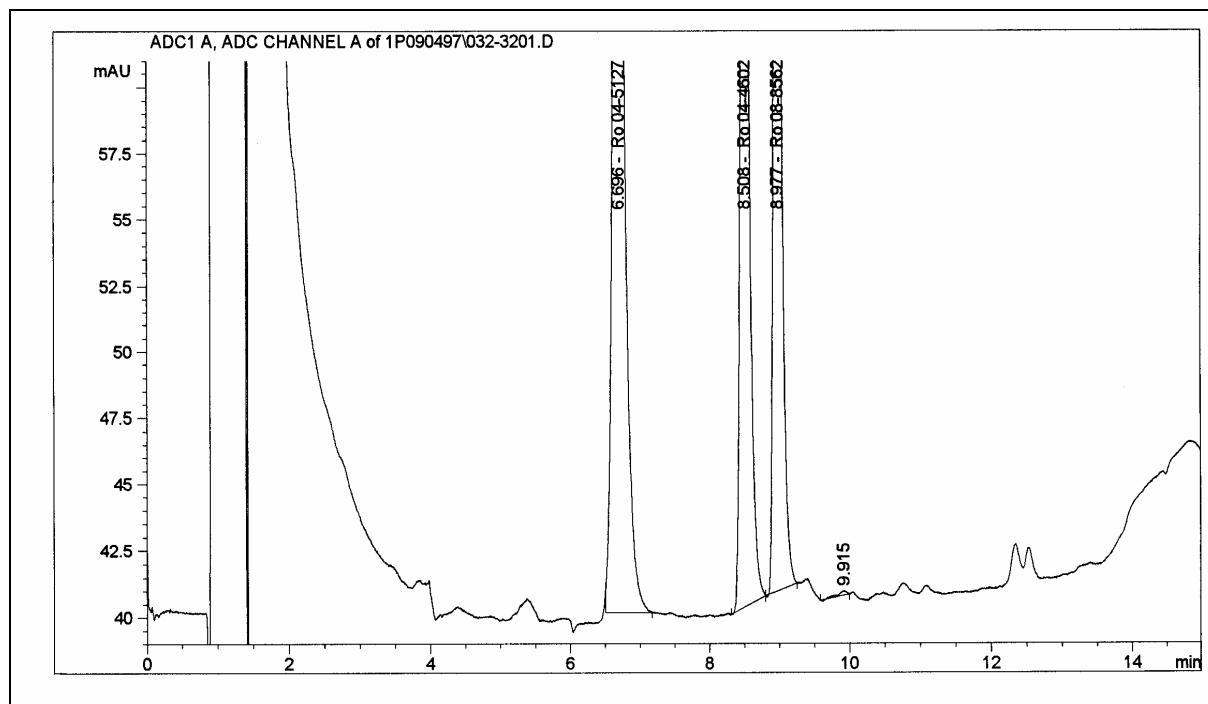
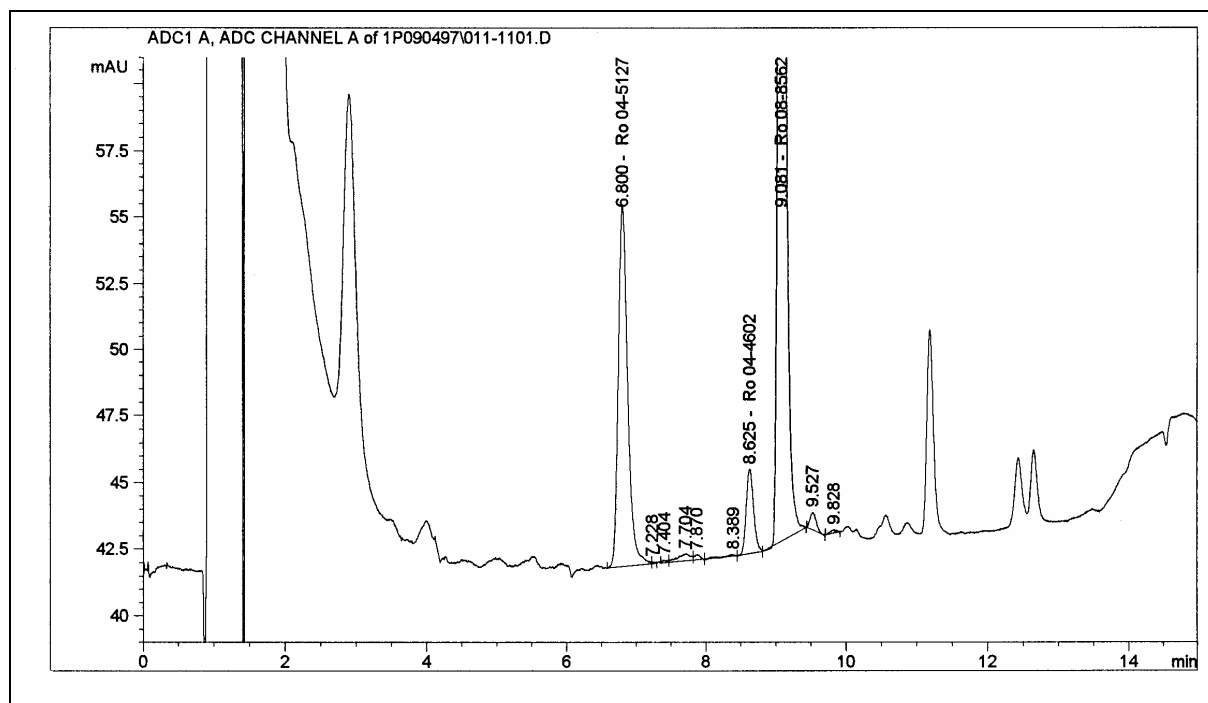
B.6 Benserazide and Ro 04-5127 Assay: Chromatograms

B.6.1 Chromatogram of human blank plasma



B.6.2 Chromatogram of human blank plasma spiked with additional 4.33 µg/L benserazide (Ro 04-4602) and 3.74 µg/L Ro 04-5127



B.6.3 Chromatogram of human blank plasma spiked with additional 43.7 µg/L benserazide (Ro 04-4602) and 45.0 µg/L Ro 04-5127**B.6.4 Chromatogram of plasma from rat A6 5 minutes after an oral dose of 20 mg/kg benserazide**

Appendix C: PHARMACOKINETIC DATA

The concentrations of L-dopa, 3-OMD, benserazide, and Ro 04-5127 are listed in µg/L. For the mathematical modeling they were converted into µmol/L. The molecular weights for the four compounds were 197.19 (L-dopa), 211.22 (3-OMD), 257.24 (benserazide), 170.17 (Ro 04-5127).

C.1 Listings of Individual Plasma Concentrations of L-Dopa and 3-OMD

C.1.1 L-Dopa plasma concentrations (µg/L) after a single oral dose of 80 mg/kg L-dopa

Scheduled time, h	Rat b1	Rat b2	Rat b3	Rat b4	Rat b5
0.00	BLC	BLC	NOP	BLC	BLC
0.08	1341	4502	4643	1506	1103
0.17	1749	1786	7645	2227	1911
0.25	1612	2588	4503	1835	2409
0.50	2101	4078	3131	2420	2659
1.00	2609	3162	3026	2862	2721
2.00	1154	755	721	1121	1838
4.00	25.8	18.5	24.6	457	59.5
6.00	BLC	BLC	NOP	33.1	BLC
8.00	BLC	NOP	BLC	15.0	NOP
10.00	BLC	NOP	NOP	10.8	BLC
24.00	NOP	BLC	NOP	BLC	BLC

BLC: below limit of calibration, **NOP:** no peak

C.1.2 3-OMD plasma concentrations (µg/L) after a single oral dose of 80 mg/kg L-dopa

Scheduled time, h	Rat b1	Rat b2	Rat b3	Rat b4	Rat b5
0.00	27.9	27.4	31.6	21.4	16.8
0.08	80.8	153	90.0	80.7	43.4
0.17	177	190	228	155	77.2
0.25	243	246	369	216	143
0.50	488	533	727	532	380
1.00	1004	1146	1388	1123	820
2.00	1849	2139	2146	1988	1895
4.00	1925	2186	1926	2239	2186
6.00	1631	1741	1839	1957	1784
8.00	1441	1534	1438	1488	1470
10.00	1266	1486	1266	1217	1202
24.00	589	712	526	476	637

C.1.3 L-Dopa plasma concentrations ($\mu\text{g/L}$) after a single oral dose of 80 mg/kg L-dopa and 20 mg/kg benserazide

Scheduled time, h	Rat c1	Rat c2	Rat c3	Rat c4	Rat c5	Rat c6	Rat c7	Ratc8	Rat c9
0.00	BLC	NOP	NOP	NOP	NOP	BLC	BLC	BLC	NOP
0.08	11360	16898	18766	13164	21494	13310	3717	4190	2001
0.17	24157	21616	29926	14824	26080	15866	11525	11484	8157
0.25	26219	20025	21612	11939	27430	17207	17423	9247	9735
0.50	14508	25022	15902	15693	17458	14946	25630	14804	8112
1.00	13863	13944	25589	14302	16378	14424	28436	21270	13293
2.00	9773	13770	20305	13069	11554	6842	12846	15159	11866
4.00	3375	9765	14289	11699	3857	4548	2803	5578	7070
6.00	300	4767	3446	3600	404	1813	330	1182	2053
8.00	30.0	347	315	1065	56.9	1137	61.4	107	274
10.00	11.8	30.4	27.1	49.7	18.3	241	14.8	22.5	66.5
24.00	NOP	NOP	10.4	NOP	NOP	BLC	BLC	8.88	30.1

BLC: below limit of calibration, **NOP:** no peak

C.1.4 3-OMD plasma concentrations ($\mu\text{g/L}$) after a single oral dose of 80 mg/kg L-dopa and 20 mg/kg benserazide

Scheduled time, h	Rat c1	Rat c2	Rat c3	Rat c4	Rat c5	Rat c6	Rat c7	Rat c8	Rat c9
0.00	22.1	31.8	32.9	BLC	BLC	18.9	38.2	38.5	39.5
0.08	869	1412	1316	1039	2207	971	399	231	94.0
0.17	2388	2700	3315	2462	4213	2056	1853	1719	1184
0.25	4459	3745	3750	2887	6317	3345	3258	2103	2242
0.50	6589	7618	6775	5885	8376	6177	9429	6530	2812
1.00	10395	10938	12353	10135	12082	11341	15611	13192	10484
2.00	16303	18964	22578	17910	18254	16553	24433	24594	18312
4.00	24627	29019	33408	34016	27777	25204	28838	38001	31024
6.00	22055	38821	39315	37902	24112	24547	29082	36399	32245
8.00	17192	34560	38320	34016	24254	24012	25377	32169	29685
10.00	15529	29117	33086	28941	20464	15871	19589	27247	23827
24.00	4401	12471	11394	10260	7498	6933	7251	8855	7748

BLC: below limit of calibration

C.2 Listings of Individual Plasma Concentrations of Benserazide and Ro 04-5127

C.2.1 Benserazide plasma concentrations ($\mu\text{g/L}$) after a single oral dose of 20 mg/kg benserazide

Scheduled time, h	Rat a1	Rat a2	Rat a3	Rat a5	Rat a6
0.00	BLC	BLC	NOP	NOP	NOP
0.08	6.64	26.0	23.6	17.8	13.7
0.17	3.96	34.7	29.7	20.9	20.1
0.25	7.41	53.3	37.6	31.9	26.0
0.50	9.01	73.9	41.7	42.5	29.8
1.00	8.50	38.5	18.3	28.8	NS
2.00	18.8	20.9	12.3	10.2	11.3
3.00	NSP	NSP	11.9	9.71	8.94
4.00	6.67	4.35	NSP	NSP	NSP

BLC: below limit of calibration, **NOP:** no peak, **NS:** no sample, **NSP:** no sample planned

C.2.2 Ro 04-5127 plasma concentrations ($\mu\text{g/L}$) after a single oral dose of 20 mg/kg benserazide

Scheduled time, h	Rat a1	Rat a2	Rat a3	Rat a5	Rat a6
0.00	0.257	0.273	0.240	0.291	NOP
0.08	7.94	BLC*	BLC*	55.8	41.4
0.17	8.60	191	167	63.8	37.8
0.25	24.4	196	101	49.3	16.7
0.50	14.6	69.9	59.6	10.7	18.3
1.00	11.2	6.93	5.15	4.07	NS
2.00	12.3	2.56	1.86	7.28	2.35
3.00	NSP	NSP	1.20	5.06	1.46
4.00	1.64	1.01	NSP	NSP	NSP

BLC*: below limit of calibration; samples were diluted too much, **NOP:** no peak, **NS:** no sample, **NSP:** no sample planned

C.2.3 Benserazide plasma concentrations ($\mu\text{g/L}$) after a single oral dose of 20 mg/kg benserazide and 80 mg/kg L-dopa

Scheduled time, h	Rat c1	Rat c2	Rat c3	Rat c4	Rat c5	Rat c6	Rat c7	Rat c8	Rat c9
0.08	213	29.3	29.7	21.8	43.8	35.0	54.0	21.6	13.3
0.17	176	28.8	45.1	26.2	45.7	38.5	44.4	31.7	43.3
0.50	84.0	37.0	28.7	34.0	19.2	35.0	30.4	12.0	62.9
1.00	59.1	18.1	37.4	19.2	22.4	23.8	21.0	25.9	72.7
2.00	16.6	7.33	13.8	NSP	NSP	NSP	2.32	10.4	NSP
4.00	NSP	NSP	NSP	7.27	2.93	1.95	NSP	NSP	NOP

NOP: no peak, **NSP:** no sample planned

C.2.4 Ro 04-5127 plasma concentrations ($\mu\text{g/L}$) after a single oral dose of 20 mg/kg benserazide and 80 mg/kg L-dopa

Scheduled time, h	Rat c1	Rat c2	Rat c3	Rat c4	Rat c5	Rat c6	Rat c7	Rat c8	Rat c9
0.08	98.8	110	188	92.6	202	131	33.6	33.4	10.2
0.17	111	69.8	101	44.8	180	74.1	50.9	22.8	15.9
0.50	27.5	27.7	11.3	24.7	7.89	15.7	37.9	16.8	31.4
1.00	23.1	5.50	17.5	6.32	7.98	10.4	21.7	28.5	11.3
2.00	4.59	2.84	3.10	NSP	NSP	NSP	8.76	8.70	NSP
4.00	NSP	NSP	NSP	2.03	0.927	8.65	NSP	NSP	4.95

NSP: no sample planned

C.3 Listings of Mean Plasma Concentrations of L-Dopa and 3-OMD

C.3.1 Average (\pm SD) L-dopa plasma concentrations after 80 mg/kg L-dopa

Scheduled time, h	Mean $\mu\text{g/L}$	SD $\mu\text{g/L}$	CV %	Median $\mu\text{g/L}$	Min $\mu\text{g/L}$	Max $\mu\text{g/L}$	N
0.00	BLC			BLC	BLC	BLC	0
0.08	2619	1790	68	1506	1103	4643	5
0.17	3064	2568	84	1911	1749	7645	5
0.25	2589	1142	44	2409	1612	4503	5
0.50	2878	769	27	2659	2101	4078	5
1.00	2876	223	8	2862	2609	3162	5
2.00	1118	450	40	1121	721	1838	5
4.00	117	191	163	25.9	18.5	457	5
6.00						33.1	1
8.00						15.0	1
10.00						10.8	1
24.00							0

BLC: below limit of calibration, **N:** number of observations used for descriptive statistics

C.3.2 Average (\pm SD) 3-OMD plasma concentrations after 80 mg/kg L-dopa

Scheduled time, h	Mean $\mu\text{g/L}$	SD $\mu\text{g/L}$	CV %	Median $\mu\text{g/L}$	Min $\mu\text{g/L}$	Max $\mu\text{g/L}$	N
0.00	25.0	5.89	24	27.4	16.8	31.6	5
0.08	89.6	39.7	44	80.8	43.4	153	5
0.17	165	56.0	34	177	77.2	228	5
0.25	243	81.7	34	243	143	369	5
0.50	532	126	24	532	380	727	5
1.00	1096	208	19	1123	820	1388	5
2.00	2003	137	7	1989	1849	2146	5
4.00	2092	154	7	2186	1925	2239	5
6.00	1791	121	7	1784	1631	1957	5
8.00	1474	39.4	3	1470	1438	1534	5
10.00	1288	115	9	1266	1202	1486	5
24.00	588	92.5	16	589	476	712	5

N: number of observations used for descriptive statistics

C.3.3 Average (\pm SD) L-dopa plasma concentrations after 80 mg/kg L-dopa and 20 mg/kg benserazide

Scheduled time, h	Mean $\mu\text{g/L}$	SD $\mu\text{g/L}$	CV %	Median $\mu\text{g/L}$	Min $\mu\text{g/L}$	Max $\mu\text{g/L}$	N
0.00	BLC			BLC	BLC	BLC	0
0.08	11655	6999	60	13164	2001	21494	9
0.17	18182	7534	41	15866	8157	29926	9
0.25	17871	6672	37	17423	9247	27430	9
0.50	16897	5432	32	15693	8112	25630	9
1.00	17944	5723	32	14424	13293	28436	9
2.00	12798	3708	29	12846	6842	20305	9
4.00	6998	4055	58	5578	2803	14289	9
6.00	1988	1629	82	1813	300	4767	9
8.00	377	427	113	274	30.0	1137	9
10.00	53.6	72.6	135	27.1	11.8	241	9
24.00				10.4	8.88	30.1	3

BLC: below limit of calibration, **N:** number of observations used for descriptive statistics

C.3.4 Average (\pm SD) 3-OMD plasma concentrations after 80 mg/kg L-dopa and 20 mg/kg benserazide

Scheduled time, h	Mean $\mu\text{g/L}$	SD $\mu\text{g/L}$	CV %	Median $\mu\text{g/L}$	Min $\mu\text{g/L}$	Max $\mu\text{g/L}$	N
0.00	31.7	8.22	26	32.9	18.9	39.5	7
0.08	949	661	70	971	94.0	2207	9
0.17	2432	906	37	2388	1184	4213	9
0.25	3567	1271	36	3345	2103	6317	9
0.50	6688	1844	28	6589	2812	9429	9
1.00	11837	1742	15	11341	10135	15611	9
2.00	19767	3236	16	18312	16303	24594	9
4.00	30213	4352	14	29019	24627	38001	9
6.00	31609	6875	22	32245	22055	39315	9
8.00	28843	6644	23	29685	17192	38320	9
10.00	23741	6254	26	23827	15529	33086	9
24.00	8535	2493	29	7748	4401	12471	9

N: number of observations used for descriptive statistics

C.4 Listings of Mean Plasma Concentrations of Benserazide and Ro 04-5127

C.4.1 Average (\pm SD) benserazide plasma concentrations after 20 mg/kg benserazide

Scheduled time, h	Mean $\mu\text{g/L}$	SD $\mu\text{g/L}$	CV %	Median $\mu\text{g/L}$	Min $\mu\text{g/L}$	Max $\mu\text{g/L}$	N
0.00	BLC			BLC	BLC	BLC	0
0.08	17.5	7.79	44	17.8	6.64	26.0	5
0.17	21.9	11.7	54	20.9	3.96	34.7	5
0.25	31.2	16.8	54	31.9	7.41	53.3	5
0.50	39.4	23.5	60	41.7	9.01	73.9	5
1.00	23.5	13.0	55	23.6	8.50	38.5	4
2.00	14.7	4.81	33	12.3	10.2	20.9	5
3.00	10.2	1.56	15	9.71	8.94	11.9	3
4.00					4.35	6.67	2

BLC: below limit of calibration, **N:** number of observations used for descriptive statistics

C.4.2 Average (\pm SD) Ro 04-5127 plasma concentrations after 20 mg/kg benserazide

Scheduled time, h	Mean $\mu\text{g/L}$	SD $\mu\text{g/L}$	CV %	Median $\mu\text{g/L}$	Min $\mu\text{g/L}$	Max $\mu\text{g/L}$	N
0.00	0.265	0.0218	8	0.265	0.240	0.291	4
0.08	35.0	24.5	70	41.4	7.94	55.8	3
0.17	93.6	80.8	86	63.8	8.60	191	5
0.25	77.5	74.1	96	49.3	16.7	196	5
0.50	34.6	27.9	81	18.3	10.7	69.9	5
1.00	6.85	3.16	46	6.04	4.07	11.2	4
2.00	5.26	4.48	85	2.56	1.86	12.3	5
3.00	2.58	2.16	84	1.46	1.20	5.06	3
4.00					1.01	1.64	2

N: number of observations used for descriptive statistics

C.4.3 Average (\pm SD) benserazide plasma concentrations after 80 mg/kg L-dopa and 20 mg/kg benserazide

Scheduled time, h	Mean $\mu\text{g/L}$	SD $\mu\text{g/L}$	CV %	Median $\mu\text{g/L}$	Min $\mu\text{g/L}$	Max $\mu\text{g/L}$	N
0.08	51.2	61.7	121	29.7	13.3	213	9
0.17	53.3	46.5	87	43.3	26.2	176	9
0.50	38.1	22.2	58	34.0	12.0	84.0	9
1.00	33.3	19.6	59	23.8	18.1	72.7	9
2.00	10.1	5.57	55	10.4	2.32	16.6	5
4.00	4.05	2.83	70	2.93	1.95	7.27	3

N: number of observations used for descriptive statistics

C.4.4 Average (\pm SD) Ro 04-5127 plasma concentrations after 80 mg/kg L-dopa and 20 mg/kg benserazide

Scheduled time, h	Mean $\mu\text{g/L}$	SD $\mu\text{g/L}$	CV %	Median $\mu\text{g/L}$	Min $\mu\text{g/L}$	Max $\mu\text{g/L}$	N
0.08	100	67.3	67	98.8	10.2	202	9
0.17	74.5	50.9	68	69.8	15.9	180	9
0.50	22.3	9.94	45	24.7	7.89	37.9	9
1.00	14.7	8.28	56	11.3	5.50	28.5	9
2.00	5.60	2.93	52	4.59	2.84	8.76	5
4.00	4.14	3.46	83	3.49	0.927	8.65	4

N: number of observations used for descriptive statistics

C.5 Listings of In Vitro Protein Binding Study Results

C.5.1 L-Dopa: In vitro binding to dialyzed human plasma¹⁾

Sample No	Concentration of L-Dopa ($\mu\text{g/L}$) ²⁾		% unbound	% bound
	plasma	ultrafiltrate	in dialyzed plasma	in dialyzed plasma
H 31 ³⁾	3.85	3.72	96.6	3.4
H 1	9.82	8.97	91.3	8.7
H 2	28.4	26.3	92.6	7.4
H 3	57.5	55.0	95.7	4.3
H 4	96.3	92.6	96.2	3.8
H 5	282	277	98.2	1.8
H 6	557	543	97.5	2.5
H 7 ⁴⁾	946	939	99.3	0.7
H 7 ⁴⁾		934	98.7	1.3
H 8	2820	2750	97.5	2.5
H 9	5540	5460	98.6	1.4
H 10	9190	9330	102	-2.0
H 11	27800	26900	96.8	3.2

1) Determined by centrifugal ultrafiltration (37°C, pH 7.3)

2) Measured by radiocounting

3) Different experimental day, same matrix

4) Duplicates were analyzed for H7

C.5.2 L-Dopa: In vitro binding to human plasma (untreated)¹⁾

Sample No	Concentration of L-Dopa ($\mu\text{g/L}$) ²⁾		% unbound	% bound
	plasma	ultrafiltrate	in untreated plasma	in untreated plasma
H 41 ³⁾	3.97	3.20	80.6	19.4
H 41 ³⁾		3.38	85.1	14.9
H 42 ³⁾	11.8	10.1	85.6	14.4
H 42 ³⁾		10.2	86.4	13.6

1) Determined by centrifugal ultrafiltration (37°C, pH 7.3).

2) Measured by radiocounting.

3) Duplicates were analyzed for H 41 and H42.

C.5.3 L-Dopa: In vitro binding to dialyzed rat plasma¹⁾

Sample No	Concentration of L-Dopa ($\mu\text{g/L}$) ²⁾		% unbound	% bound
	plasma	ultrafiltrate	in dialyzed plasma	in dialyzed plasma
R 31 ³⁾	3.98	3.01	75.6	24.4
R 1	9.05	7.98	88.2	11.8
R 32 ³⁾	10.5	8.68	82.7	17.3
R 2	28.0	24.7	88.2	11.8
R 3	56.0	47.6	85.0	15.0
R 4	93.3	82.8	88.7	11.3
R 5	286	254	88.8	11.2
R 6	547	518	94.7	5.3
R 7 ⁴⁾	953	897	94.1	5.9
R 7 ⁴⁾		901	94.5	5.5
R 8	2800	2700	96.4	3.6
R 9	5500	5370	97.6	2.4
R 10	9430	9200	97.6	2.4
R 11	27500	27100	98.5	1.5

1) Determined by centrifugal ultrafiltration (37°C, pH 7.3).

2) Measured by radiocounting.

3) Different experimental day, same matrix.

4) Duplicates were analyzed for H7.

C.5.4 3-OMD: In vitro binding to dialyzed human plasma¹⁾

Sample No	Concentration of 3-OMD ($\mu\text{g/L}$) ²⁾		% unbound	% bound
	plasma	ultrafiltrate	in dialyzed plasma	in dialyzed plasma
H 1	5.79	5.46	94.3	5.7
H 2	9.39	9.19	97.9	2.1
H 3	27.9	26.6	95.3	4.7
H 4	55.8	53.7	96.2	3.8
H 5	92.9	90.0	96.9	3.1
H 6	277	267	96.4	3.6
H 7	552	539	97.6	2.4
H 8	899	892	99.2	0.8
H 9	2550	2620	103	-3
H 10	5210	5280	101	-1
H11	8650	8820	102	-2
H 12	25900	25900	100	0

1) Determined by centrifugal ultrafiltration (37°C, pH 7.3).

2) Measured by radiocounting.

C.5.5 3-OMD: In vitro binding to human plasma (untreated)¹⁾

Sample No	Concentration of 3-OMD ($\mu\text{g/L}$) ²⁾		% unbound	% bound
	plasma	ultrafiltrate	in untreated plasma	in untreated plasma
M 1	5.94	5.72	96.3	3.7
M 2	9.81	9.62	98.1	1.9
M 3	28.0	28.0	100	0
M 4	58.4	57.7	98.8	1.2
M 5	97.2	95.8	98.6	1.4
M 6	282	283	100	0
M 7	572	569	99.5	0.5
M 8	952	941	98.8	1.2
M 9	2820	2780	98.6	1.4
M 10	5650	5590	98.9	1.1
M11	9400	9490	101	-1
M 12	26500	26100	98.5	1.5

1) Determined by centrifugal ultrafiltration (37°C, pH 7.3).

2) Measured by radiocounting.

C.5.6 3-OMD: In vitro binding to dialyzed rat plasma¹⁾

Sample No	Concentration of 3-OMD ($\mu\text{g/L}$) ²⁾		% unbound	% bound
	plasma	ultrafiltrate	in dialyzed plasma	in dialyzed plasma
R 1	5.57	5.45	97.8	2.2
R 2	9.22	9.23	100	0
R 3	27.5	27.0	98.2	1.8
R 4	55.8	54.3	97.3	2.7
R 5	93.0	90.3	97.1	2.9
R 6	274	268	97.8	2.2
R 7	543	534	98.3	1.7
R 8	915	889	97.2	2.8
R 9	2600	2620	101	-1
R 10	5350	5270	98.5	1.5
R11	8900	8970	101	-1
R 12	26100	25900	99.2	0.8

1) Determined by centrifugal ultrafiltration (37°C, pH 7.3).

2) Measured by radiocounting.

Appendix D: NONLINEAR MIXED EFFECTS MODELING

D.1 Results of NONMEM run doAP01_FOCEI

Fixed Effects		
θ_1 V_{dopa} [L]	Estimate	0.426
	CV%	26
θ_2 $V_{\text{OMD,b}}$ [L]	Estimate	0.177
	CV%	10
θ_3 CL_{dopa} [L/h]	Estimate	0.685
	CV%	10
θ_4 $CL_{\text{OMD,b}}$ [L/h]	Estimate	0.0126
	CV%	2
Random Effects		
<i>Inter-individual variance / Exponential model</i>		
ω^2_1 on V_{dopa}	Estimate	0.269
	CV%	24
	Inter-individual variability [%]	52
ω^2_2 on $V_{\text{OMD,b}}$	Estimate	0.0521
	CV%	63
	Inter-individual variability [%]	23
ω^2_3 on CL_{dopa}	Estimate	0.0323
	CV%	78
	Inter-individual variability [%]	18
ω^2_4 on $CL_{\text{OMD,b}}$ *	Estimate (fixed in this run)	0
	CV%	N/A
	Inter-individual variability [%]	0
<i>Proportional residual error</i>		
σ^2 for L-dopa	Estimate	0.213
	CV%	13
	Variability [%]	46
σ^2 for 3-OMD	Estimate	0.0792
	CV%	40
	Variability [%]	28
<i>Additive residual error</i>		
σ^2 for L-dopa §	Estimate (fixed in this run)	0.000019
	CV%	N/A
	SD [$\mu\text{mol/L}$]	0.00436
σ^2 for 3-OMD #	Estimate (fixed in this run)	0.000016
	CV%	N/A
	SD [$\mu\text{mol/L}$]	0.00400
Objective function: 94	Number of significant digits: 3.3	Minimization successful

*: The estimated variance for η of $CL_{\text{OMD,b}}$ was very small and therefore was fixed to zero in the final run, § σ^2 for L-dopa was fixed to 0.004311^2 which is the squared BLQ value of L-dopa in $\mu\text{mol/L}$, #: σ^2 for 3-OMD was fixed to 0.004024^2 which is the squared BLQ value of 3-OMD in $\mu\text{mol/L}$, **CV%:** derived from asymptotic standard error of estimate, **N/A:** not assessed, because estimate was fixed, **SD:** standard deviation

D.2 Results of NONMEM run bensAP13_FOCEI

Fixed Effects		
$\theta_1 V_{1B}$ [L]	Estimate (CV%)	0.185 (19)
$\theta_2 V_{2B}$ [L]	Estimate (CV%)	0.113 (7)
$\theta_3 CL_B$ [L/h]	Estimate (CV%)	1.55 (8)
$\theta_4 CL_{dB}$ [L/h]	Estimate (CV%)	0.0691 (9)
$\theta_5 ka_B$ [h ⁻¹]	Estimate (CV%)	0.713 (13)
$\theta_6 V_{1M}$ [L]	Estimate (CV%)	0.0717 (9)
$\theta_7 V_{2M}$ [L]	Estimate (CV%)	1.93 (90)
$\theta_8 CL_{dM}$ [L/h]	Estimate (CV%)	1.25 (76)
$\theta_9 ka_M$ [h ⁻¹]	Estimate (CV%)	1.92 (27)
Random Effects		
<i>Inter-individual variance / Exponential model</i>		
ω^2_1 on V_{1B}	Estimate (CV%)	0.412 (88)
	Inter-individual variability [%]	64
ω^2_2 on V_{2B} **	Estimate (fixed in this run)	0
	Inter-individual variability [%]	0
ω^2_3 on CL_B	Estimate (CV%)	0.0935 (48)
	Inter-individual variability [%]	31
ω^2_4 on CL_{dB} *	Estimate (fixed in this run)	0
	Inter-individual variability [%]	0
ω^2_5 on ka_B	Estimate (CV%)	0.200 (51)
	Inter-individual variability [%]	45
ω^2_6 on V_{1M}	Estimate (CV%)	0.0886 (58)
	Inter-individual variability [%]	30
ω^2_7 on V_{2M}	Estimate (CV%)	0.487 (60)
	Inter-individual variability [%]	70
ω^2_8 on CL_{dM} *	Estimate (fixed in this run)	0
	Inter-individual variability [%]	0
ω^2_9 on ka_M	Estimate (CV%)	0.749 (40)
	Inter-individual variability [%]	87
<i>Proportional residual error</i>		
σ^2 for benserazide	Estimate (CV%)	0.0678 (21)
	Variability [%]	26
σ^2 for Ro 04-5127	Estimate (CV%)	0.206 (16)
	Variability [%]	45
<i>Additive residual error</i>		
σ^2 for benserazide §	Estimate (fixed in this run)	1E-6
	SD [$\mu\text{mol/L}$]	0.000777
σ^2 for Ro 04-5127 #	Estimate (fixed in this run)	1E-6
	SD [$\mu\text{mol/L}$]	0.001175
Objective function: -1355	Number of significant digits: 3.1	Minimization successful

*: The variance for η of CL_B and CL_{dM} was fixed to zero, **: The estimated variance for η of V_{2B} was very small and therefore was fixed to zero in the final run, §: σ^2 for benserazide was fixed to 0.0007772 which is the squared BLQ value of benserazide in $\mu\text{mol/L}$, #: σ^2 for Ro 04-5127 was fixed to 0.0011752 which is the squared BLQ value of Ro 04-5127 in $\mu\text{mol/L}$, **CV%:** derived from asymptotic standard error of estimate, **SD:** standard deviation

D.3 Results of NONMEM run bedoAP06

Fixed Effects		
θ_3 $V_{\text{OMD},c}$ [L]	Estimate	0.0363
	CV%	NC
θ_6 $CL_{\text{OMD},c}$ [L/h]	Estimate	0.00591
	CV%	NC
θ_7 ki	Estimate	0.000856
	CV%	NC
Random Effects		
<i>Inter-individual variance / Exponential model</i>		
ω^2_3 on $V_{\text{OMD},c}$	Estimate (fixed in this run)	0.0521
	CV%	N/A
	Inter-individual variability [%]	23
ω^2_6 on $CL_{\text{OMD},c}$	Estimate (fixed in this run)	0
	CV%	N/A
	Inter-individual variability [%]	0
ω^2_7 on ki	Estimate (fixed in this run)	0
	CV%	N/A
	Inter-individual variability [%]	0
<i>Proportional residual error</i>		
σ^2 for L-dopa	Estimate	0.770
	CV%	NC
	Variability [%]	88
σ^2 for 3-OMD	Estimate	0.400
	CV%	NC
	Variability [%]	63
<i>Additive residual error</i>		
σ^2 for L-dopa §	Estimate (fixed in this run)	0.000019
	CV%	N/A
	SD [$\mu\text{mol/L}$]	0.00436
σ^2 for 3-OMD #	Estimate (fixed in this run)	0.000016
	CV%	N/A
	SD [$\mu\text{mol/L}$]	0.00400
Objective function: 3392	Number of significant digits: 3.1	Minimization successful Covariance step aborted

§: σ^2 for L-dopa was fixed to 0.004311^2 which is the squared BLQ value of L-dopa in $\mu\text{mol/L}$, #: σ^2 for 3-OMD was fixed to 0.004024^2 which is the squared BLQ value of 3-OMD in $\mu\text{mol/L}$, CV%: derived from asymptotic standard error of estimate, NC: not calculated due to abortion of covariance step, N/A: not assessed, because estimate was fixed, SD: standard deviation

Appendix E: REPARAMETERIZATION OF MICHAELIS-MENTEN EQUATION

The reparameterization of the Michaelis-Menten equation is based on the published reparameterized E_{\max} model ^[217] described in Eq. 98 which can be written as Eq. 99.

$$E = E_0 + \frac{(\beta^\gamma + 1) * (E^* - E_0) * C^\gamma}{(C^{*\gamma} + \beta^\gamma * C^\gamma)} \quad \text{Eq. 98}$$

$$E = E_0 + \frac{(1 + \beta^{-\gamma}) * (E^* - E_0) * C^\gamma}{\left(C^\gamma + \frac{C^{*\gamma}}{\beta^\gamma}\right)} \quad \text{Eq. 99}$$

E: effect, **E₀**: baseline effect, **C**: measure of drug exposure (e.g. concentration or dose), **γ**: sigmoidicity parameter, **E***: estimated effect resulting from C*, **β**: measure of degree of which the function deviates from linearity in C^γ

According to Eq. 99 EC_{50} and E_{\max} are defined using Eq. 100 and Eq. 101.

$$EC_{50} = \frac{C^{*\gamma}}{\beta^\gamma} \quad \text{Eq. 100}$$

$$E_{\max} = (1 + \beta^{-\gamma}) * (E^* - E_0) \quad \text{Eq. 101}$$

E_{max}: maximum effect, **EC₅₀**: concentration at which 50 % of the maximum effect is reached

Eq. 99 was transcribed to describe Michaelis-Menten kinetics, setting the hill coefficient, γ , to 1 resulting in Eq. 102.

$$V = \frac{(1 + \beta^{-1}) * V^* * C}{\left(C + \frac{C^*}{\beta}\right)} \quad \text{Eq. 102}$$

C: drug concentration, **V**: metabolic rate, **V***: estimated metabolic rate resulting from the concentration C*, **β**: measure of degree of which the function deviates from linearity in C

The parameters K_m and V_{\max} can be written as Eq. 103 and Eq. 104 using the parameters beta (β) and V^* . C^* is a concentration chosen within the range of the observed data.

$$K_m = \frac{C^*}{\beta} \quad \text{Eq. 103}$$

$$V_{\max} = (1 + \beta^{-1}) * V^* = \left(1 + \frac{1}{\beta}\right) * V^* \quad \text{Eq. 104}$$

K_m: Michaelis-Menten constant (concentration at which 50 % of the maximum metabolic rate is reached), **V_{max}**: maximum metabolic rate

Curriculum Vitae

Name: Susan Grange
Date of Birth: August 22, 1967
Place of Birth: Basel, Switzerland
Nationality: Swiss

Education:

1978-1986 Gymnasium am Kohlenberg Basel, Switzerland
 March 1986 Matura Typus D (modern languages)
 1986-1992 School of Pharmacy, University of Basel, Switzerland
 Nov. 1992 Graduation with Federal Diploma

Postgraduate Education:

1996-2000 Thesis (PhD) at the Phil II Faculty of the University of Basel, Switzerland, in collaboration with F. Hoffmann-La Roche Ltd, Pharma Division, Non-Clinical Drug Safety, Basel, Switzerland under the supervision of Prof. T.W. Guentert and Prof. N.H.G. Holford: Assessment of the pharmacokinetic interaction of L-dopa and benserazide.

Professional Experience:

At F. Hoffmann-La Roche Ltd, Basel, Switzerland: Department Clinical Pharmacology

1993-1995 Clinical Research Associate
 2000-2002 Clinical Science Specialist
 Since 2002 Clinical Pharmacologist

The lectures of the following lecturers were attended during the Pharmacy studies and the PhD:

Barras JP, Bartels H, Battegay E, Baumgartner E, Fallab S, Guentert TW, Haefeli WE, Haegeli A, von Hahn HP, Hofbauer KG, Kress A, Leuenberger H, Linde HHA, Lüdin E, Maître L, Meyer UA, Monard D, Moroni C, Nicholls JG, Pfeilschifter J, Plattner GR, Schaffner W, Scholer A, Seiler H, Senn E, Sequin U, Spornitz U, Vozeh S, Weiss P.

Publications and Presentations

Thesis publication:

1. Grange S, Holford NHG, and Guentert TW. A pharmacokinetic model to predict the PK interaction of L-dopa and benserazide in rats. *Pharmaceutical Research* 18: 1174-1184, 2001.

Other publications:

1. Reigner B, Watanabe T, Schüller J, Lucraft H, Sasaki Y, Bridgewater J, Saeki T, McAleer J, Kuranami M, Poole C, Kimura M, Monkhouse J, Yorulmaz C, Weidekamm E, and Grange S. Pharmacokinetics of Capecitabine (Xeloda®) in Japanese and Caucasian Patients with Breast Cancer. *Cancer Chemotherapy and Pharmacology*. Published online May 29, 2003.
2. Gram LF, Guentert TW, Grange S, Vistisen K, and Brøsen K. Moclobemide, a substrate of CYP2C19 and an inhibitor of CYP2C19, CYP2D6, and CYP1A2: a panel study. *Clinical Pharmacology and Therapeutics* 57: 670-677, 1995.

Thesis poster presentations:

1. Grange S, Holford NHG, and Guentert TW. Model to predict the PK interaction of L-dopa and benserazide in rats. *Millennial World Congress of Pharmaceutical Sciences 2000*, April 16-20; San Francisco, California, USA.
2. Grange S, Holford NHG, and Guentert TW. Prediction of human L-dopa kinetics after L-dopa treatment with and without benserazide from *in vivo* L-dopa kinetics in rats. *Millennial World Congress of Pharmaceutical Sciences 2000*, April 16-20; San Francisco, California, USA.

Other poster presentations:

1. Hijazi J, Riek M, Gaudeul-Ehrhart E, and S. Grange. Saquinavir 500 mg tablet, a new formulation, has similar bioavailability to Invirase 200 mg capsule for healthy volunteers at 1000/100 mg BID dosing with ritonavir. *2nd IAS Conference on HIV Pathogenesis and Treatment 2003*, July 13-16; Paris, France.
2. Grange S, Guentert TW, Banken L, and Birnböck H. Lack of influence of multiple-dose acetyl-L-carnitine on the pharmacodynamics and pharmacokinetics of captopril. *AAPS Annual Meeting 1996*, October 27-31; Seattle, Washington, USA.
3. Guentert TW, Grange S, Bock J, Waldburger R, and Birnböck H. Lack of an important influence of CYP2D6 oxidation status on the pharmacokinetics of moclobemide. *96th Annual Meeting of the American Society for Clinical Pharmacology and Therapeutics 1995*, March 13-18; San Diego, California, USA.

4. Guentert TW, Gram LF, Grange S, and Brøsen K. Reversible interaction of moclobemide with CYP2D6 and CYP2C_{meph}. *95th Annual Meeting of the American Society for Clinical Pharmacology and Therapeutics 1994*, March 30 – April 1; New Orleans, Louisiana, USA.